AD-A050 116 AGBABIAN ASSOCIATES EL SEGUNDO CALIF F/G 20/11
IMPEDANCE-BASED MOTION PREDICTION, SCALING, AND ENVIRONMENTAL S--ETC(U)
DEC 77 F B SAFFORD N00173-76-C-0249
UNCLASSIFIED AA-R-7710-4500 NRL-MR-3676 NL

1 OF 3
AD
A050116

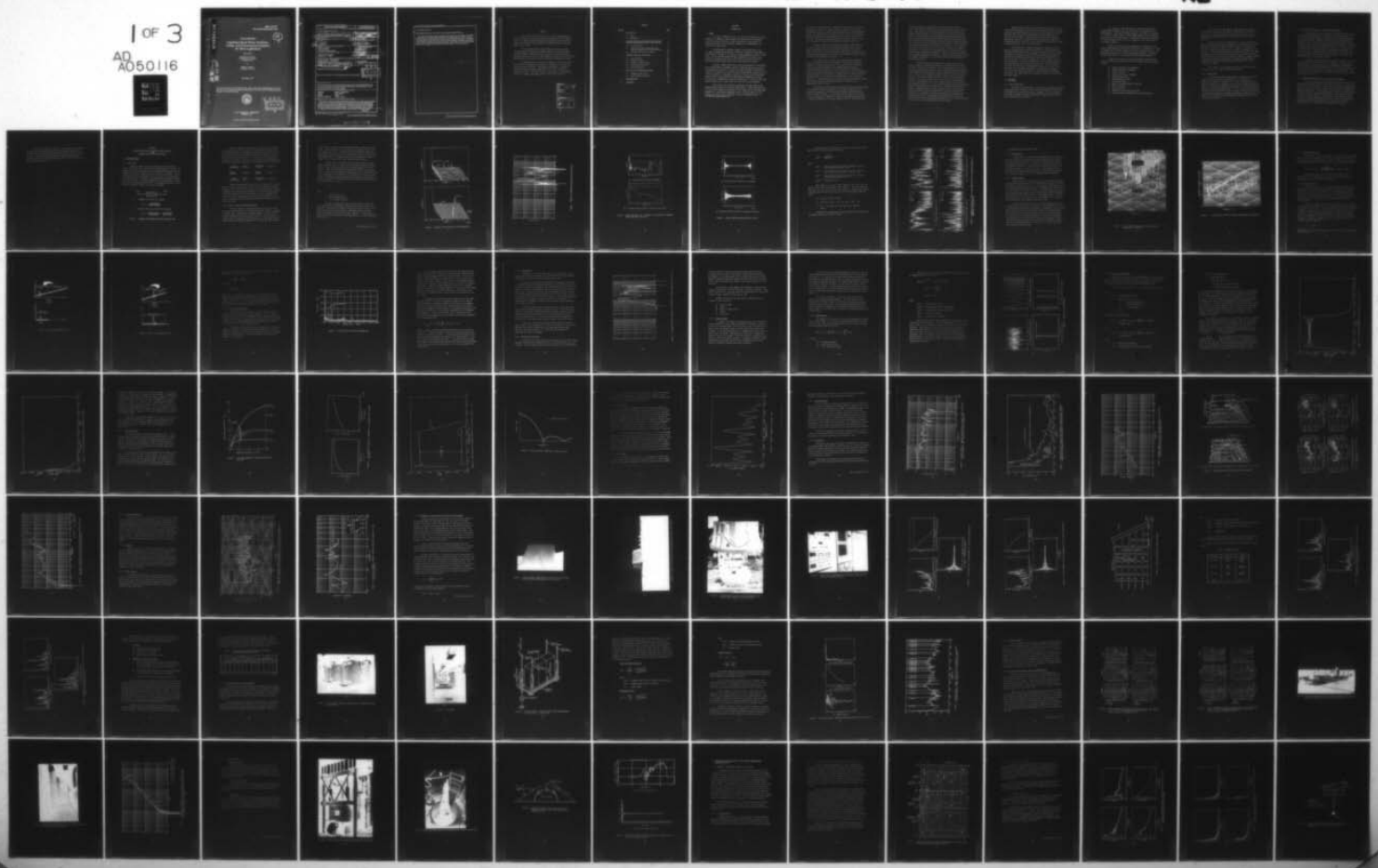

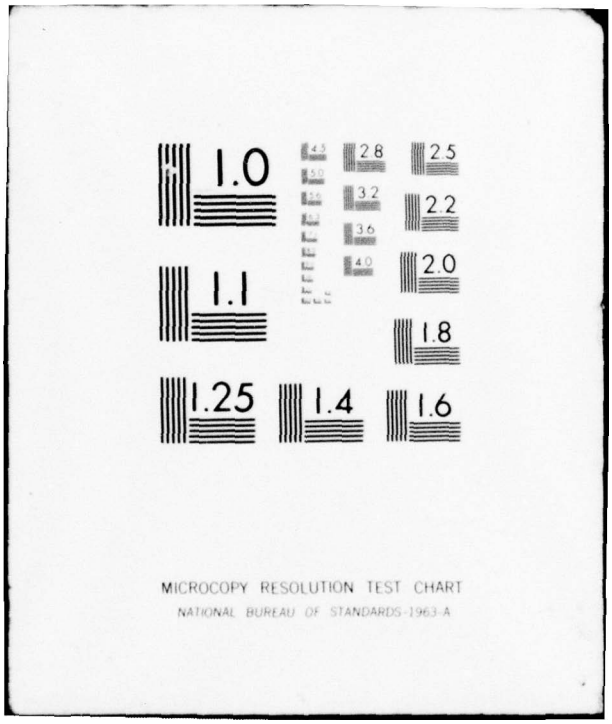
1.0
1.1
1.25
1.4
1.6
1.8
2.0
2.2
2.5
2.8
3.2
3.6
4.0
MICROCOPY RESOLUTION TEST CHART
NATIONAL BUREAU OF STANDARDS-1963-A

ade 000109
NRL Memorandum Report 3676

(12)

FINAL REPORT

Impedance-Based Motion Prediction, Scaling, and Environmental Simulation for Shock Applications

Prepared for

Department of the Navy
Naval Research Laboratory
Washington, D.C.

by

Agbabian Associates
El Segundo, California

December 1977

This work was sponsored by the Defense Nuclear Agency under subtask Y99QAXSF503, work unit 05, and work unit title Mechanical Impedance Measurement, with CFEA 03511 of Naval Sea Systems Command as a secondary manager.

NAVAL RESEARCH LABORATORY
Washington, D.C.

SECURITY CLASSIFICATION OF THIS PAGE (When Data Entered)

REPORT DOCUMENTATION PAGE

READ INSTRUCTIONS BEFORE COMPLETING FORM

1. REPORT NUMBER: NRL Memorandum Report 3676
2. GOVT ACCESSION NO.
3. RECIPIENT'S CATALOG NUMBER

4. TITLE (and Subtitle): IMPEDANCE-BASED MOTION PREDICTION, SCALING, AND ENVIRONMENTAL SIMULATION FOR SHOCK APPLICATIONS
5. TYPE OF REPORT & PERIOD COVERED: Final report on an NRL problem. Jun[illegible]76 - Oct[illegible]77
6. PERFORMING ORG. REPORT NUMBER: AA-R-7710-4500
7. AUTHOR(s): F. B. Safford
8. CONTRACT OR GRANT NUMBER(s): N00173-76-C-0249
9. PERFORMING ORGANIZATION NAME AND ADDRESS: Agbabian Associates, 250 N. Nash Street, El Segundo, California 90245
10. PROGRAM ELEMENT, PROJECT, TASK AREA & WORK UNIT NUMBERS: Y99QAXSF503
11. CONTROLLING OFFICE NAME AND ADDRESS: Naval Research Laboratory, Washington, D. C. 20375
12. REPORT DATE: Dec[illegible]77
13. NUMBER OF PAGES: 219
14. MONITORING AGENCY NAME & ADDRESS (if different from Controlling Office): NRL, SBIE
15. SECURITY CLASS. (of this report): UNCLASSIFIED
15a. DECLASSIFICATION/DOWNGRADING SCHEDULE
16. DISTRIBUTION STATEMENT (of this Report): MR-3676, AD-E000 109

Approved for public release; distribution unlimited.

DDC RECEIVED FEB 17 1978 B

17. DISTRIBUTION STATEMENT (of the abstract entered in Block 20, if different from Report)

18. SUPPLEMENTARY NOTES

This work was sponsored by the Defense Nuclear Agency under subtask Y99QAXSF503, work unit 05, and work unit title Mechanical Impedance Measurement, with CFEA 03511 of Naval Sea Systems Command as a secondary manager.

19. KEY WORDS (Continue on reverse side if necessary and identify by block number)

Impedance	Parameter Identification
Inertance	Pulse excitation
Mobility	Scaling
Multivariate regression	Transfer function

20. ABSTRACT (Continue on reverse side if necessary and identify by block number)

The ability to predict and simulate acceleration-time histories at the actual mounting locations of weapon system components will provide vital knowledge for protecting and hardening these components to meet present and changing mission requirements of naval ships and submarines. Mechanical impedance/mobility techniques, long a tool of the experimenter, have now evolved to practical methods under engineering conditions. This report summarizes current activities in the measurement of structural dynamic functions, usable methods for predicting response to

(Continues) over

DD FORM 1 JAN 73 1473 EDITION OF 1 NOV 65 IS OBSOLETE S/N 0102-014-6601

SECURITY CLASSIFICATION OF THIS PAGE (When Data Entered)

407 844 JOB

20. Abstract (Continued)

environmental threats, and a new method for environment-simulation testing.

The report is replete with example applications that demonstrate the practicality of impedance/mobility techniques. Problems that may become more tractable include the scaling of previous test results from one ship to another, and from one kind of equipment to another. The techniques could be applied to quasi-linear systems, nonlinear systems, parametric identification multivariate regression analysis, and pulsed environmental simulation. Some projects that could yield important information are suggested for review extension, and elaboration by the naval community.

PREFACE

This report presents the results of a study on impedance-based motion prediction, scaling, and environmental simulation for shock applications. G.J. O'Hara was project manager for the Naval Research Laboratory (NRL); F.B. Safford was project engineer for Agbabian Associates (AA) and author of this report.

Dr. R.O. Belsheim, NRL, (now with NKF Engineering) furnished information about the effects of equipment loading on structural motions. Dr. Vernon Neubert, Pennsylvania State University, provided considerable background information on the U.S. Navy impedance projects, as did R.E. Walker, Waterways Experiment Station, on the U.S. Army Corps of Engineers projects.

Dr. Robert Plunkett, University of Minnesota, served as a consultant during the development and evaluation of techniques for response prediction and pulse simulation. Optimization investigations were made in consultation with Dr. George A. Bekey and Dr. S.F. Masri, University of Southern California. Transient air-blast scaling analysis was furnished by Dr. Arthur R. Maddox, Naval Weapons Center, China Lake, California.

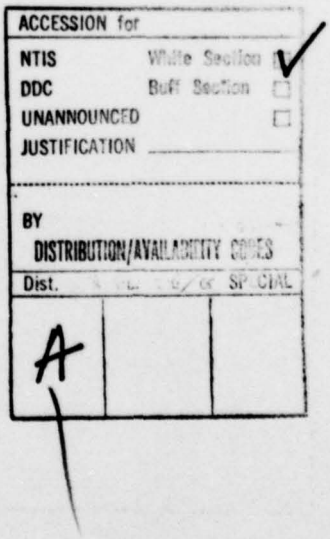

CONTENTS

SECTION 1

INTRODUCTION

1.1 SCOPE

This report summarizes the state of the art (with emphasis on recent advances) for impedance, response predictions therefrom, and environmental simulation by pulse techniques. Useful applications of these methods to ongoing naval needs are also presented, together with recommendations for future work in these areas.

The background of impedance, based on the contributions of the U.S. Navy, aerospace and machine tool industries, the Defense Nuclear Agency, and the Corps of Engineers, is reviewed. Although impedance is based on linear theory, various feasible methods have been considered for projecting the technique to parameter identification for nonlinear structural conditions and for approximate methods such as multivariate regression analysis.

Excellent response predictions in both the frequency and time domains can be accomplished with impedance records of magnitude and phase, and their associated impulse functions. The ability to make time-domain predictions for large physical systems is a relatively recent accomplishment, obtained from continuous improvement in measurement systems and in digital processing methods. Response motions can be conveniently predicted from impedance and transfer functions over a bandwidth of a few hertz to 5000 hertz. Predictions that were compared against actual records from field tests were in good agreement.

Some informal, but incomplete, comparisons have been made between impedance-based predictions and finite element models. These comparisons were not satisfactory because of differences in test ranges and finite element model assumptions. A more formal comparative study is now being made of the two methods, and results will be published in the next eight months (Ref. 1).

Note: Manuscript submitted December 6, 1977.

As a result of the availability of computers in the last 10 to 15 years for developments in the area of dynamic response, many analytical solutions on the dynamic response of structures have evolved based on assumed mathematical models. This development has advanced the analysis many years ahead of the knowledge of material and member behavior (which serves as the basis for modeling), thus leaving a broad gap between the two areas. Closure of this gap is essential to improve and to check finite element predictions.

Equipment survival is of paramount importance in the design of U.S. Navy strategic and tactical systems against weapon effects, and frequently becomes a driving consideration when the overall cost of such a system is considered. As is to be expected, every effort is made during the conceptual and design phases to minimize system equipment costs while trying to ensure a high probability of survival.

The expected levels of shock and vibration must be established before deciding how to protect the equipment. Because current computer technology limitations cause excessive run times with their accompanying large costs, modeling assumptions, and somewhat awkward structural and blast-loading approximations, reliable predictions of the shock and vibration environment inside protective structures are limited. The equipment must be assessed for survivability by determining failure, malfunction, and degradation levels (often referred to as "fragility") in terms of threat motions, i.e., the characteristic acceleration time histories expected, rather than simple sine waves, saw-tooth shock pulses, or presently used approximations (Refs. 2 to 5).

An alternative procedure for determining the internal response motions of a protective structure, particularly in the higher frequencies, is to measure the impedances of the structure from exterior loading surfaces to internal points of interest. In this manner, selected points on the structure are vibrated with a fixed-force vibrator as the frequency of vibration is smoothly changed over the frequency range of interest. By measuring the

structural response at selected points inside and on the structure, a quantitative measure is obtained of the structure response to the vibratory force. The complex ratio of the output acceleration to the input force (magnitude and phase) can then be multiplied by an arbitrary input force to predict structural motions. With an adequate structural description, the motions generated at equipment mounting by an attack may be predicted, and the structural path can be analyzed for methods mitigating shock transmission. When the appropriate transmitted shock time histories at the mounting points of equipment are obtained, the equipment can be hardened. One of the better and more practical descriptions of the structural load paths is impedance and mobility. The severity of postulated attacks will range from linear to varying degrees of nonlinear response of a structure, such that high-force-level impedance measurements are required. The high-force levels are required for impedance measurements in a quasi-linear sense or for the formation of nonlinear functionals.

Transient shock tests on equipment and systems to simulate the motions induced by a conventional explosive or nuclear attack are largely limited to single-axis test machines. Further limitations exist in the size and weight of equipment that can be tested. Simulating multiaxis loading on large equipment with many degrees of freedom represents a difficult problem, as it is impractical to generate continuously varying forces of sufficient magnitude. This problem becomes extremely difficult or impossible where in-place or field tests are required. On the other hand, short duration forces of large magnitudes over a wide frequency range can be generated by pulse generators (Refs. 6, 7). Since a discrete number of pulses superficially presents an appearance quite different from a continuous input excitation signal, it becomes necessary to select the pulses in such a way that the resulting vibration of the structure matches as closely as possible the response (e.g., displacement, velocity, or acceleration) produced by the continuous input force, as determined by an appropriate error criterion. Pulse excitation can be readily demonstrated analytically to induce structural response motions closely approximating predicted motions.

Numerous physical devices can be applied for pulse testing. Their selection and use depends on thrust levels, pulse duration, number of pulses, and spatial distribution required. The class of pulse generators includes mechanical (Ref. 8), cold gas, gas/hydraulic, hot gas (chemical), and explosive (point charges). Pulse simulation to match threat-criterion response for several massive weapons-systems equipment has already been accomplished (Ref. 9). Plans for pulse testing very large structural systems to damage/destruction levels are now being made.

The combination of impedance measurements, response predictions based on these measurements, and pulse-simulation testing when applied to large systems offers very attractive economic alternatives to other methods. For example, the simulation tests of Reference 9 provided a satisfactory demonstration of adequacy and hardness to meet mission requirements at a cost of less than 1% of what was expended on a different weapon system for the same purpose. In this other weapon system, more conventional methods were used, and the results were less than conclusive. Another example is the present construction of a $200,000,000, two-axis, 50 ft x 50 ft shake-table facility by the Japanese government in association with Japanese industry to test nuclear-power components and scale models to earthquake levels (Ref. 10). Model construction, transport, and test costs would be an additional expense.

1.2 BACKGROUND

1.2.1 UNITED STATES NAVY

The onset of the development of nuclear-powered submarines generated a sustained need for silencing. One of the principal tools for the analysis and mitigation of structure-borne sound is impedance. Under the leadership of the Navy, impedance was studied, evaluated, and applied by naval laboratories, universities, and industry.

A.O. Sykes was a major contributor at the Naval Ships Research and Development command, as was Fred Schloss with his development of the impedance head. At the Naval Research Laboratory, R.E. Blake, R.O. Belsheim, G.J. O'Hara, I. Vigness, and G.M. Remmers added substantial new information, both analytically and experimentally. Through the Office of Naval Research, N. Perrone provided project direction on impedance in both industry and in the academic community.

Analysis, applications, and implementation of impedance at the Electric Boat Company were principally carried out by L.H. Chen and I.P. Vatz. R. Plunkett and D.F. Muster conducted similar work at General Electric. The Pennsylvania State University established academic leadership in impedance research, particularly in its associated Ordnance Research Laboratory.

Impressive contributions to structural dynamics evolved from the above activities as can be observed from the following structural impedance listings:

- Complex damping and loss mechanisms
- Thévenin and Norton equivalents
- Dynamic absorbers
- Isolation with finite impedances
- Component connections
- Lumped parameter systems
- Distributed systems
- Beams with numerous boundary conditions
- Built-up structures
- Plates and shells
- Complex and statistical force fields
- Systems impedance measurements (ships and submarines)

The listing is far from complete. Published work originating from this list is extensive, with much of it being found in the *Journal of the Acoustical Society of America* and in the *Shock and Vibration Bulletin* published by the Shock and Vibration Information Center, Naval Research Laboratory.

Fortunately, many of the fundamentals of U.S. Navy research have been preserved and consolidated in monographs and reference books such as the following: *Colloquium on Mechanical Impedance Methods*, R. Plunkett, ed. Amer. Soc. of Mech. Engrs., New York, Dec. 2, 1958; J.C. Snowden, *Vibration and Shock in Damped Mechanical Systems*, John Wiley and Sons, New York, 1968; E. Skudrzyk, *Simple and Complex Vibratory Systems*, the Pennsylvania State University Press, University Park, PA, 1968; V.H. Neubert, "Impedance Related to Modeling and Analysis of Structures," monograph, Shock and Vibration Information Center, Naval Research Laboratory, Washington, D.C. (to be published circa 1978).

This summary of the impedance activities of the U.S. Navy omits many contributors only because of the need for brevity.

1.2.2 EUROPEAN WORK

In the United Kingdom, impedance work on structures has been of a long and consistent duration, commencing after its formulation by Professor A.G. Webster of Clark University in 1914. Significant work was done by R.G. White and F. Kandianis at the Institute of Sound and Vibration Research, University of Southampton, England, where time-series digital data analysis was extensively applied (Refs. 11 to 17). The work at Southampton was sponsored by the Royal Navy. Both the French and Swedish Navies are also involved in the application of impedance techniques for submarines (Ref. 18). Swedish efforts proceed from their underwater depth-charge tests on a submarine section (Ref. 19).

1.2.3 AEROSPACE, MACHINE TOOL, AND AUTOMOTIVE INDUSTRIES

The introduction of the Fast Fourier Transform and systems identification altered the direction of impedance to one of modal analysis. In this approach, data measurements are processed into a form compatible with finite element modeling. Numerous digital-processing methods have been developed for the conversion of data into mode shapes, frequencies, mass and stiffness matrices, and damping representation (Refs. 20 to 26). Thus, while an impedance measurement is a nonparametric sample of a distributed system, this type of data is altered to the form of uncoupled normal modes. The primary objective of performing modal vibration tests is to develop, verify, refine, evaluate, correlate with or obtain confidence in, the analytical mathematical model and the dynamic analyses.

Applications have been made to orbiting vehicles, missiles, aircraft, ground transportation, nuclear facilities, automobiles, and power plants. These applications have been facilitated by improvements in measurement and testing techniques, sensor developments, and on-line digital processing. The latter case has occurred with the introduction of the minicomputer. These changes have yielded improvement in measurement accuracy, and a very substantial reduction in costs.

1.2.4 DEFENSE NUCLEAR AGENCY AND U.S. ARMY CORPS OF ENGINEERS

The need for accurate environmental/structural motions over a wide-frequency band, caused by nuclear weapon effects, motivated C.C. Huang, Corps of Engineers, Huntsville, and J.G. Lewis and E.P. Sevin of the Defense Nuclear Agency to direct projects where structural responses could be computed from impedance measurements. The Corps of Engineers' projects involved the motion prediction of massive equipment (200,000 lb) from input-mounting locations to critical-internal locations of the equipment as determined by transfer functions. The Defense Nuclear Agency projects involved motion predictions of aboveground and flush-buried protective structures as determined by impedance functions. These projects are summarized in Section 2.

The Corps of Engineers, Huntsville, also required in-place testing of large massive equipment where the test motions would reasonably match the acceleration time histories predicted from transfer functions. To meet this need, a mechanical-phase generator was developed and successfully applied. Details of this pulse system were briefly discussed in Section 1.1, and are elaborated in Section 2.

SECTION 2

RESPONSE PREDICTIONS AND INDUCED MOTION SIMULATION FROM MEASURED AND SCALED SYSTEM FUNCTIONS

2.1 SYSTEM FUNCTIONS

2.1.1 DEFINITIONS

Dynamic properties of passive systems may be represented by a complex ratio of the input loading to the output response of a system. This complex ratio may be presented in the form of magnitude and phase, real and imaginary, and real vs. imaginary, all as a function of frequency. Inverse transformation provides yet another form of this ratio in the time domain, the impulse function. The complex ratios obtained may be viewed as samples from a continuum both in space and bandwidth, and are nonparametric. These functions can be determined analytically from a mathematical model or can be physically measured. Figure 1 illustrates the concept:

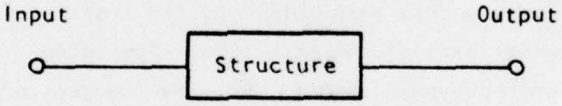

- Impedance as function of frequency

$$Z(\omega) = \frac{\text{Input Force}}{\text{Output Velocity}}$$

- Transfer function as function of frequency

$$\tau(\omega) = \frac{\text{Output Motion}}{\text{Input Motion}} = \frac{\text{Output Force}}{\text{Input Force}}$$

FIGURE 1. IMPEDANCE AND TRANSFER FUNCTIONS CONCEPTUALIZED

Mechanical impedance is an indicator of how a structure responds to a vibratory force. The response of a vibrated point on a structure is inversely proportional to the impedance, which will be defined herein for a given frequency as the driving force on the structure divided by the peak velocity at a point on the structure. The motion of the structure may be recorded as displacement, velocity, or acceleration, and, when ratioed with input force, the various system functions are defined by the following terms:

$$\frac{\text{Force}}{\text{Displacement}} = \text{Dynamic Stiffness} \qquad \frac{\text{Displacement}}{\text{Force}} = \text{Compliance}$$

$$\frac{\text{Force}}{\text{Velocity}} = \text{Impedance} \qquad \frac{\text{Velocity}}{\text{Force}} = \text{Mobility}$$

$$\frac{\text{Force}}{\text{Acceleration}} = \text{Dynamic Mass} \qquad \frac{\text{Acceleration}}{\text{Force}} = \text{Inertance}$$

Another important function is the ratio of input motion to output motion or of input force to output force. This is defined as a transfer function. Thus, if the base of a structure is put into motion by a blast or earthquake, multiplying this base motion by the transfer function produces the motion at another part of the structure. The terms "impedance" and "transfer function" have been used to simplify the presentation of this report; and where specific functions are displayed, as in data plots, these terms are defined.

2.1.2 EFFECTS OF NOISE AND SIGNAL PROCESSING

The total output of the data measurement device is the signal. This output signal passes into a recording system that produces a signature on magnetic tape. Subsequently, the analog signature is converted to a digital signature also on magnetic tape. The digital data are then in a form suitable for analysis by digital processors. In this chain of events, however, there are a number of opportunities for electronic and mechanical

errors to occur. These errors are commonly defined as noise or drift and offset. Data measurements to obtain transfer and impedance functions are very susceptible to noise, in both acquisition and processing operations. These spurious effects are often of a magnitude sufficient to highly distort the measured signal. A display of signal and noise (Ref. 27) is shown in Figure 2 for a sine wave input signal sweeping from 40 to 80 Hz.

Complex ratios of signals containing moderate amounts of noise exhibit a pattern similar to Figure 3 for the inertance magnitude function $[\ddot{X}/F(j\omega)]$. Noise both enhances and reduces resonant peaks with no clear pattern. A more sensitive indication of noise can be found in phase plots, $\phi(j\omega)$, of Figure 4 when the phase is presented for 0 to $-n\pi$ deg rather than in the conventional form of ± 180 deg. For noise-free, multiresonant linear systems, the phase plot should be essentially a monotonic line of phase as a function of frequency. The slope of this curve provides the arrival time of the signal, which is given as:

$$\tau = \frac{\phi}{\omega}$$

where

τ = Arrival time (sec)
ϕ = Phase change (radians)
ω = $2\pi f$ frequency (radians)

Examination of Figure 4a shows an erratic pattern of phase, and this phase pattern can be observed in the plot of the impulse function of Figure 5a. The phase plot of Figure 4b tends to be a better signal, yet the impulse function of Figure 5b exhibits a high degree of noise and some effects of symmetry at the end of the trace. Obviously, if these data in Figures 4 and 5 were to be used in their present forms, very poor computations would result.

(Text continued on p. 16.)

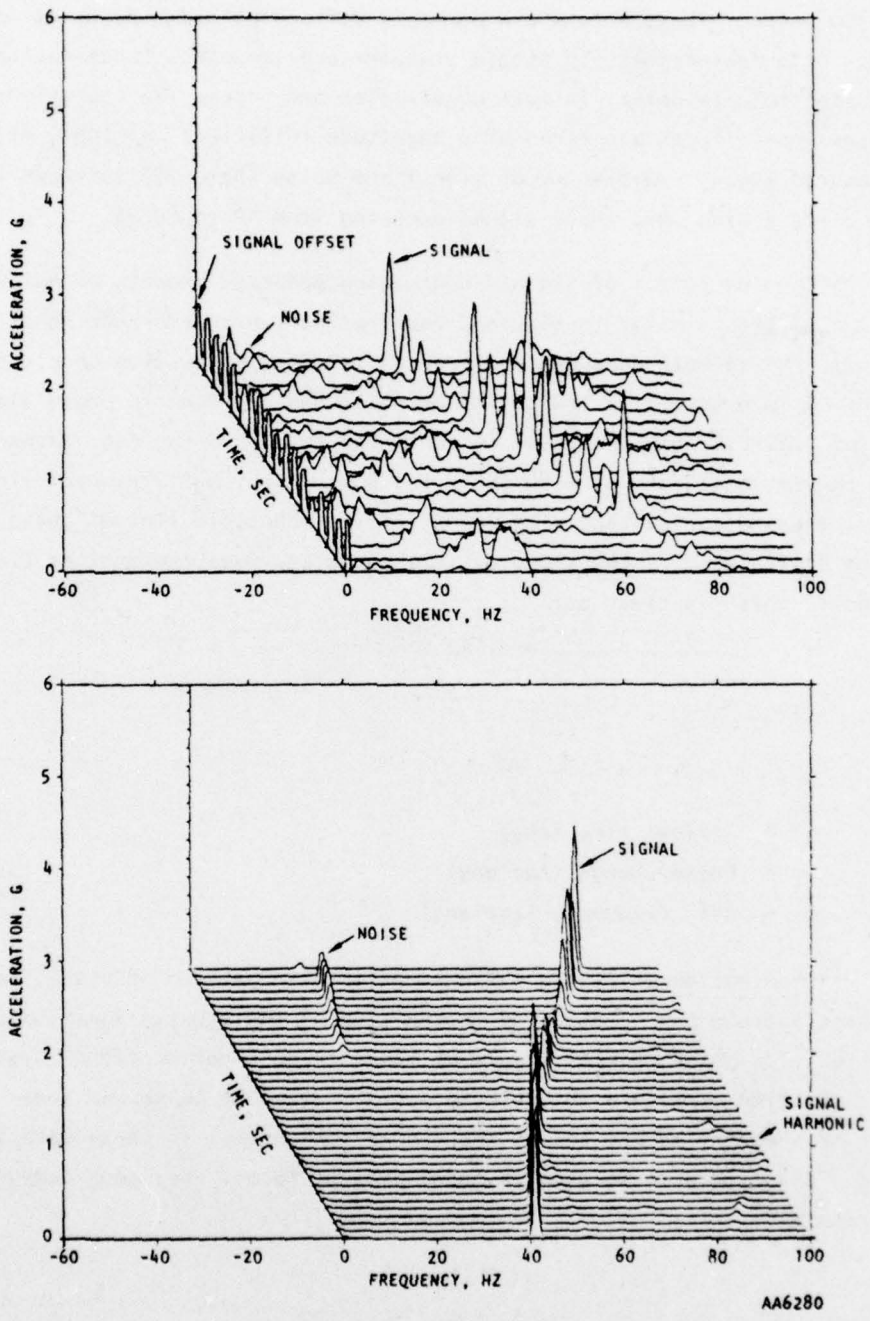

FIGURE 2. DISPLAYS OF SIGNAL AND NOISE FOR DATA ANALYSIS

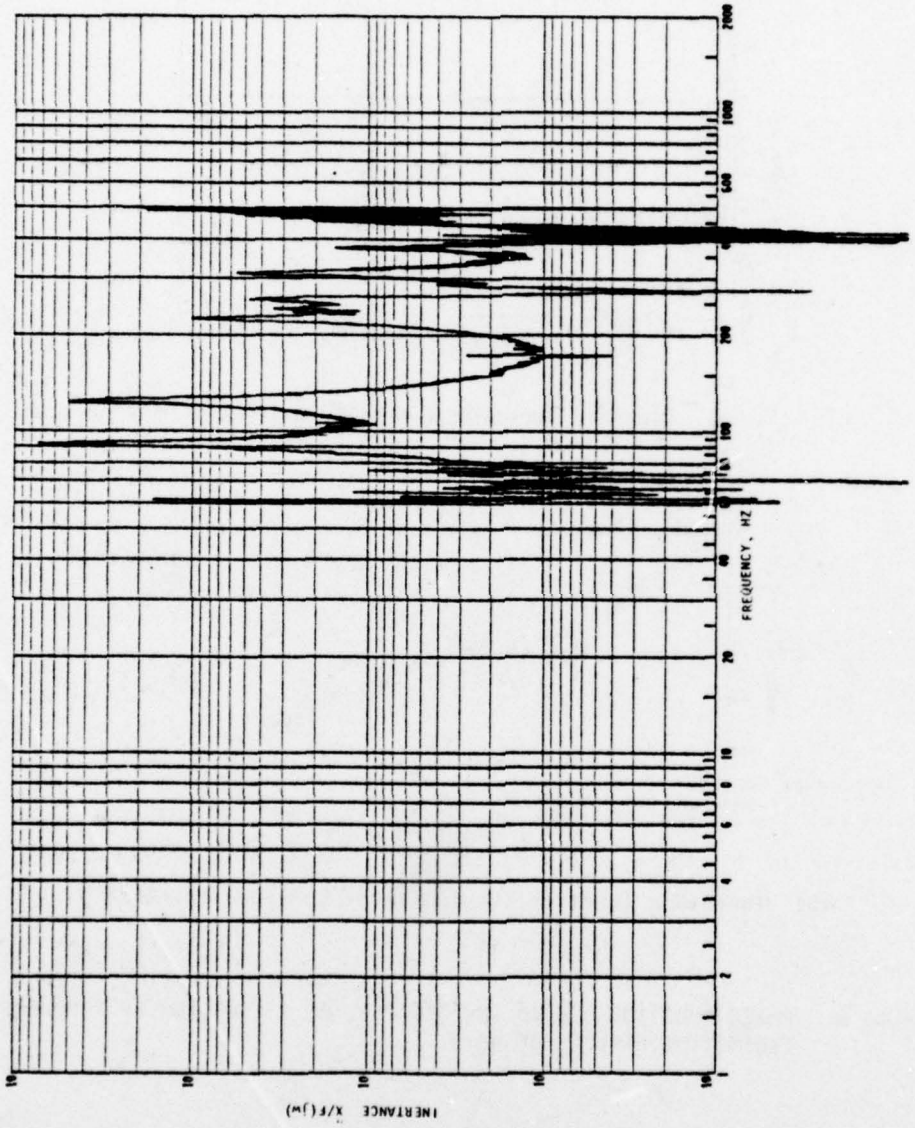

FIGURE 3. EXAMPLE OF INERTANCE MAGNITUDE AFFECTED BY NOISE

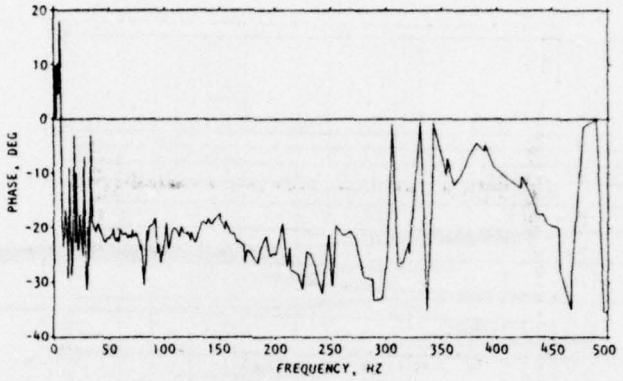

(a) Transfer function phase of equipment

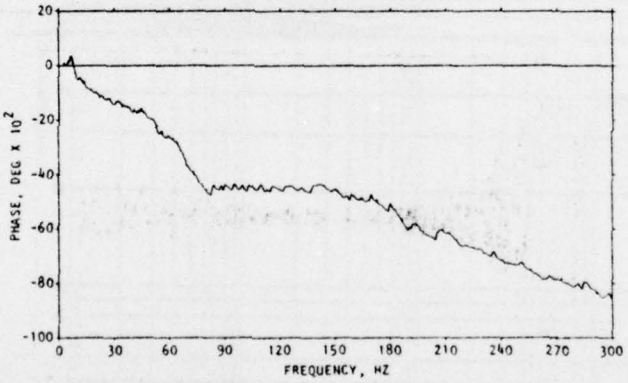

(b) Inertance function phase of a protective structure

FIGURE 4. PHASE FUNCTIONS, 0 TO -nπ DEGREES, AS A FUNCTION OF FREQUENCY EXHIBITING EFFECTS OF NOISE

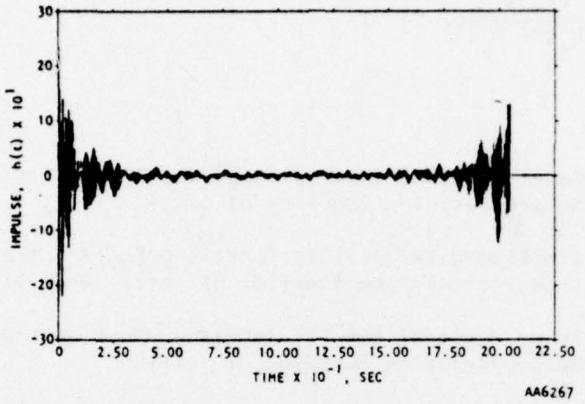

(a) Transfer function impulse of an equipment

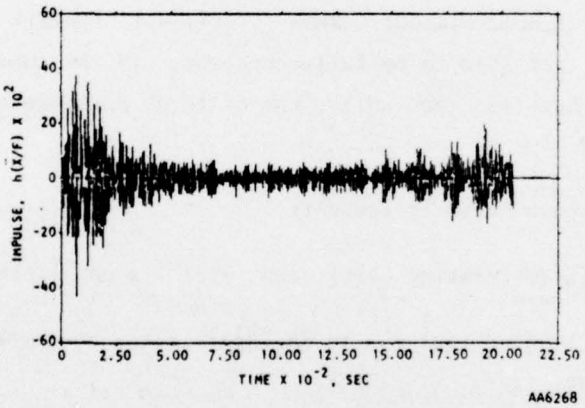

(b) Inertance function impulse of a protective structure

FIGURE 5. IMPULSE FUNCTIONS SHOWING EFFECTS OF NOISE

Another method for the detection of noise is the coherence function (Ref. 28), which is expressed by the following:

$$\gamma^2_{xy}(f) = \frac{|G_{xy}(f)|^2}{G_x(f)\, G_y(f)} \leq 1$$

where

$G_x(f)$ = Power spectral density function, Fourier transform of *autocorrelation function* of $x(t)$

$G_{xy}(f)$ = Cross-spectral density function, Fourier transform of cross-correlation function of $x(t)$ and $y(t)$

$G_y(f)$ = Power spectral density function, Fourier transform of autocorrelation function of $y(t)$

$\gamma^2_{xy}(f)$ = Coherence function

When $\gamma^2_{xy}(f) = 0$ at a particular frequency, $x(t)$ and $y(t)$ are said to be incoherent (uncorrelated). When $\gamma^2_{xy}(f) = 1$ for all frequencies, then $x(t)$ and $y(t)$ are said to be fully coherent. If the coherence function is greater than zero but less than unity, one of three possible conditions exist:

- Extraneous noise is present.
- The system relating $x(t)$ and $y(t)$ is not linear.
- $y(t)$ is an output due to an input $x(t)$ and other inputs.

Extraneous noise suppresses the coherence fucntion, and the display of Figure 6 serves as a detector for noise.

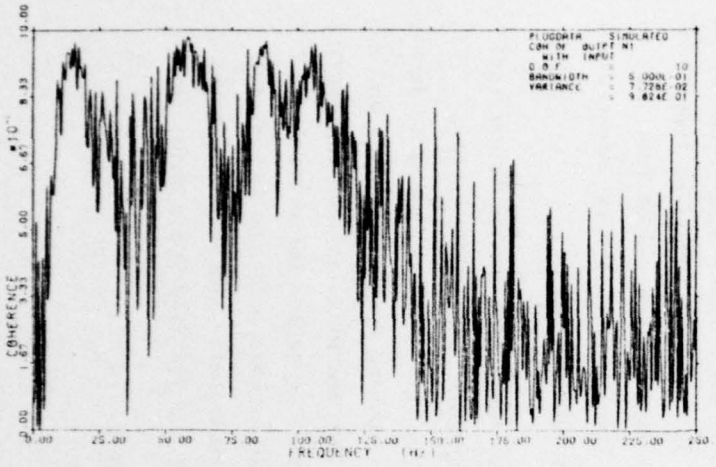

(a) Random noise added, Level N1

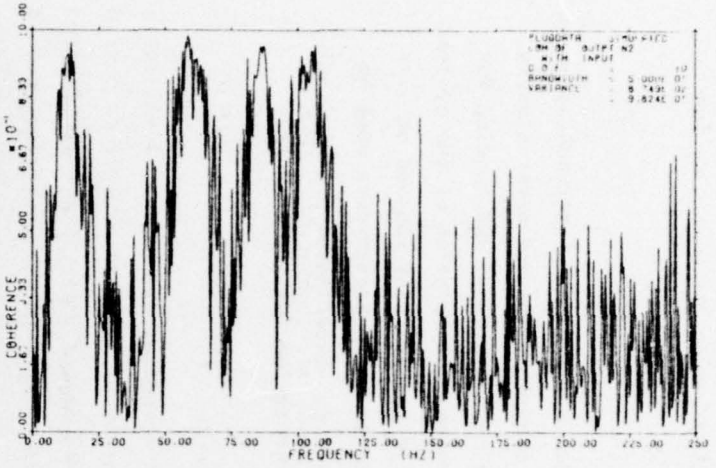

(b) Random noise added, Level N2

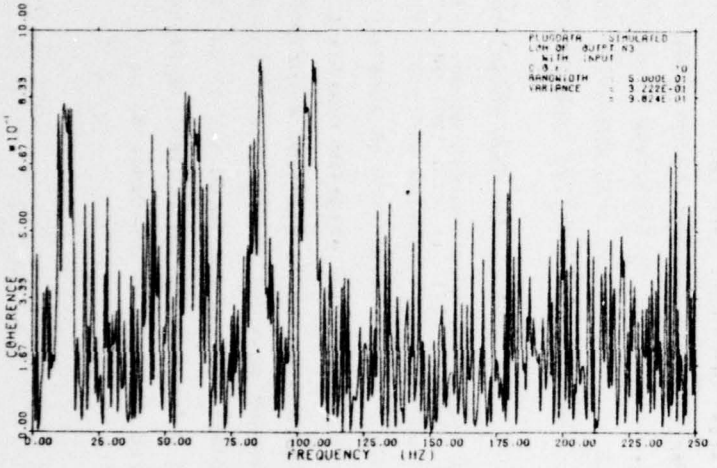

(c) Random noise added, Level N3

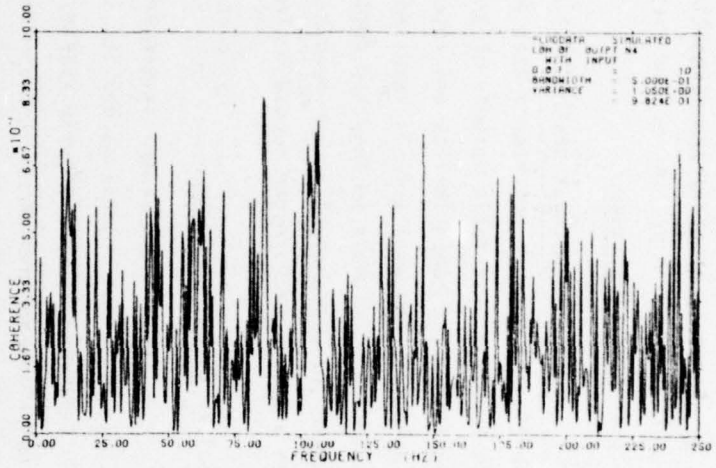

(d) Random noise added, Level N4

FIGURE 6. COHERENCE FUNCTIONS OF FOUR FILTERS SHOWING EFFECTS OF INCREASING AMOUNTS OF RANDOM NOISE CONTAMINATION

2.1.3 REDUCTION OF NOISE AND ERROR SIGNALS

2.1.3.1 Instrumentation

It goes without saying that adequate and proper instrumentation is essential to measure and record data with minimal noise and error signals. This involves systematic methods of grounding, shielding, and bonding for electromagnetic compatibility and interference. Calibration of the system in bandwidth and amplitude is required prior to each test run and on-line monitoring of signals is required during tests. All transducers must be checked for cross-coupling and acoustic pickup. Experienced professionals with a proven performance record in instrumentation must be selected.

2.1.3.2 Signal to Noise

Input-force signal levels should be set at the highest level compatible with test objectives and the linearity of the test article to obtain more favorable signal-to-noise ratios. This objective is more often limited to the force-generating equipment available. Impedance tests performed on a 1/12-scale model of a protective structure at the Defence Research Establishment, Suffield, Canada, ranged from 15 to 30 lb, while identical impedance measurements on the prototype structure in North Dakota ranged from 1000 to 5000 lb. Nominally, this change in force level between the two structures corresponded to the scaled impedance difference of 144.

Checks can be made to ensure that the system ambient electrical and mechanical noise levels do not interfere with the impedance data. This is accomplished by making plots of impedance vs. frequency, using as data the ambient signal level from an accelerometer mounted on the structure and a force signal level from the operating but mechanically isolated vibrator. The vibrator can be isolated by suspending it on cables and attaching a reaction mass; or if the size of the vibrators used preclude such direct isolation, than the force signal can be electrically simulated. Figures 7 and 8 for a prototype protective structure and its 1/12-scale model show noise overlaid on impedance data.

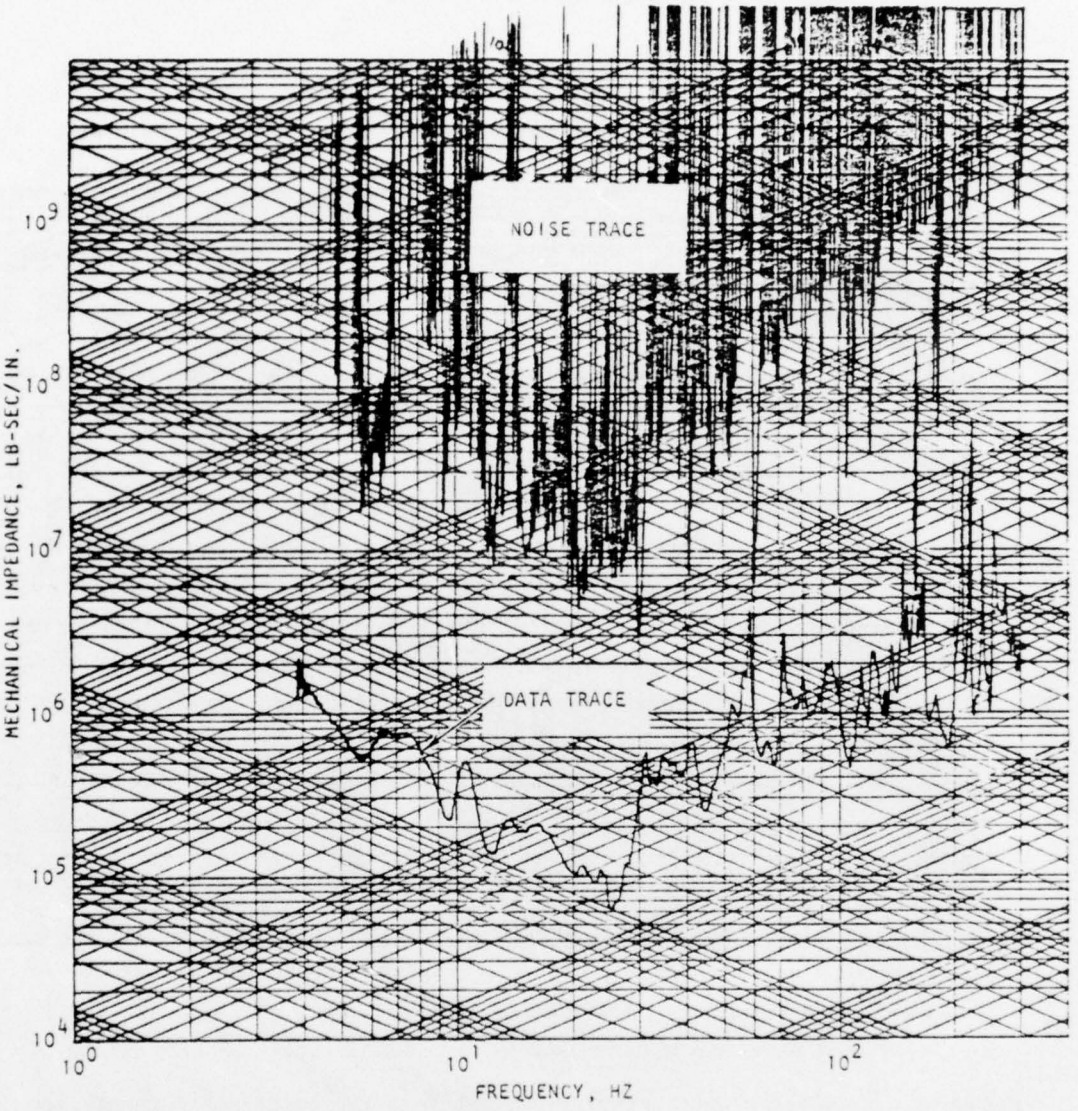

FIGURE 7. TYPICAL PROTOTYPE PROTECTIVE STRUCTURE TRANSFER IMPEDANCE/NOISE COMPARISON

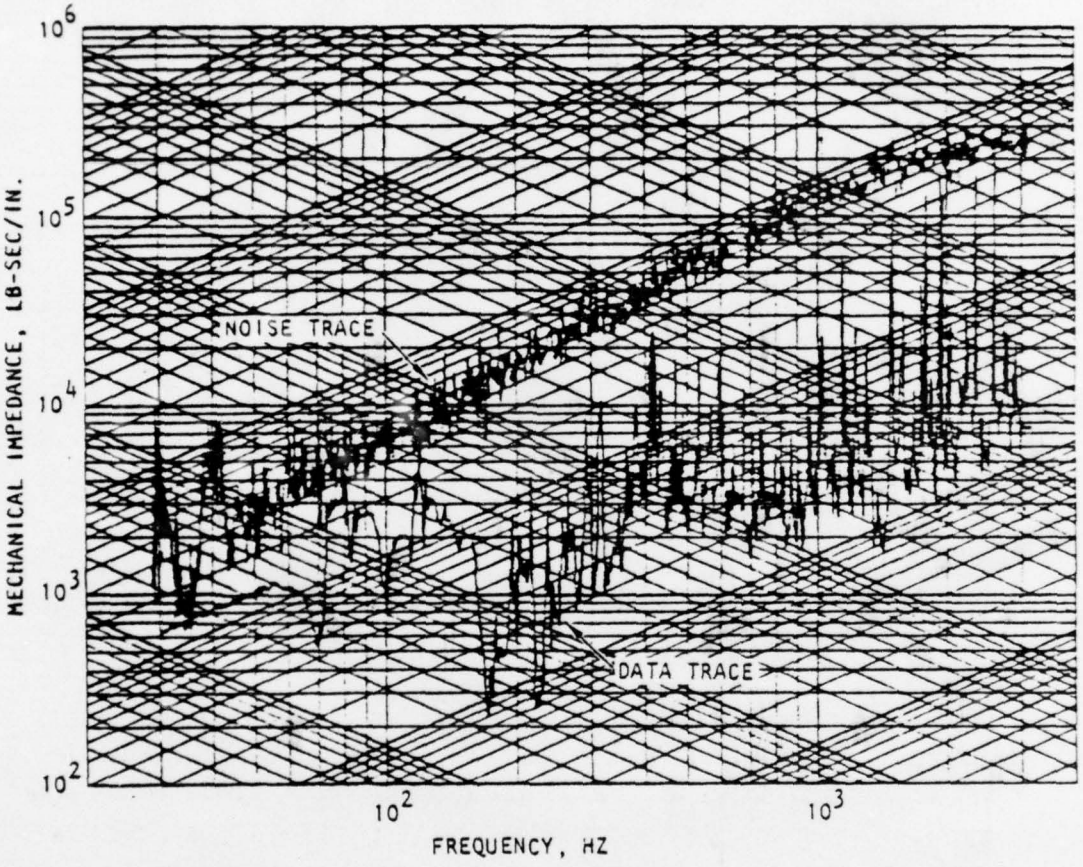

FIGURE 8. 1/12-SCALE MODEL PROTECTIVE STRUCTURE IMPEDANCE/NOISE COMPARISON

2.1.3.3 Phase-Shifting Errors

With magnetic tape recording machines, phase shifts occur even though the heads are within manufacturer's tolerance. Recording data on one machine and playing back on another compounds the problem. Phase shifts vary directly with frequency and inversely with tape speed as per the following expression:

$$\text{Phase shift error} = \frac{\text{Head Misalignment, in.}}{\text{Tape Speed, ips}} \times \text{frequency} \times 360 \text{ deg}$$

Tape machines should be calibrated for each channel with an oscillator over the frequency band of interest. Phase corrections may be used subsequently when the data have been digitized.

2.1.3.4 Drift and Offset

Offsets and drifts occur in many cases and are independent of the measurement instrument response to externally applied loads. In such cases, record offsets or drifts are stationary, i.e., the same error is present before, during, and after the transient era. A simple means of correcting these errors is to determine the offset and/or drift on a time segment before the shock arrival and to extrapolate the appropriate correction to the transient segment.

Experience has shown that late-time detrending is the most reliable way of correcting most baseline errors. The technique (Ref. 29) is illustrated in Figure 9. In many cases, a linear least-squares fit to the late-time data is adequate to achieving the desired correction. When the record length is too short to use the preceding method, the baseline error is corrected by the early-time procedure illustrated in Figure 10. Again, linear detrending is adequate* to removing the baseline's errors. The line fitted to the early-time segment is defined as

$$g(t) = a + bt$$

*Occasionally, the data justify a higher order correction, such as a parabolic fit to the data.

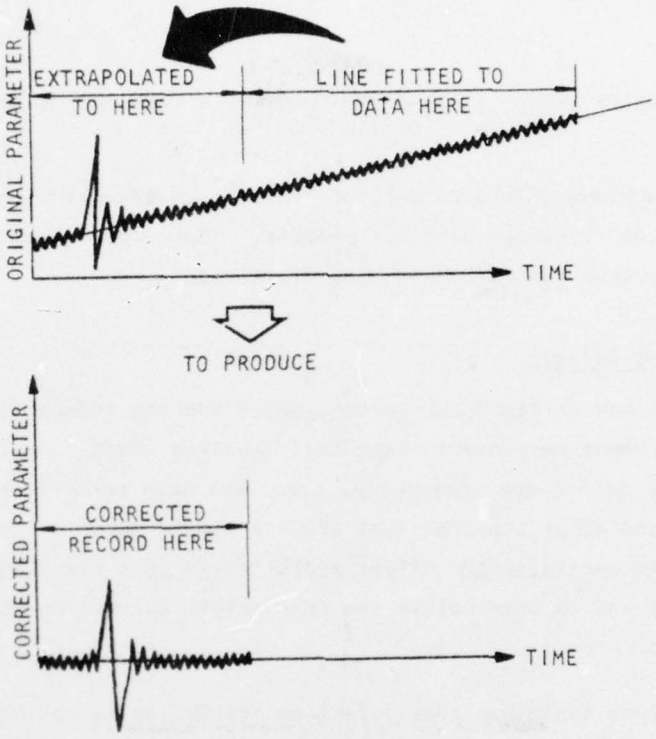

FIGURE 9. LATE-TIME DETRENDING OF DATA

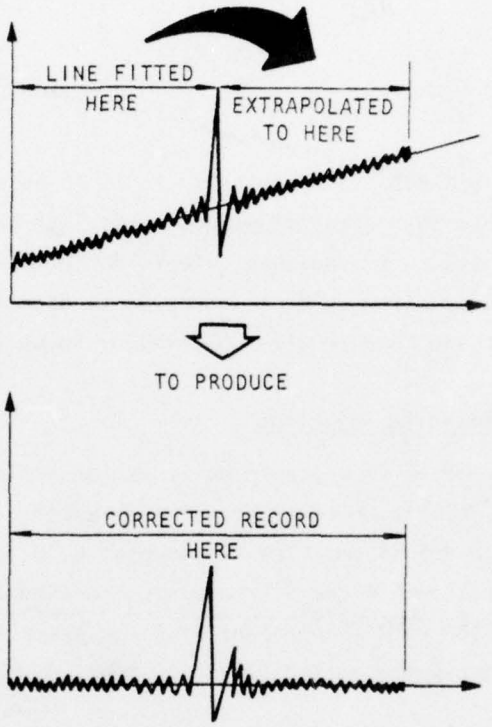

FIGURE 10. EARLY TIME DETRENDING OF DATA

where a is the intercept and b is the slope. The constants a and b are evaluated by minimizing the function

$$Q = \left[f(t) - g(t)\right]^2$$

such that

$$\frac{\partial Q}{\partial a} = \frac{\partial Q}{\partial b} = 0$$

where $f(t)$ is the data to be fitted. It is to be noted that the first equation considers both data offset and drift. If only offset is to be removed, the constant b vanishes. Tests for effectiveness of the offset and detrending correction is by integration to determine residual velocity and displacement and compare with observed or known results.

2.1.3.5 Discrete Noise Rejection

The presence of discrete noise is identified from the Fourier transform of the record where no signal is present. Figure 11 shows an example of such a transform. The fundamental 60 Hz power-supply noise and the even harmonics out to the 8th harmonic are clearly evident. Also noted in Figure 11 is the random component of noise exemplified by the nearly constant gain across the entire frequency band.

The removal of discrete noise can be accomplished in various ways, notably by band-reject filtering and time-domain subtraction. The former technique is tedious and unreliable because band-reject filtering can remove important signal components. The latter technique is potentially more accurate as described below.

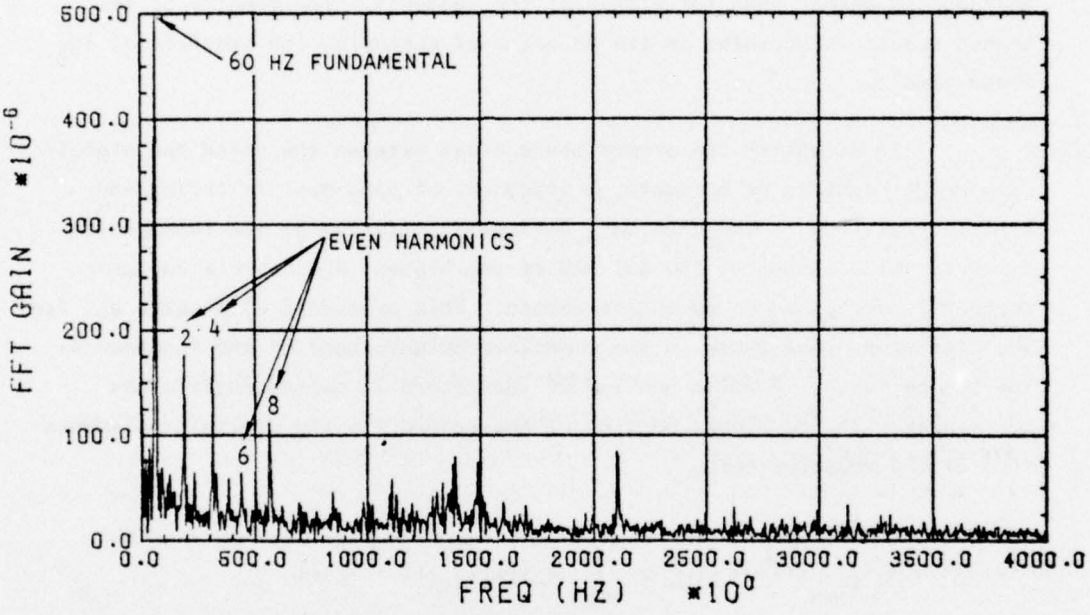

FIGURE 11. ILLUSTRATION OF DISCRETE AND RANDOM NOISE

The time-domain subtraction technique (Ref. 29) consists of subtracting the discrete noise segment of a record from the signal-plus-noise segment. Two major changes will result from this process. First, if the noise is properly phased with the signal plus noise, the discrete noise components will cancel. Implicit in this result is the assumption and fact that the entire measurement and playback systems are linear for the measurement voltages. Second, the random component of noise will be amplified because the subtraction of two random segments will result in a record whose variance is larger than for either of the segments. The penalty of the second result is accepted in the interest of achieving the benefits of the first result.

To establish the proper phase times between the noise and signal-plus-noise segments of a record, a procedure of band-pass filtering and cross correlation is implemented. Band-pass filtering at the fundamental discrete noise component (60 Hz) and at the highest discernible harmonic thereof is performed on an entire record. This procedure eliminates all frequencies other than those in the immediate neighborhood of the fundamental and the harmonic. A noise portion of the record is subsequently cross correlated with the signal portion of the record via the digital implementation of the equation below

$$R_{x_n x_{s+n}}(\tau) = \lim_{T \to \infty} \frac{1}{T} \int_0^T x_n(t)\, x_{s+n}(t + \tau)\, dt$$

where x_n and x_{s+n} denote the band-passed noise and signal plus noise, respectively. The cross-correlation function derived from evaluating the equation for successive lag times τ ultimately establishes the particular delay when both the fundamental and harmonic are in-phase between x_n and x_{s+n}. Taking into account the particular τ thus derived, the unfiltered noise segment of the record can be subtracted from the unfiltered signal-plus-noise segment to achieve the desired result, i.e., a record purged of the discrete noise.

2.1.3.6 Random Noise

Random noise of the same bandwidth as the signal presents special problems, particularly for single tests. When repetitive tests can be made, averaging will substantially reduce the random noise content.

Repetitive tests of the same measurement can be made, and transfer or impedance functions are formed for each test. These functions are treated as repetitive waveforms and averaged. The variance of the noise present in the function is reduced by the number of samples and consequently the rms value of the noise is reduced by the square root of the number of samples averaged. This method assumes that the mean value of the noise is zero, that the noise is a random variable, and that each sample (noise) is statistically independent. An example of this procedure is shown in Figure 12 for 20 averages. This figure should be compared to Figure 3, which represents a single measurement of the same test article.

Repetitive system function averaging as well as single measurement tests can be supplemented by curve fitting to the data. This curve-fitting method is a very useful procedure and produces response predictions that are often reasonable and not excessively in error even when used with system functions containing noise. In this latter case, technical judgments and end objectives of the project must determine whether to use curve fitting.

Other noise reduction and evaluation methods have been developed and are useful in varying degrees for single test measurements. These include PSD (Ref. 29), Fourier transform (Ref. 29), phase optimization methods (Ref. 30), and coherence (Ref. 31). At this time, these methods are approximate and costly to implement.

2.1.4 EXCITATION OF STRUCTURES

Selection of driving functions are constrained by the physical hardware available to generate the required force levels, shaping characteristics, and bandwidth. The most commonly used force-function generators are electrodynamic

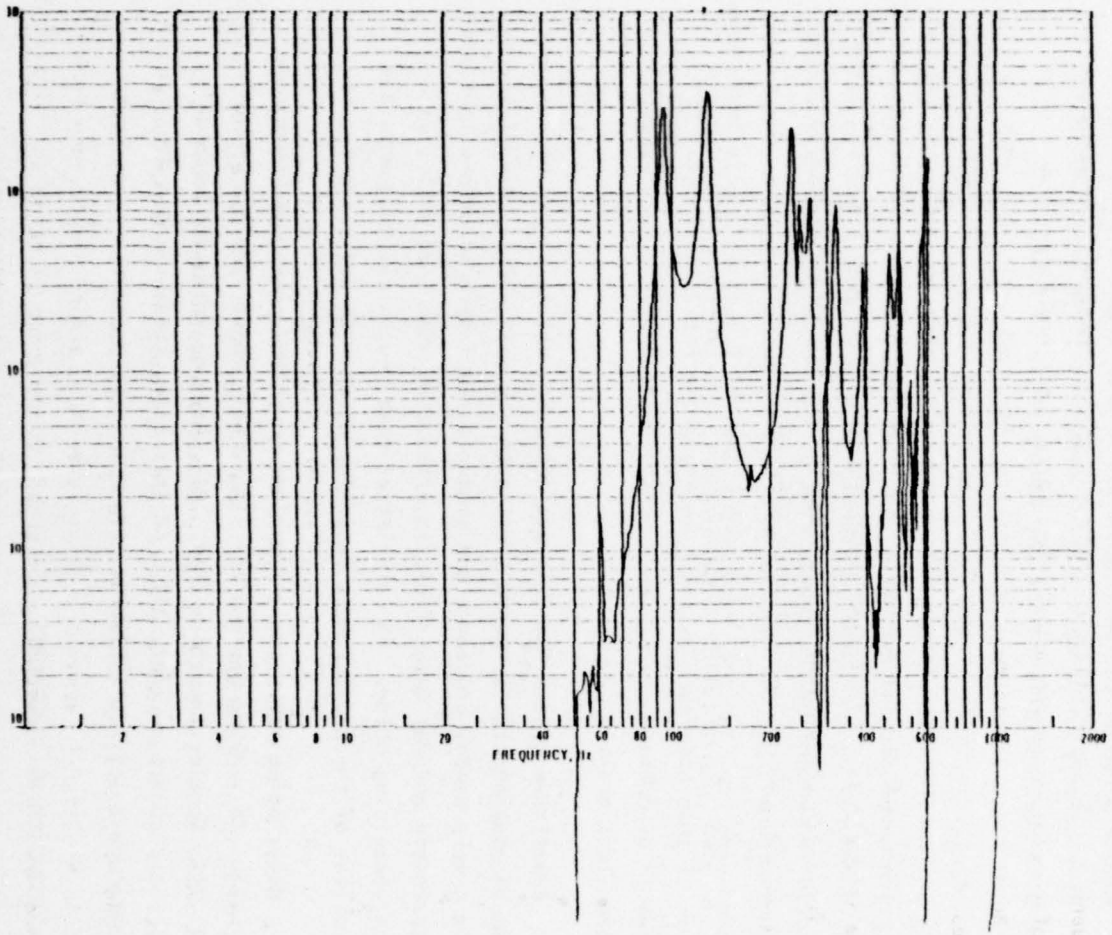

FIGURE 12. INERTANCE MAGNITUDE AVERAGE OF 20 FUNCTIONS TO REDUCE RANDOM NOISE (See Fig. 3)

and electrohydraulic shakers that produce continuous periodic (usually sinusoidal) functions that are controllable in amplitude, time duration, and frequency. With sophisticated control systems, these devices are also capable of generating random and complex force functions as well as simple pulses. Rotating eccentric mass shakers are also used, primarily for civil structures.

Shock machines, impact hammers, pulse generators, and explosives produce a second family of driving functions, the transient functions. These types of functions may include many pulses of varying forms (e.g., half-sine, triangle, square), depending on the required input.

Methods of excitation that have come into common use and are discussed in this section are

- Slow sine sweep
- Random
- Rapid sine sweep (chirp)
- Impulse
- Pulse train

2.1.4.1 Slow Sine Sweep

In the past, the frequency response characteristics of structures have been measured by quasi-steady-state methods. One method, referred to as the slow sine-sweep method, involves varying an input sinusoidal forcing function over the frequency region of interest and measuring the output responses. It has been used extensively in impedance and transfer function testing (Refs. 30 and 32). Considerable error may occur if steady-state response is arbitrarily assumed. To minimize such error, convergence techniques are used in the testing procedures. Convergence techniques involve progressively slower sweep rates (or time-of-frequency variation) until essentially asymptotic response amplitudes are obtained.

A/D conversion and the subsequent computer processing of slow sine-sweep data generate cost and technical problems owing to the large amount of data required. To circumvent this problem, sophisticated A/D conversion techniques have been developed that allow for selective windowing of the real-time response data (Refs. 30 and 32). The window-sampled data are processed for frequency, magnitude, and phase, and these data are stored as sets of digital channel elements. For many large data acquisition projects, however, this processing method is impractical due to the large time and cost requirements. In addition, averaging the system functions to reduce noise is not practical.

The slow sine excitation is useful for quick-look field data processing with analog impedance equipment. On large structures, this method permits resonance buildup of the structure, thereby generating more favorable signal-to-noise ratios. Vibration machines ranging from a few pounds to 50,000 lb of output force are available. Both low and high frequency rolloff of force occurs and is a function of the design characteristics of each vibrator.

2.1.4.2 Random Function

The random driving function can include all frequencies of interest over a selected range. It is defined as an uncorrelated function for which the mean is zero and the power spectral density (PSD) is constant or shaped over the frequency region of interest.

$$\text{PSD} = G_x = \lim_{B \to 0} \frac{a^2}{B} \quad \text{or} \quad a^2 = \int_{f_1}^{f_2} G(f)\,df$$

in which

B = Frequency bandwidth
G_x = Power spectral density
a = rms of random-force input

System functions (Ref. 28) may be measured from input-output records of random excitation by the following:

$$|G_{xy}(f)|e^{-\Theta_{xy}(f)} = |H(f)|e^{-j\phi(f)}\, G_x(f)$$

$$|H(f)| = \frac{|G_{xy}(f)|}{G_x(f)}$$

$$\Theta_{xy}(f) = \phi(f)$$

where

$G_x(f)$ = Input spectral density

$G_{xy}(f)$ = Cross-spectral density (input/output)

$\Theta_{xy}(f)$ = Cross-spectral density phase factor

$\phi(f)$ = Phase system function

$|H(f)|$ = System function magnitude

This type of excitation permits sampling of the data records to form a succession of system functions, which when averaged substantially reduce noise. Figure 12 is an averaged system function from 20 trials using random excitation. Input power per frequency from the vibrator is reduced for broad band random compared to the slow sine excitation method. Quick-look at the system function must be delayed until the records have been processed, unless a minicomputer processor is available (Time-Data, HP, Spectral Dynamics). Force input rolloffs at both low and high frequencies are functions of the particular vibrator. Figure 13a is an example of a random force-time history.

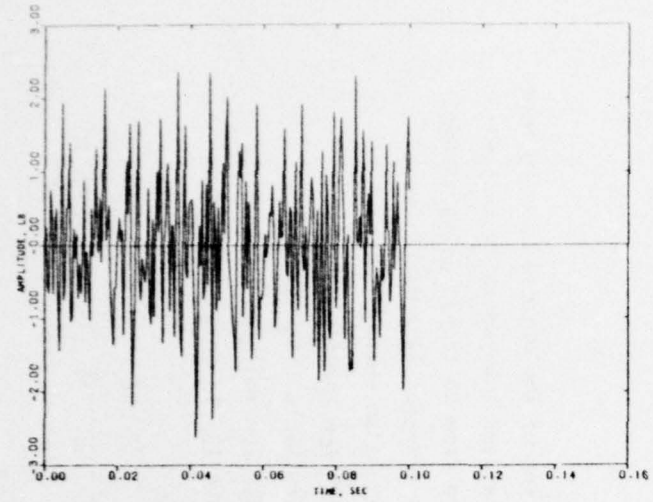

(a) Random-force input function

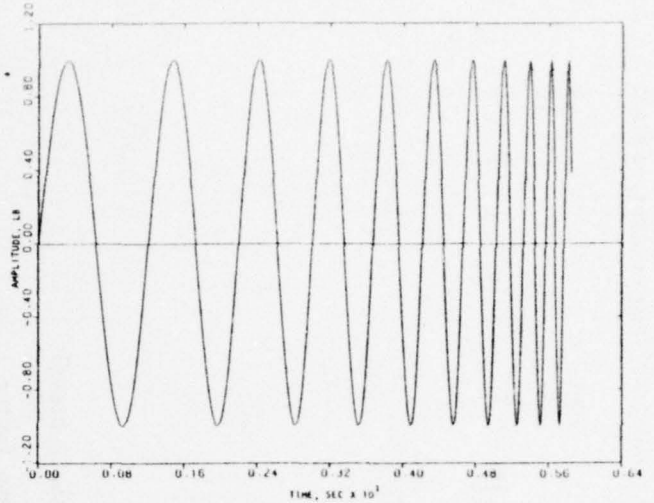

(b) Rapid sine-sweep input function

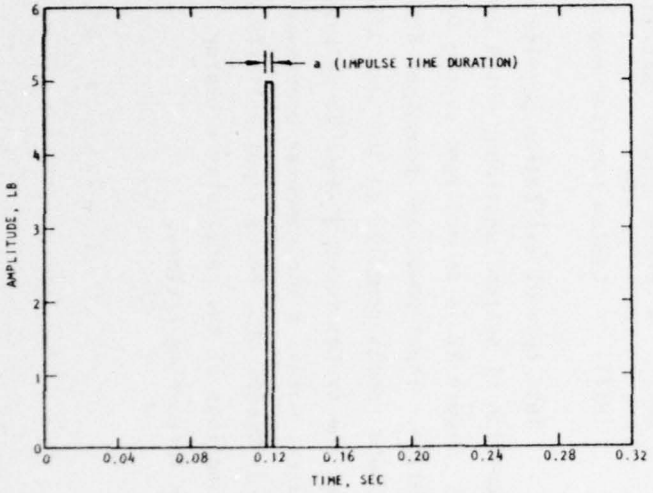

(c) Impulse input function

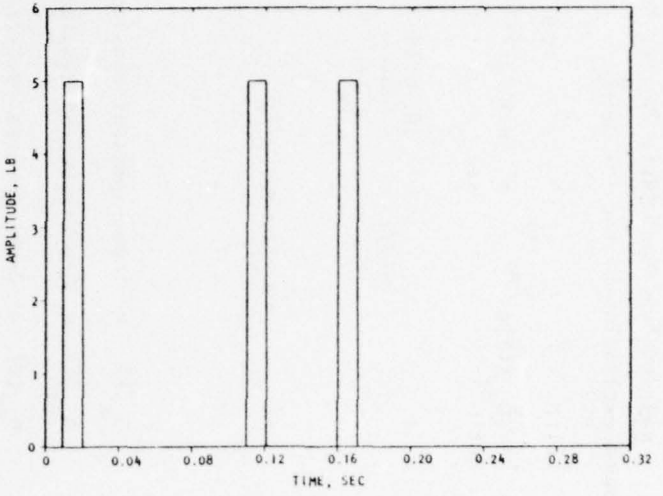

(d) Pulse train input function

FIGURE 13. FORCE EXCITATION FUNCTIONS

2.1.4.3 Rapid Sine Sweep (CHIRP)

Generally similar to the slow sine-sweep function is the rapid sine-sweep (chirp) function, which differs mainly in the time duration of frequency sweeping. Figure 13b is a force-time history upsweep chirp. Two forms of this function are commonly used in testing, one from Reference 33.

$$F(t) = Fo \sin (at^2 + bt),\ 0 < t < T,\ \text{increasing frequency sweep}$$

where

Fo = Maximum force amplitude

$a = \frac{\pi}{T}(f_2 - f_1)$, $f_2 > f_1$

T = Total record length, sec

f_1 = Initial frequency, Hz

f_2 = Final frequency, Hz

$b = 2\pi f_1$

and the second from Reference 34:

$$F(t) = Fo \sin\left[-2\pi N' \log_e \left(1 - \frac{fot}{N'}\right)\right],\ \text{for increasing frequency sweep}$$

and

$$F(t) = Fo \sin\left[2\pi N' \log_e \left(1 + \frac{fot}{N'}\right)\right],\ \text{for decreasing frequency sweep,}$$

where

Fo = Maximum force amplitude

N' = Effective number of cycles at each frequency

fo = Initial frequency, Hz

f = Final frequency, Hz

t = Sweep time from fo to f

$= N' \left(\frac{1}{fo} - \frac{1}{f}\right)$, increasing frequency

$= -N' \left(\frac{1}{fo} - \frac{1}{f}\right)$, decreasing frequency

Chirp testing may be performed in either direction, from low to high frequency or the reverse. As in random testing, short-record lengths may be obtained for the frequency bandwidth of interest with consequent ease in digitizing the record. Function generators controlling the vibrators may be programmed for numerous chirp sweeps to permit averaging of the system functions for noise reduction. For chirp testing, additional control systems may be required for the vibrator to maintain programmed input. An example of a single chirp sweep is the system function shown in Figure 3. Limitations of quick-look data and frequency rolloff of the vibrator are the same as for random excitation. Major advantage of the chirp test is the higher force input attainable per frequency.

Chirp testing in the form of $F_o \sin (at^2 + bt)$ provides a reasonably constant force input spectrum as may be observed in Figure 14. For general testing this is the desired form. The log sweep form provides the frequency spectrum given in Figure 15. In this log sweep form, the low spectrum amplitudes at the high frequency yield undesirable signal-to-noise ratios. The log sweep chirp is desired by some investigators for the form or shape of the shock spectrum, which may be generated.

The shock spectrum is an envelope of the response amplitudes of n single-degree-of-freedom (SDOF) oscillators as $n \to \infty$. The amplitudes are dependent on the nature of the input and the damping assumed for the oscillators. The shock spectrum is used to determine how the oscillators (and the modes for real structures) are excited towards their maximum amplitudes. It is not enough just to have a frequency present in the input. It must be

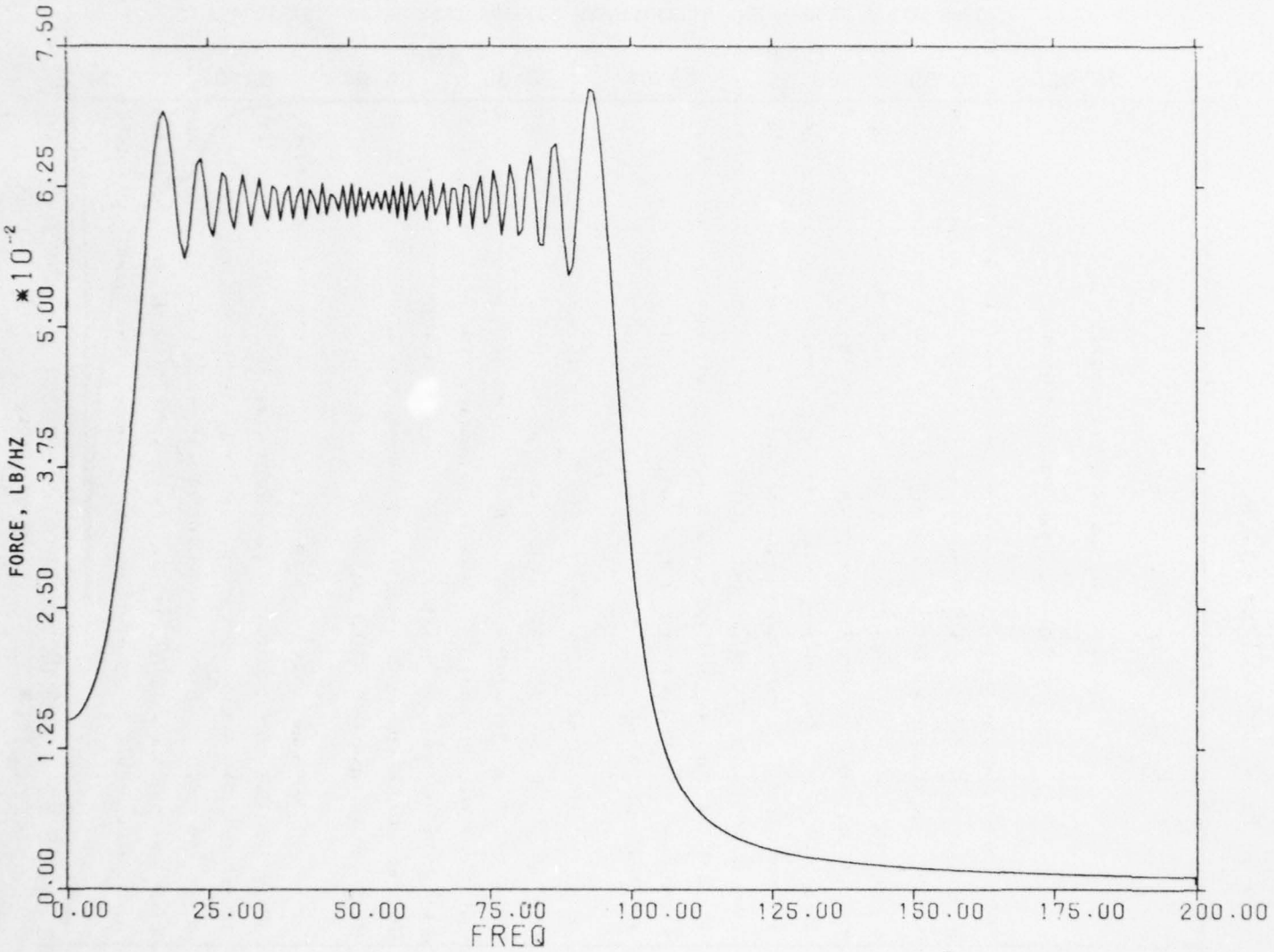

FIGURE 14. CHIRP TEST FOURIER MAGNITUDE, IN THE FORM OF F_o SIN $(at^2 + bt)$

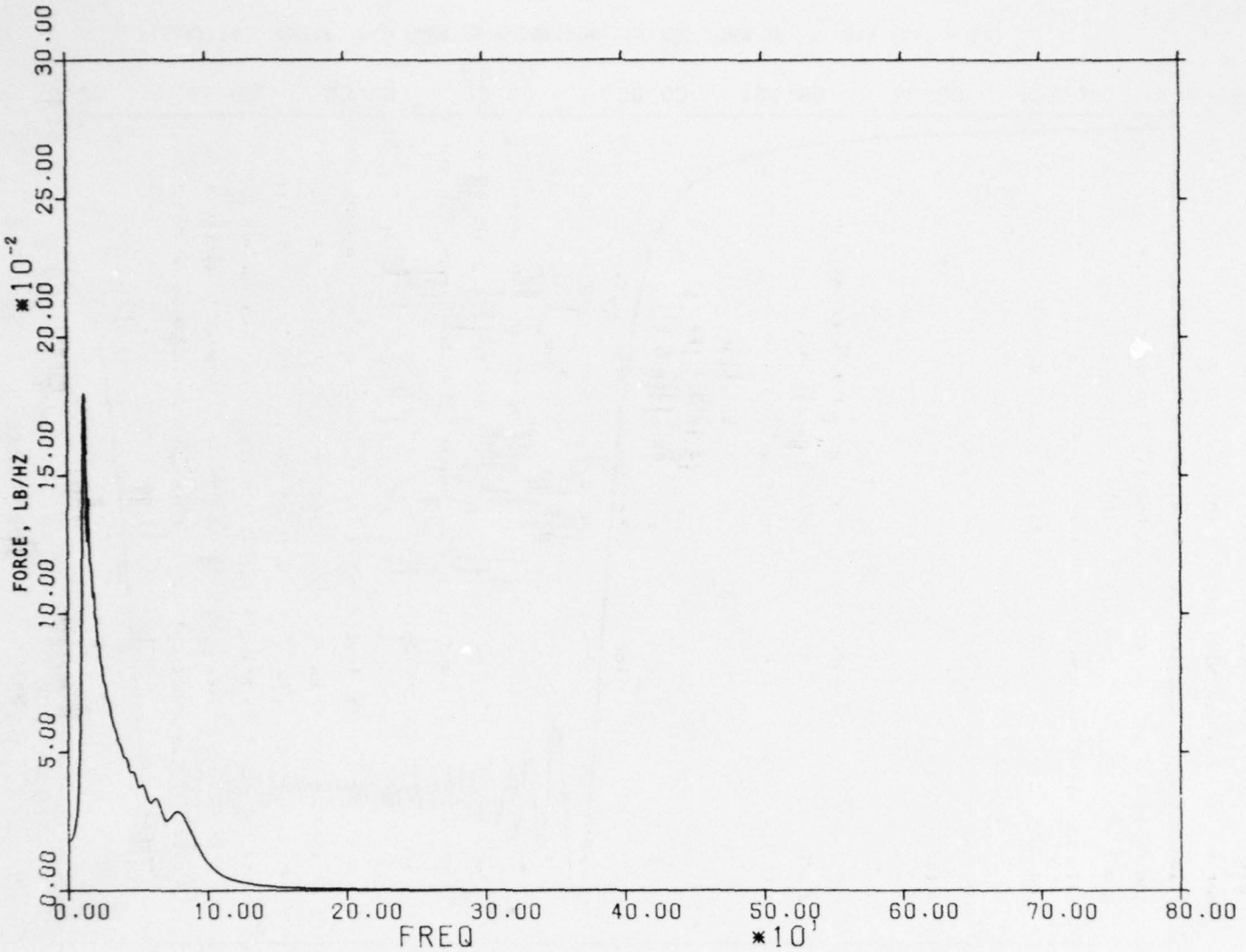

FIGURE 15. CHIRP TEST FOURIER MAGNITUDE IN THE FORM OF A LOG SWEEP

present with adequate oscillations to fully excite the mode. The evaluation of whether or not an input will produce this desired effect is accomplished by comparing the shock spectrum for several values of damping. As Figure 16 shows, the number of cycles required is heavily dependent on the value of Q, ($C/Cc = \zeta = 1/2Q$). For $Q = 5 (\zeta = 0.10)$, the response amplitude has essentially reached a maximum of 5 cycles, but for $Q = 25$ ($\zeta = 0.02$), the maximum has not been reached at 20 cycles. $Q = 5$ is a reasonable value to assume for structural modes and, therefore, from Figures 16 and 17 it can be concluded that whenever $Q_{25}/Q_5 \geq 2$, the input is adequate to fully excite the structural modes.

Shock spectra calculated at values of $Q = 5$ and $Q = 25$ for the chirp (log sweep) driving function is shown in Figure 18 from which the ratio Q_{25}/Q_5 will give an effective number of oscillations of 15. This shock spectrum technique is a useful tool in selecting sweep times for chirp testing.

2.1.4.4 Impulse Functions

The impulse-function family comprises a number of types. Two of the types that are mechanically producible are the short duration, single-impulse functions from shock machines, and periodic impulses from impact hammers. The simplicity and portability of some of the devices used to generate impulses make them advantageous for many engineering applications. A typical impulse function and associated Fourier transform magnitude are presented in Figures 13c and 19.

A single impulse function that can populate a high-frequency region must be of short duration as seen in Figure 19 (e.g., let $F_{max} = 1/2 \frac{2\pi}{a} =$ 500 Hz; then $a \simeq 5$ ms). The short duration imposes practical restrictions on shock devices in formulating acceptable pulses. For lightweight test articles, a shock hammer was developed at the Naval Research Laboratories (Ref. 35) circa 1958. Practical use of this device did not come about until

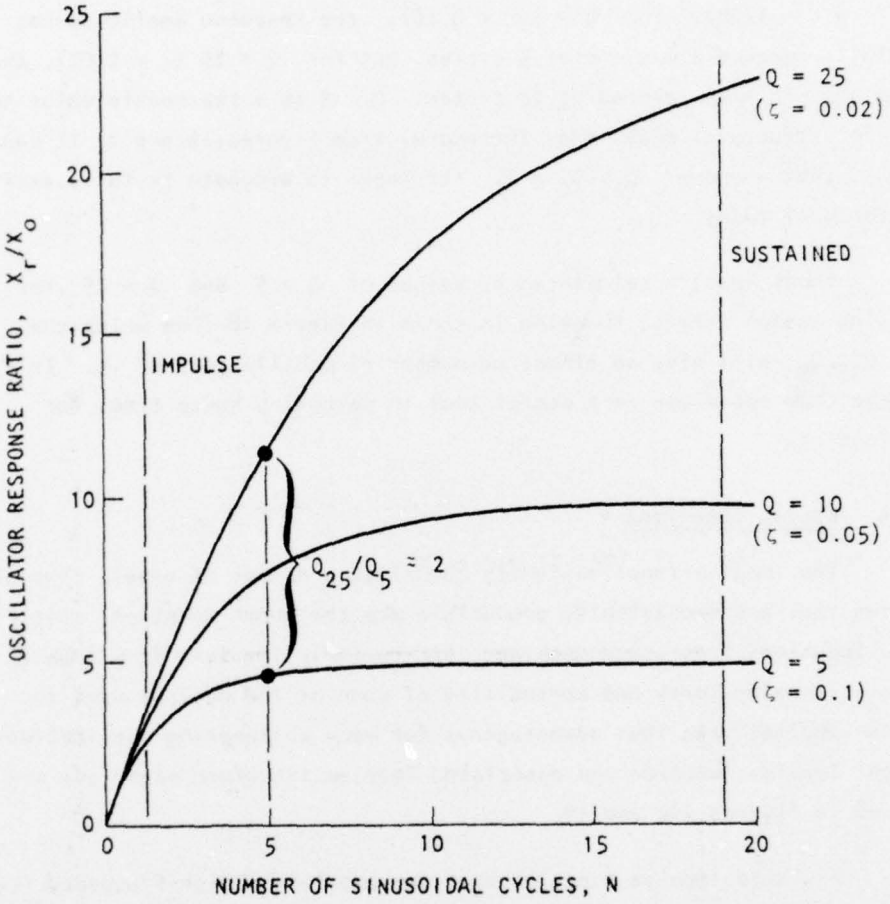

FIGURE 16. OSCILLATOR RESPONSE TO SINUSOIDAL BASE MOTION (Ref. 34)

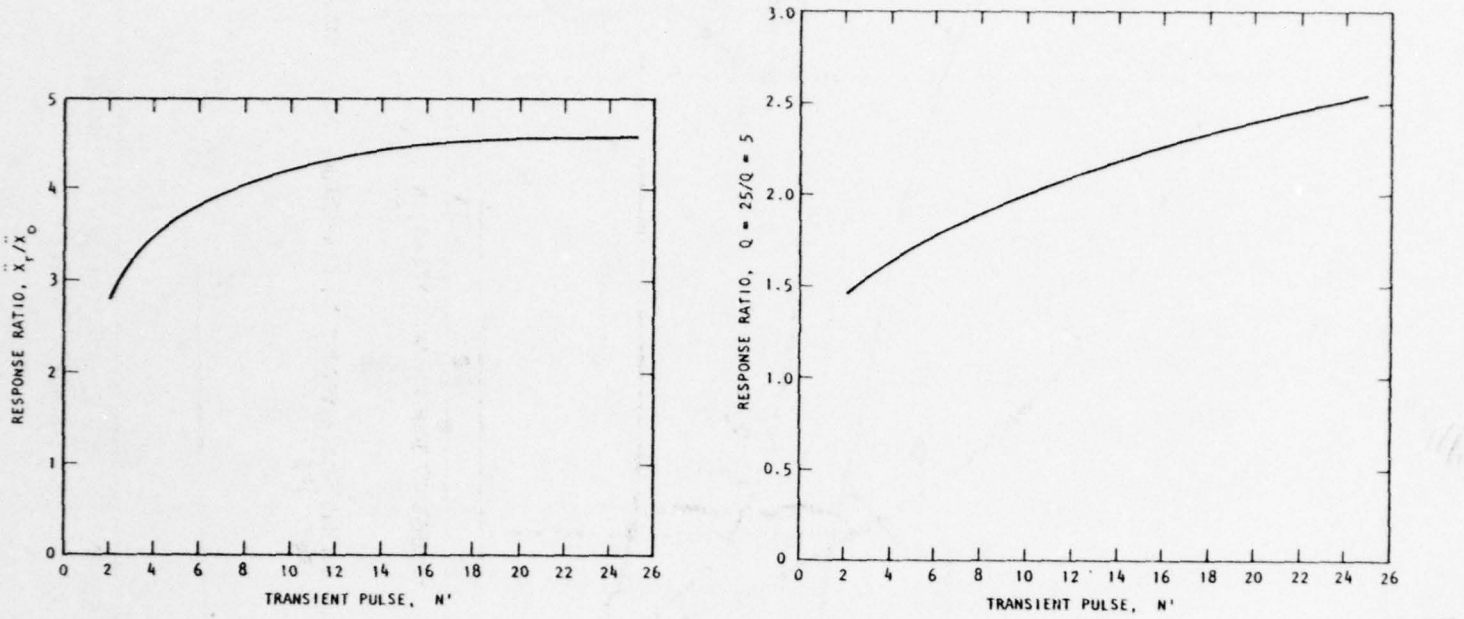

(a) Q = 5

(b) Q=25/Q=5

FIGURE 17. Q-5 OSCILLATOR RESPONSE VS. PARAMETER N' FOR TRANSIENT PULSE UPSWEEP (Ref. 34)

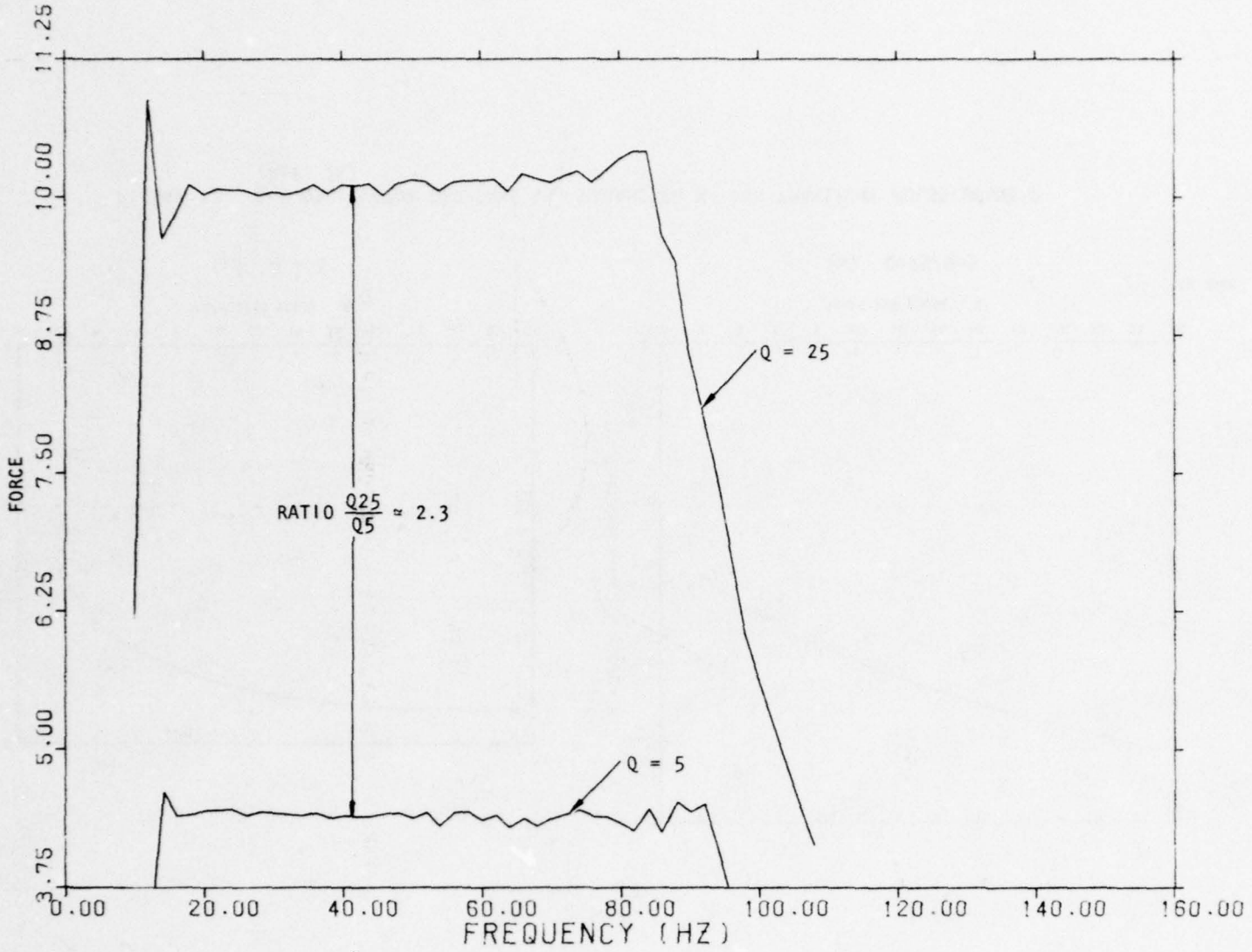

FIGURE 18. SHOCK SPECTRA FOR LOG SWEEP CHIRP AT Q = 25 AND Q = 5 (See Fig. 17b)

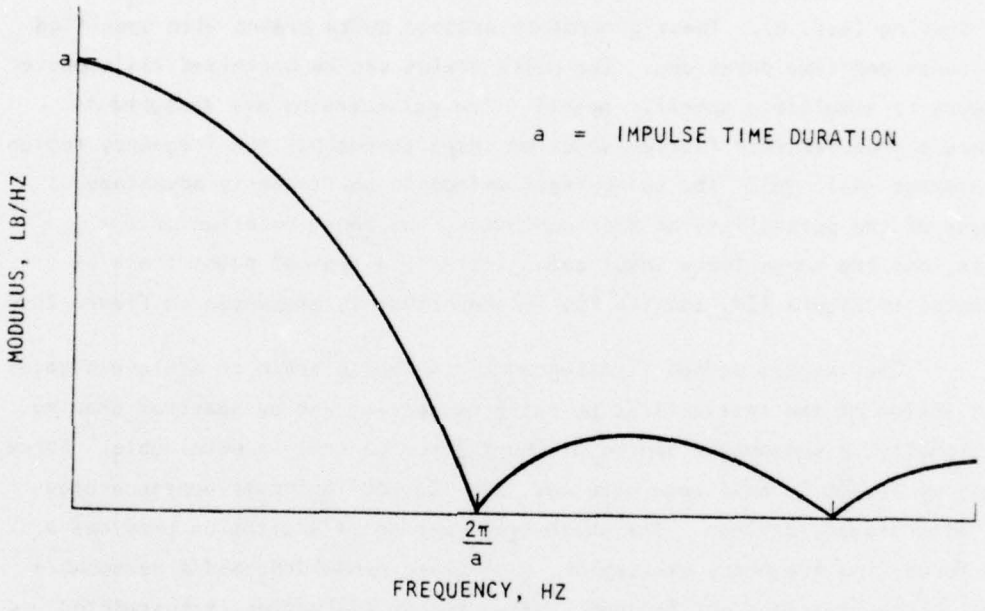

FIGURE 19. FOURIER MAGNITUDE TRANSFORM OF IMPULSE FUNCTION

recently with the advent of digital spectrum analyzers. Today, one can flail away using numerous repeat tests to average down noise inherent in this excitation method. Given sufficient weight or force, impulse excitation can be used to excite and measure very low frequencies.

2.1.4.5 Pulse Trains

Specially designed mechanical force pulse generators have been used quite successfully to simulate known acceleration excitations for vibration testing (Ref. 6). These generators produce pulse trains with specified amplitudes and time durations. The pulse trains can be optimized via computer software to simulate a specific output. The pulse trains are designed to produce a predetermined Fourier spectrum shape throughout the frequency region of interest (Ref. 36). The pulse-train method is particularly advantageous because of the portability of test equipment, the short duration of the inputs, and the large force input capabilities. A typical pulse train is presented in Figure 13d, and its Fourier magnitude is presented in Figure 20.

The impulse method is extended by the pulse train to achieve greater mobilization of the test article by pulse sequencing and by spectrum shaping. Additionally, a reasonable degree of input force control is obtainable. Force levels of 20,000 lb have been obtained, and 100,000-lb inputs appear achievable with present devices. The pulse train method of excitation provides a high force, low frequency excitation, a moderate bandwidth, and a reasonable number of oscillations per frequency. Quick-look evaluation is restricted to oscillograph time histories. System functions must be processed digitally.

2.1.5 SYSTEM SURVEY

At the onset of a test, a survey is recommended to ascertain the linearity of the system by multilevel tests and reciprocity, system symmetry, and cross-axes coupling. Quantitative information gained at an early stage

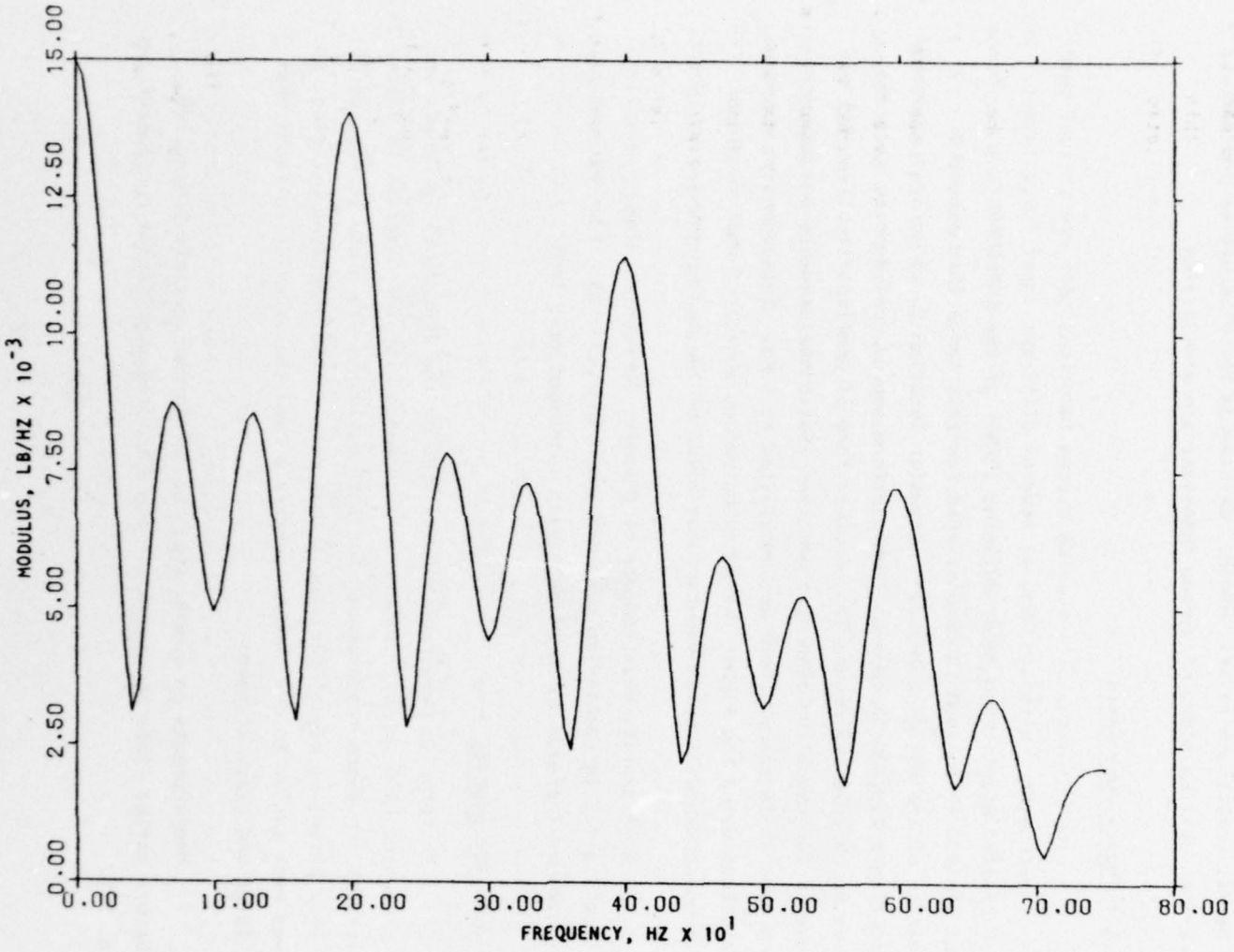

FIGURE 20. FREQUENCY TRANSFORM OF FORCE-PULSE INPUT

can permit reductions in test efforts or provide for alternative procedures. Quick-look on-line plots of system functions are a necessity.

2.1.5.1 Multilevel Tests

Linear systems will provide system functions that are virtual overlays of each other, although made at several different input force levels. For the Perimeter Acquisition Radar Building (PARB) of the SAFEGUARD system, force input of 1000 lb to 7000 lb demonstrated for this range that essential linearity of the building existed. Transfer function tests across isolators supporting a 200,000-lb control room platform showed nonlinearity existing, as may be observed in Figure 21. Another form of nonlinearity (Fig. 22) was uncovered for shock-isolated platform from static measurements and measurements made while the platform was oscillated at 1 Hz. Subsequently, response predictions using the higher transmission values indicated that the local environment was well below the hardness value of the nearby mounted equipment.

Nonlinearity measurements of transfer inertances along a missile-silo wall sited in backfilled soil are shown in Figure 23. For the most part, they show an increase in compliance with increased test load.

2.1.5.2 Reciprocity

Reciprocity measurements were made on the PARB model in Canada and the prototype PARB in North Dakota in accordance with the diagrams in Figure 24. Reciprocal impedance measurements for both buildings are given in Figures 25 and 26. Extensive use of reciprocity was made in the prototype building, as it was much easier to move accelerometers around the exterior surfaces than the large and heavy vibrator.

Measurements on a moderate size reinforced-concrete protective structure buried flush to ground surface disclosed significant nonlinearities (Fig. 27).

(Text continued on p. 51.)

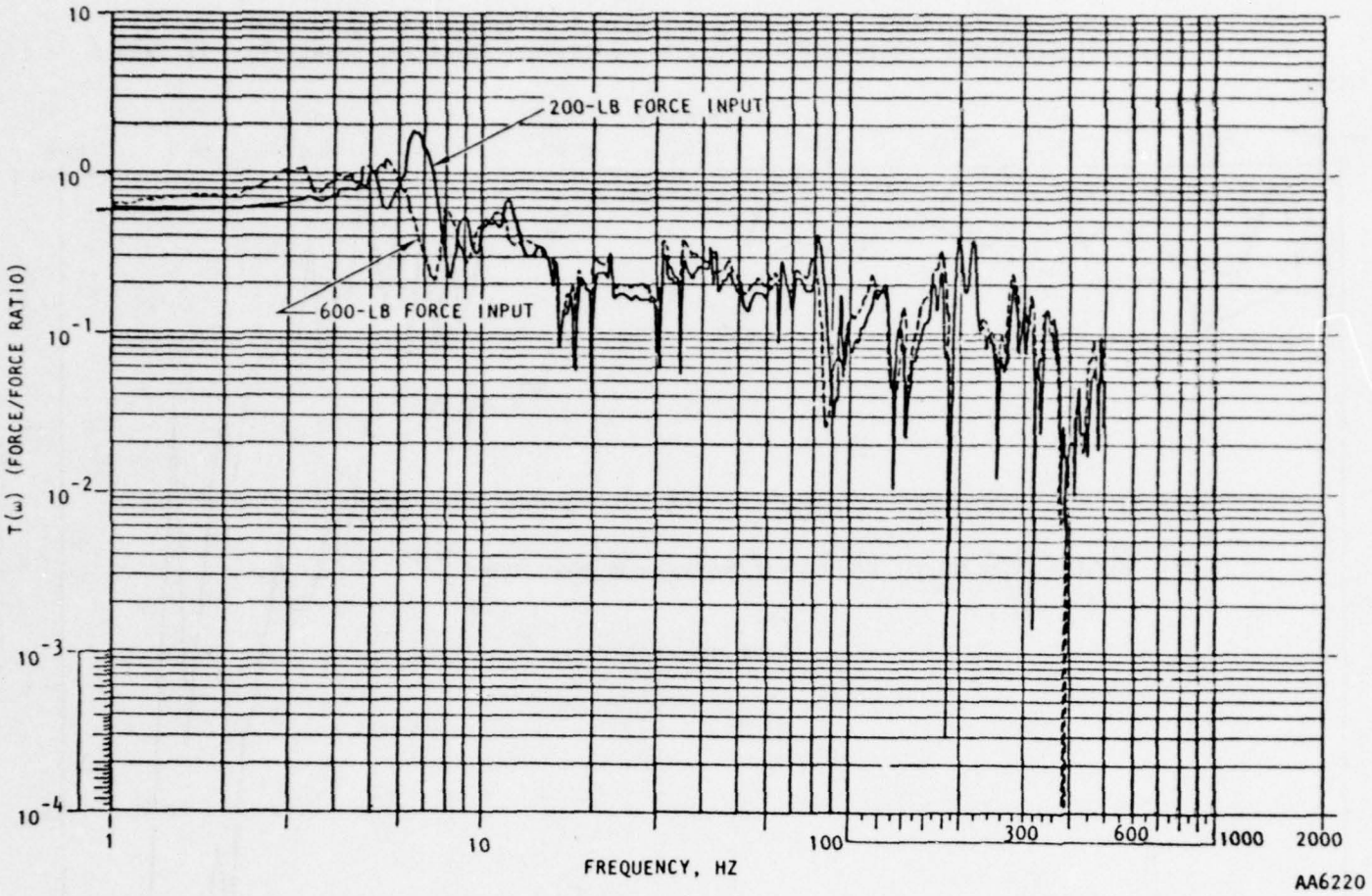

FIGURE 21. PLATFORM PARPP-CR: TRANSFER FUNCTION MODULUS (ANALOG) FORCE RATIO ACROSS SPRING ISOLATOR AT INPUT FORCE LEVELS OF 200 LB AND 600 LB

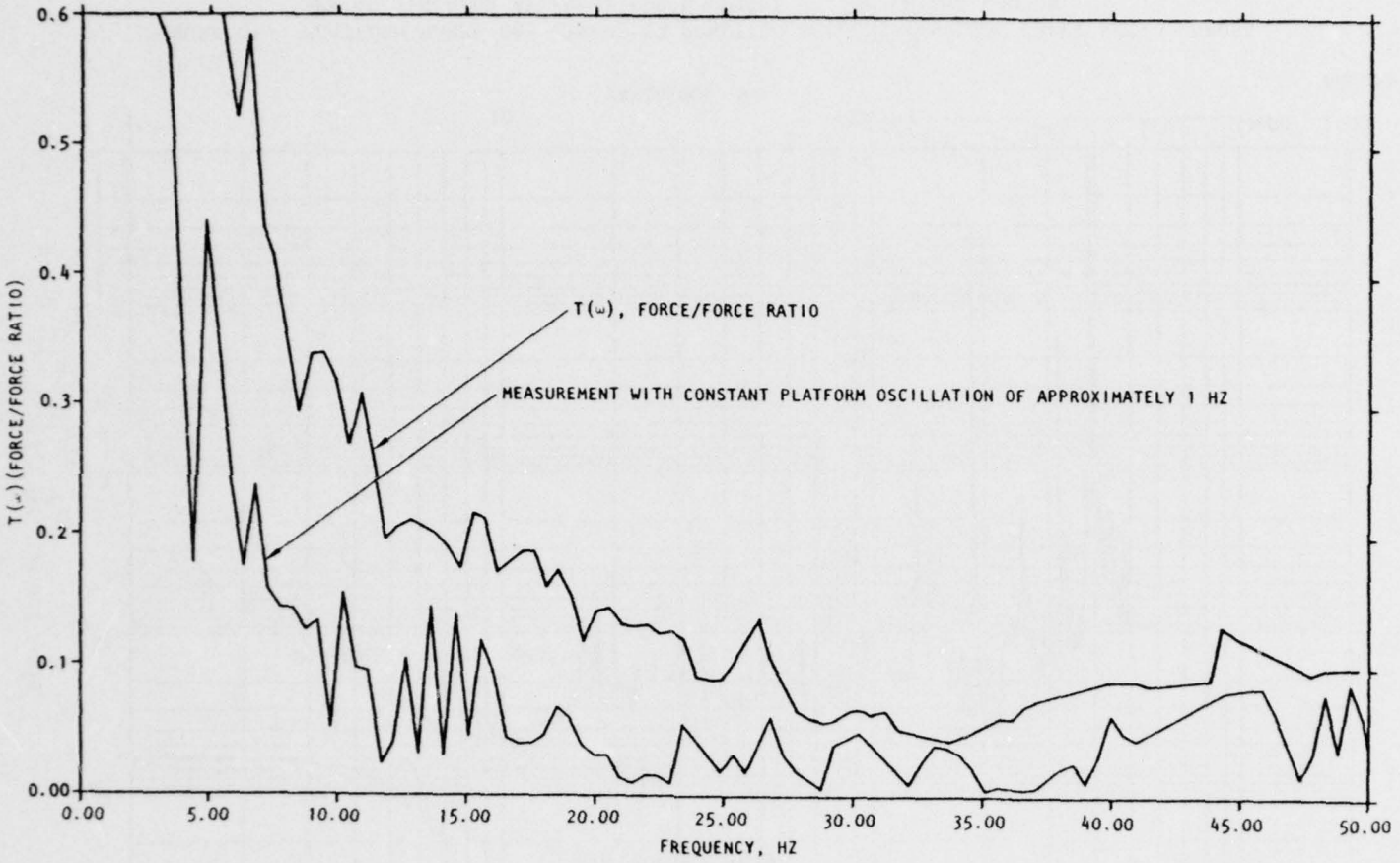

FIGURE 22. PLATFORM MSRB-125B: TRANSFER FUNCTION MODULUS ACROSS PNEUMATIC ISOLATOR, COMPARISON OF MEASUREMENTS WITH AND WITHOUT 1-HZ CONSTANT OSCILLATION

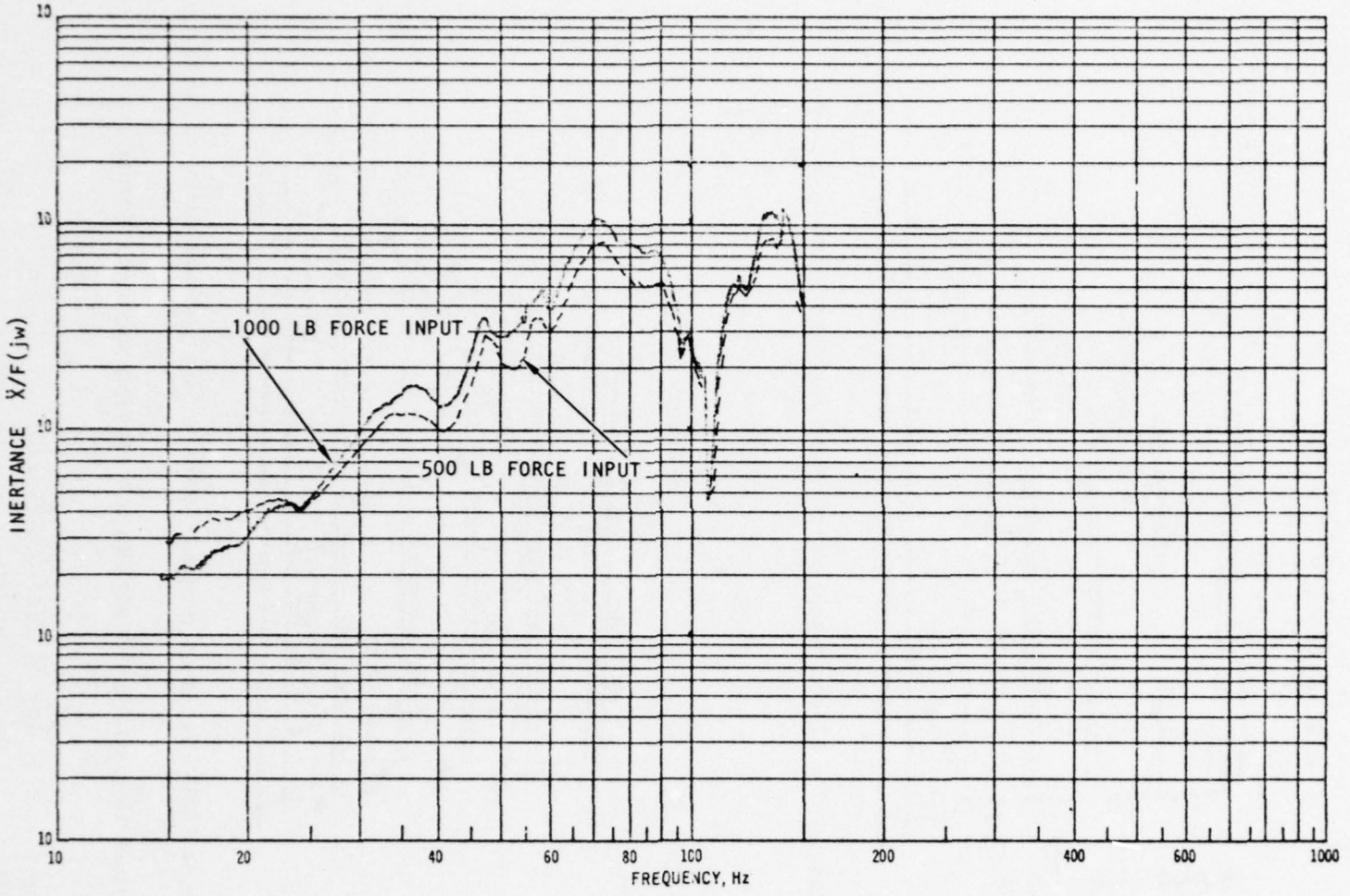

FIGURE 23. TRANSFER INERTANCE, X/F(jw), MAGNITUDE FUNCTION ALONG A MISSILE SILO WALL SITED IN BACKFILLED AND COMPACTED SOIL

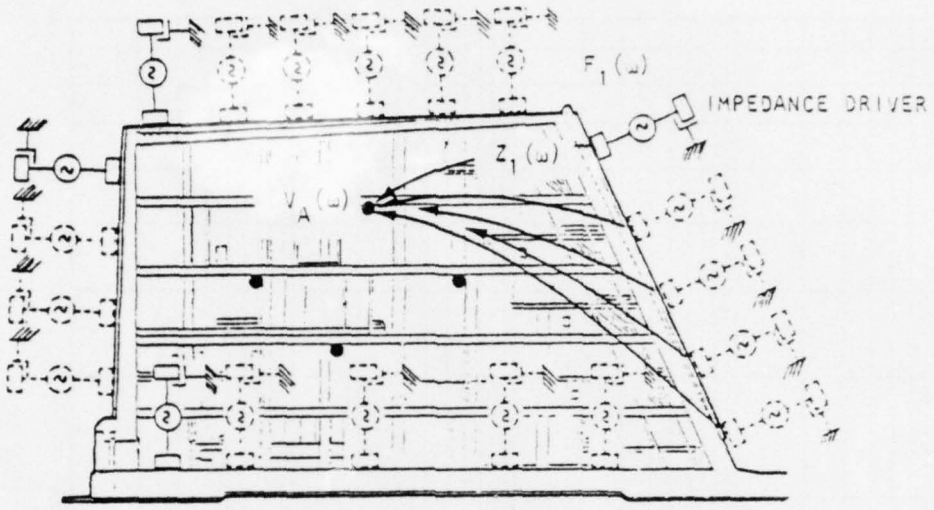

(a) Model PARB: Direct measurements (from surface to response point)

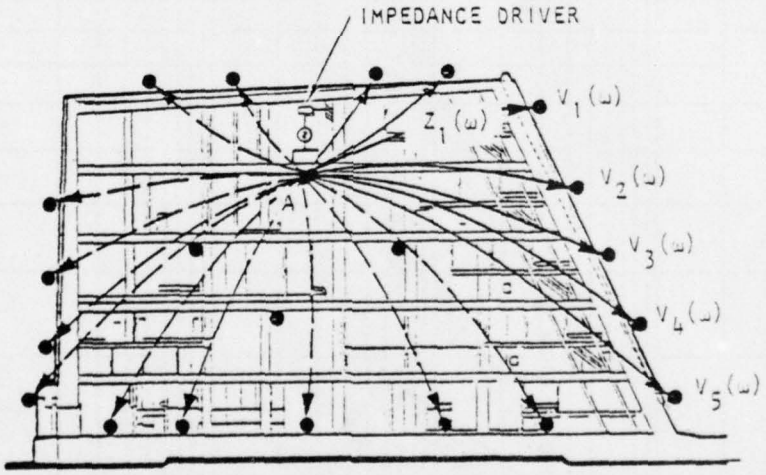

(b) Prototype PARB: Reciprocity measurements (from response point to surfaces)

FIGURE 24. MEASUREMENT METHODS USED ON PARB MODEL AND PROTOTYPE

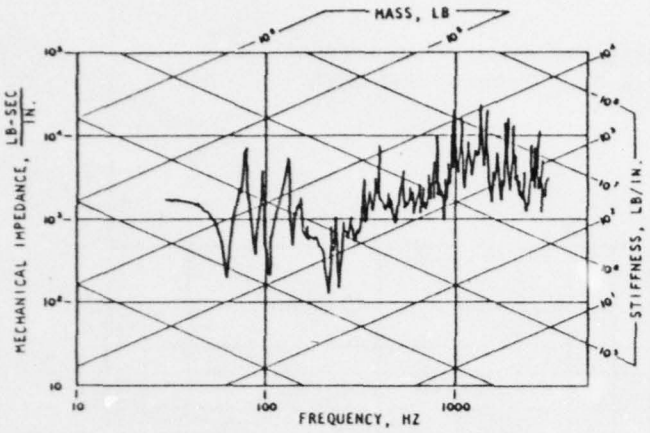

(a) Drive point, roof center (T-7); Measurement point, 5th floor center (1-VT)

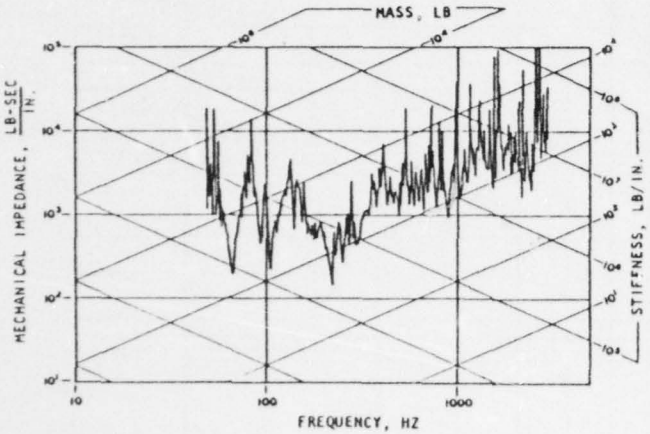

(b) Drive point, 5th floor center (1-VT); Measurement point roof center (T-7)

FIGURE 25. MODEL PARB DATA FOR DETERMINING RECIPROCITY

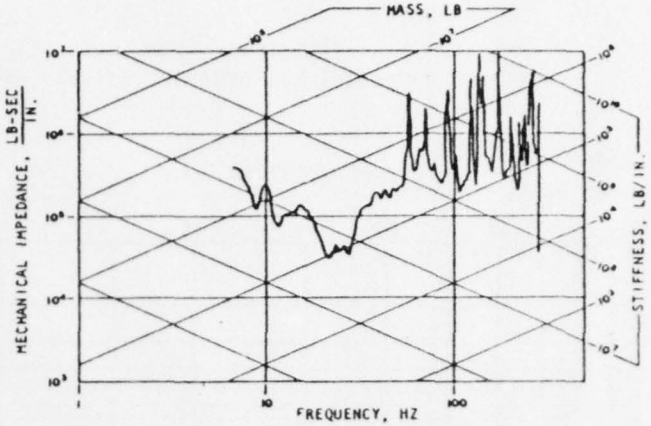

(a) Drive point, roof center (T-7); Measurement point, 5th floor center (1-VT)

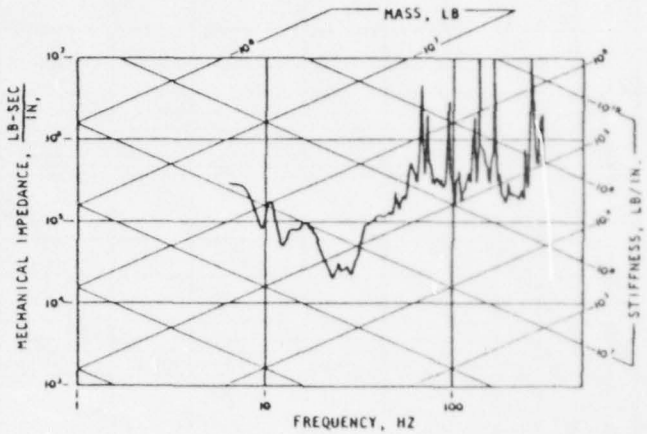

(b) Drive point, 5th floor center (1-VT); Measurement point roof center (T-7)

FIGURE 26. PROTOTYPE PARB DATA FOR DETERMINING RECIPROCITY

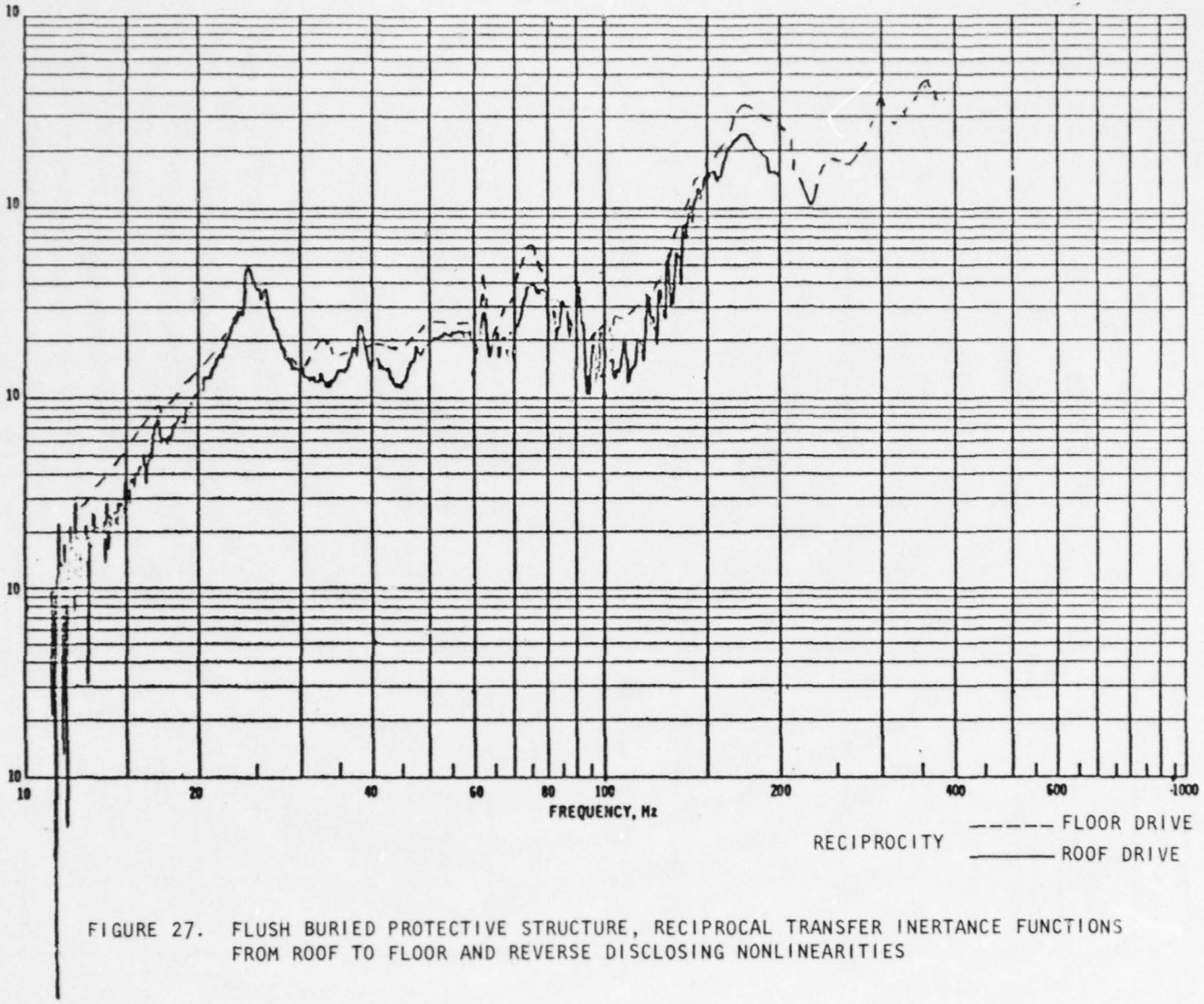

FIGURE 27. FLUSH BURIED PROTECTIVE STRUCTURE, RECIPROCAL TRANSFER INERTANCE FUNCTIONS FROM ROOF TO FLOOR AND REVERSE DISCLOSING NONLINEARITIES

2.1.5.3 Cross-Axes Coupling

Cross-axes coupling is the motion induced in a test article orthogonal to the direction of input force or motion. Figure 28 overlays cross-axes coupling impedance on an axially aligned impedance measurement for the same accelerometer location. Accounting for cross-axes coupling was not required for response predictions on this building. The frequency magnitudes of the external blast loads were very small in the frequency range where cross-coupling was a significant proportion of the regular impedance measurements. The root sum square for all four walls contributed less than 5% to vertical motion. In the present ongoing missile silo tests, cross axes coupling is significant and response predictions will have to include this effect.

2.1.5.4 Symmetry

Where a test article or structure possesses geometric symmetry, or at least reasonable-appearing symmetry, testing may be shortened by measurements on one-half or one-quarter of the structure, as the case may be. Decisions to use symmetric measurements should be made by impedance surveys. Where unsymmetric elements or components exist, either local measurements, substitution, or a strategy of redistribution of the measurement matrix can often be judiciously used. Figure 29 shows inertance transfer measurements overlaid for symmetry comparison on a Ballistic Missile Defense System Impedance Test Unit (hog trough).

2.1.6 SYSTEM FUNCTIONS

Since 1972 numerous impedance projects have been conducted to ascertain system functions and to predict response motions therefrom for a variety of external threats. From these projects, the following topics have been selected because of project uniqueness, phenomena observed, and techniques employed. The data presented are consistent in this report but factored for declassification.

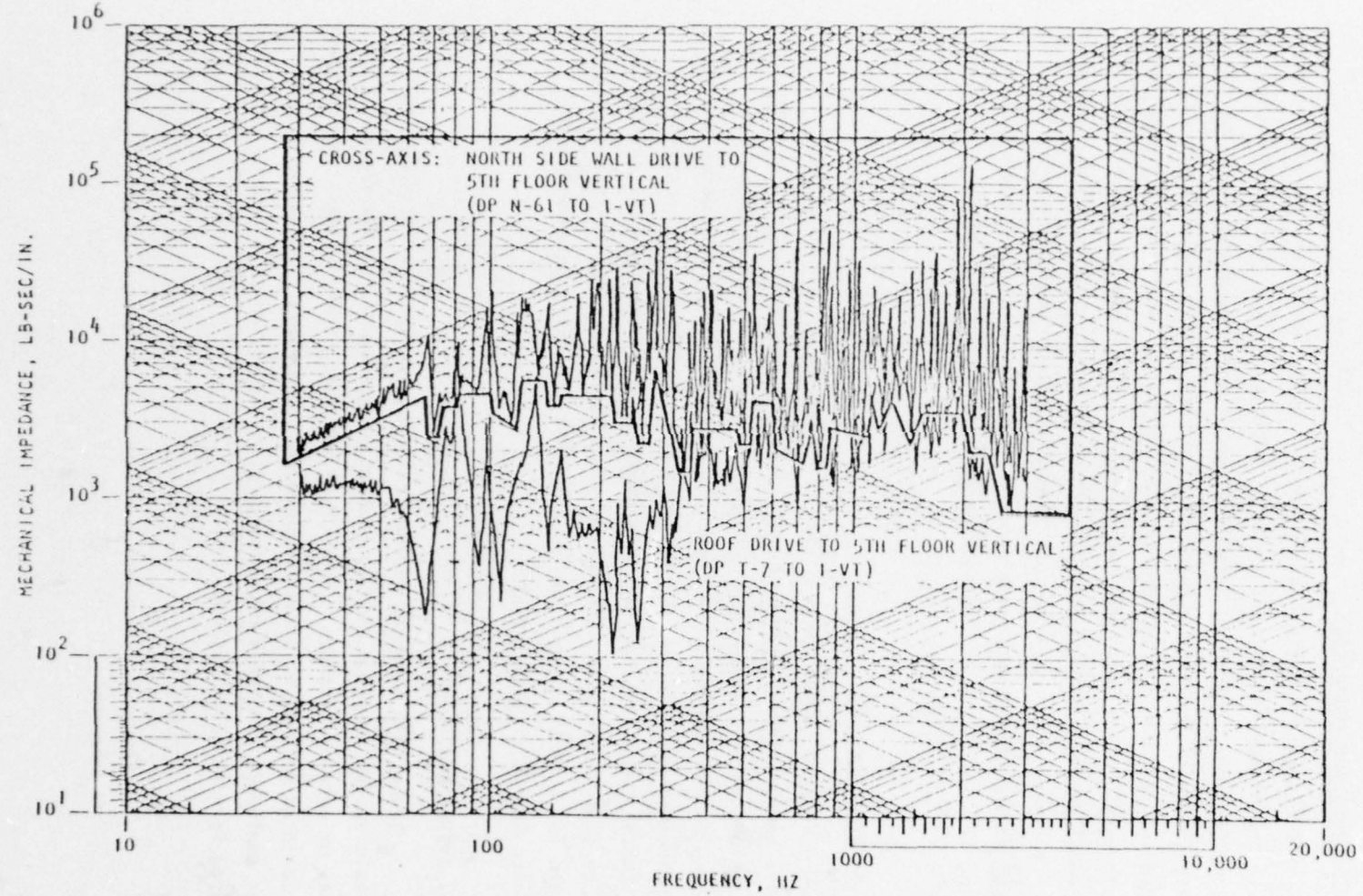

FIGURE 28. MODEL PARB CROSS-AXIS TRANSFER IMPEDANCES TO 5TH FLOOR VERTICAL RESPONSE POINT: NORTH WALL HORIZONTAL DRIVE POINT COMPARED WITH ROOF VERTICAL DRIVE POINT

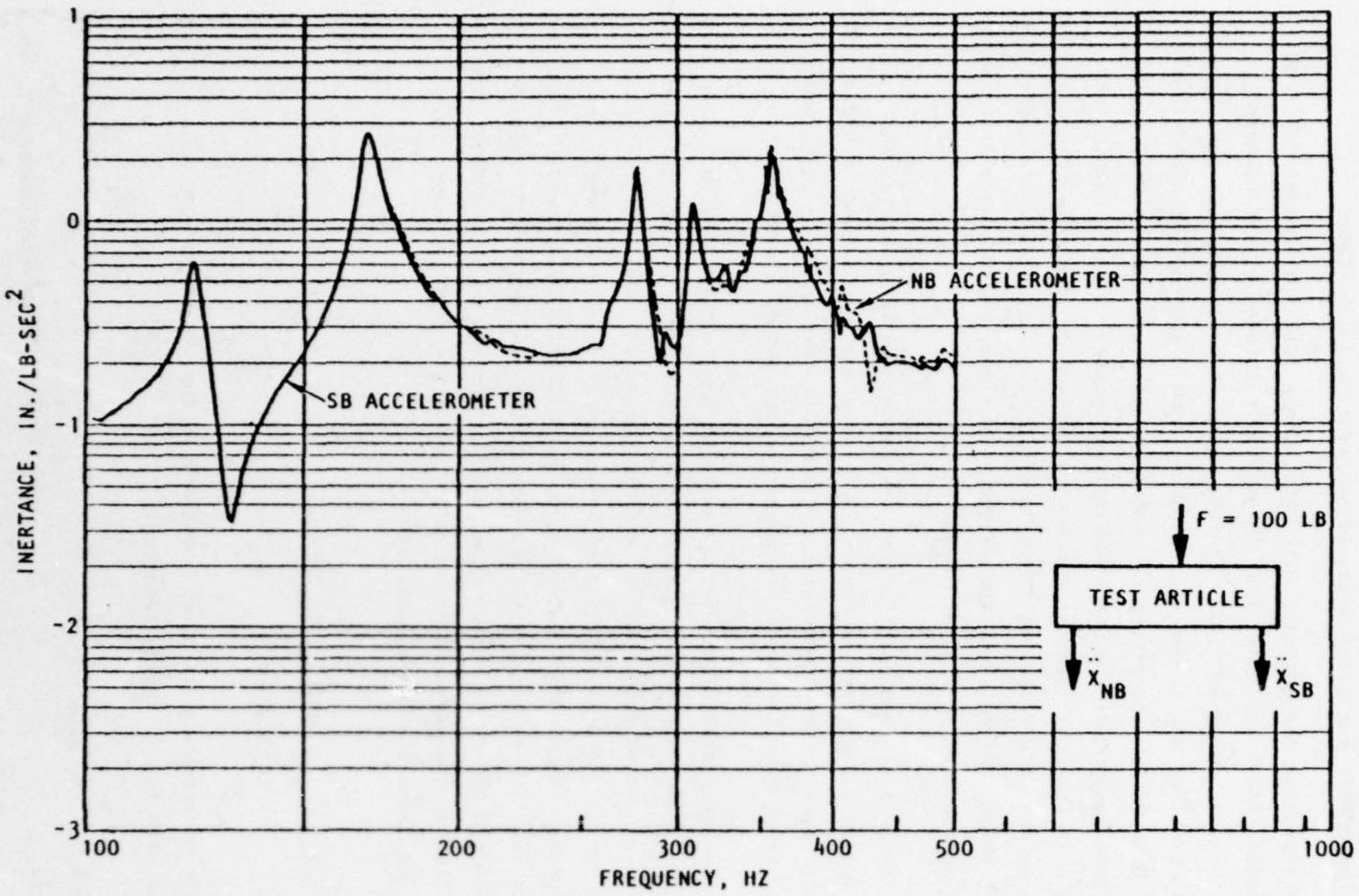

FIGURE 29. TEST ARTICLE SYMMETRY, INERTANCE TRANSFER MEASUREMENT COMPARISON: INPUT AT TOP OF TEST ARTICLE

2.1.6.1 SAFEGUARD, Perimeter Acquisition Radar Building (PARB)

Impedance measurements were made upon a 1/12-scale model PARB and the prototype PARB. The model PARB (Fig. 30) is located at the Defence Research Establishment, Suffield, Canada, where it had previously been subjected to air-blast and ground-shock loading from a 500-ton TNT explosion in the EVENT DIAL PACK. The prototype PARB (Fig. 31) is an operational radar system, formerly part of the SAFEGUARD system located in North Dakota. The prototype building is a reinforced-concrete protective structure that measures 125 ft in height, 194 ft on its front, and 210 ft on its side, with exterior walls 3 ft thick. Pictures of the vibrator used and the impedance processing equipment are covered in Figures 32 and 33.

Typical systems functions of inertance magnitude, phase, and impulse functions are given in Figure 34 for the scale model and in Figure 35 for the prototype. These nonparametric functions have been digitally processed into final form for use in response predictions of the structures.

Response predictions for a few locations involve a large number of measurements taken over the structure external surfaces. For efficiency, these predictions can be used to predict responses at additional internal locations of the building. This is facilitated by use of transfer functions. The response prediction at the first location is multiplied by a transfer function to another location to obtain the response at the new location. Transfer functions are obtained by the complex ratio of the motion at a remote location to the motion at the drive point location, as illustrated in Figure 36. Transfer functions are represented as:

$$\tau(\omega) = \left| \frac{\ddot{X}_{out}}{\ddot{X}_{in}} (\omega) \right| e^{-j\phi\omega}$$

Calculation of responses at other locations in the structure were made in accordance with the following equations:

$$\ddot{X}_i(\omega) = \ddot{X}_5(\omega)\ \tau_{i/5}(\omega)$$

(Text continued on p. 65.)

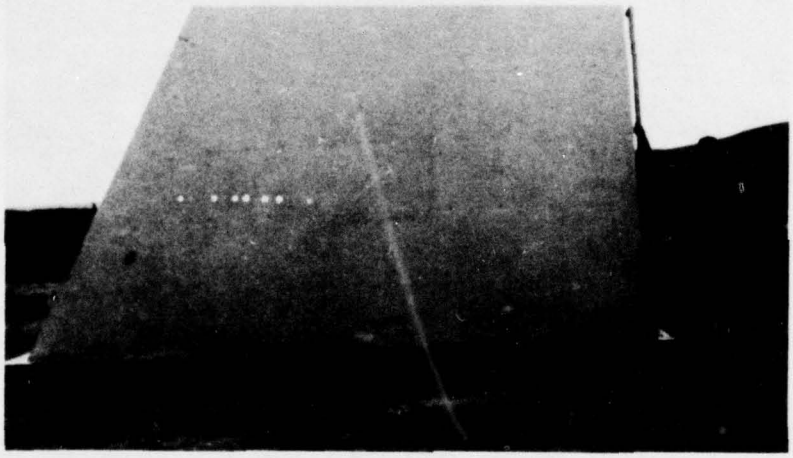

FIGURE 30. 1/12-SCALE MODEL PERIMETER ACQUISITION RADAR BUILDING (PARB), DEFENCE RESEARCH ESTABLISHMENT, SUFFIELD, CANADA

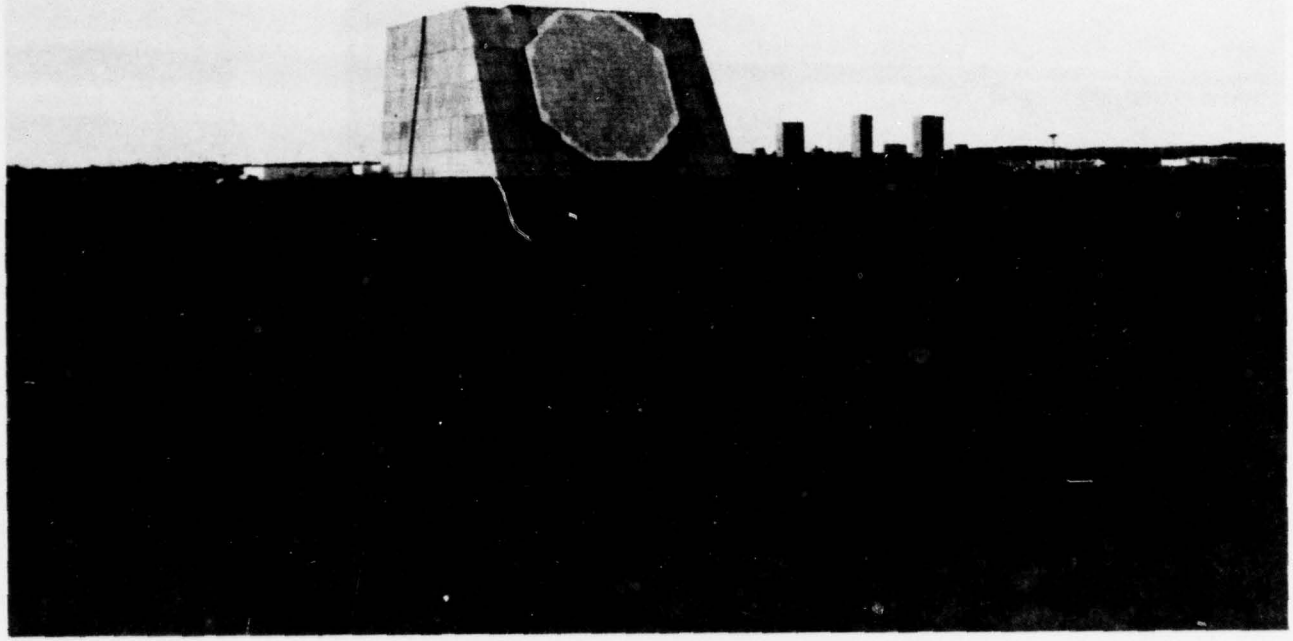

FIGURE 31. PROTOTYPE PERIMETER ACQUISITION RADAR BUILDING (PARB), NORTH DAKOTA

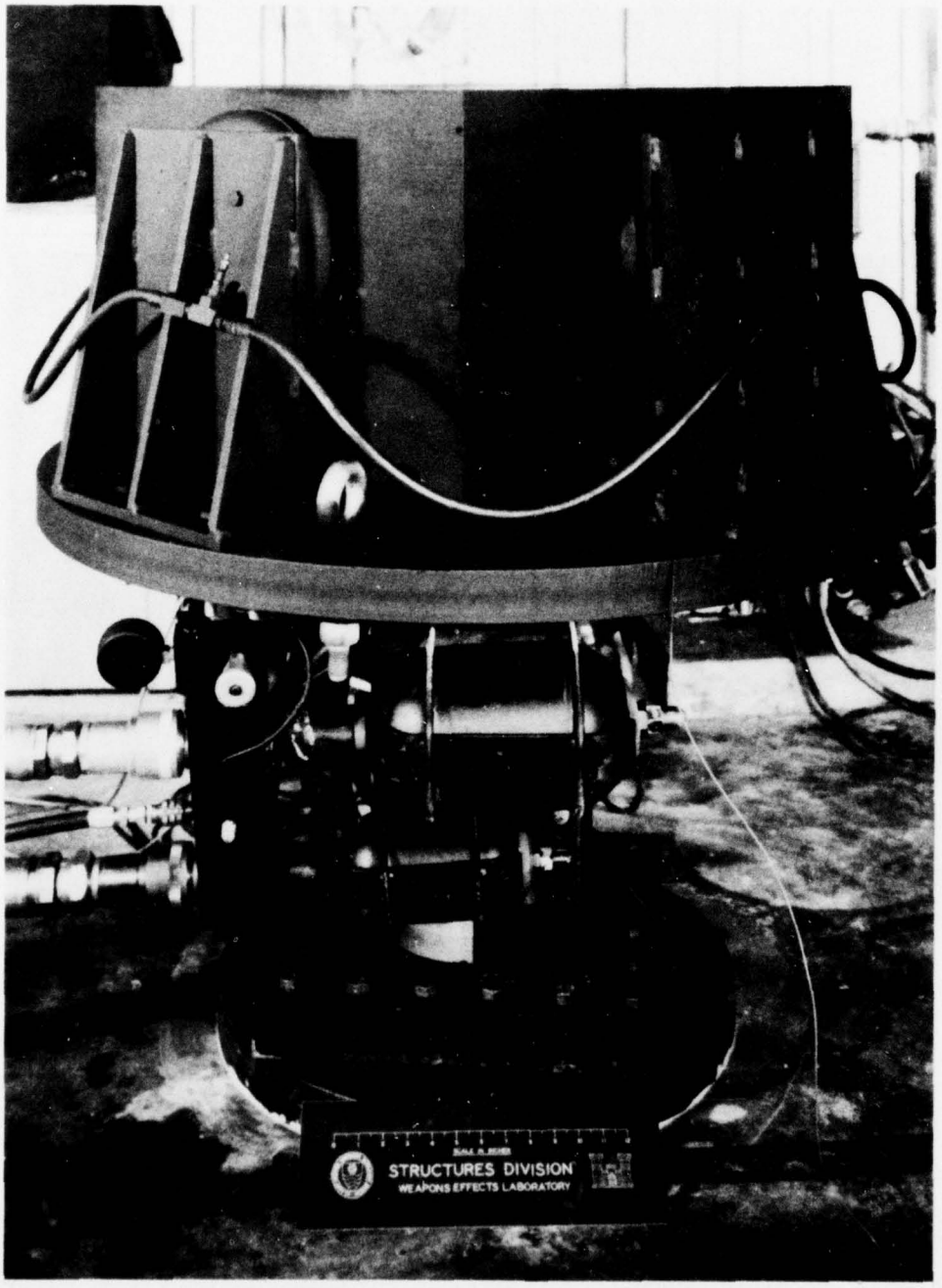

FIGURE 32. ELECTROHYDRAULIC SHAKER USED FOR MEASUREMENTS OF THE PROTOTYPE PARB (Waterways Experiment Station)

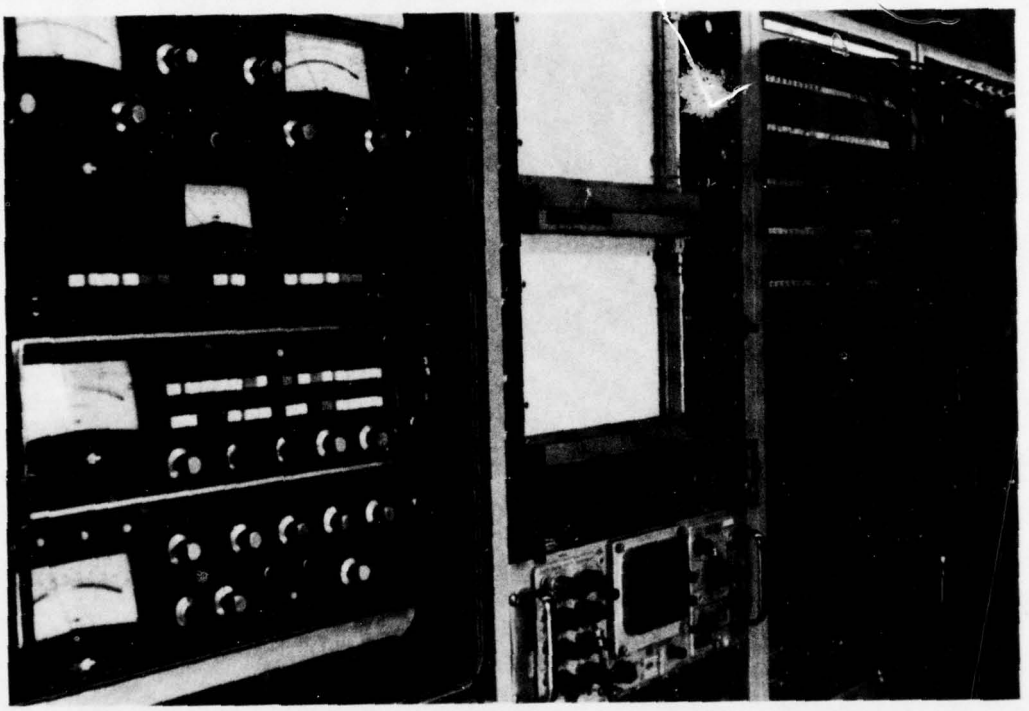

FIGURE 33. INSIDE VIEW OF INSTRUMENTATION AND IMPEDANCE PROCESSING VAN (Waterways Experiment Station)

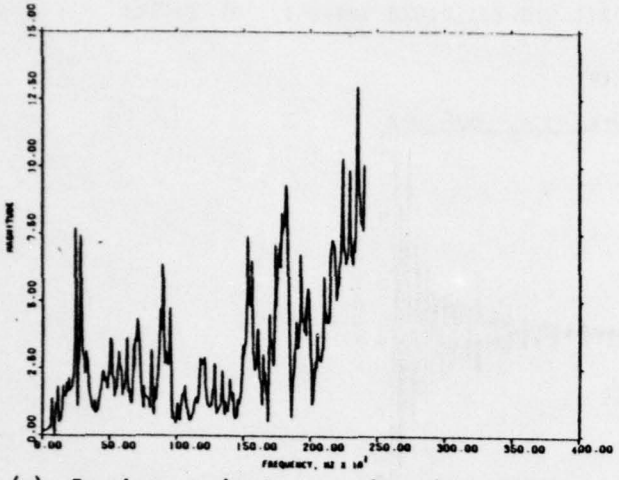

(a) Fourier magnitude: acceleration acceptance

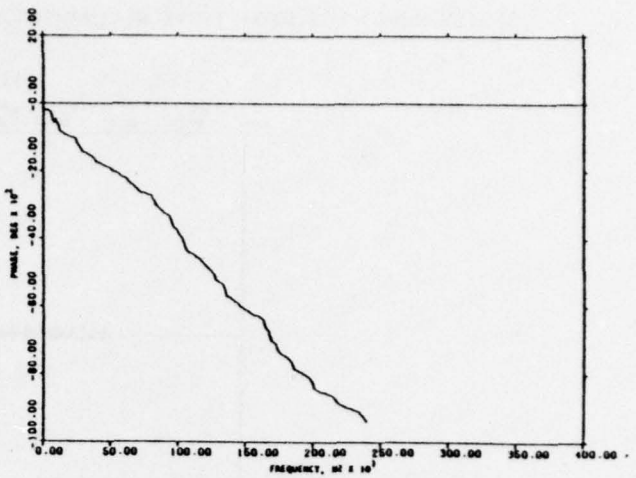

(b) Fourier phase: acceleration acceptance

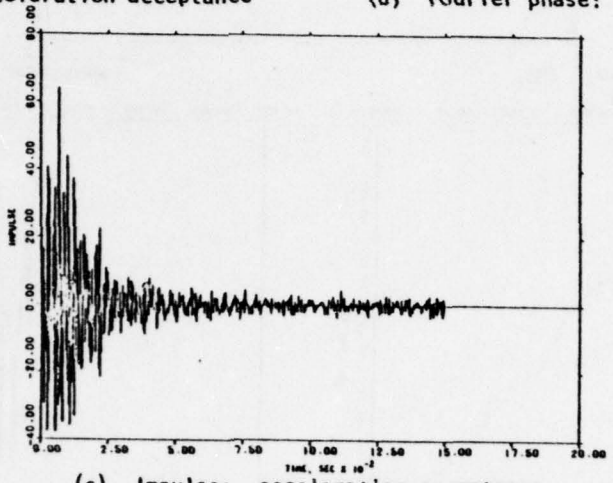

(c) Impulse: acceleration acceptance

FIGURE 34. TYPICAL MODEL DIGITIZED MEASUREMENT IN FINAL FORM FOR COMPUTATIONS

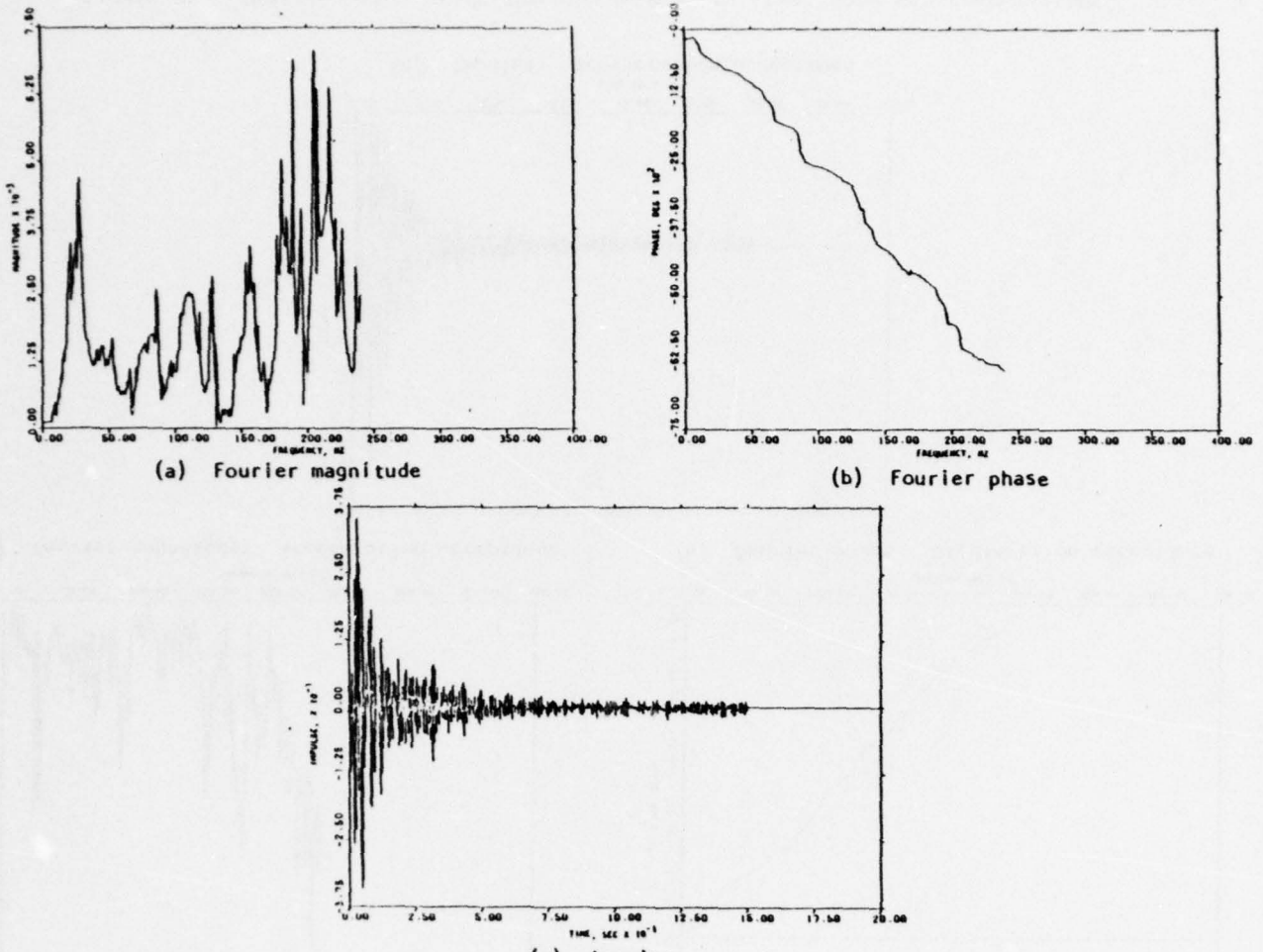

FIGURE 35. TYPICAL PROTOTYPE DIGITIZED MEASUREMENT IN FINAL FORM FOR COMPUTATIONS

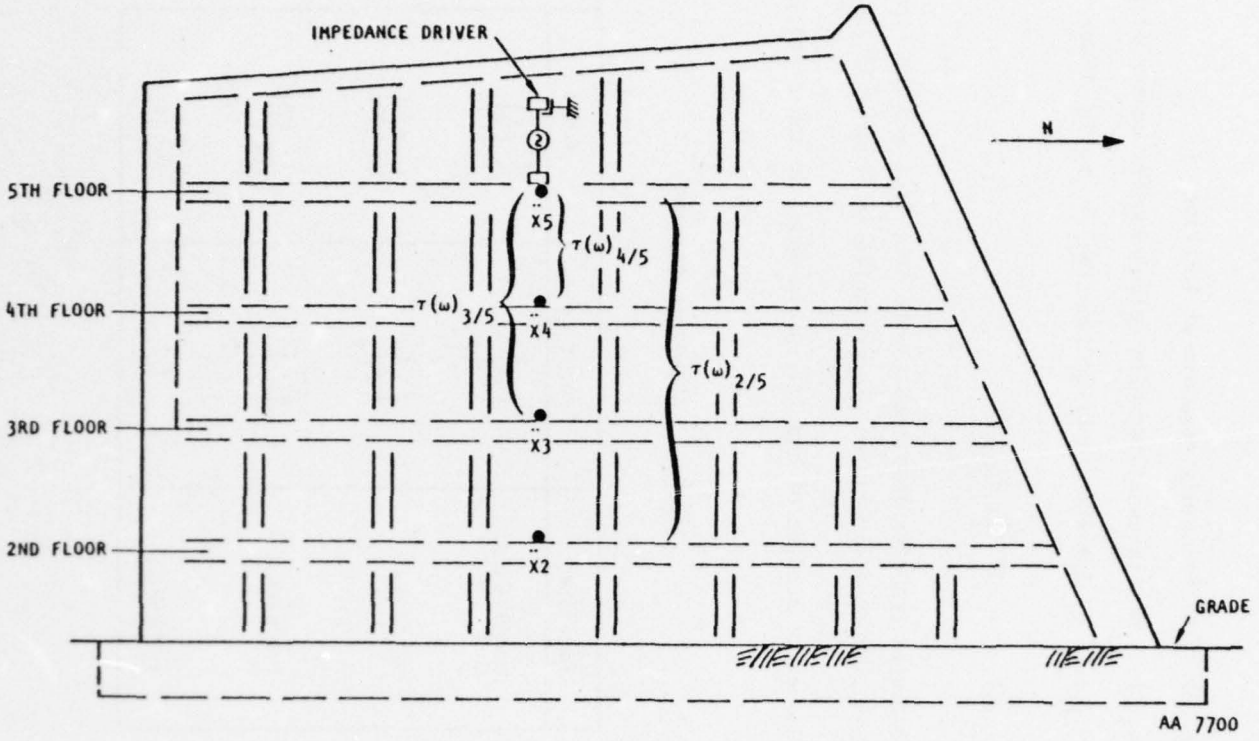

FIGURE 36. METHOD OF MEASUREMENT OF TRANSFER FUNCTIONS

where

$\ddot{X}_i(\omega)$ = Frequency response at location i

$\ddot{X}_5(\omega)$ = Frequency response calculated for center of the 5th floor

$T_{i/5}(\omega)$ = Transfer function location i to 5th floor

$$\ddot{x}_i(t) = \mathfrak{F}^{-1}\left[\ddot{X}_i(\omega)\right]$$

Measured transfer functions to the 4th, 3rd, and 2nd floors of both the model and prototype structures are presented in Figures 37 and 38.

Geometric scaling of the 1/12-scale model to the prototype is given in Table 1.

TABLE 1. GEOMETRIC SCALING

Function	Prototype	Model
Compliance	$\left(\frac{X}{F}\right)_P$	$\frac{1}{12}\left(\frac{X}{F}\right)_m$
Mobility	$\left(\frac{\dot{X}}{F}\right)_P$	$\frac{1}{144}\left(\frac{\dot{X}}{F}\right)_m$
Inertance	$\left(\frac{\ddot{X}}{F}\right)_P$	$\frac{1}{1728}\left(\frac{\ddot{X}}{F}\right)_m$
Frequency	f_P	$\frac{1}{12}\ f_m$

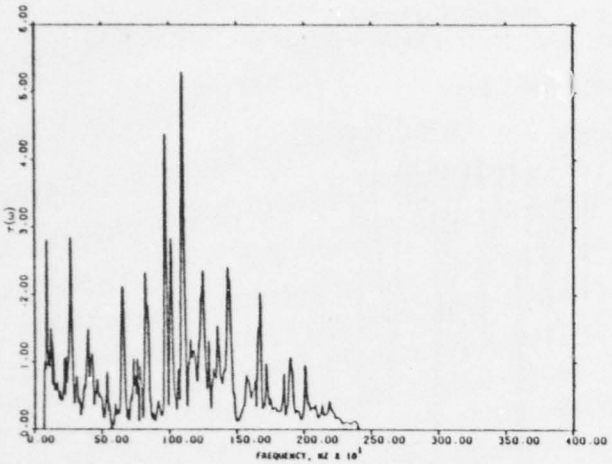

(a) 5th floor to 4th floor

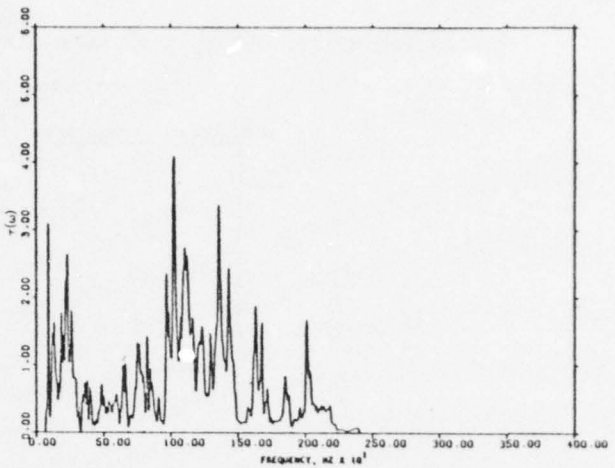

(b) 5th floor to 3rd floor

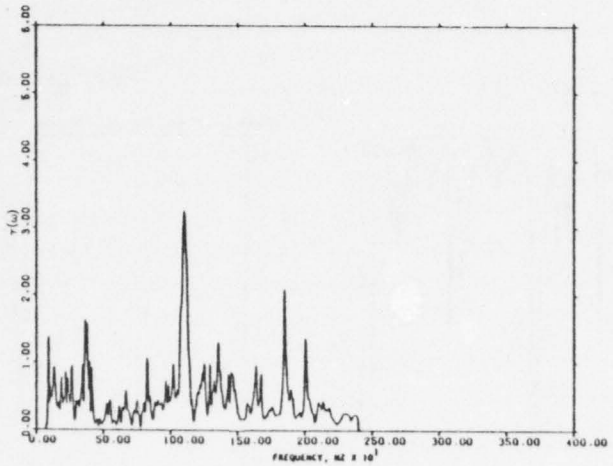

(c) 5th floor to 2nd floor

FIGURE 37. MODEL PARB: TRANSFER FUNCTION MAGNITUDES (ACCELERATION RATIO) FOR CALCULATION OF RESPONSE PREDICTION

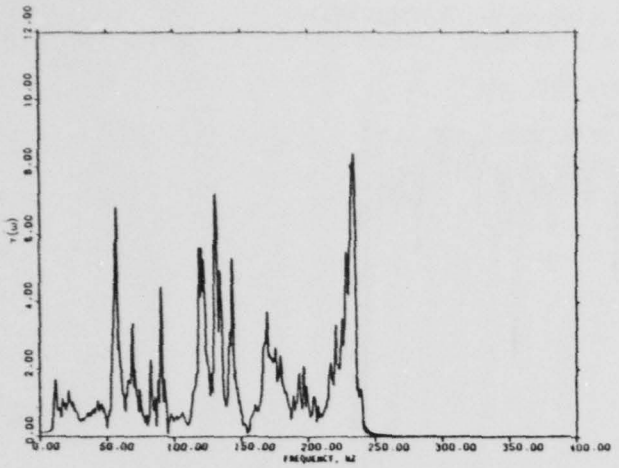

(a) 5th floor to 4th floor

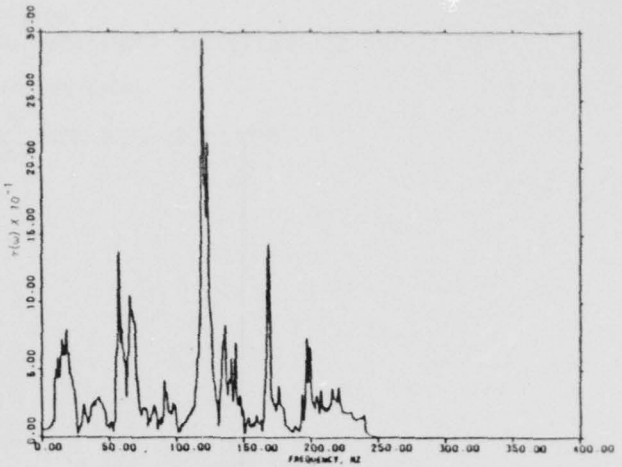

(b) 5th floor to 3rd floor

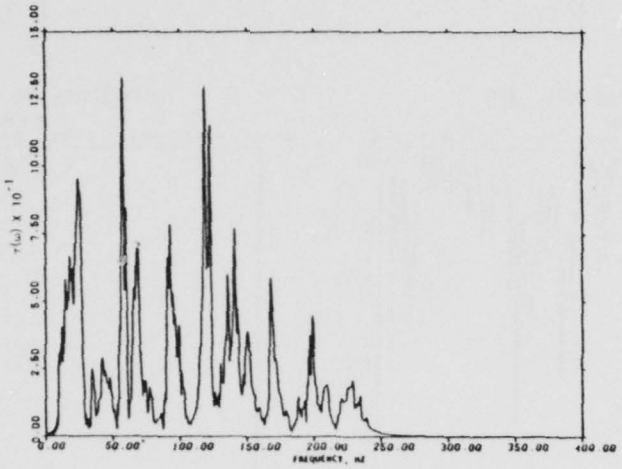

(c) 5th floor to 2nd floor

FIGURE 38. PROTOTYPE PARB: TRANSFER FUNCTION MAGNITUDES (ACCELERATION RATIO) FOR CALCULATION OF RESPONSE PREDICTION

Scaling the model data geometrically did not provide a good fit. Several not-to-scale effects existed in the prototype that had not been or could not be accounted for in the model. These effects included:

a. Structure

- Prototype roof--radar base slab
- Prototype--2nd floor mezzanine
- Prototype--utility tunnel
- Model--excessively large base slab

b. Equipment in Prototype Structure

- Tactical support equipment on shock-isolated platforms, 2nd floor 365,000-lb sprung weight of 22 platforms, and 3rd floor 203,000-lb sprung weight of 4 platforms
- SAFCA communication equipment on shock-isolated platforms, 3rd floor 86,126-lb sprung weight of 3 platforms
- Weapons systems equipment hard mounted on 3rd floor

The radar base slab on the prototype roof stiffens the area covered and adds weight. The 2nd floor mezzanine, the utility tunnel of the prototype, and the extra large base slab in the model contribute to the scaling problem. Equipment installed in the prototype, particularly on the 2nd and 3rd floors, has a decided effect in altering the floor frequency responses. The weapon system equipment hard mounted to the 3rd floor is massive and, in the case of the precise power units, acts as stiffeners. These power units cover approximately one-third of the 3rd floor area. The numerous shock-isolated platforms are dynamically responsive over a wide frequency band and dynamically interact with the floors to alter floor responses substantially.

A scaling comparison in both magnitude and frequency was made between representative and paired inertance measurements of the model and prototype buildings. These functions, such as those shown in Figures 34 and

35, are compared for the 5th floor and similarly for each floor. Scaling parameters were determined by keying corresponding model and prototype functions at their peak amplitudes and then iteratively determining amplitude and frequency scale factors for a minimum error difference. The scale factors determined by this procedure are given in Table 2 for each location.

TABLE 2. SCALING FACTORS, MODEL TO PROTOTYPE, FOR GEOMETRIC AND INERTANCE MEASUREMENT SCALING

Floor	Scale Factors				Difference (Reference Geometric)	
	Inertance		Geometric			
	Displacement Factor, a	Frequency Factor, b	Displacement Factor, λ	Frequency Factor, λ	Displacement, %	Frequency, %
5th	18.4	10.2	12	12	+53	-15
4th	10.5	12.7	12	12	-12	+6
3rd	25.3	14.0	12	12	+111	+17
2nd	34.5	9.7	12	12	+188	-19

AA 7696

2.1.6.2 System Functions of Massive Equipment

System functions were measured on ten large shock-isolated platforms, which ranged in weight from 7,500 lb to 244,000 lb. The method of measurement presented herein is of more interest than the systems measured, for its general applicability to in-place massive machinery and equipments. Typical shock-isolated platforms for which transfer functions were measured are pictured in Figure 39.

The indirect method of transfer function measurement is illustrated in Figure 40, which measures the transfer function at a point of practical and physical convenience. The size of machines and equipment often make it impossible to jack up an equipment mounting leg and insert a vibrator. By

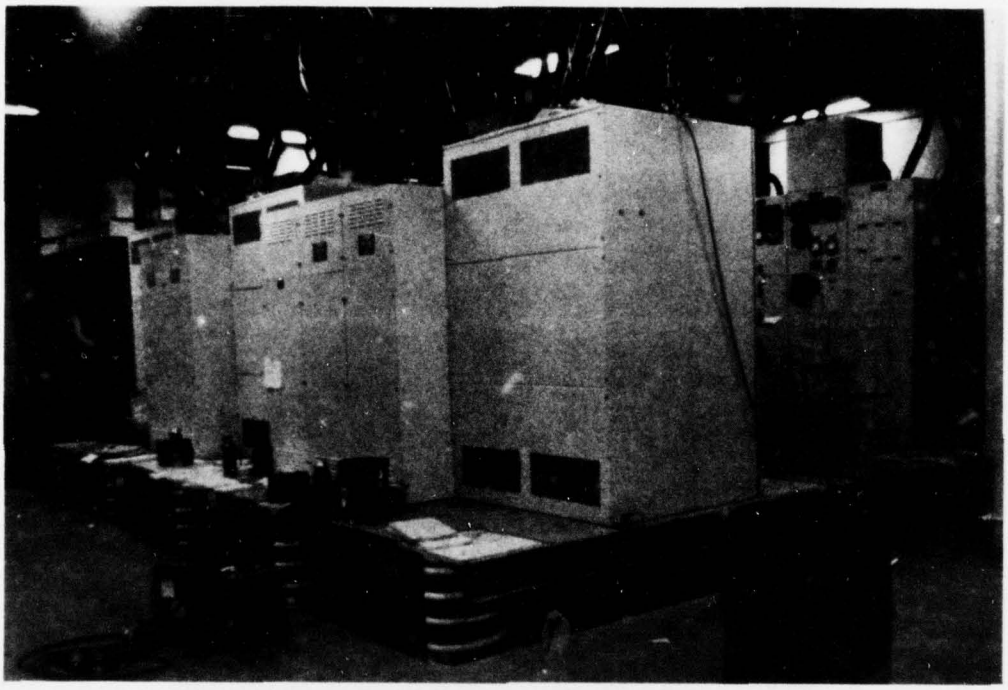

(a)

FIGURE 39. TYPICAL SHOCK ISOLATED PLATFORMS UPON WHICH TRANSFER FUNCTIONS WERE MEASURED

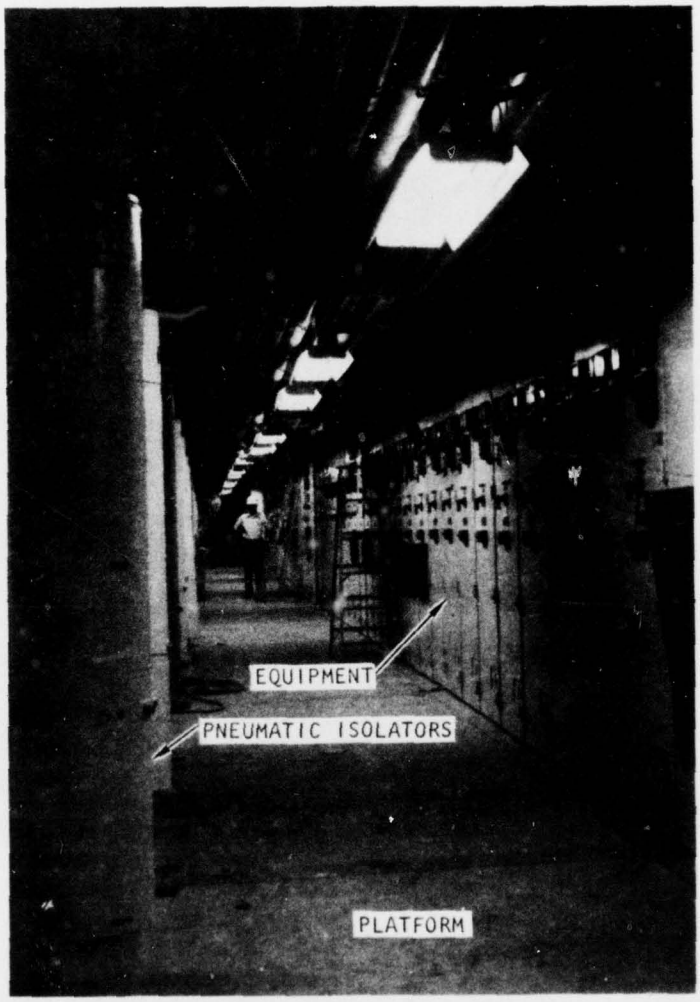

(b)

FIGURE 39. (CONCLUDED)

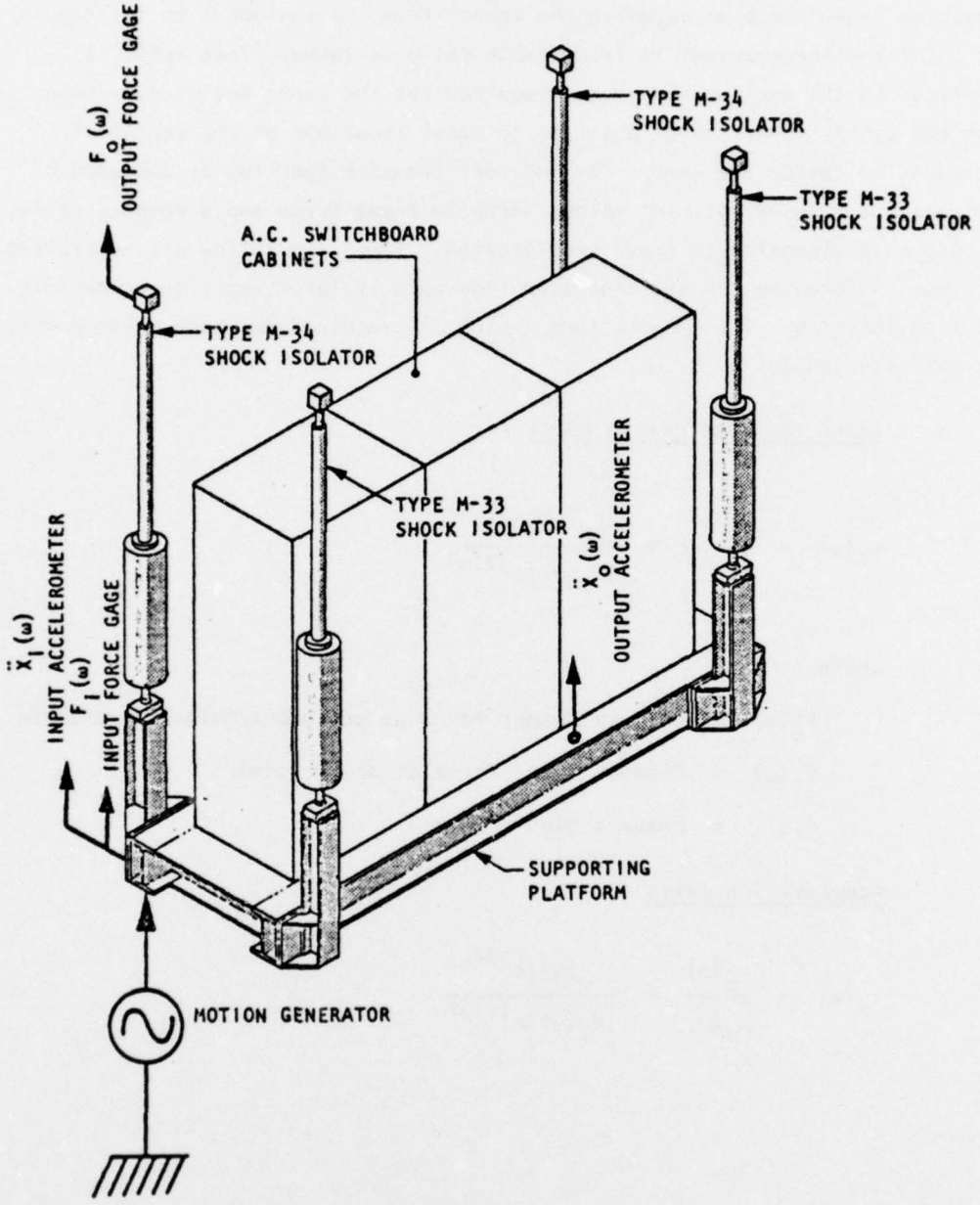

FIGURE 40. PLATFORM PARPP-D: INDIRECT TRANSFER FUNCTION MEASUREMENTS
$\tau(\omega) = F_o(\omega)/F_i(\omega) \cdot \ddot{X}_o(\omega)/\ddot{X}_i(\omega)$

measuring in a direction opposite the input--from the equipment to its mounting points--a force-output to force-input ratio is taken. This ratio is identical to the acceleration ratio required for the input motion direction. From the vibration-generator position to other locations on the equipment, acceleration ratios are used. The indirect transfer function is composed of two parts, a complex ratio of output force to input force and a complex ratio of output acceleration to input acceleration. These two ratios are multiplied together to form the transfer function from each isolator input to a specific platform location. The computations, which are required for each drive point, are expressed as follows:

Force ratio per drive point

$$\tau_F(\omega) = \frac{F_o(\omega)}{F_i(\omega)} = \frac{|F_o(\omega)|e^{j\theta(\omega)}}{|F_i(\omega)|e^{j\phi(\omega)}}$$

where

$F_o(\omega)$ = Complex output force at equipment/building junction

$F_i(\omega)$ = Complex input force at drive point

θ, ϕ = Phase angles

Acceleration ratio

$$\tau_a(\omega) = \frac{\ddot{x}_o(\omega)}{\ddot{x}_i(\omega)} = \frac{|\ddot{x}_o(\omega)|e^{j\beta(\omega)}}{|\ddot{x}_i(\omega)|e^{j\gamma(\omega)}}$$

where

$x_o(\omega)$ = Complex platform accelerometer signal

$x_i(\omega)$ = Complex drive-point accelerometer signal

β, γ = Phase angles

Transfer function

$$\tau(\omega) = \tau_F(\omega) \cdot \tau_a(\omega)$$

$$= \frac{F_o(\omega)}{F_i(\omega)} \cdot \frac{\ddot{x}_o(\omega)}{\ddot{x}_i(\omega)}$$

The transfer function, computed as a product of both the force and acceleration ratios, is summed for all isolators of a platform to generate an overall (global) platform transfer function.

A plot of transfer function magnitude (Fig. 41) reveals that resonance amplifications from modes occur from 0.5 Hz to 10 Hz, with magnitudes from 1.2 to 2.3. The resonance at 17 Hz for a magnitude of 0.7 was identified during measurements as spring surge in the coil isolators.

Another example of a transfer function is shown (Fig. 42) for Platform D. This platform measures 4 ft x 12 ft, weighs 13,100 lb, and is supported by four undamped coil-spring isolators, pendulum mounted. Three a.c. switchboard cabinets are mounted on this platform. Data measurements are from 35 Hz to 500 Hz, and rigid-body modes have been added to Figure 42 for vertical, pitch, and roll frequencies at 0.85, 1.08, and 1.45 Hz.

A comparison is made in the plot of Figure 42 between the measured resonance frequencies and the modal frequencies of a finite element model for this platform. It is to be noted that 28 modal frequencies were found by the model and approximately 77 modal frequencies are present by measurement.

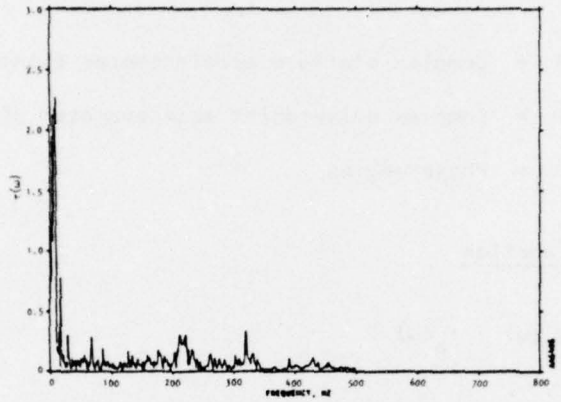

(a) Transfer function magnitude

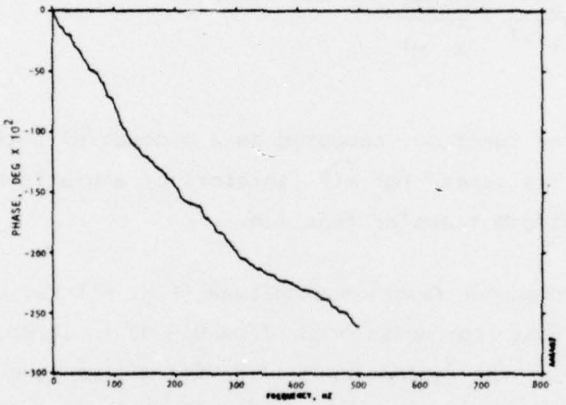

(b) Transfer function phase

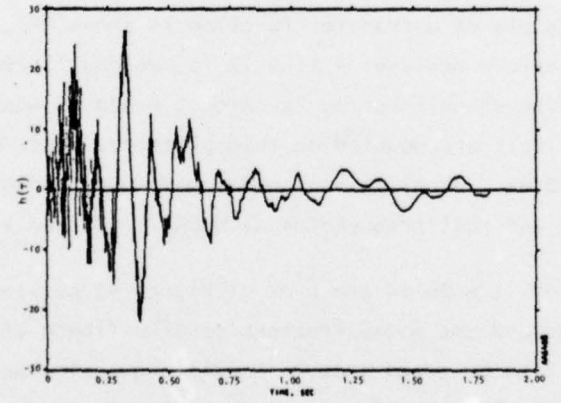

(c) Impulse function

FIGURE 41. PARPP CONTROL ROOM: MEASURED TRANSFER FUNCTION FOR 0.5 HZ TO 500 HZ

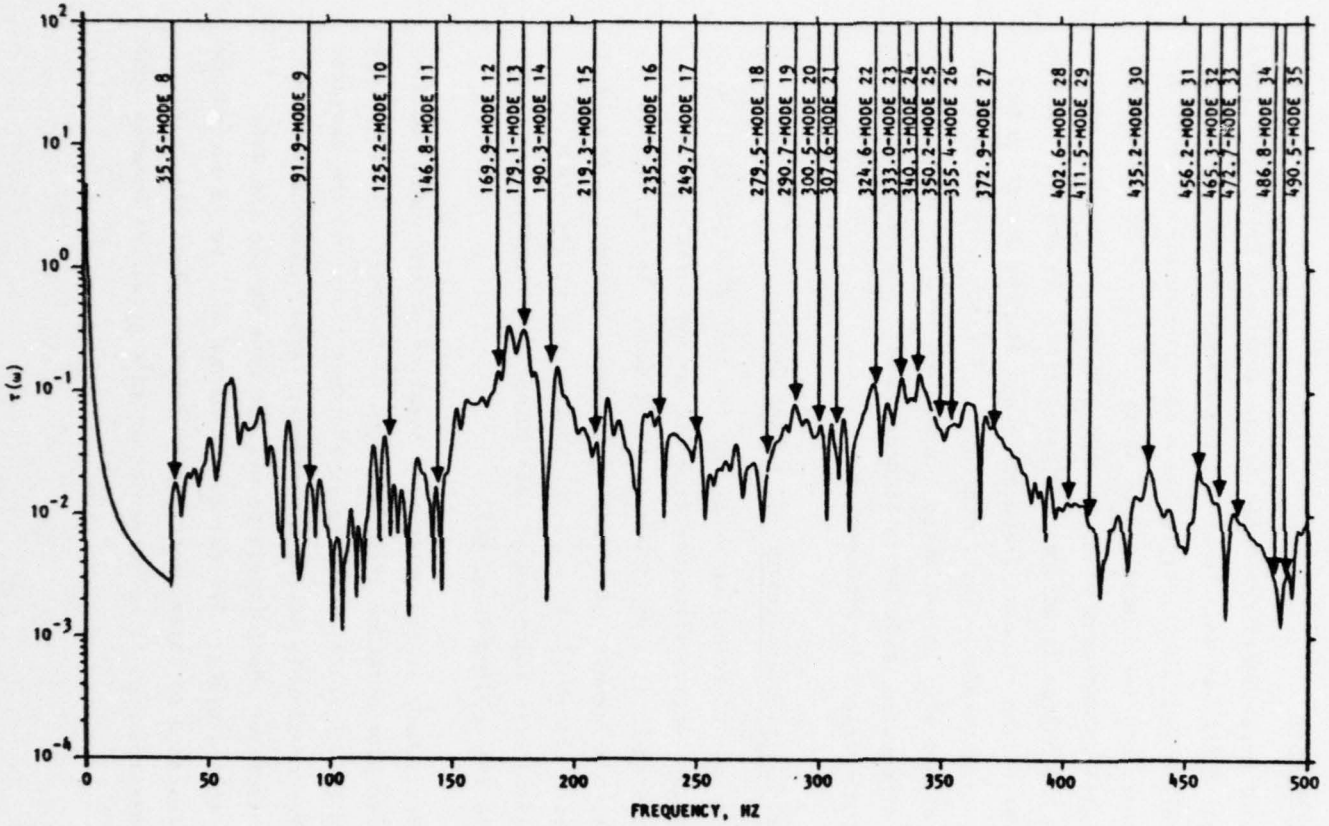

FIGURE 42. PLATFORM PARPP-D: GLOBAL TRANSFER FUNCTION, RESONANCES OF THE MEASURED FUNCTION COMPARED TO MODAL FREQUENCIES OF A FINITE ELEMENT MODEL

2.1.6.3 Buried Structures

A series of experiments performed by the Waterways Experiment Station (Ref. 37) in Project ESSEX was made to assess the effects of soil coupling on structures. Two reinforced box structures were constructed with both structures having the same interior dimensions of 16 ft x 4 ft x 4 ft. The structures differed in wall thicknesses of 13 in. and 5.6 in. The results of impedance tests on the buried structures indicated (Figs. 43 and 44) that the effect of soil cover on the resonant frequencies and damping appear to be dependent upon the structure/soil impedance ratio. Further work is planned by which the soil effect will be extracted and modeled from the experimental data. Extraction procedures would be in accordance with the method presented on component interconnections in Reference 9.

2.1.6.4 Electrical Distribution Center, SAFEGUARD System

The Electrical Distribution Center of the SAFEGUARD SYSTEM is a reinforced-concrete protective structure flush to ground surface (Fig. 45). This structure measures 26 ft x 43 ft and is 19 ft deep. The ceiling is approximately 2 ft in thickness. Internal electrical equipment is mounted on a shock-isolated platform (30 ft x 20 ft) that weighs on the order of 40,000 lb. The platform is supported at each corner by pneumatic isolators, pendulum mounted to the ceiling (Fig. 46).

Measurements made at the attachment location of the shock isolator with and without isolator attached (Fig. 47) show differences. This measurement difference, although small, illustrates the sensitivity of the measurement system even for components having a decidedly large impedance mismatch. Extraction of the isolator input impedance will be made during the data analysis phase of this project. The extraction method will be in accordance with procedures presented on interconnection in Reference 35. Figure 27 also shows nonlinear reciprocity measurements on this structure between roof and floor.

(Text continued on p. 80.)

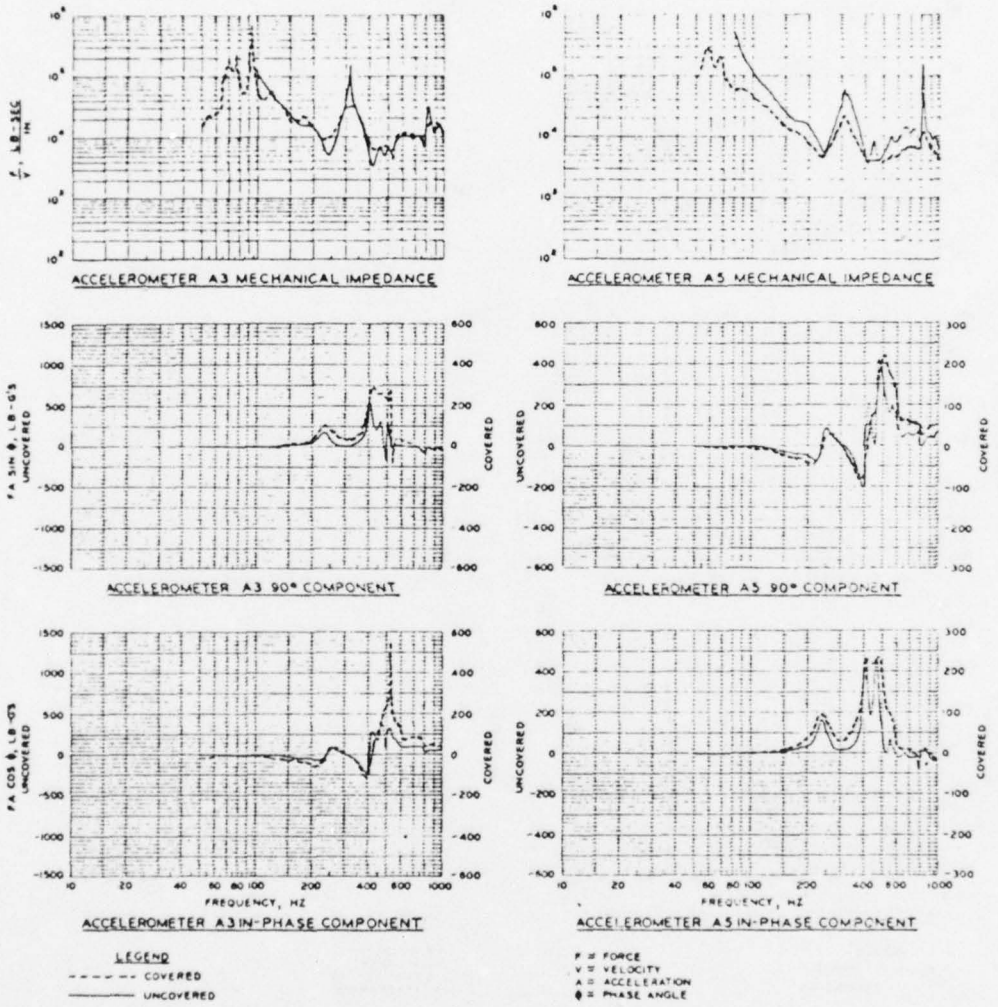

FIGURE 43. TYPICAL IMPEDANCE FUNCTIONS FOR THICK WALLED (13 IN.) BOX STRUCTURE (16 FT X 4 FT x 4 FT) SHOWING EFFECTS OF SOIL COVER (Courtesy Waterways Experiment Station)

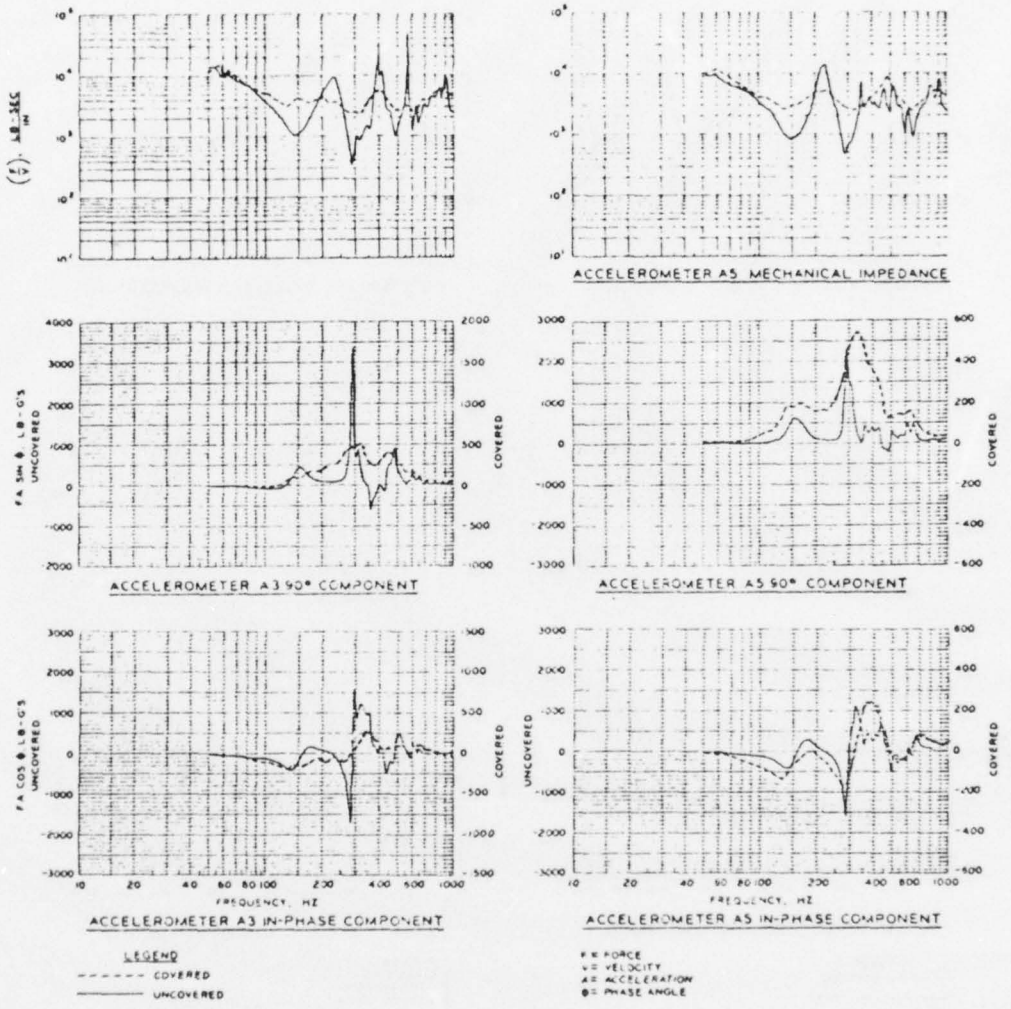

FIGURE 44. TYPICAL IMPEDANCE FUNCTIONS FOR THIN WALLED (5.6 IN.) BOX STRUCTURE (16 FT X 4 FT X 4 FT INTERIOR) SHOWING EFFECTS OF SOIL COVER (Courtesy Waterways Experiment Station)

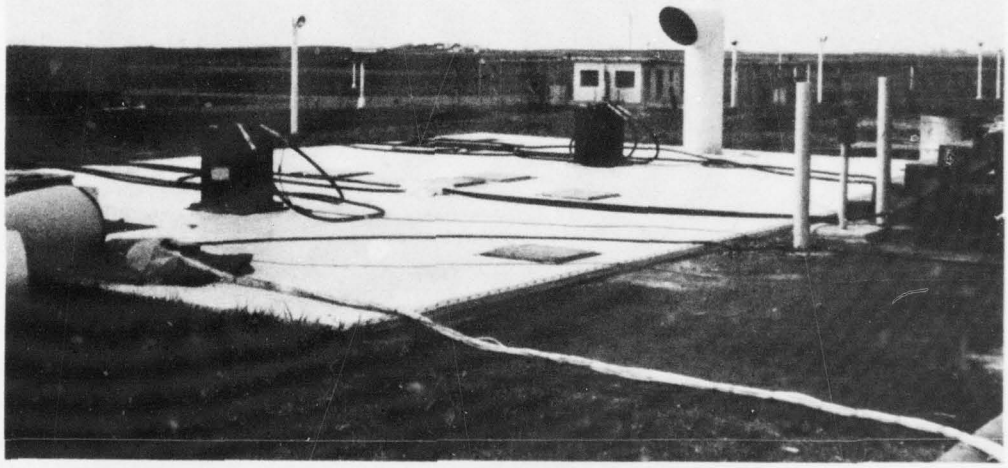

FIGURE 45. ELECTRICAL DISTRIBUTION CENTER, A FLUSH-TO-GROUND SURFACE REINFORCED PROTECTIVE STRUCTURE (Two electrohydraulic vibrators on roof)

FIGURE 46. SHOCK ISOLATED PLATFORM (30 FT X 20 FT) WEIGHING 40,000 LB IN ELECTRICAL DISTRIBUTION CENTER

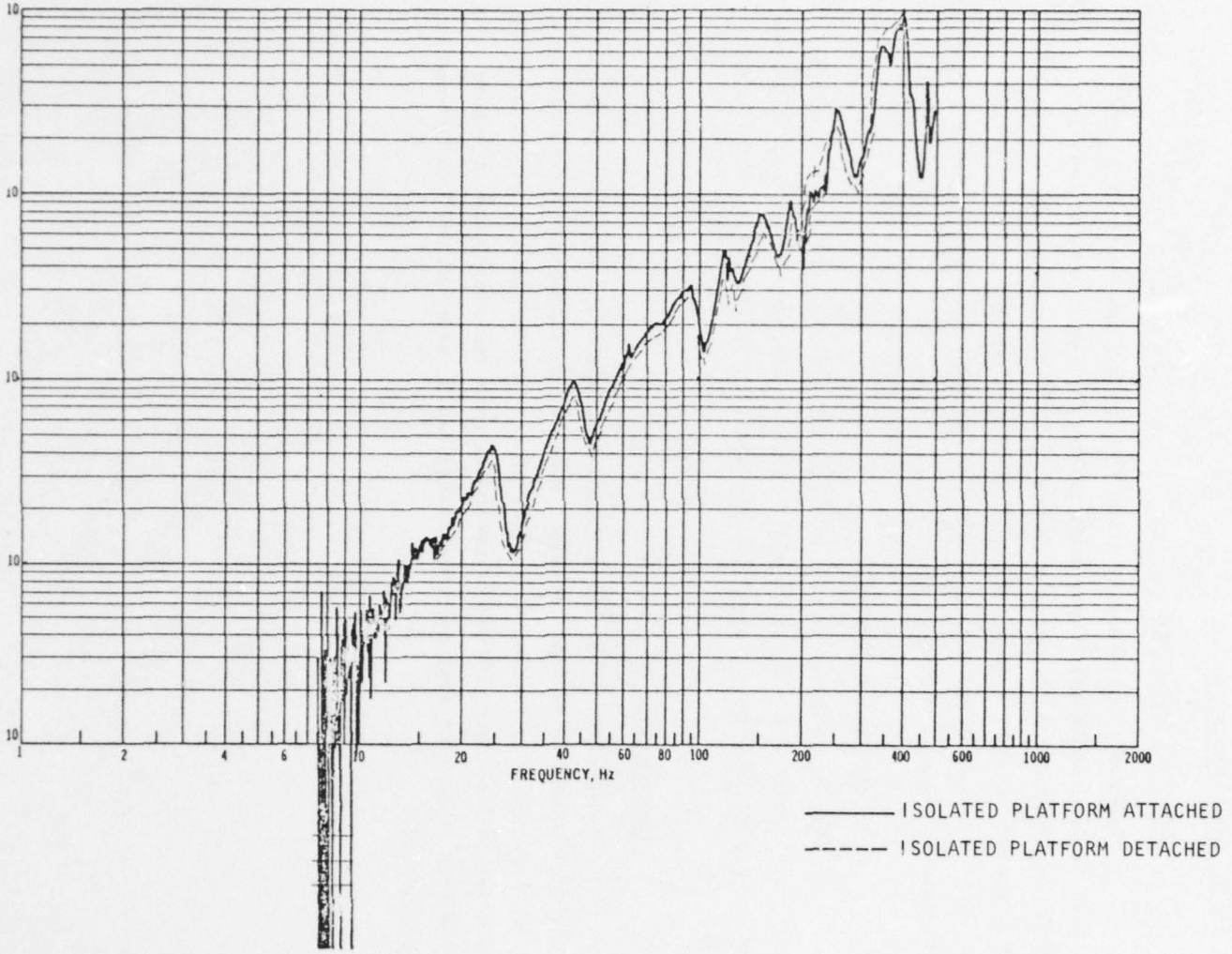

FIGURE 47. DRIVING POINT IMPEDANCE TESTS OF ELECTRICAL DISTRIBUTION CENTER AT ATTACHMENT LOCATION OF A SHOCK ISOLATOR (Measurements made with and without isolator attached)

2.1.6.5 Other Projects

BMD Test Structure

Impedance measurements shown in Figure 3 for chirp tests and Figure 12 for random tests were made on the Ballistic Missile Division (BMD) test structure pictured in Figure 48. This structure of reinforced concrete was used as a test device to study various methods of vibration excitation and data processing to improve accuracy of data and to reduce test and data processing costs.

Sprint Missile and Silo

Impedance measurements of Figure 23 exhibit effects of nonlinear soil coupling to a missile silo wall. These measurements were recently taken on an ongoing impedance project for the Sprint Silo and Sprint Missile (Fig. 49).

Hangerette

Hangerettes (Fig. 50) are used to protect aircraft from both conventional bombs and nuclear threats. Mobility measurements (Vel/Force) were made (Fig. 51) from the inside surface of the reinforced-concrete arch to the external soil surface. These measurements in a reciprocity sense assume linearity from which response predictions can be made, as will be covered in Section 2.2.

(Text continued on p. 85.)

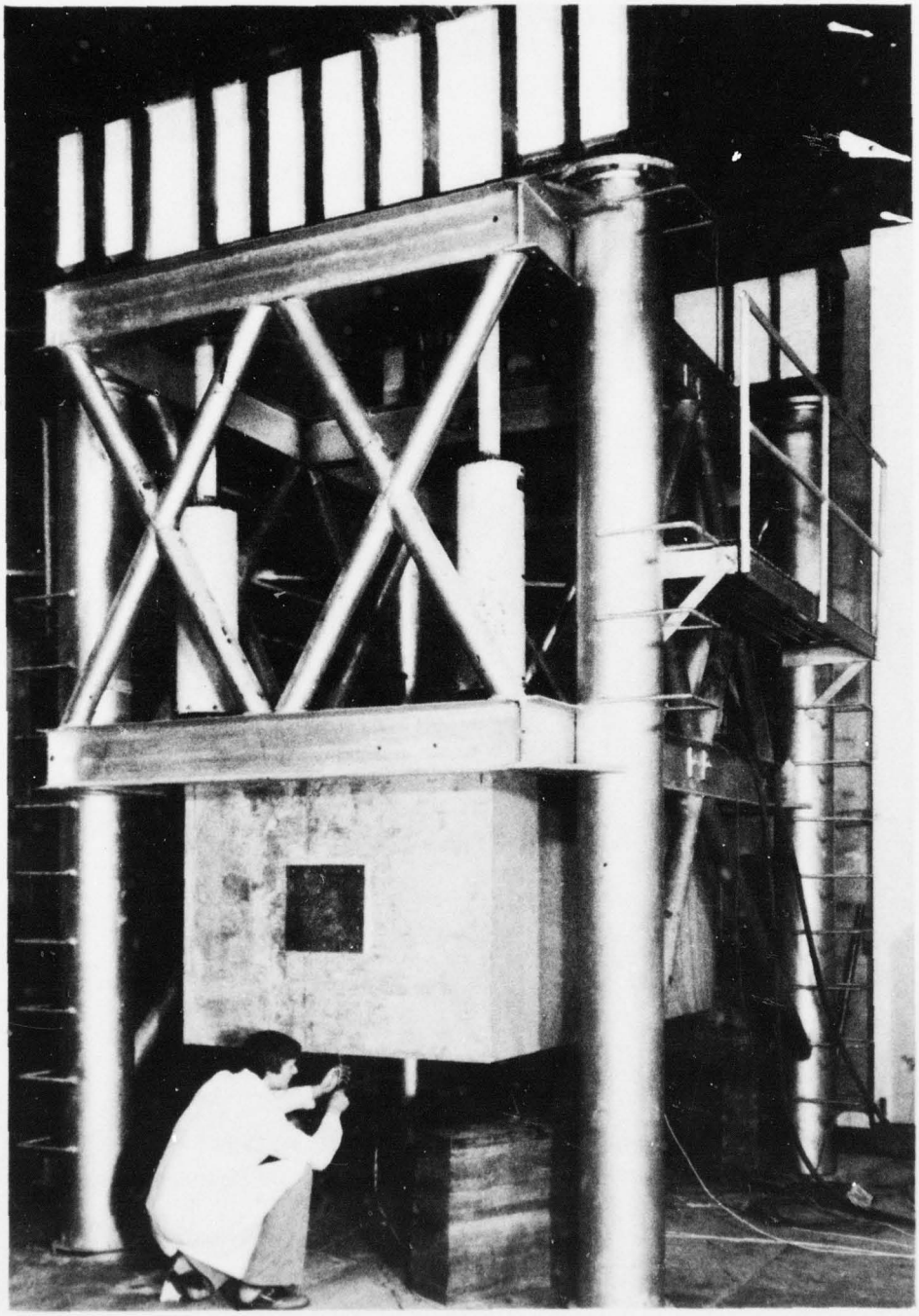

FIGURE 48. BALLISTIC MISSILE DIVISION (BMD) IMPEDANCE TEST STRUCTURE

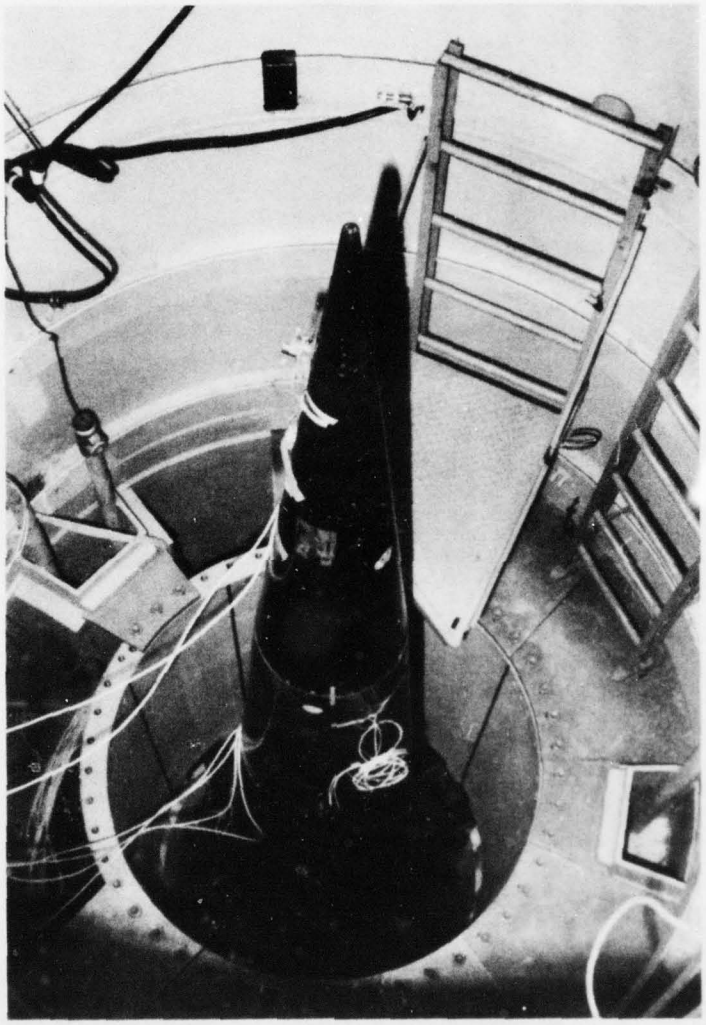

FIGURE 49. SPRINT SILO AND SPRINT MISSILE INSTRUMENTED FOR IMPEDANCE MEASUREMENTS

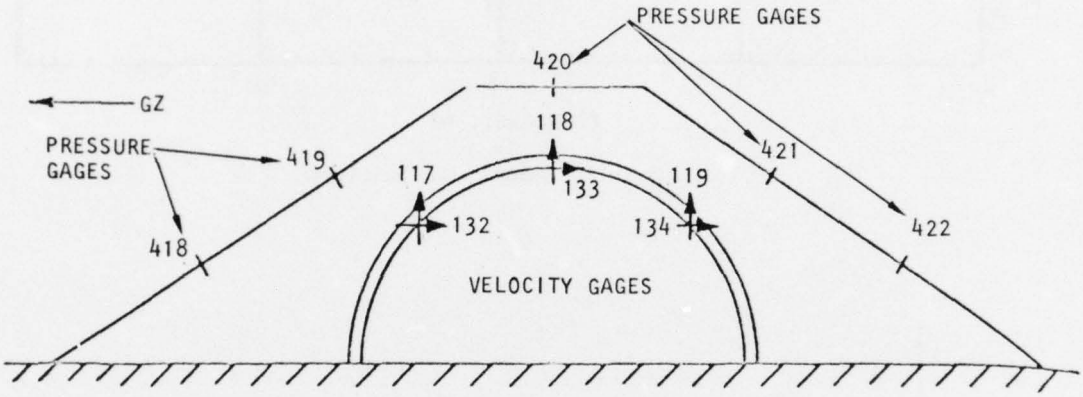

FIGURE 50. HANGARETTE-AIRCRAFT SHELTER SHOWING LOCATION OF PRESSURE AND VELOCITY GAGES MIXED COMPANY EVENT (500-TON TNT TEST)

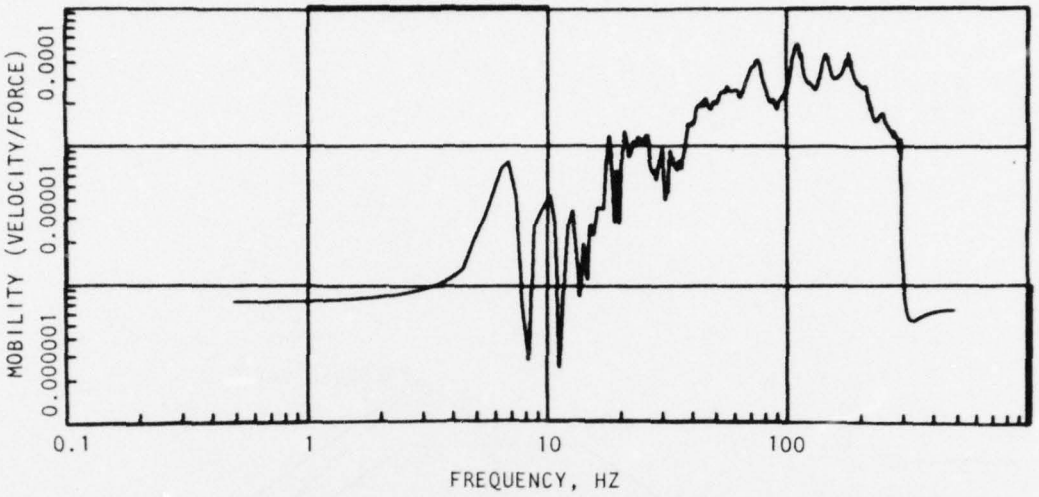

(a) Mobility magnitude function

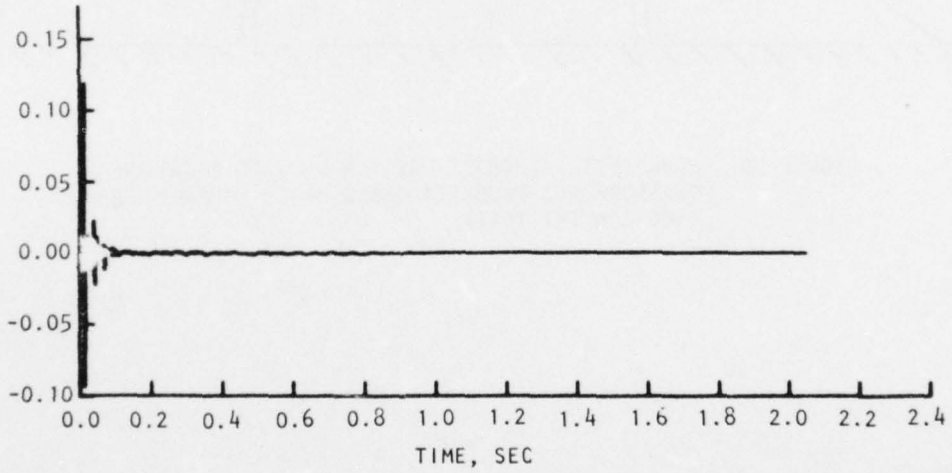

(b) Mobility impulse function

FIGURE 51. MOBILITY OF HANGARETTE FROM MID-ARCH TO SOIL SURFACE (Courtesy Waterways Experiment Station)

2.2 PREDICTION OF SYSTEM RESPONSES USING MEASURED IMPEDANCE AND TRANSFER FUNCTIONS

2.2.1 RESPONSE OF ABOVEGROUND STRUCTURES TO AIR BLAST

The method used to calculate the response accelerations of the 1/12-scale model and prototype Perimeter Acquisition Radar Buildings (PARB) is similar for each. Verification or checks on the accuracy of the response predictions is made by comparing the predictions with response records of the scale model taken during Event DIAL PACK (Ref. 3). Event DIAL PACK was a 500-ton TNT explosion that subjected air-blast and ground-shock loads to several targets. Calculations for both structures were made for the vertical direction only, and as such, the traveling air-blast pressure loading over the roof surface comprises the external forcing function. Exclusion of the cross-coupling contributions to structural motions from pressure loads on the external four walls is considered to have minimal effect on the calculated responses. As discussed in Section 2.1, the rapid rolloff of pressure amplitudes with frequency permitted this reduction in computational effort.

All data and calculations are internally consistent and show comparable amplitudes for pressures, motions, yield, time, and frequency. However, the absolute values have been normalized so that this report could be declassified.

2.2.1.1 1/12-Scale Model

Response predictions use inertance functions, a pressure zone for each inertance function, air-blast pressure functions, pressure area zone engulfment, traveling pressure wave function, and transfer functions. Each of the above elements is described and quantified in the following paragraphs.

2.2.1.1.1 *Inertance Functions and Associated Pressure Area Zoning*

The use of inertance measurements to predict the response of a structural system to blast loading is basically a special application of the impedance technique. An inertance test measures the point acceleration response of a structure due to a point force load. Blasts such as the air-pressure loads acting on the model PARB structure in Event DIAL PACK is a continuous forcing function acting on a continuous structure. Thus, the sampled impedance information must be summed over the structure (as an approximation of an integral) to obtain the internal point responses of the structure due to loads acting everywhere on the external surfaces of the structure.

Each inertance function must be associated with a specific area of the structure upon which the air-blast pressure acts. This assumes that the inertance function is essentially constant for this area. Finite-element plate models were initially used to map the model and to provide, thereby, preliminary measurement and drive point locations. Additional refinement of drive point locations was made during field testing where quick-look analog impedance measurements verified that a reasonable density of measurements for the model structure would be acquired. The smooth change in functions obtained when moving from one area to the next indicated that a reasonable number of measurements consistent with computational costs had been obtained. Potentially, interpolation of the measurements could have been made during computation, should the need have arisen. Additional measurements also showed a high degree of symmetry for the structure (see Sec. 1), and this fact permitted a higher density of measurement per surface area.

Boundaries for local areas of each acceptance measurement were drawn by observation and evaluation of the data. For the 29 measurements selected, the associated impedance zone and input pressure zone for each measurement is shown in Figure 52.

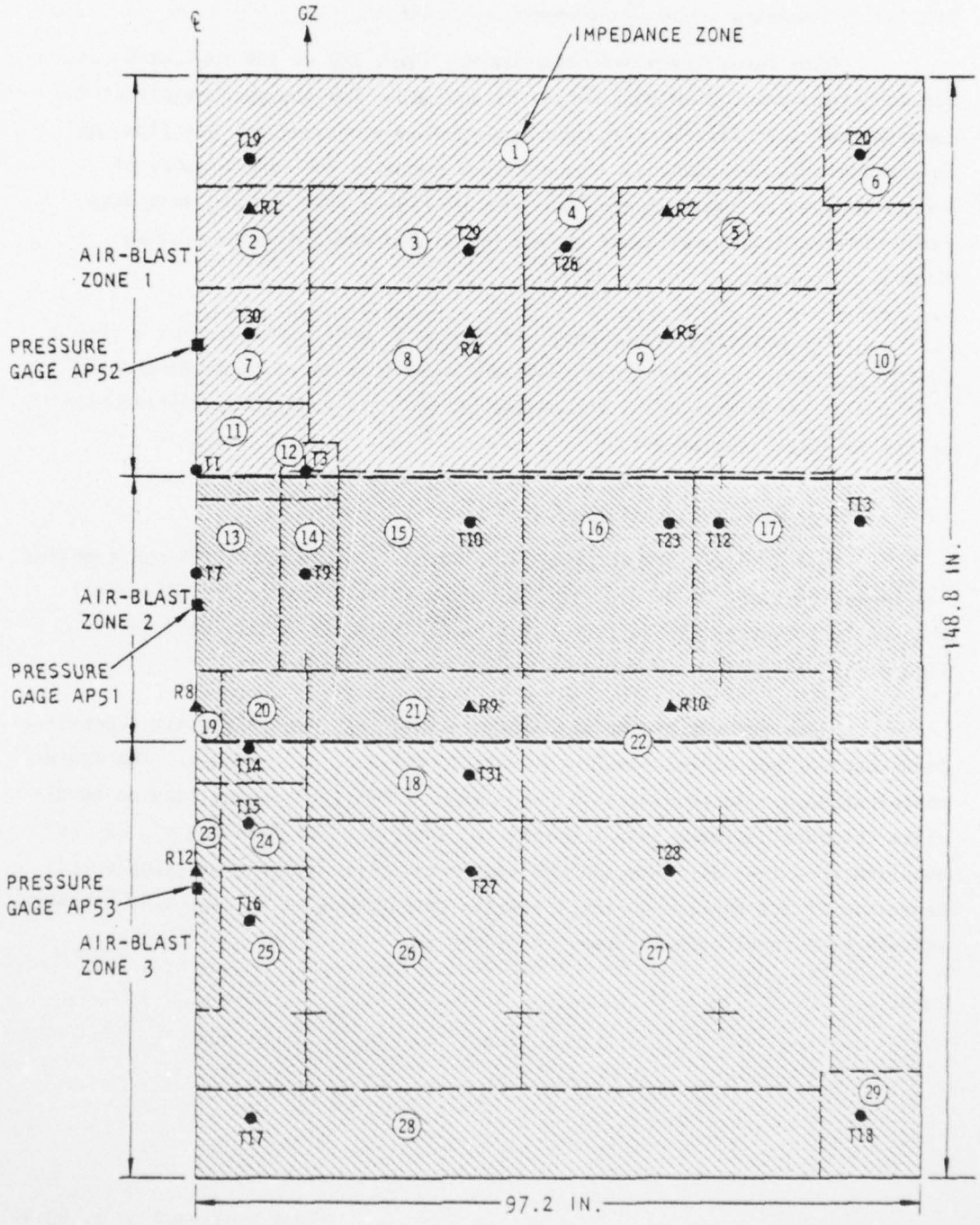

FIGURE 52. ZONED ROOF ON PARB MODEL SHOWING IMPEDANCE ZONES, AIR-BLAST ZONES, AND IMPEDANCE MEASUREMENT DRIVE LOCATIONS

2.2.1.1.2 *Pressure Input Development*

Only three air-blast measurements (Ref. 29) on the roof were obtained from Event DIAL PACK (Figs. 53 and 54). The aboveground structure perturbs the air-blast loading by overexpanding the transient air flow, as is particularly observable in the pressure notch in the time history of Figure 53b and in the frequency spectrum of Figure 54b. Hence, test data rather than conventional blast curves (Figs. 53d and 54d) were used as forcing functions.

The air-blast zones shown in Figure 52 were configured on a simple geometric basis. The air-blast functions were considered to be constant within each air-blast zone. The potential for extrapolation and interpolation exists for this type of data.

a. Pressure Area Zones

For a local surface area, A_{ik}, which is associated with one transfer inertance function, it is necessary to account for the velocity of the air load as it traverses the surface. This accounting, as illustrated in Figure 55, is required to assure a proper surface loading.

Upon arrival of the air blast at time τ_i, the air blast successively loads the surface in increments ΔX where $n\Delta X = d_i$ the length. The incremental loading time is given by: $\Delta t = \Delta X/V$. This incremental loading subdivides the local surface into segments $A_{ik}(\Delta X/d_i)$. The fineness of ΔX is obtained from the Δt selected and can be as small as the digitizing rate. Depiction of air-blast engulfment and the development of an effective pressure as seen by a local area is shown in Figure 56.

(Text continued on p. 93.)

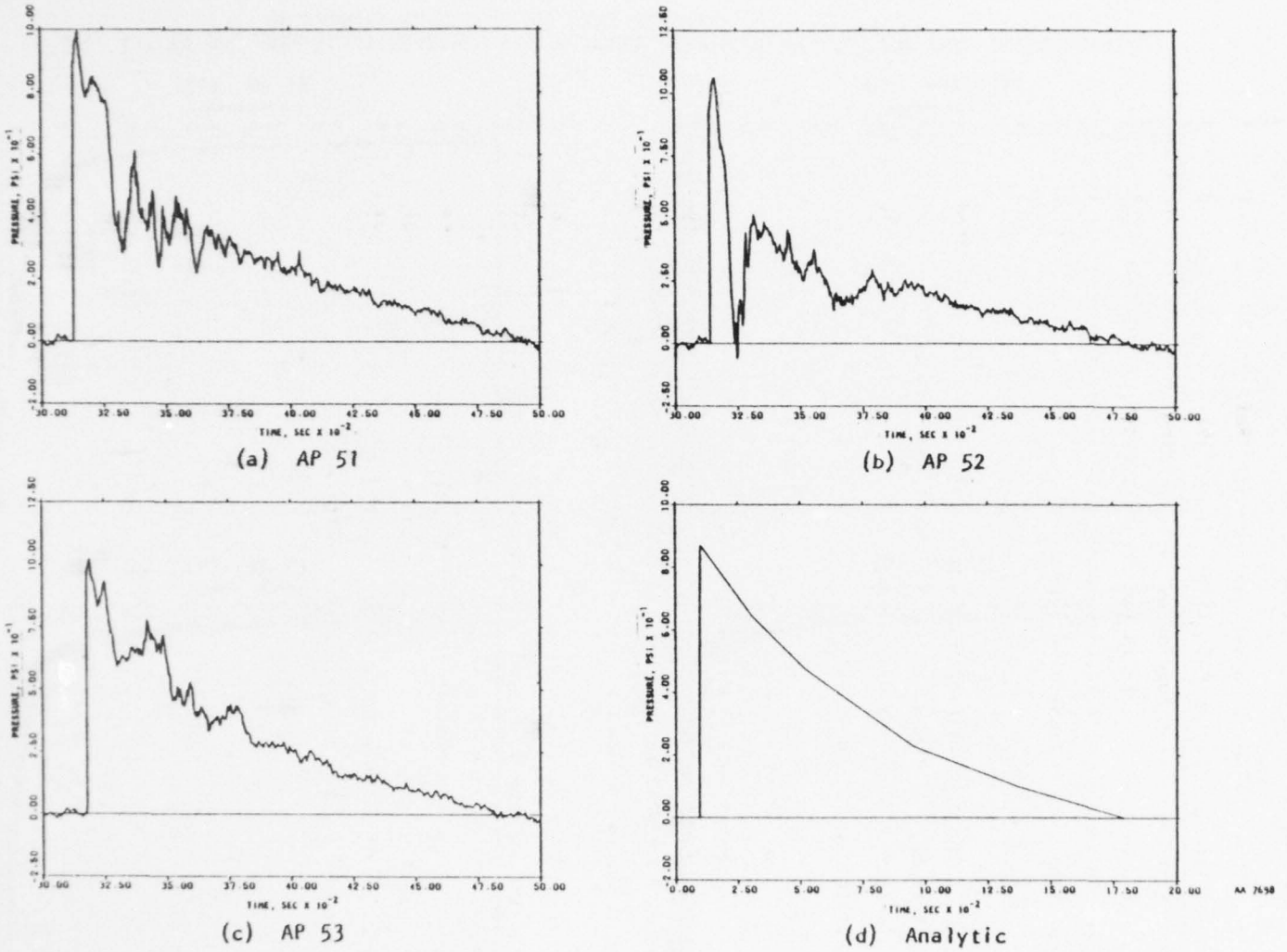

FIGURE 53. AIR-BLAST MEASUREMENTS ON MODEL PARB ROOF AND CONVENTIONAL AIR-BLAST REPRESENTATION OF PRESSURE-TIME HISTORIES

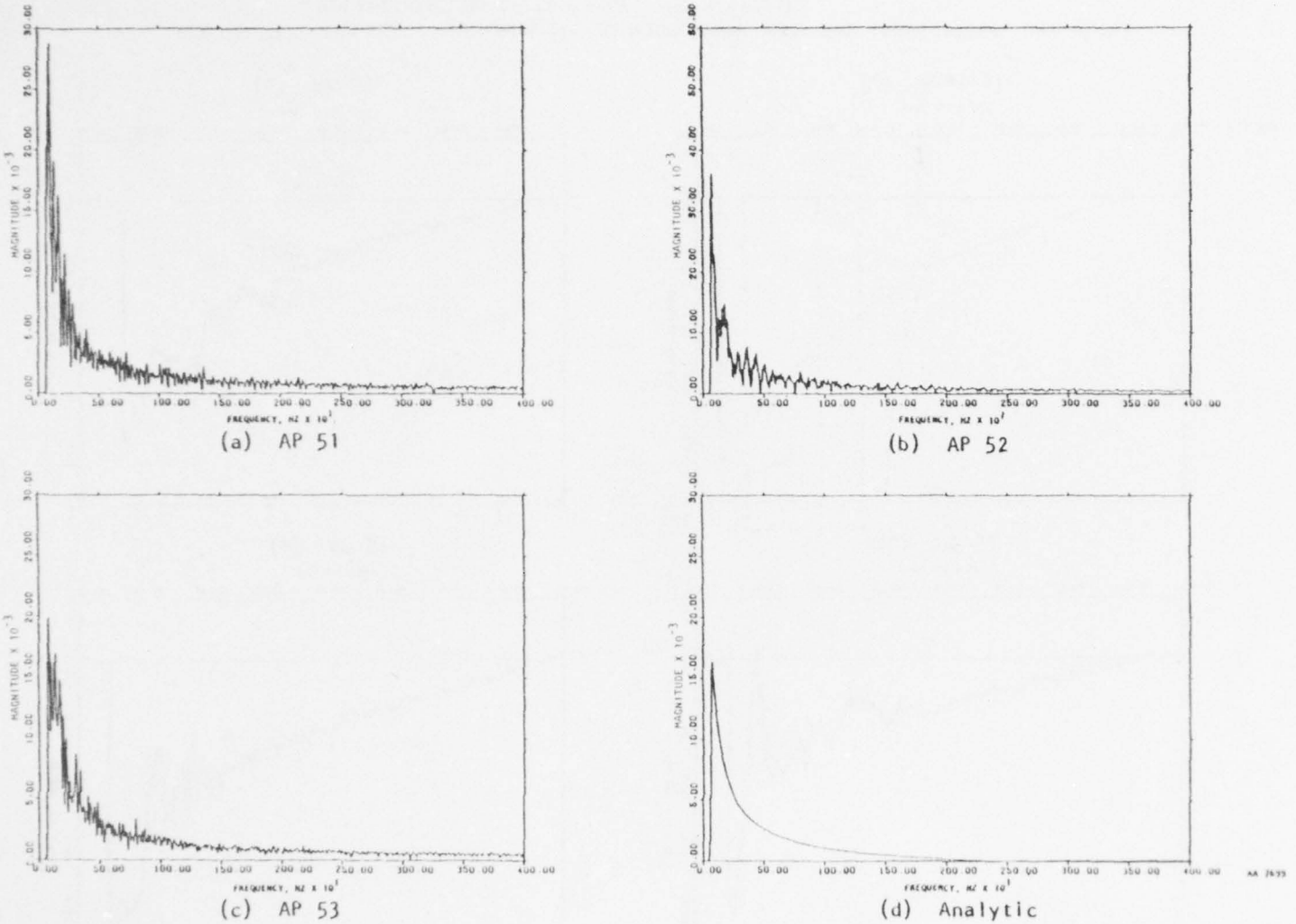

(a) AP 51

(b) AP 52

(c) AP 53

(d) Analytic

FIGURE 54. AIR-BLAST MEASUREMENTS ON MODEL PARB ROOF AND CONVENTIONAL REPRESENTATION OF FOURIER MAGNITUDE PRESSURE SPECTRA

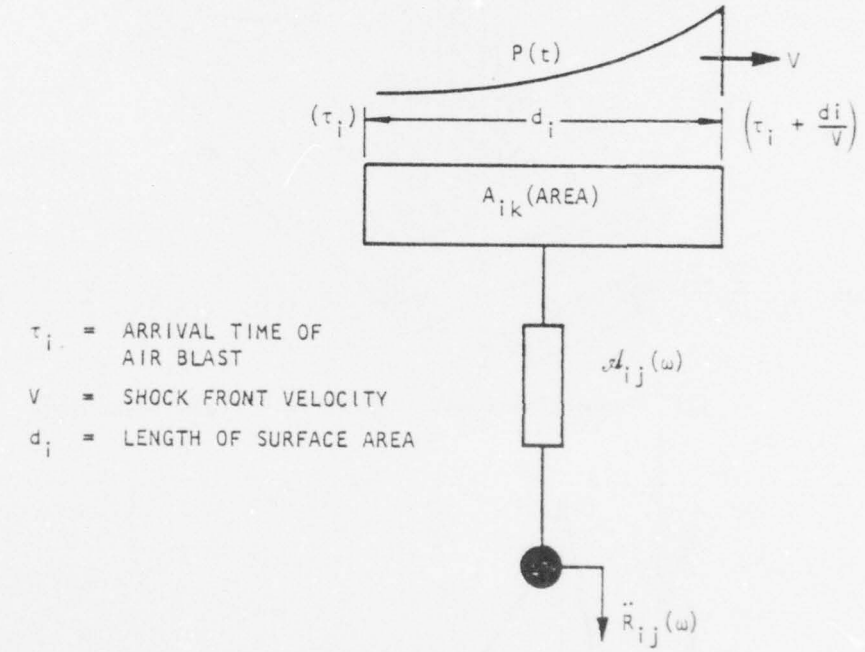

FIGURE 55. MOVING AIR LOAD OVER A LOCAL SURFACE AREA ASSOCIATED WITH A TRANSFER INERTANCE FUNCTION TO AN INTERNAL POINT IN STRUCTURE

AD-A050 116 AGBABIAN ASSOCIATES EL SEGUNDO CALIF F/G 20/11
IMPEDANCE-BASED MOTION PREDICTION, SCALING, AND ENVIRONMENTAL S--ETC(U)
DEC 77 F B SAFFORD N00173-76-C-0249
UNCLASSIFIED AA-R-7710-4500 NRL-MR-3676 NL

2 OF 3
AD
A050116

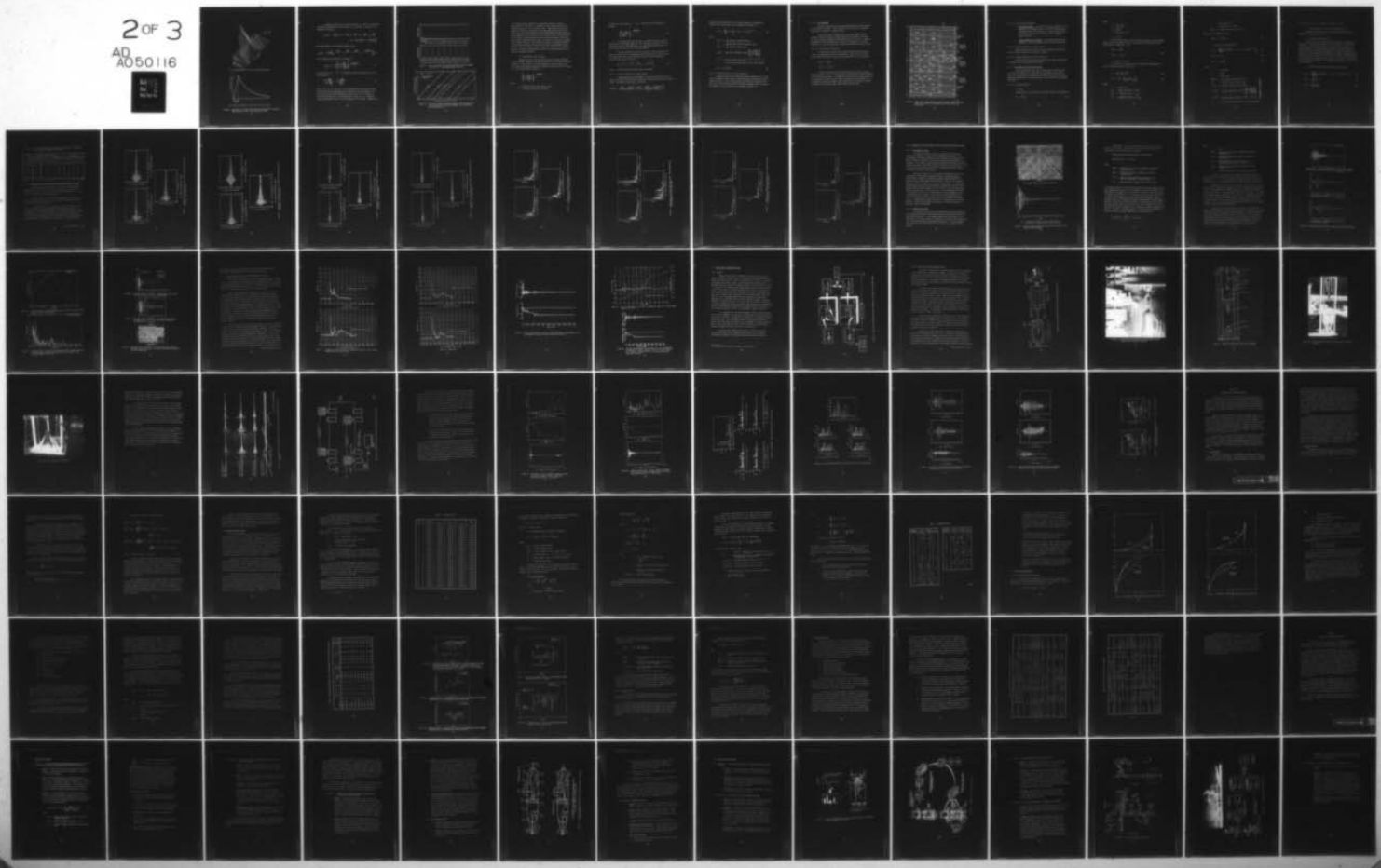

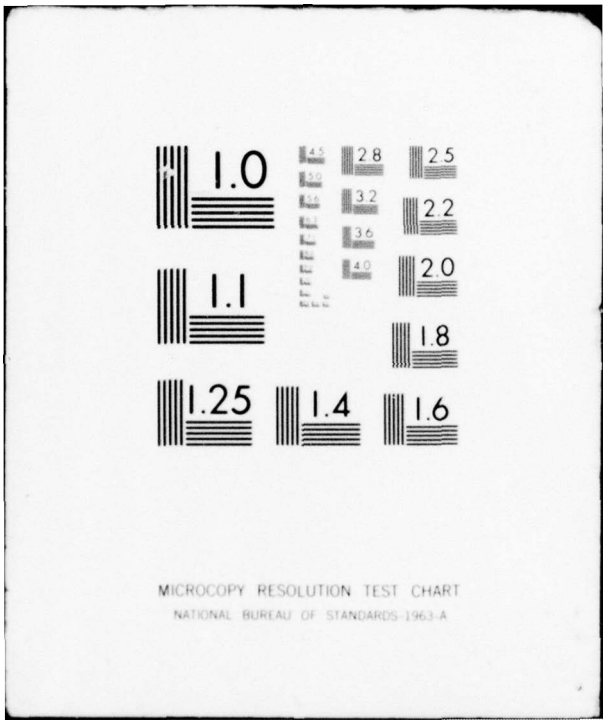
1.0
1.1
1.25
1.4
1.6
1.8
2.0
2.2
2.5
2.8
3.2
3.6
4.0
4.5
MICROCOPY RESOLUTION TEST CHART
NATIONAL BUREAU OF STANDARDS-1963-A

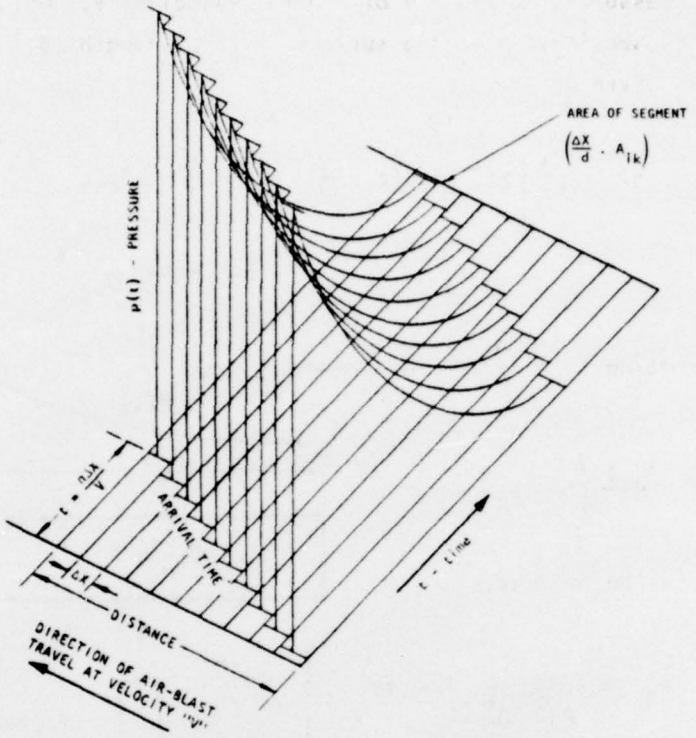

(a) Three-dimensional view of air-blast engulfment

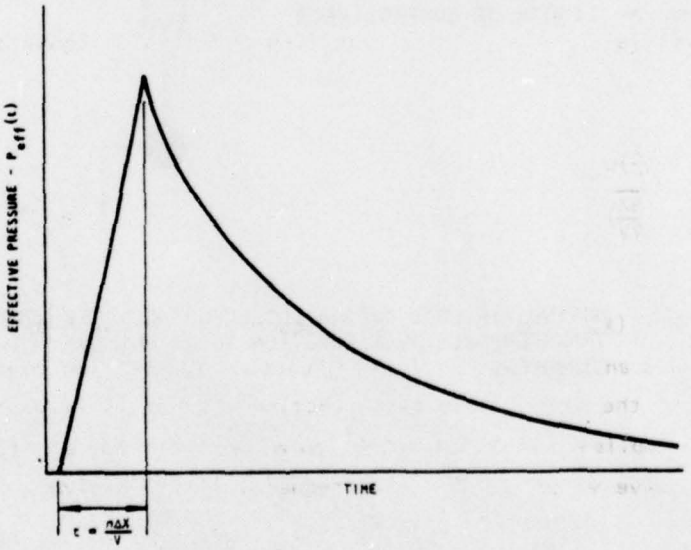

(b) Profile of effective pressure over a local area

FIGURE 56. DEPICTION OF AIR-BLAST ENGULFMENT AND DEVELOPMENT OF EFFECTIVE PRESSURE OVER A LOCAL AREA (EXAGGERATED SCALE)

A pressure-time history of frontal velocity V, which is successively translated and sectioned over the surface A_{ik} of length d_i equal to $n\Delta X$ increments is given by:

$$P_{eff}(t) = \frac{1}{n}\left[p(t) + p(t - \frac{\Delta X}{V})\, u(t - \frac{\Delta X}{V}) + p(t - \frac{2\Delta X}{V})\, u(t - \frac{2\Delta X}{V}) \right.$$
$$\left. \cdots\ p(t - \frac{(n-1)\Delta X}{V}\, u(t - \frac{(n-1)\Delta X}{V}\right] \tag{1}$$

and transformation in the frequency domain gives:

$$P_{eff}(\omega) = \frac{P(\omega)}{n}\left(1 + e^{-j\frac{\Delta X}{V}\omega} + e^{-j\frac{2\Delta X}{V}\omega} + e^{-j\frac{3\Delta X}{V}\omega} \cdots + e^{-j\frac{(n-1)\Delta X}{V}\omega}\right) \tag{2}$$

and the expression of Equation 2 converges to:

$$P_{eff}(\omega) = P(\omega)\left[\frac{\sin\ (\frac{n\Delta X}{2V})\omega}{n \sin\ (\frac{\Delta X}{2V})\omega}\right] e^{-j\frac{(n-1)\Delta X}{2V}\omega} \tag{3}$$

For small angles ($\theta \simeq \sin\ \theta$) the engulfing function of Equation 3 may be represented by:

$$\frac{\sin\ (\frac{n\Delta X}{2V})\omega}{n \sin\ (\frac{\Delta X}{2V})\omega} \simeq \frac{\sin\ (\frac{n\Delta X}{2V})\omega}{n\ (\frac{\Delta X}{2V})\omega} \tag{4}$$

which is the $S_i\ (X)$ function in the frequency domain such as represented in Figure 57a and an approximate box car function in the time domain. The cyclic nature of the actual engulfing function (Eq. 3) is illustrated in Figure 57b and implies a critical selection of a time step Δt (dependent on mesh length/wave velocity) for the frequency limit involved. Somewhat akin

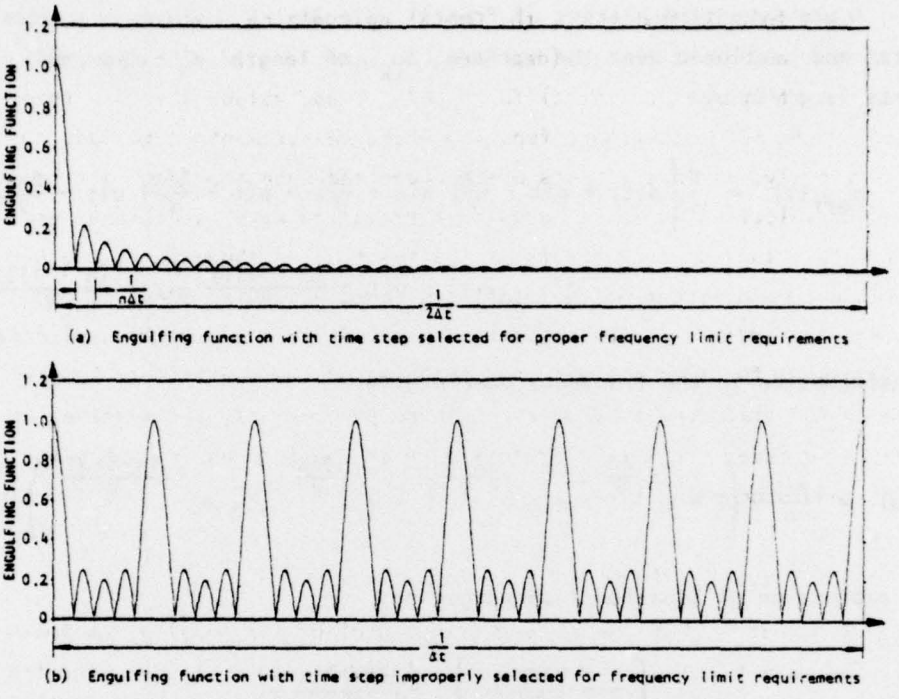

FIGURE 57. PLOT OF MAGNITUDE OF ENGULFING FUNCTION FOR TWO DIFFERENT TIME STEPS Δt = (MESH LENGTH/BLAST VELOCITY)

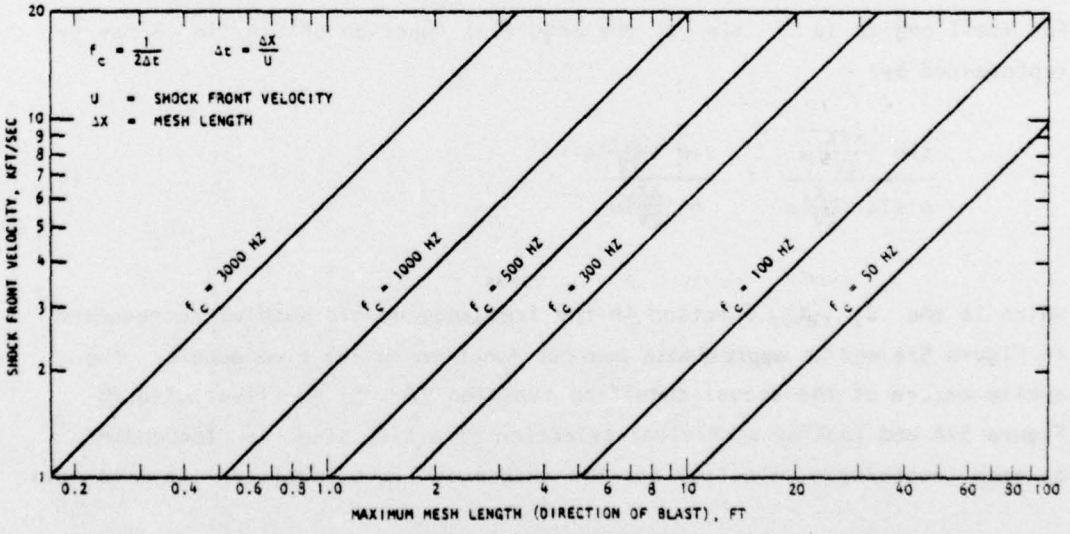

FIGURE 58. TRAVELING AIR-BLAST LOADING ON SURFACE; MAXIMUM MESH LENGTH IN BLAST DIRECTION AT FOLDING FREQUENCY (f_c) FOR RANGE OF SHOCK FRONT VELOCITIES

to the Nyquist folding frequency, the engulfing function, as shown in Figure 57a has a time step Δt (dependent on mesh length/velocity) and a frequency cutoff 1/2 Δt (0.1 msec) for 5 KHZ. These values are more than adequate for the model inertance function where measurements were made to 3 KHz. Obviously, serious effects are encountered when too large a time step (mesh length/velocity) is taken in using a traveling wave, since the results will ultimately include the effects of the function as shown in Figure 57b, where frequency amplitudes above cutoff are contained in the data or computations. Not too obvious in the engulfing functions is the maximum amplitude in the frequency function of unity and the area of the approximate boxcar function in the time domain of unity. Figure 58 provides, for a traveling load over a surface, the maximum mesh length at the folding frequency for a range of traversing velocities.

b. Traveling Wave over a Surface

Somewhat similar to the engulfing function for local areas (mesh size) is the wave travel over the entire structure. In this case, the travel distance or time increment is from the boundary of one local area to the next. Where the boundary distances are equal and the blast velocity constant, the traveling wave function would be:

$$\left[\frac{\sin\left(\frac{N\Delta t}{2}\right)\omega}{\sin\left(\frac{\Delta t}{2}\right)\omega}\right] e^{-j\frac{(N-1)\Delta t}{2}\omega} \qquad (5)$$

where

N = Number of equal local areas on roof

Δt = Traverse time across local area

As before for small angles, $\theta \simeq \sin\theta$ and the function of Equation 5 becomes:

$$\left[\frac{\sin\left(\frac{N\Delta t}{2}\right)\omega}{\left(\frac{\Delta t}{2}\right)\omega}\right] e^{-j\frac{(N-1)\Delta t}{2}\omega} \tag{6}$$

The traveling wave for the roof is a summation having a maximum amplitude in the frequency domain of $N\Delta t$ (the total traverse time of the wave over the roof). The amplitude of the approximate boxcar function is unity and has an area of $N\Delta t$ in the time domain.

The local areas of the roof are not equal, and the foregoing discussion is useful only in understanding the characteristics of the function. The unequalness of the local roof areas requires that the function of Equation 5 be placed in the form

$$\left[1 + e^{-j\tau_1\omega} + e^{-j\tau_2\omega} + e^{-j\tau_3\omega} + \ldots e^{-j\tau_{N-1}\omega}\right] \tag{7}$$

where τ_i = time of arrival at each local area boundary

2.2.1.1.3 *Response Prediction at First Location*

Response calculations were made in the vertical direction from roof loads of a traveling air blast for the center of the 5th floor of the 1/12-scale model. The method of calculation is given as:

$$\text{Response} = \begin{pmatrix}\text{Local}\\ \text{Inertance}\end{pmatrix}\begin{pmatrix}\text{Local}\\ \text{Area}\end{pmatrix} \times \begin{pmatrix}\text{Local}\\ \text{Pressure}\end{pmatrix} \times \begin{pmatrix}\text{Local}\\ \text{Engulfment}\\ \text{Function}\end{pmatrix}\begin{pmatrix}\text{Traveling}\\ \text{Wave}\\ \text{Function}\end{pmatrix}$$

Computations were performed in the frequency domain as represented by Equation 8 and transformed to the time domain by Equation 9.

$$\ddot{X}(\omega) = \sum_{i=0}^{N} \mathcal{I}_i(\omega) \left[A_i \cdot P_i(\omega) \cdot Si_i(\omega) \right] e^{-j\tau_i\omega} \tag{8}$$

where

$\mathcal{I}_i(\omega)$ = ith inertance function $[\ddot{X}/F_i(\omega)]$

A_i = ith local area (mesh) of external load

$P_i(\omega)$ = ith external pressure load

$Si_i(\omega)$ = ith local engulfment function $\left[\dfrac{\sin\left(\frac{n\Delta t\omega}{2}\right)}{n \sin\left(\frac{\Delta t\omega}{2}\right)} \right]$

$e^{-j\tau_i\omega}$ = Traveling wave function $\left[1 + e^{-j\tau_1\omega} + e^{-j\tau_2\omega} \ldots \right]$

τ_i = Arrival time of blast wave at local area boundary

$$\ddot{x}(t) = \mathcal{F}^{-1}\left[\ddot{X}(\omega) \right] \tag{9}$$

2.2.1.1.4 *Response Prediction to Other Locations*

Response predictions at additional internal locations (i.e., locations in addition to the "first") of the building are facilitated by use of transfer functions. The response prediction at the first location on the 5th floor is multiplied by a transfer function to another location to obtain the response at the new location, as discussed in Section 2.1.

2.2.1.2 Prototype PARB

Response predictions of the prototype PARB follow the same procedure as that used for the model. Each variable will be discussed, with emphasis placed where differences in procedure occur.

Selection of local impedance zones and pressure areas for each inertance function followed the methods employed for the model. The zones for the 36 impedance measurements selected are shown in Figure 59. Impedance measurements A-1 and A-29 were used on the basis of symmetry in two other locations (Fig. 59), since poor data records were obtained in Zones 34 and 36.

2.2.1.2.1 *Pressure Input Development*

Pressure-time histories from Event DIAL PACK were scaled geometrically for computations on the prototype PARB. Pressures for both model and prototype are identical but scaling of characteristic time is required.

$$P_p(t) = P_m\left(\frac{t}{\lambda}\right)$$

$$P_p(\omega) = \lambda\, P_m(\lambda\omega) \qquad (13)$$

Effects on waveforms of the DIAL PACK pressure records by scaling (Reynolds number, $\rho VL/\mu$) to the prototype were evaluated to determine whether serious errors would result. Information on transient blast waves interacting with structures is quite limited. Some information having applicability to the PARB configuration has been found and evaluated for scale factor effects. These data are from shock tubes, water tables, and nose cones.

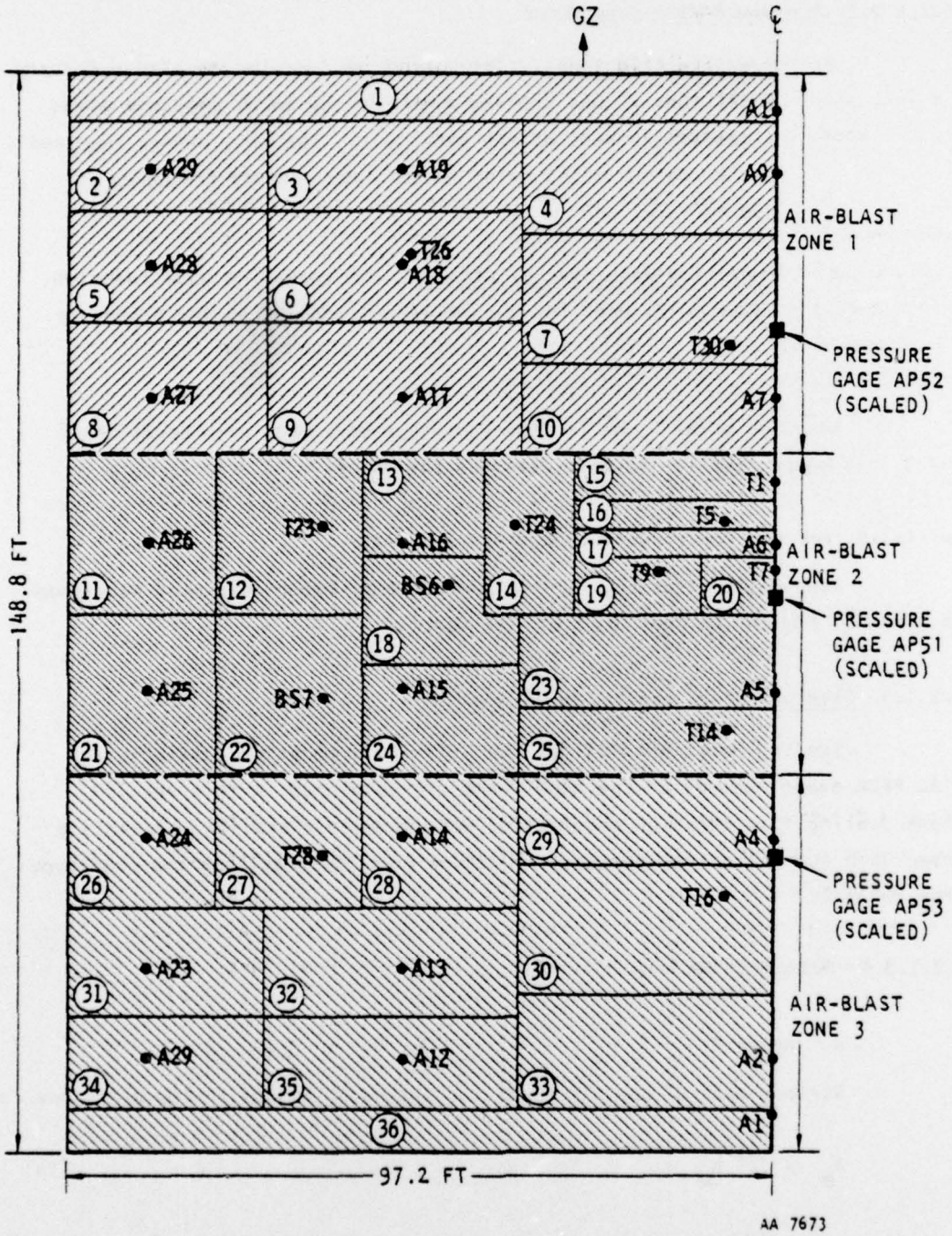

FIGURE 59. ZONED ROOF OF PARB PROTOTYPE SHOWING IMPEDANCE ZONES, AIR-BLAST ZONES, AND IMPEDANCE MEASUREMENT DRIVE POINTS (DIRECT AND RECIPROCITY)

2.2.1.2.2 *Air-Blast-Wave Engulfment*

a. Pressure Area Zones. The engulfing function developed for the model (Eq. 4) was applied also for the local pressure areas (impedance zones) of the prototype. The only change required was a coarser mesh, owing to the lower cutoff frequency of 300 Hz (Fig. 58).

b. Traveling Wave over a Surface. The traveling wave function, Equation 7, used for the model was applied to the prototype.

2.2.1.2.3 *Response Prediction at First Location*

Response predictions for the prototype were made with Equations 8 and 9 in a manner similar to that used for the model.

2.2.1.2.4 *Response Predictions for Other Locations*

Response predictions for the prototype at other locations were made in a manner similar to that used for the model.

2.2.1.3 Development of Scaling Relationships

Scaling relationships for the 1/12-scale model calculations and DIAL PACK event records of the model PARB are developed in this section. These scaling relationships provide for both geometric scaling and scaling based upon comparison of inertance functions from the model and the prototype from Table 2.

2.2.1.3.1 *Geometric Scaling*

a. Areas

Surface area of the air blast for the model scaled to the prototype is

$$A_p = \lambda^2 A_m \qquad (14)$$

where

A = Area (sq ft)

p = Prototype

m = Model

λ = Scale factor (12)

b. Air Blast

The air-blast pressures from DIAL PACK are scaled for the prototype where pressure amplitudes for model and prototype are equivalent, but the time duration is scaled by λ(12).

$$p_p(t) = p_m\left(\frac{t}{\lambda}\right)$$

$$p_p(\omega) = \lambda\, p_m(\lambda\omega) \qquad (15)$$

c. Inertance Functions

For simplicity, a generalized single-degree-of-freedom model was used to develop the scaling relationship

$$F = \left[\left(M - \frac{K}{\omega^2}\right) - j\frac{C}{\omega}\right]\ddot{X} \qquad (16)$$

$$\mathcal{A}(\omega) = \frac{\ddot{X}}{F} = \left[\frac{\omega^2}{(\omega^2 M - K) - j\omega C}\right] \qquad (17)$$

where

F = Force (lb)

M_p = Mass (lb-sec^2/in.) = $\lambda^3 M_m$

K_p = Stiffness (lb/in.) = λK_m

C_p = Damping (lb-sec/in.) = $\lambda^2 C_m$

λ = Scale factor (12)

$\ddot{X}$ = Accelerations (in./sec^2)

$\mathcal{A}(\omega)$ = Inertance function (in./sec^2-lb)

Substitution in Equation 17 gives:

$$\mathcal{A}_p(\omega) = \frac{1}{\lambda^3}\mathcal{A}_m(\lambda\omega) \tag{18}$$

d. Geometrically Scaled Response

$$\ddot{X}_p(\omega) = \sum_{i=0}^{N}\left\{\frac{1}{\lambda^3}\mathcal{A}_i(\lambda\omega)\left[\lambda^2 A_i \cdot \lambda P_i(\lambda\omega) \cdot Si_i(\lambda\omega)\right] e^{-j\tau_i\lambda\omega}\right\}_m \tag{19}$$

$$\ddot{X}_p(\omega) = \ddot{X}_m(\lambda\omega) \tag{20}$$

$$\ddot{x}_p(t) = \frac{1}{\lambda}\ddot{x}_m\left(\frac{t}{\lambda}\right) \tag{21}$$

where

p = Prototype

m = Model

λ = Scale factor

$\mathcal{A}_i(\lambda\omega)$ = ith impedance function $[\ddot{X}/F_i(\omega)]$

A_i = ith local area of external load

$P_i(\lambda\omega)$ = ith static external pressure load

$Si_i(\lambda\omega)$ = ith local engulfment function $\left[\frac{\sin\left(\frac{n\Delta t\lambda\omega}{2}\right)}{n\sin\left(\frac{\Delta t\lambda\omega}{2}\right)}\right]$

$e^{-j\tau_i\lambda\omega}$ = Traveling wave function $\left[1 + e^{-j\Delta t\lambda\omega} + e^{-2j\Delta t\omega}\ldots\right]$

τ_i = Arrival time of blast wave at local area boundary

2.2.1.3.2 *Scaling by Use of Measured Inertance Functions*

a. Scaling of Areas, Pressures, and Wave Engulfment

Scaling of areas, pressure, and wave engulfment are geometric as presented in Section 2.2.1.3.1.

b. Inertance Function Scaling

Several not-to-scale conditions existed between the prototype and model PARB. These conditions cannot really be quantitatively established, although discussion and identification of each is given in Section 1. A scaling comparison in both magnitude and frequency was made between representative and paired acceptance measurements of the model and prototype buildings. Scaling parameters were determined by keying corresponding model and prototype functions at their peak amplitudes and then iteratively determining amplitude and frequency scale factors for a minimum error difference. The scale factors determined by this procedure are presented in Tables 2 and 3 for each location.

c. Measured Inertance Scaling (not-to-scale effects)

$$\ddot{X}_p(\omega) = \sum_{i=0}^{N} \left\{ \frac{1}{ab^2} \mathcal{A}_i(b\omega) \left[\lambda^2 A_i \cdot \lambda P_i(\lambda\omega) \cdot Si_i(\lambda\omega) \right] e^{-j\tau_i \lambda\omega} \right\}_m \tag{22}$$

$$\ddot{x}_p(\omega) = \frac{\lambda^3}{ab^2} \ddot{x}_m(b\omega) \tag{23}$$

$$\ddot{x}_p(t) = \frac{\lambda^3}{ab^3} \ddot{x}_m\left(\frac{t}{b}\right) \tag{24}$$

TABLE 3. ACCELERATION RESPONSE SCALING, MODEL TO PROTOTYPE, OF GEOMETRIC AND INERTANCE MEASUREMENT SCALE FACTORS

Floor	Acceleration Response Scaling				Difference (Reference Geometric)	
	Inertance		Geometric			
	Fourier Magnitude, λ^3/ab^2	Time History & Shock Spectra, λ^3/ab^2	Fourier Magnitude	Time History & Shock Spectra, $1/\lambda$	Fourier Magnitude, %	Time History & Shock Spectra, %
5th	$\frac{1}{1.11}$	$\frac{1}{11.3}$	1	$\frac{1}{12}$	+10	-6
4th	$\frac{1}{0.98}$	$\frac{1}{12.4}$	1	$\frac{1}{12}$	-2	+3.3
3rd	$\frac{1}{2.87}$	$\frac{1}{40}$	1	$\frac{1}{12}$	+65	+70
2nd	$\frac{1}{1.88}$	$\frac{1}{18.2}$	1	$\frac{1}{12}$	+47	+34

AA 7697

2.2.1.4 Comparison of Prototype Responses to Response Scaled from Model

Acceleration response motions from DIAL PACK records and model calculations are scaled to the prototype calculations and presented in Figures 60 through 67. Scaling was made by inertance function ratios, since geometric scaling did not provide a good fit.

Overall similarity of scaled DIAL PACK and model calculations to prototype calculations is quite good for acceleration-time histories and Fourier magnitude frequency spectra.

Deviations noted in the calculated rise and fall times for time histories involve both data measurements and subsequent processing. Some improvements in technique were applied to the prototype calculations. Differences observable in the Fourier transforms, particularly in the 4th and 3rd floors, are attributable to not-to-scale effects in the prototype and to measurement processing techniques for floor-to-floor transfer functions.

(Text continued on p. 113.)

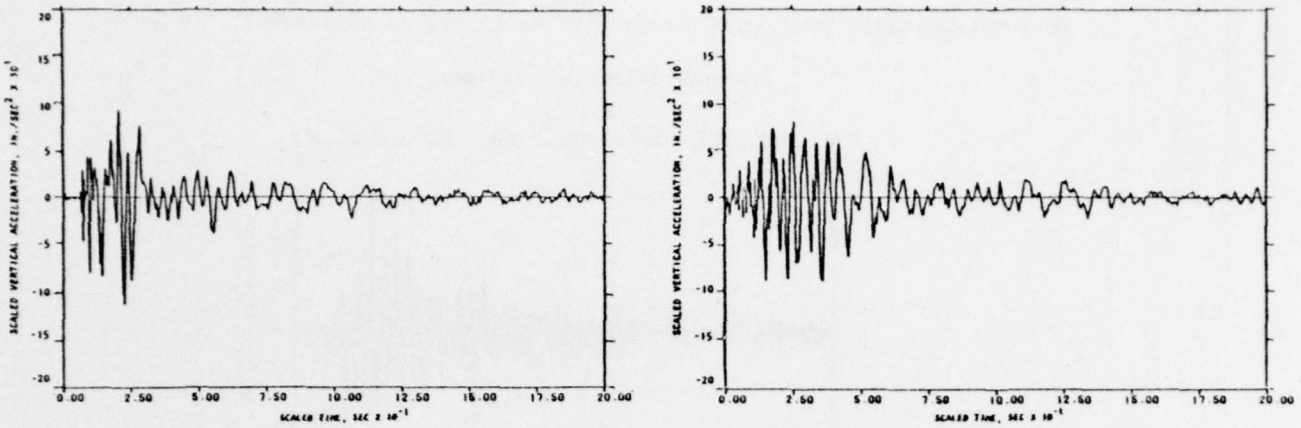

(a) DIAL PACK model response

(b) Predicted model response

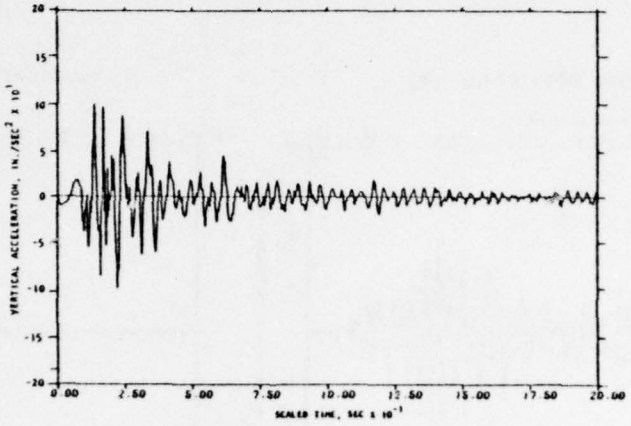

(c) Predicted prototype response

FIGURE 60. COMPARISON OF PROTOTYPE AND SCALED MODEL PARB ACCELERATION-TIME HISTORIES: 5TH FLOOR CENTER

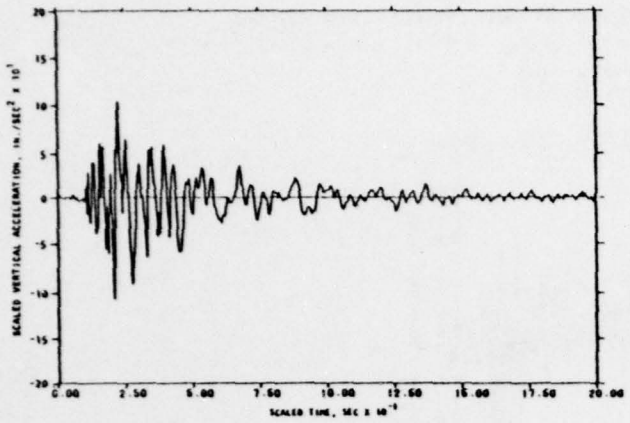

(a) DIAL PACK model response

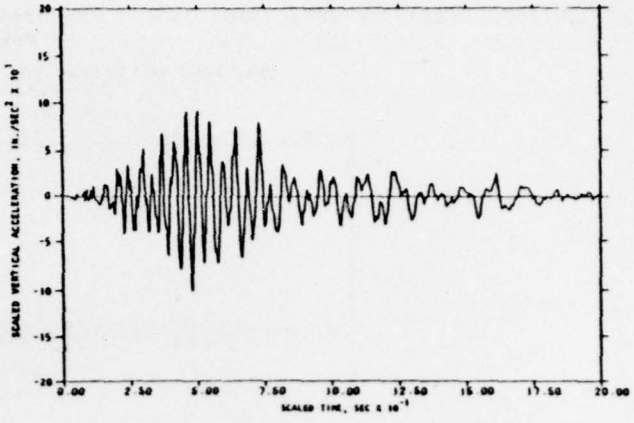

(b) Predicted model response

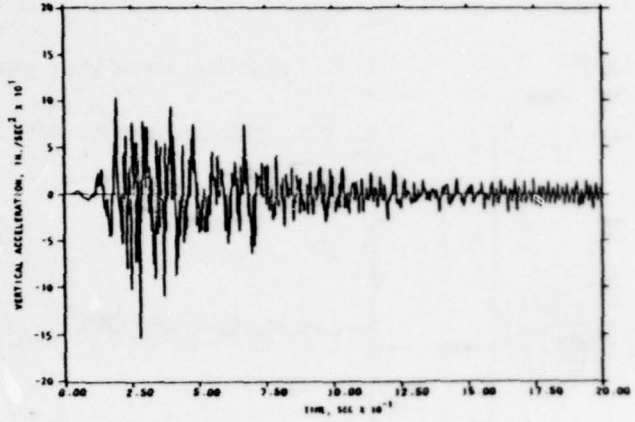

(c) Predicted prototype response

FIGURE 61. COMPARISON OF PROTOTYPE AND SCALED MODEL PARB ACCELERATION-TIME HISTORIES: 4TH FLOOR CENTER

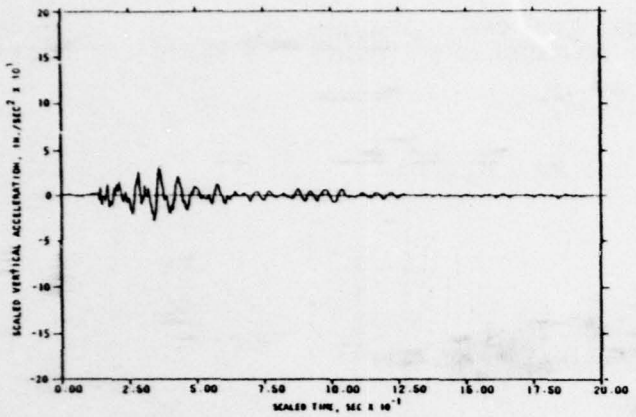

(a) DIAL PACK model response

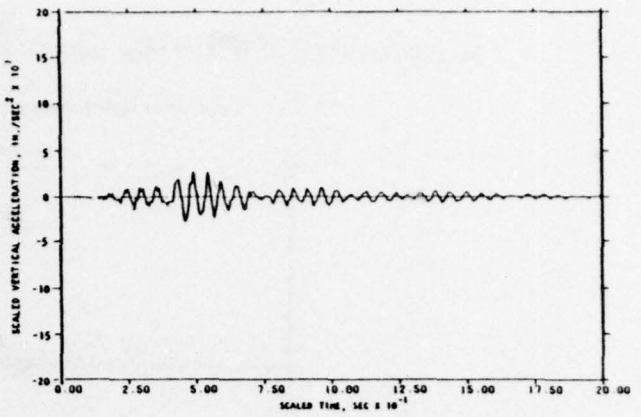

(b) Predicted model response

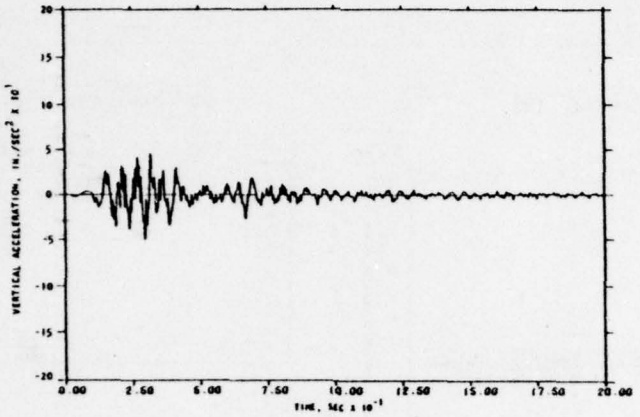

(c) Predicted prototype response

FIGURE 62. COMPARISON OF PROTOTYPE AND SCALED MODEL PARB ACCELERATION-TIME HISTORIES: 3RD FLOOR CENTER

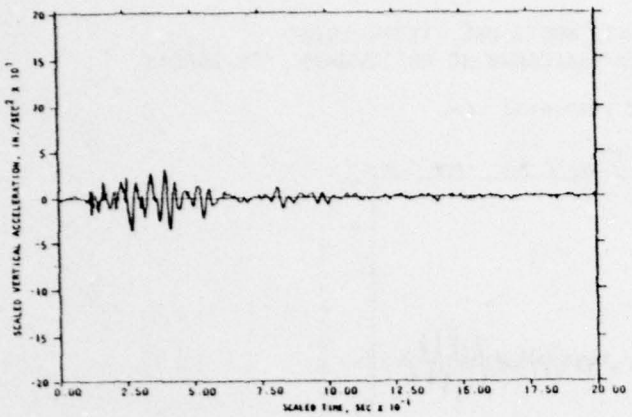

(a) DIAL PACK model response

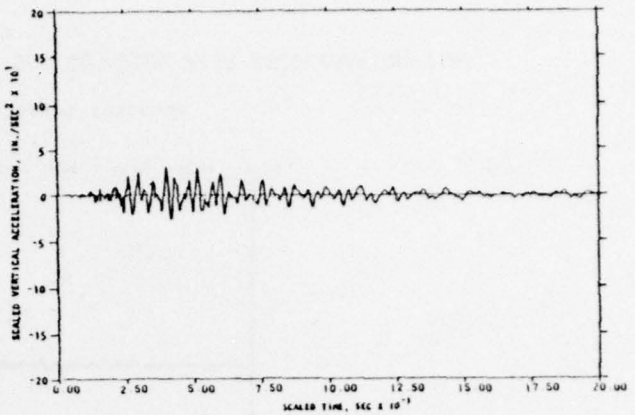

(b) Predicted model response

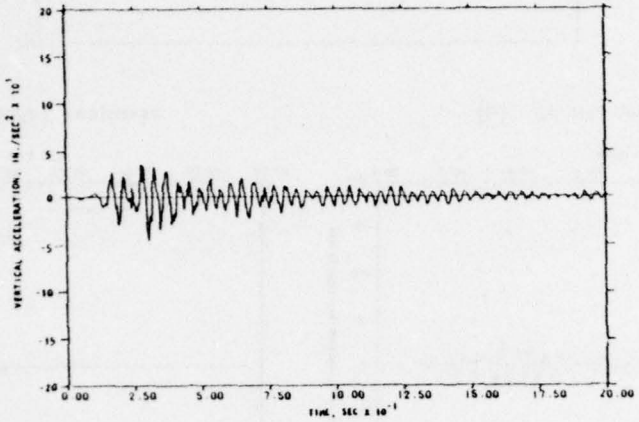

(c) Predicted prototype response

FIGURE 63. COMPARISON OF PROTOTYPE AND SCALED MODEL PARB ACCELERATION-TIME HISTORIES: 2ND FLOOR CENTER

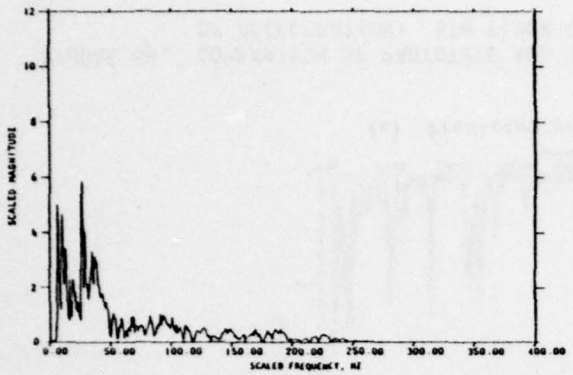

(a) Scaled DIAL PACK model response

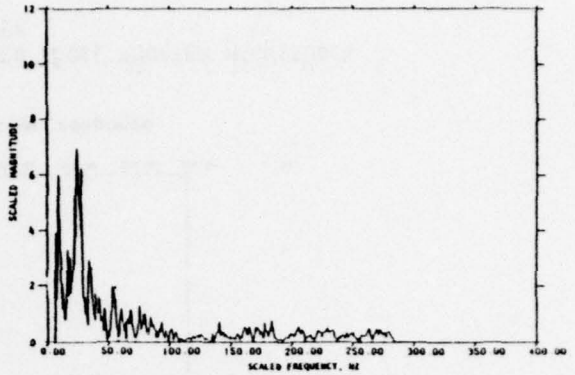

(b) Scaled predicted model response

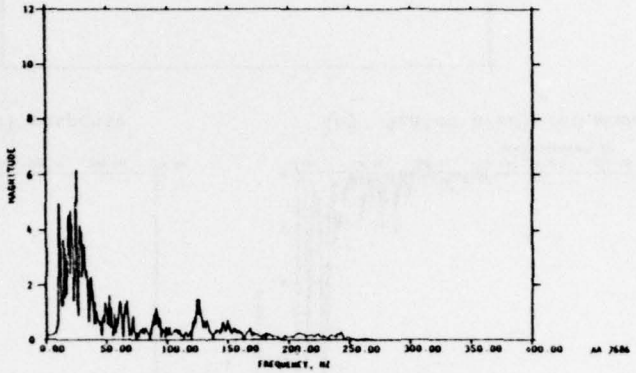

(c) Predicted prototype response

FIGURE 64. COMPARISON OF PROTOTYPE AND SCALED MODEL FOURIER MAGNITUDES OF ACCELERATION: 5TH FLOOR CENTER

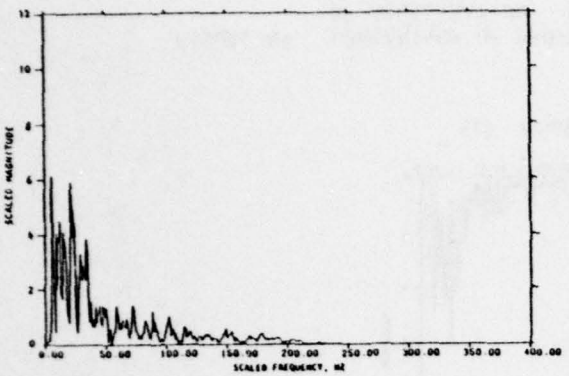

(a) Scaled DIAL PACK model response

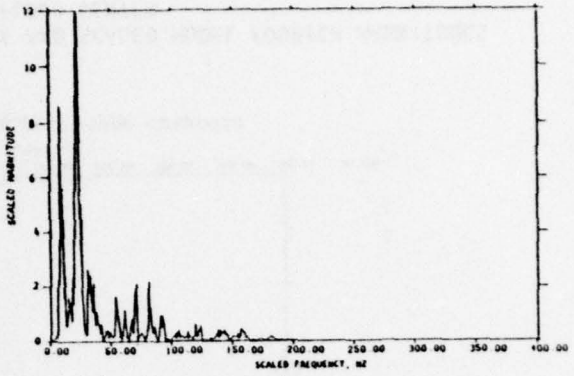

(b) Scaled predicted model response

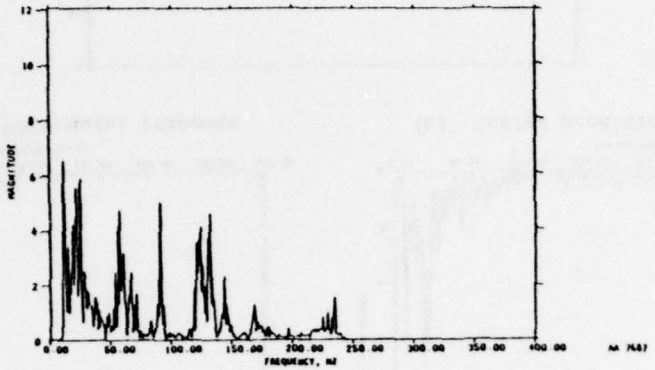

(c) Predicted prototype response

FIGURE 65. COMPARISON OF PROTOTYPE AND SCALED MODEL FOURIER MAGNITUDES OF ACCELERATION: 4TH FLOOR CENTER

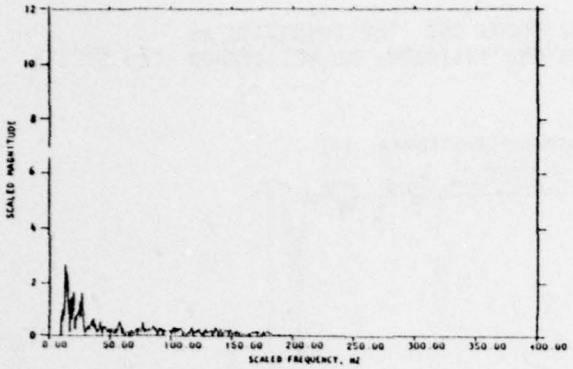

(a) Scaled DIAL PACK model response

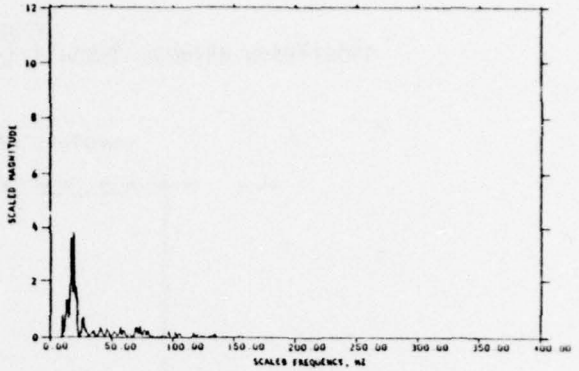

(b) Scaled Predicted model response

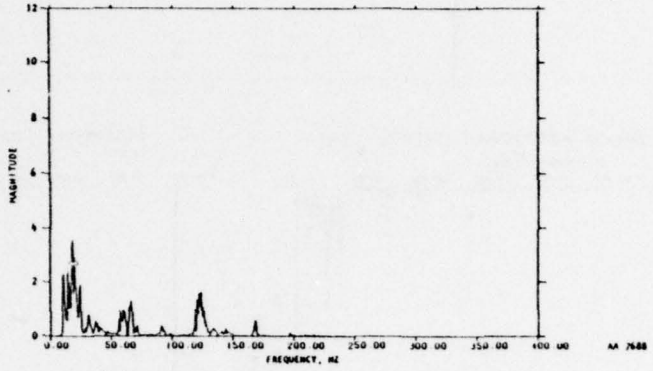

(c) Predicted prototype response

FIGURE 66. COMPARISON OF PROTOTYPE AND SCALED MODEL FOURIER MAGNITUDES OF ACCELERATION: 3RD FLOOR CENTER

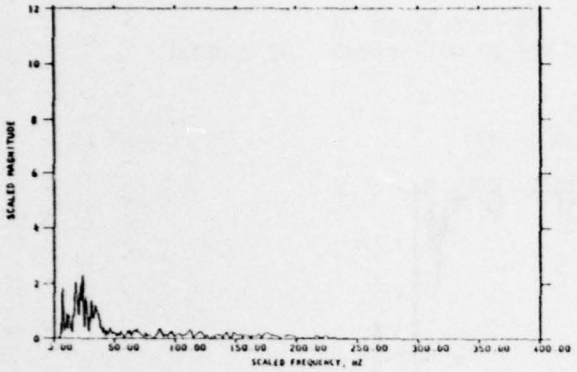

(a) Scaled DIAL PACK model response

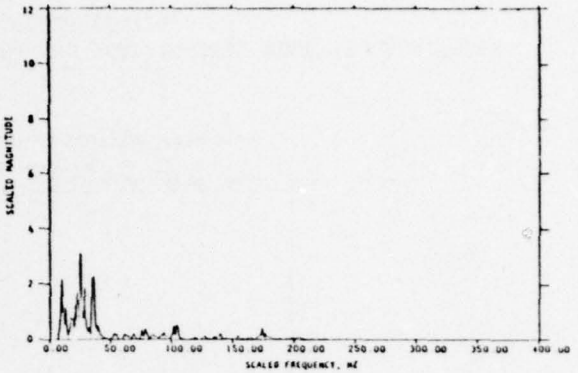

(b) Scaled predicted model response

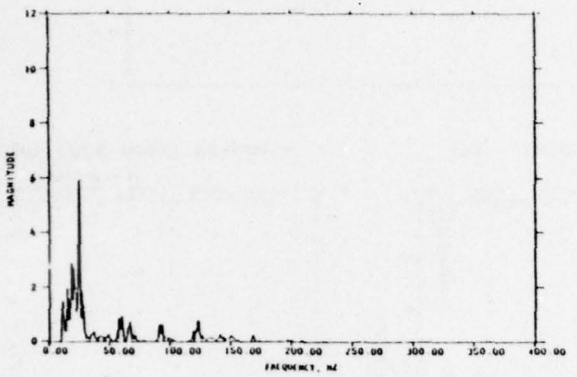

(c) Predicted prototype response

FIGURE 67. COMPARISON OF PROTOTYPE AND SCALED MODEL FOURIER MAGNITUDES OF ACCELERATION: 2ND FLOOR CENTER

2.2.2 RESPONSE OF MASSIVE EQUIPMENT TO SPECIFIED BASE MOTION INPUT CRITERIA

2.2.2.1 Environmental Threat

The shock environments internal to structures at the mounting locations of equipments were specified as undamped shock spectra. The environmental shock spectra selected to test and predict the response of all weapons systems in protective structures were those designated as Annex M and shown in Figure 68a. These worst-case (envelope) environments were chosen because they equal or exceed the envelope of local input shock spectra for all structures of the system at practically all frequencies, and are therefore considered the reference shock spectra.

For analysis and test, a time history (acceleration, velocity, or displacement, versus time) is required as input to predict and measure platform motion. However, the specified envelope spectrum (Annex M) is generalized to envelop numerous threat histories. Such lack of uniqueness therefore requires that many tests or calculations be made. An alternative was developed by Yang (Ref. 38) to generate a synthesized time history that populates specified shock spectra for the protective structures and thereby assures a conservative, or worst-case, test. This synthesized time history is the summation of a series of oscillations at selected frequencies over the range of the shock spectra. Oscillations at each frequency are from 1-1/2 oscillations (3 one-half cycles) to 6-1/2 oscillations (13 one-half cycles). The amplitude of these oscillations is constrained to a sine-beat envelope. Synthesized waveforms that populate the input shock spectra of Annex M are shown in Figure 68b.

2.2.2.2 Response Predictions

The motions of the 10 shock-isolated platforms were calculated with input from both the overall Annex M motion and the specified local motion for each platform location. In the frequency domain, the input functions are multiplied by the system functions, followed by an inverse Fourier transformation to obtain the platform acceleration-time history. In the time domain, input time history of the building is convolved with the platform impulse function.

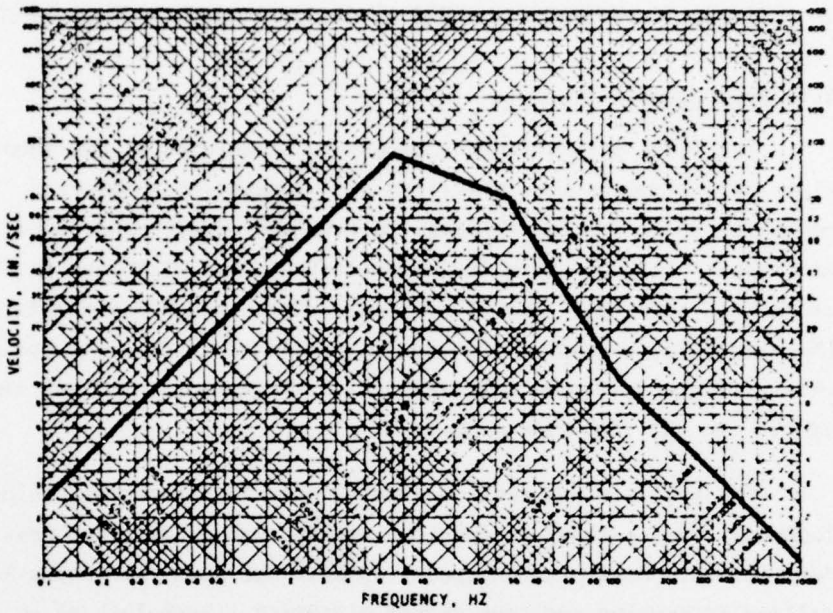

(a) Annex M shock spectrum, vertical axis

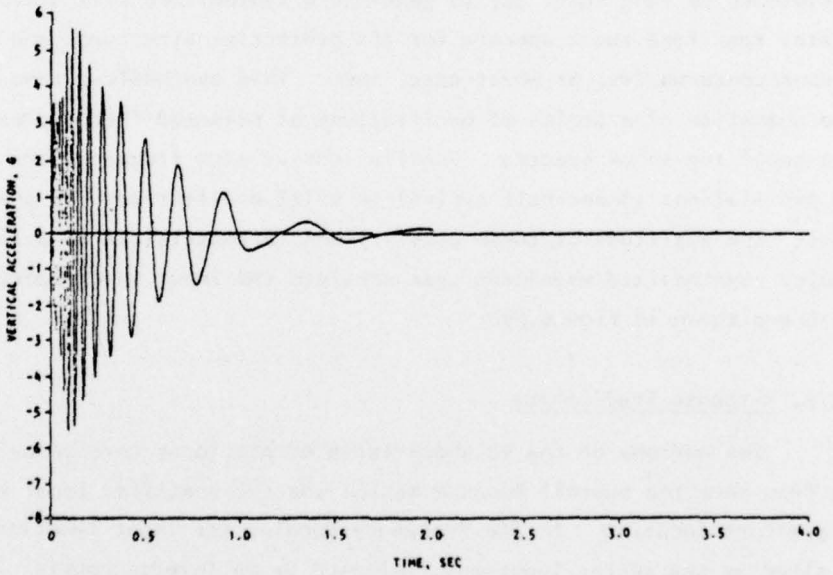

(b) Synthesized waveform, vertical acceleration time history to match Annex M shock spectrum

FIGURE 68. VERTICAL OVERALL (ENVELOPE) BUILDING INPUT MOTION FOR ALL WEAPON SYSTEMS EQUIPMENT

These data are displayed as motion-time histories, shock spectra, and Fourier magnitudes. Two examples of platform motions predicted from measurements will be discussed in this section.

Response motions were determined by the following:

$$\ddot{X}_R(t) (=) \ddot{x}_R(\omega) = \tau(\omega) \ddot{x}_i(\omega)$$

where

$\ddot{X}_R(t)$ = Acceleration-time history response of platform at reference point

$\ddot{x}_R(\omega)$ = Acceleration-frequency response of platform at reference point

$\ddot{x}_i(\omega)$ = Input building acceleration, Annex M or local, Fourier-transformed to frequency domain

$\tau(\omega)$ = Measured overall transfer function of platform

As discussed previously, the load path from each isolator was measured from the isolator/building junction to a reference point on the platform. These measurements were summed for all isolators of a platform to give an overall (or global) transfer function. This implies that the building input motion is uniform and in phase over the area covered by the platform. Such an assumption was required because the building areas covered by each platform specify a uniform input into each isolator. Alternatively, each transfer-function path and the building input motion at each attachment point could have been individually computed and all computations summed to determine the results. The dual of the above equation is the convolution integral from which the identical platform response may also be computed as:

$$\ddot{x}(\omega) (=) \ddot{X}(t) = \int_0^T h(t - \tau) \ddot{X}_i(\tau) \, d\tau$$

where

t, T = Time

$\ddot{X}(t)$ = Acceleration-time history response of platform at reference point

$\ddot{x}(\omega)$ = Acceleration-frequency response of platform at reference point

$h(t)$ = Measured impulse function of platform (transformed from transfer function $\tau(\omega)$)

$\ddot{X}_i(t)$ = Input building acceleration, Annex M or local (Appendix A)

τ = Time delay function for the convolution operation

In effect, this convolution corresponds to shifting two functions and computing the integral of its product with the other time history as t ranges from 0 to T. The total duration of platform response is equal to the duration of the impulse function plus the duration of input time history.

Response motion predictions of the control room platform of the PAR Power Plant is displayed in Figures 69 through 71. Acceleration-time histories for the frequency band 35 Hz to 500 Hz and 0.5 Hz to 500 Hz are included in Figures 69a and 69b. In the displacement-time history (Fig. 69c), it is noted that the peak-to-peak displacement is less than ± 1 in. These peak values must be considered conservative or upper bound, in view of the nonlinearities in the low frequencies as previously discussed. Rigid-body design limits for platforms is ± 6 in. The shock spectrum and Fourier spectrum for this platform response is provided in Figures 70 and 71.

Acceleration-time history response of Platform D represents two methods of determination. Figure 72 was developed by a finite-element computer model and Figure 73 was obtained at Waterways Experiment Station. Both time histories employed Annex M input motion to the platform. Rigid-body modes and properties of vertical, roll, and pitch were analytically inserted for the low frequencies of the measured data to provide comparability between the figures, most particularly for shock spectra. The shock spectra of Figure 74 are computer-model and measured-data response predictions.

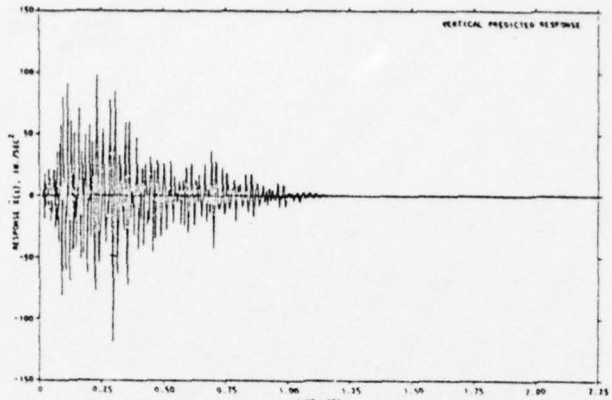

(a) Platform PARPP-CR: Predicted acceleration-time history response, using the computed global transfer function convolved with Annex M input (frequency range 35 to 500 Hz)

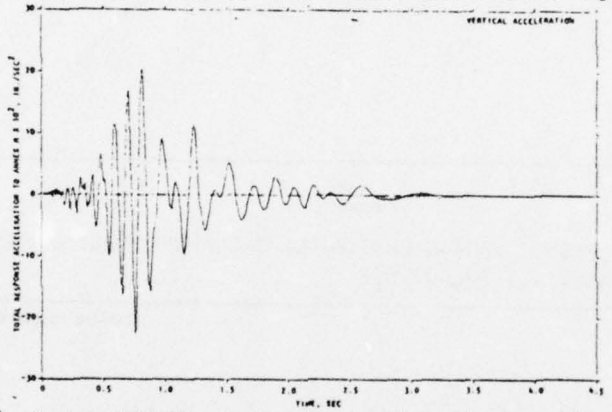

(b) Platform PARPP-CR: Acceleration-time history for Annex M input (frequency range 0.5 to 500 Hz)

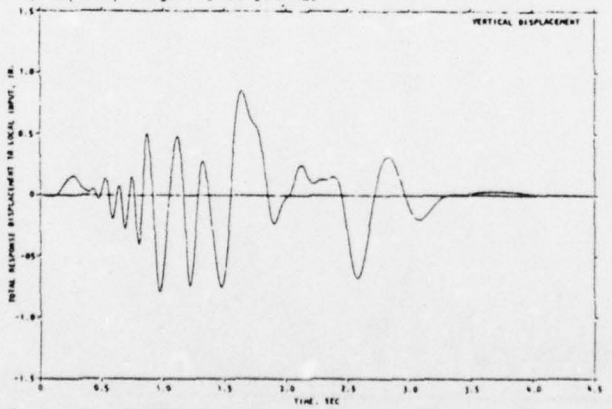

(c) Platform PARPP-CR: Displacement-time history for local input (frequency range 0.5 to 500 Hz)

FIGURE 69. RESPONSE MOTION PREDICTION OF CONTROL ROOM IN PAR POWER PLANT

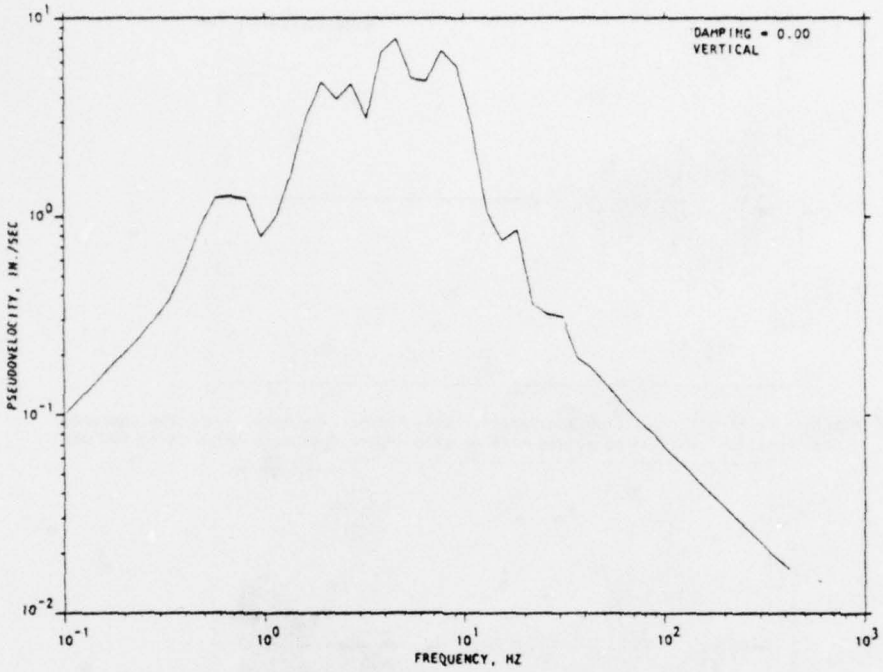

FIGURE 70. PLATFORM PARPP-CR: VERTICAL-RESPONSE SHOCK SPECTRUM FOR ANNEX M INPUT (FREQUENCY RANGE 0.5 TO 500 HZ)

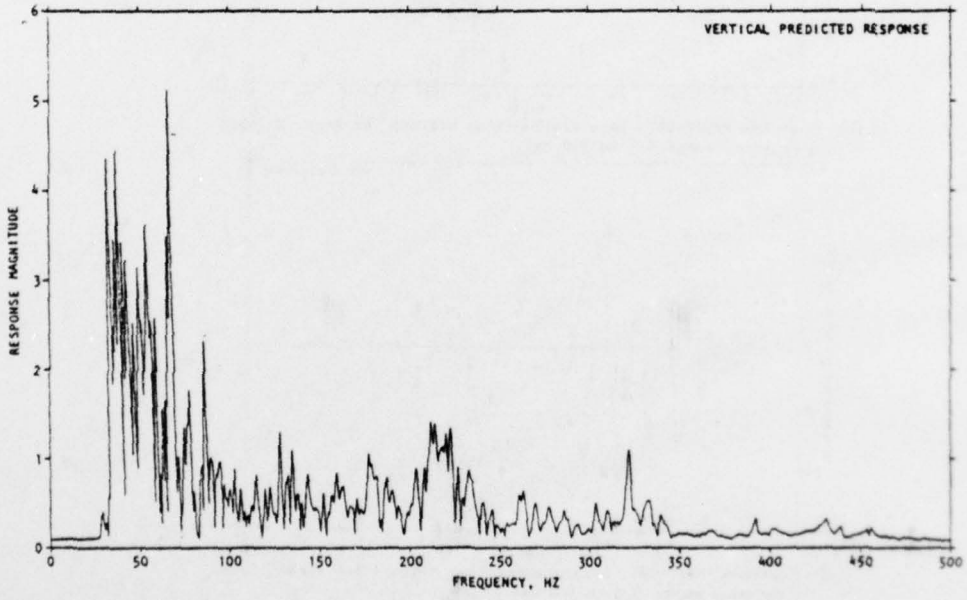

FIGURE 71. PLATFORM PARPP-CR: PREDICTED ACCELERATION FOURIER RESPONE MAGNITUDE, USING THE GLOBAL TRANSFER FUNCTION CONVOLVED WITH ANNEX M INPUT (FREQUENCY RANGE 35 TO 500 HZ)

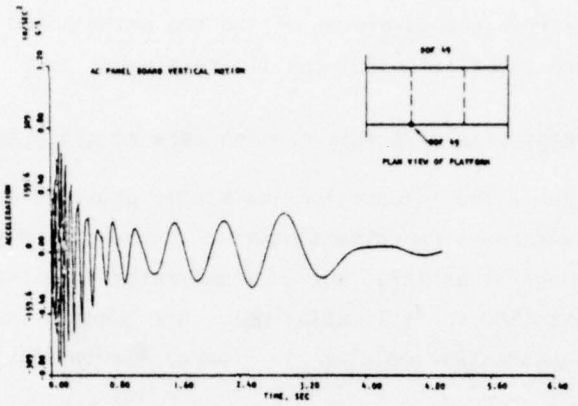

FIGURE 72. PAR POWER PLANT, PLATFORM D: ACCELERATION-TIME HISTORY RESPONSE COMPUTED BY FINITE ELEMENT METHOD

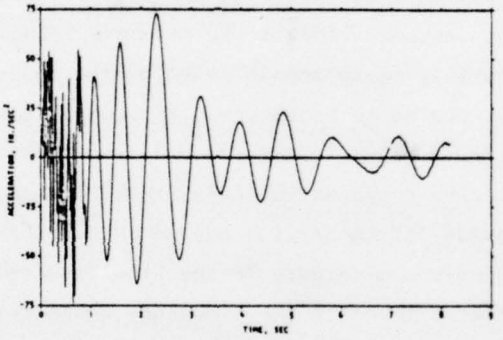

FIGURE 73. PAR POWER PLANT, PLATFORM D: ACCELERATION-TIME HISTORY RESPONSE, ANALYTIC 0 TO 10 HZ AND TRANSFER FUNCTION MEASUREMENT 10 HZ TO 150 HZ

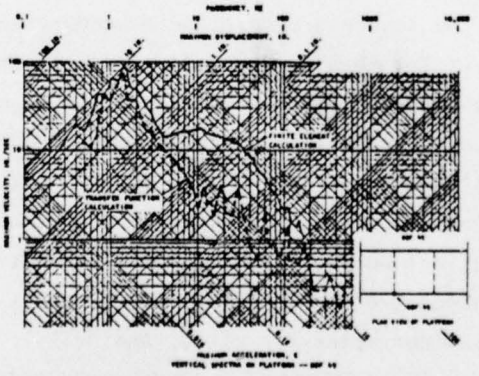

FIGURE 74. PAR POWER PLANT, PLATFORM D: FINITE-ELEMENT SHOCK SPECTRUM RESPONSE CALCULATION COMPARED WITH SHOCK SPECTRUM FROM TRANSFER FUNCTION MEASUREMENTS

Differences result from the waveforms of the two methods and the higher magnitudes of motion prediction for the finite element case.

2.2.3 RESPONSE PREDICTION OF A SOIL-COVERED ARCH TO AIR BLAST

This unpublished information was kindly provided by Robert E. Walker of the U.S. Army Waterways Experiment Station, Vicksburg, Mississippi. Several 1/3-scale model hangarettes (Fig. 50) were subjected to air-blast pressures in EVENT MIXED COMPANY (500-ton TNT explosion). Air-blast pressure records taken from one of the hangarettes are given in Figures 75a to 75d.

Mobility measurements (V/F) were made from the inside surface of the reinforced-concrete arch to soil surface near the locations of the air-blast pressure gages on a full-size structure. Using these measurements in a reciprocity sense (assumed linearity), response velocity predictions were made from the mobility measurements taken on the full-scale structure. The air-blast data was scaled to prototype. For comparison to velocity records of the arch in the MIXED COMPANY Tests, the full-scale predictions were scaled to the models. The scaled response velocity at the mid-arch position is given in Figure 76. To provide for comparison between MIXED COMPANY recorded velocity and the predictions of Figure 76 the predicted velocity-time history had to be lowpass filtered to match the frequency characteristics of the velocity gages used in the test. Test data and predictions are shown in Figures 77 and 78.

Walker used the response prediction procedure set forth in Equation 8 of Section 2.2.1, except for the local engulfment function. This omission may account for the late-time oscillation occurring at 125 msec in Figures 76 and 78. The prediction using mobility measurements in addition to the scaling employed shows surprising good agreement with actual data. It can also be concluded that soil nonlinearity for this test and at these pressure levels exerts only a moderate influence. Late-time displacement of the test record (275 msec) cannot be accounted for at this time, since it is not known whether the gage record has been corrected for offset and drift. Additionally, the mobility measurements were not low enough in frequency pick-up ground roll.

(Text continued on p. 125.)

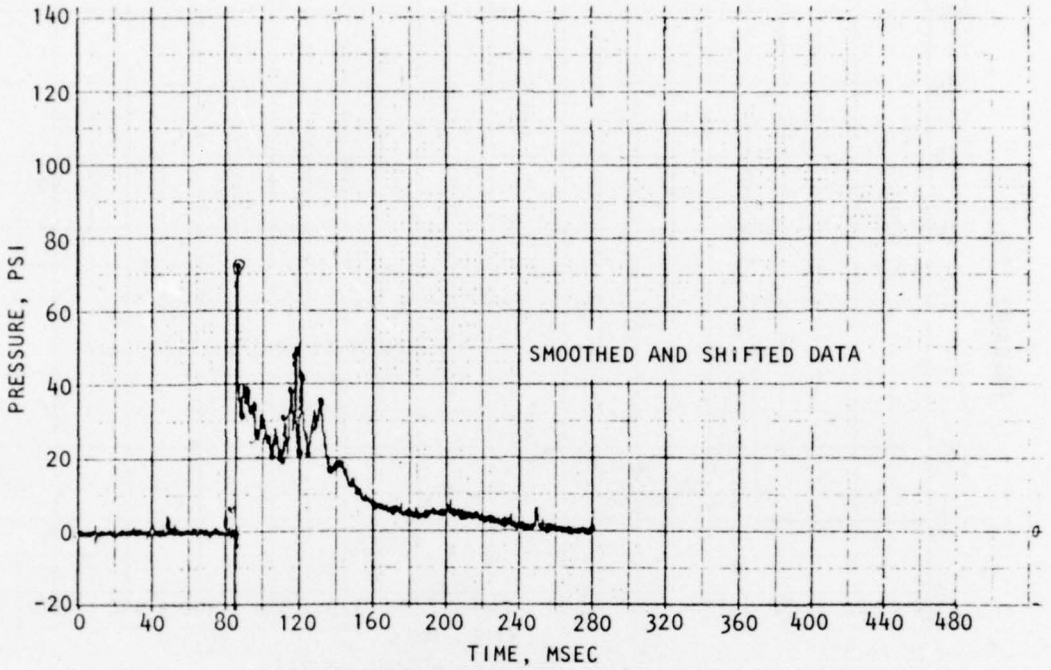

(a) Hangarette Station 418

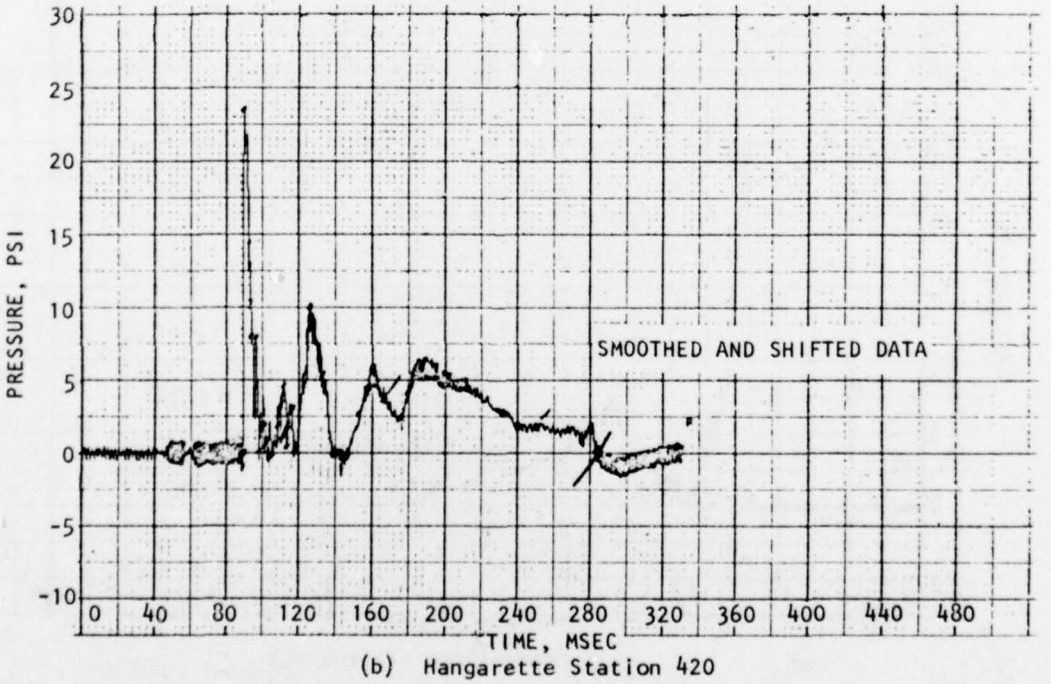

(b) Hangarette Station 420

FIGURE 75. RECORDED AIR-BLAST PRESSURES ON HANGARETTE FROM *MIXED COMPANY* EVENT (500-TON TNT TEST (See Fig. 50)

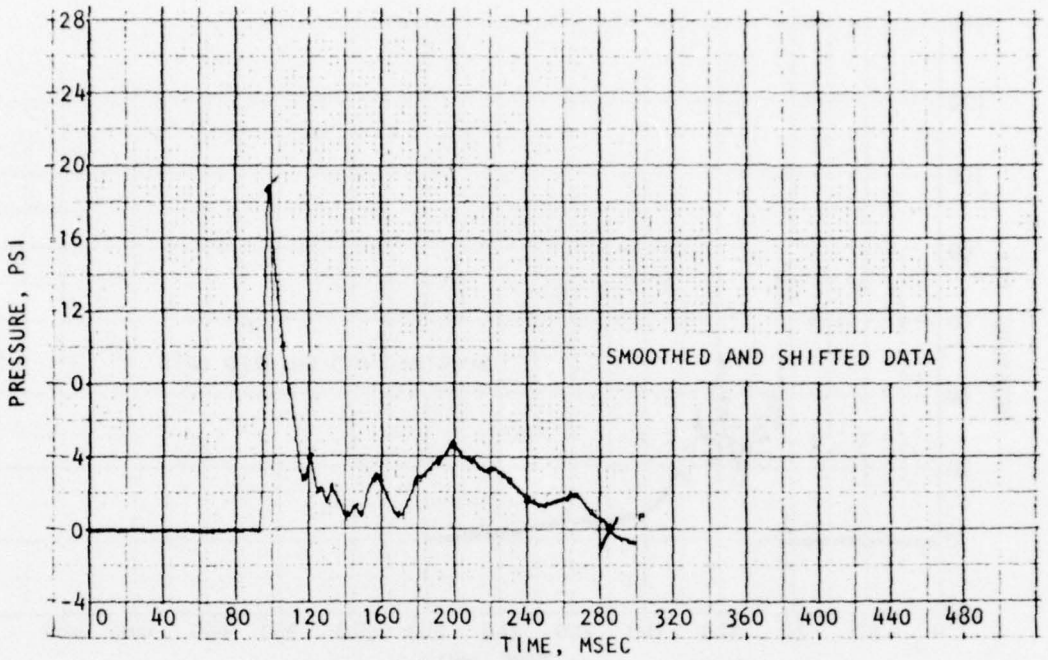

(c) Hangarette Station 421

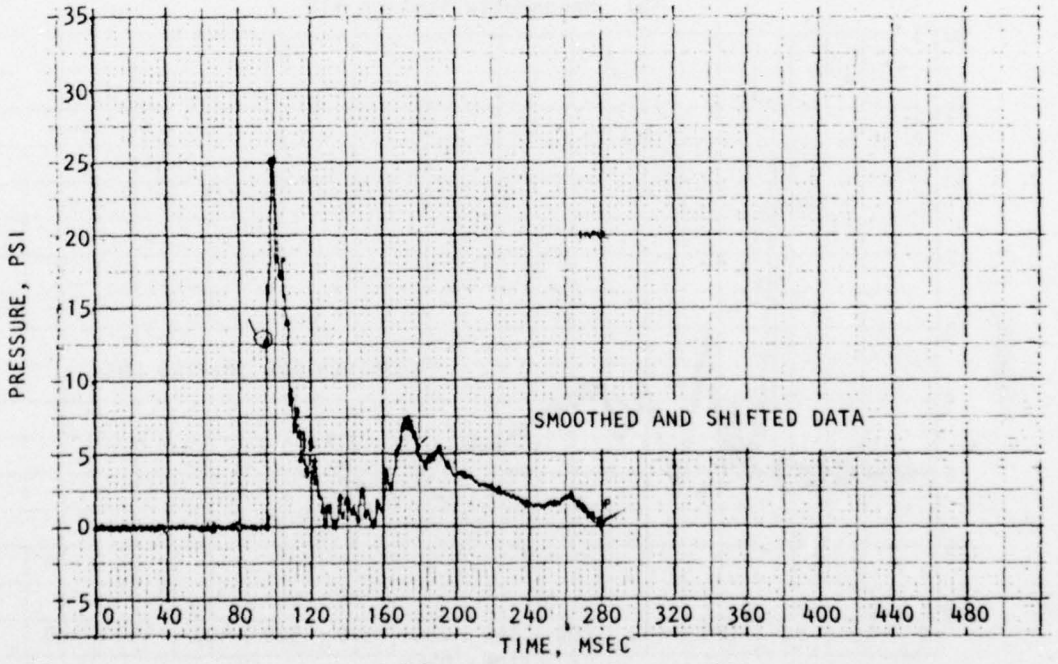

(d) Hangarette Station 422

FIGURE 75. (CONCLUDED)

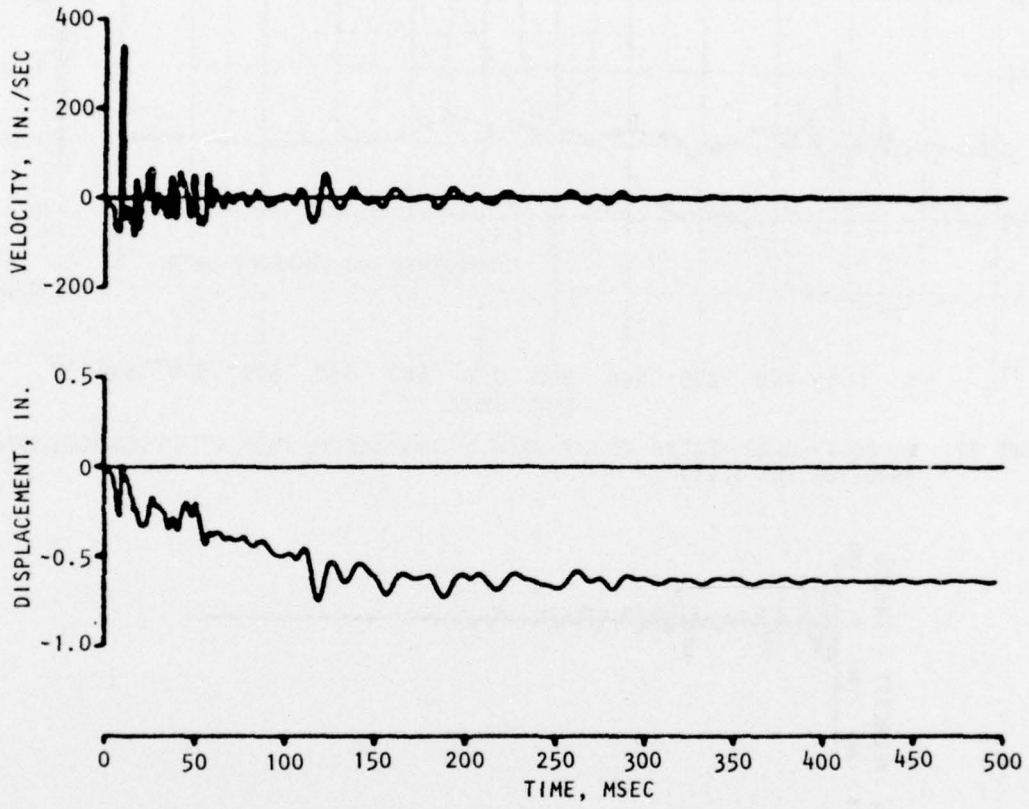

FIGURE 76. VELOCITY MOTION PREDICTION AT MID-ARCH FROM MOBILITY MEASUREMENTS (V/F) ON HANGARETTE (Courtesy Waterways Experiment Station)

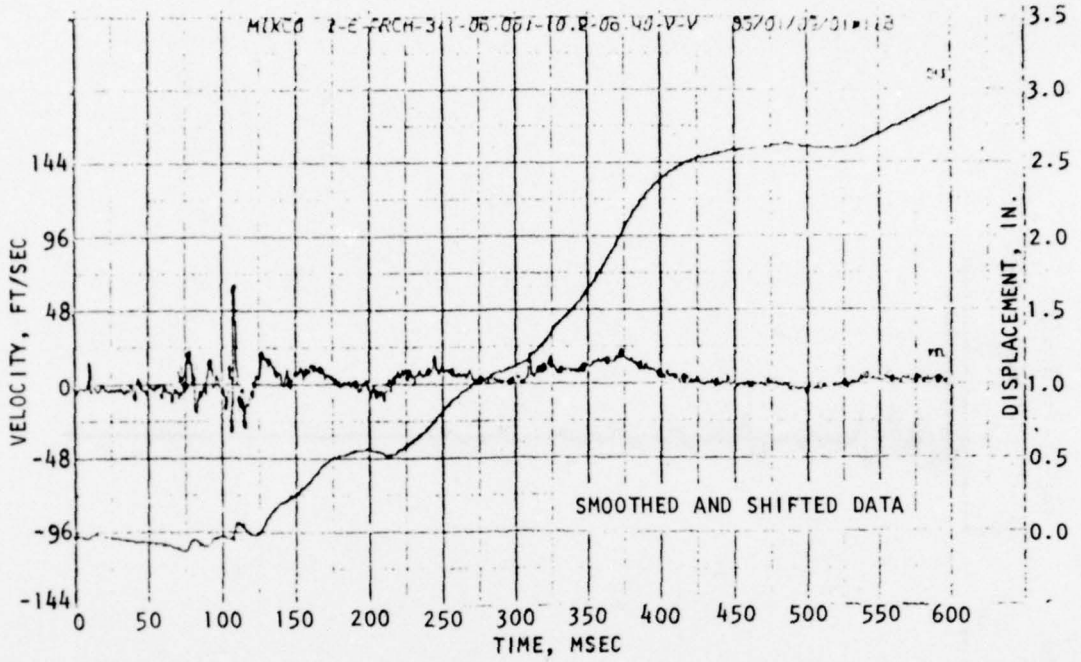

FIGURE 77. VELOCITY GAGE RECORD AT MID-ARCH OF HANGARETTE FROM *MIXED COMPANY* EVENT (500-TON TNT TEST)

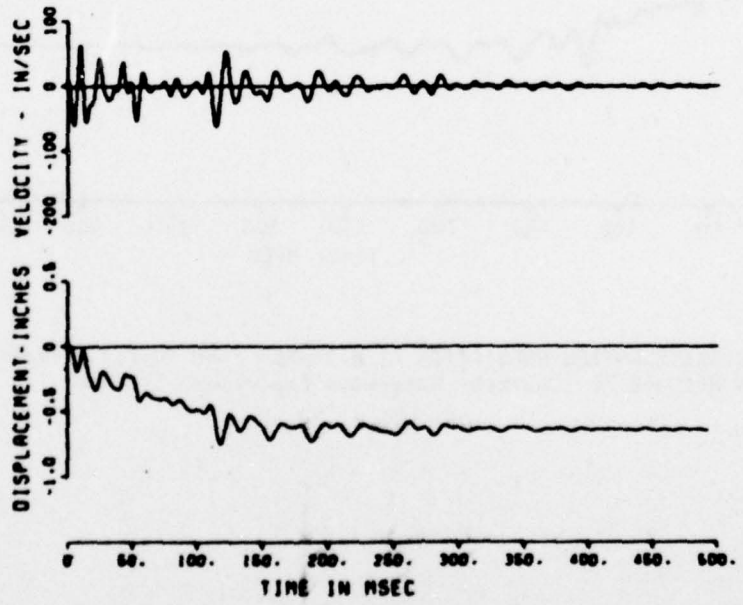

FIGURE 78. VELOCITY MOTION PREDICTION FROM MOBILITY (V/F) MEASUREMENTS ON HANGARETTE (Velocity low-pass filtered to match velocity gage frequency response of Fig. 77) (Courtesy Waterways Experiment Station)

2.3 SIMULATION OF STRUCTURAL MOTIONS

2.3.1 METHOD

Transient shock tests on equipment and systems to simulate the motions induced by a nuclear event or an earthquake are largely limited to single-axis test machines.* Further limitations exist in the size and weight of equipment which can be tested. Simulating multiaxis loading on large equipment with many degrees of freedom represents a difficult problem, because it is impractical to generate continuously varying forces of sufficient magnitude. This problem is further aggravated where in-place or field tests are required. On the other hand, short-duration forces of large magnitudes over a wide frequency range can be generated by mechanical pulse generators (Ref. 6). Since a discrete number of pulses superficially presents an appearance quite different from a continuous excitation signal, it becomes necessary to select the pulses in such a way that the resulting vibration of the structure matches as closely as possible the response (e.g., displacement, velocity, or acceleration) produced by the continuous force, as determined by an appropriate error criterion. This approach is shown in Figure 79.

It is important to note that the method of Figure 79 requires that the criterion response to the continuous input be known, which would generally not be true in practice. To accomplish this objective, the approach proposed here assumes that: (1) a mathematical model of the system under study is known, and (2) the inputs of interest (e.g., earthquake or nuclear blast) are given. Under these conditions the "criterion response" can be calculated and used to obtain the pulse train for the simulated test.

In general, the response-time history of a test article under simulated test should show a reasonable approximation to the expected environmental phenomena for meaningful hardness/vulnerability evaluation.

*A few biaxial and triaxial test machines are available.

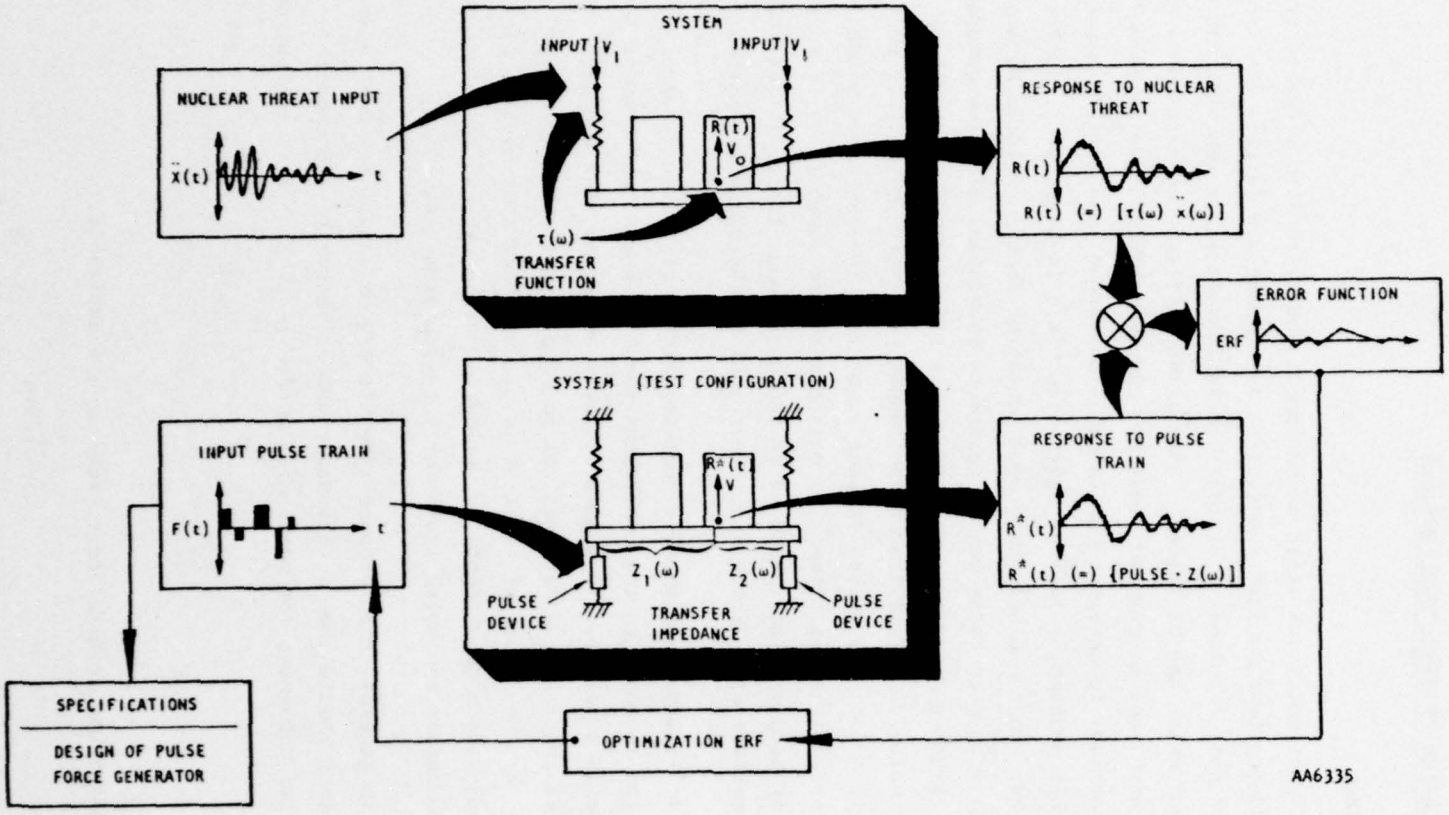

FIGURE 79. DATA FLOW TO SIMULATE PREDICTED RESPONSE OF PLATFORM TO A NUCLEAR THREAT

2.3.2 PULSE-SIMULATION ENVIRONMENTAL TESTS

The need for a mechanical force-pulse generator arose in connection with studies on how to effectively simulate, by physical test, shock transients on massive equipment located in protective structures. The force generators could not, for physical reasons, be interposed between the equipment and the building. The platform environments represent the building motions generated by nuclear attack as transmitted into the equipment through the isolation system.

By drawing a metal bar or mandrel through a cutting tool (or vice versa) with suitable motive power (air pressure, hydraulic pressure, explosive force, electrical, mechanical), a series or a set of force-time histories may be generated (Refs. 6, 39). Reaction at the attachment points of the device transmits a force output to the structure under test. Figure 80 illustrates the device using motive power supplied by the stored energy in a pneumatic cylinder. Amplitude, duration, and shape of the pulse time histories are controlled by the relative velocity between the cutting tool and the metal projection on the mandrel, and by the shape of the metal projection on the mandrel. A photograph of the pulse generator installed for in-place testing is shown in Figure 81.

Large forces may be generated from this device. Force required to cut metal is largely independent of rate (velocity), and is a function of the volume of chips cut (depth, width, and length of cut) and a function of the specific energy of cutting a material. A load cell or strain gage may be incorporated in series with the device to provide a force-time history readout as the device is operated.

Another form of pulse generator is sketched in Figure 82 and pictured in Figures 83 and 84. This form is a variation of the drop shock test machine but differs by generating multiple pulses. Expected capacity of the design of Figure 82 is 70,000-lb force; and with design modifications of the nubbins and cutter, 150,000-lb force output is expected. Currently the machine is used to generate very low frequency response of large structures

(Text continued on p. 133.)

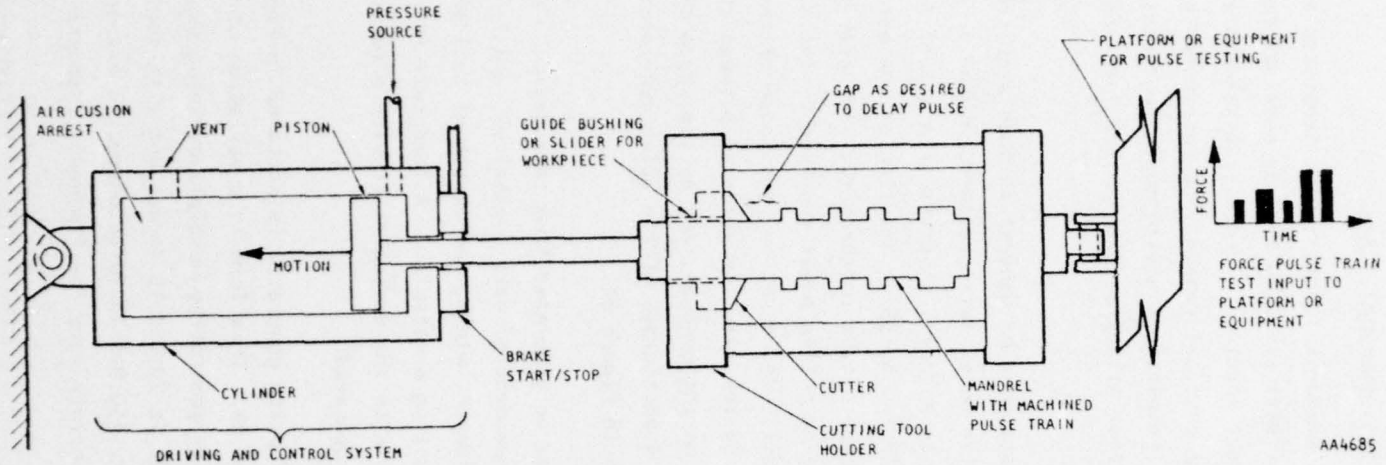

FIGURE 80. PULSE-FORMING DEVICE WITH DRIVING AND CONTROL SYSTEM

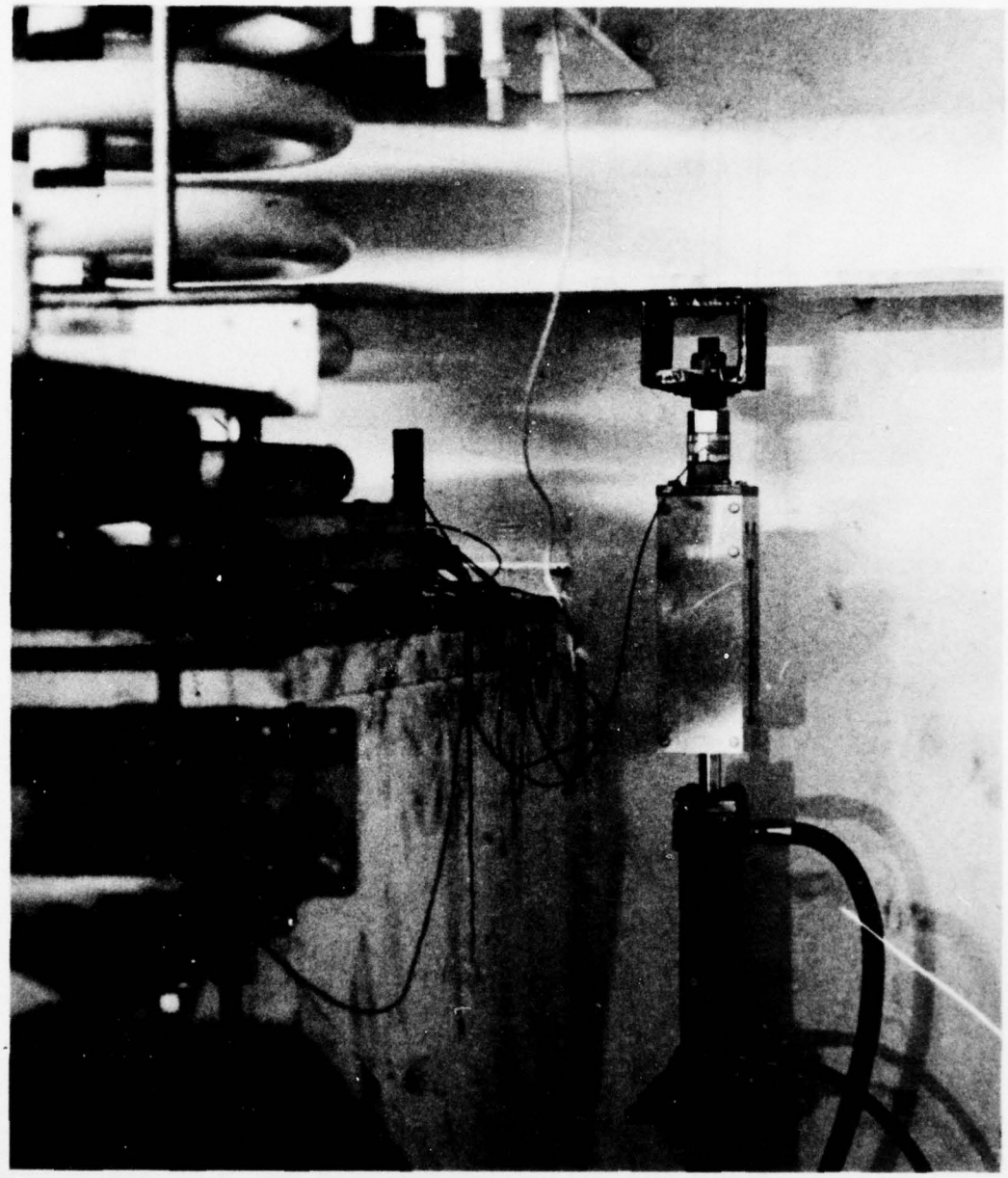

FIGURE 81. PULSE-TEST CONFIGURATION FOR CONTROL ROOM PLATFORM SHOWING ONE OF FOUR UNITS REQUIRED

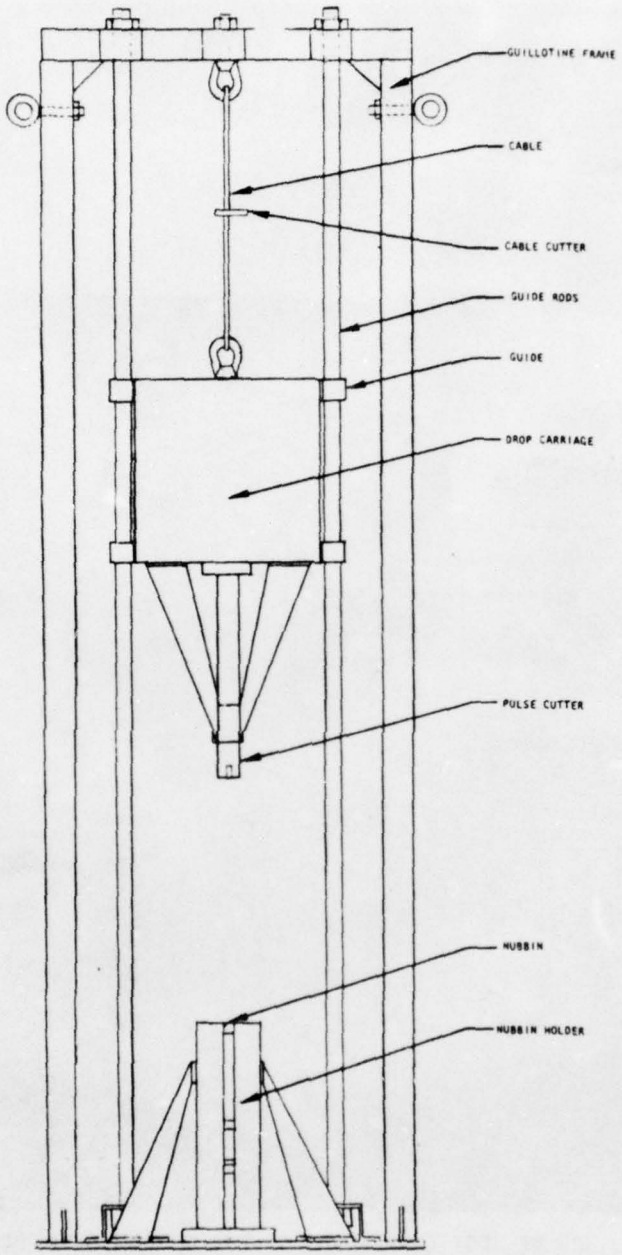

FIGURE 82. SKETCH OF MEDIUM-FORCE OUTPUT PULSE GENERATOR

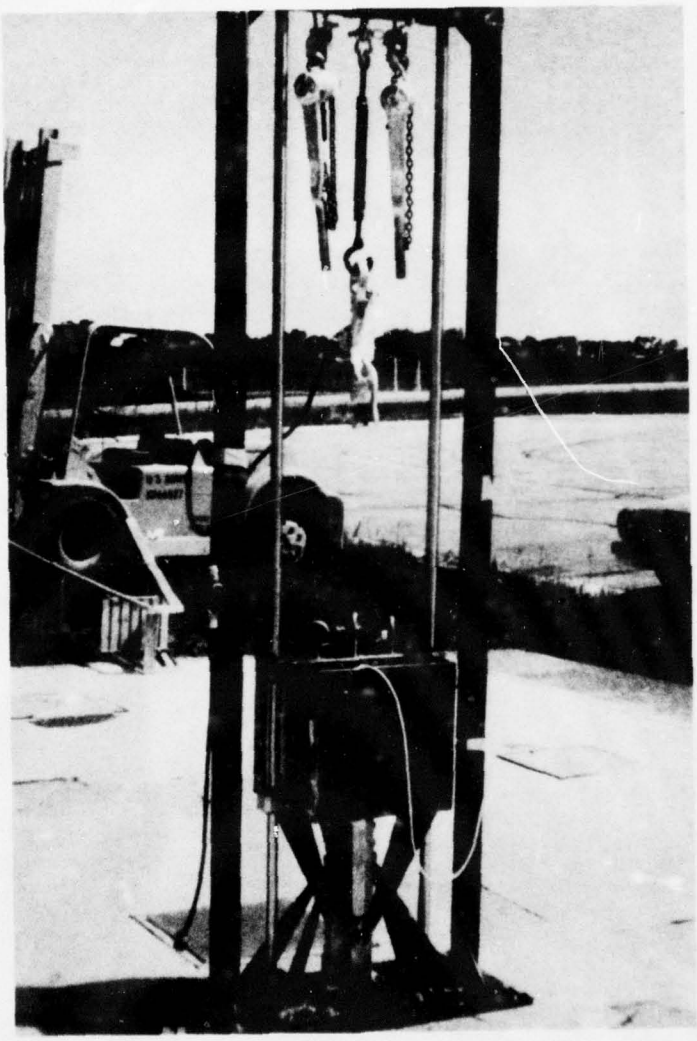

FIGURE 83. MEDIUM FORCE PULSE GENERATOR MOUNTED ON EDC STRUCTURE (Fig. 45)

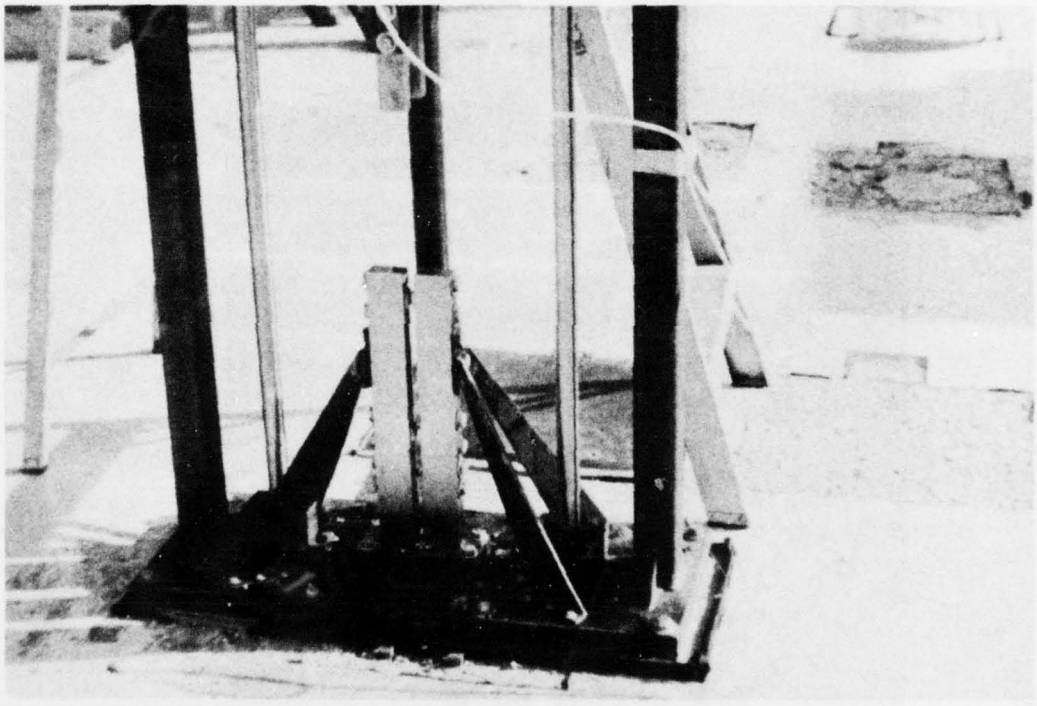

FIGURE 84. MEDIUM FORCE PULSE GENERATOR

where the force output of vibration machines is very low. This drop shock generator is so new that performance information is limited to the oscillograph data of Figure 85. Figure 85 records data taken on the Electrical Distribution Center shown in Figures 45 and 46.

Four pulse generators of Figure 81 were used for shock-isolated platform tests (Fig. 39) and were attached near the four corners of each platform. The schematic of the pulse generator and power-actuation system is given in Figure 86. Power to the pulse generators was provided by hydraulic cylinders having volumetric compensators in series. All four units were connected in series by metal piping. A pneumatic-hydraulic accumulator provided stored energy to drive the generators at line pressures to 1000 psi. Pulse-initiation timing was accounted for by pre-positioning each cutter/mandrel and performing calibration runs of the entire pulse system for each platform configuration.

For the in-place pulse-simulation process, a discrete number of pulses appears quite different from a continuous excitation signal. It is necessary, therefore, to select the pulses in such a way that the resulting vibration of the platform matches as closely as possible the response (i.e., displacement, velocity, or acceleration) produced in the platform by the continuous excitation resulting from the building motion (nuclear threat input). The accuracy of simulation is determined by an appropriate error criterion as shown in Figure 79.

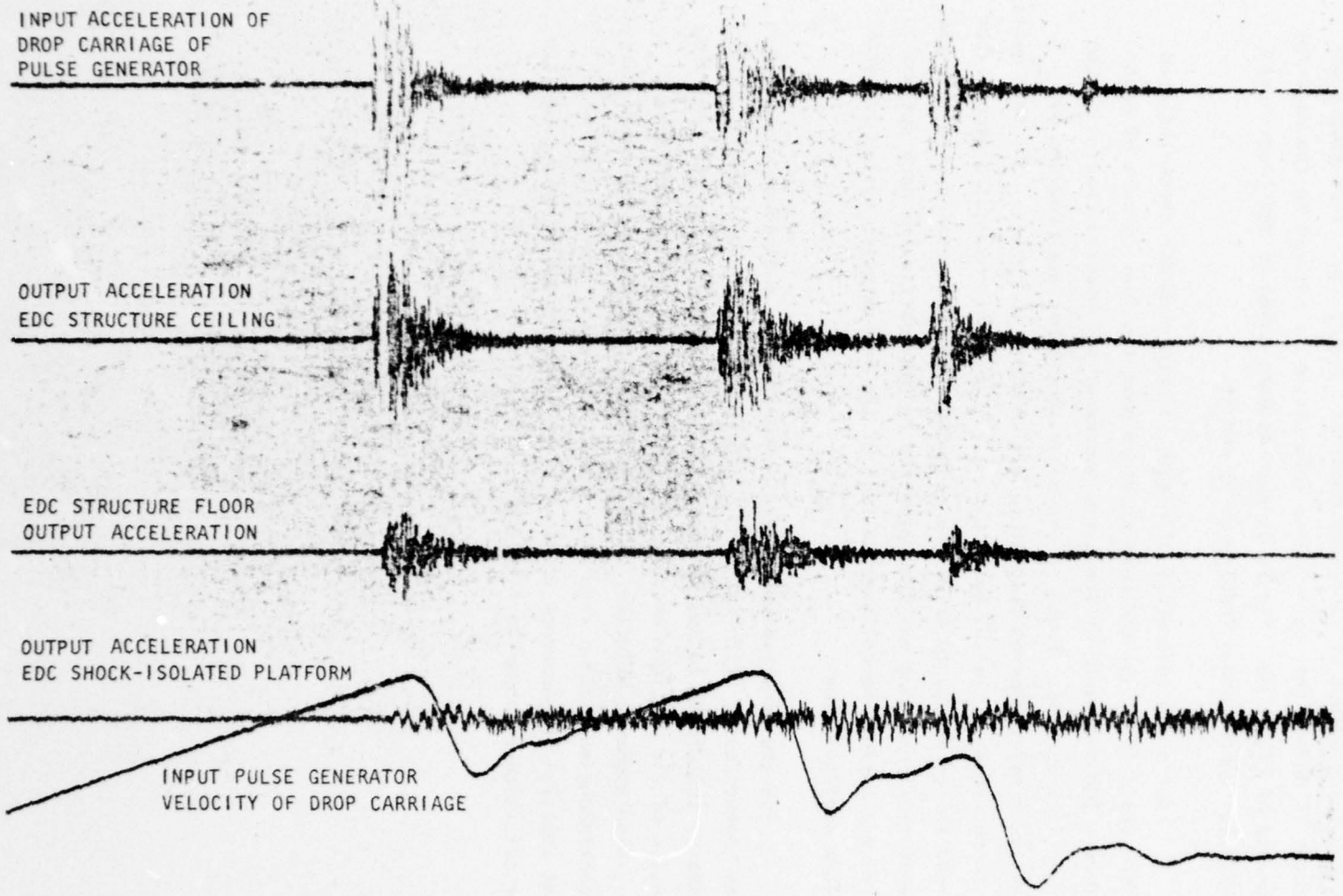

FIGURE 85. OSCILLOGRAPH RECORDS AMPLITUDE-TIME HISTORIES OF DROP CARRIAGE AND EDC STRUCTURE RESPONSE

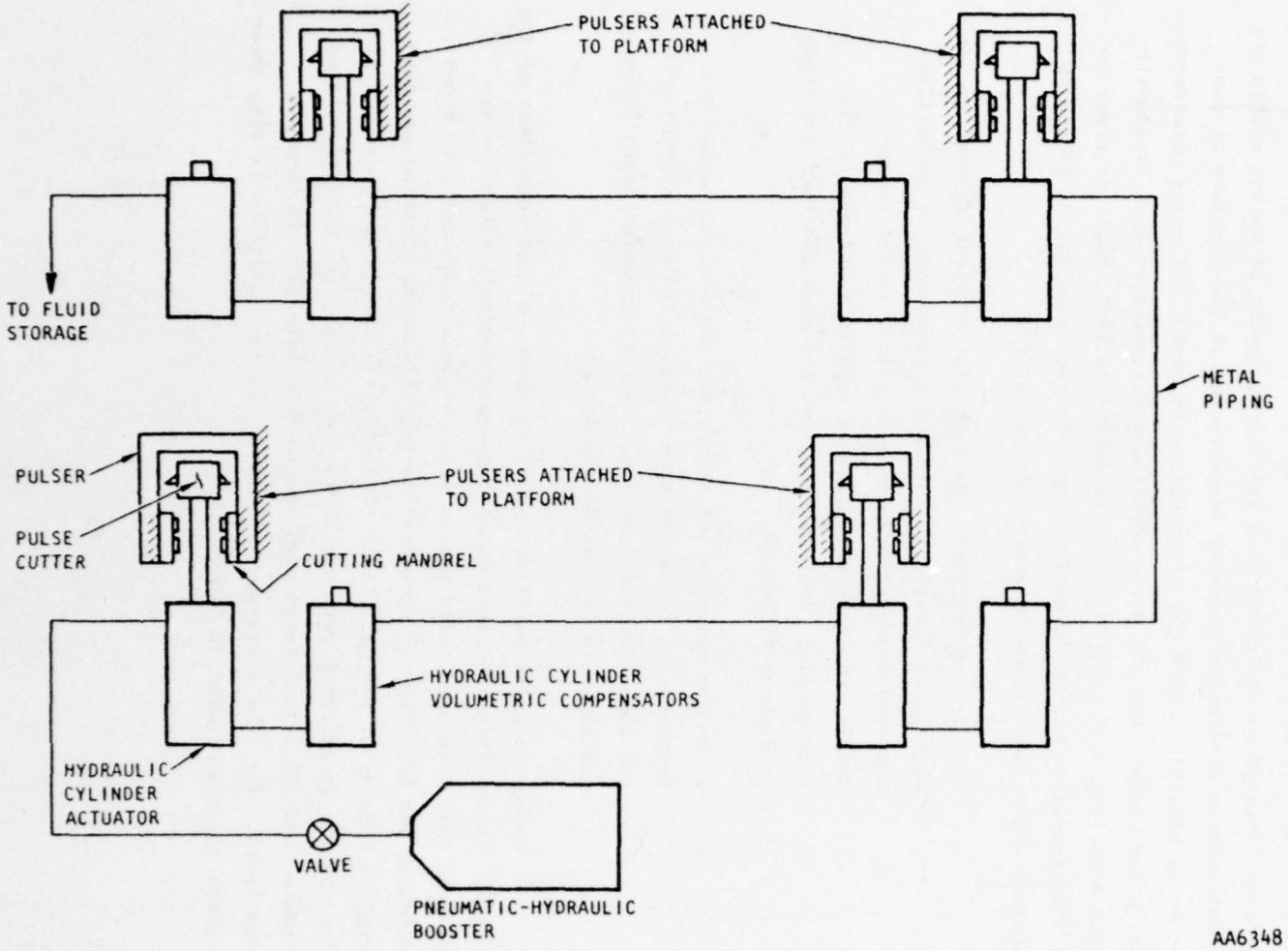

FIGURE 86. SCHEMATIC OF PULSE-GENERATOR AND POWER-ACTUATION SYSTEM

The basic criterion used for simulation accuracy is the integral squared error between the criterion and pulse-simulated platform response. The error function is evaluated at a sufficient number of points within the multiple-degree-of-freedom platform to characterize the platform as completely as possible. With the error criterion given, the pulse occurrence time, pulse widths, and the pulse amplitudes are selected by a systematic-search algorithm such that the error is minimized (Ref. 40). In order to use the simulation method in conjunction with the optimization procedure discussed above, the following steps were performed:

a. The impulse functions for each platform were determined for each pulse location. This was accomplished by converting measured transfer impedance functions in the frequency domain, to transfer impedance impulse functions in the time domain. Typical functions for each platform are shown in Figures 87 and 88.

b. Using the optimization algorithm, the criterion platform response was converged upon by pulse trains convolved with the above impulse function. Typical computed pulse trains are shown in Figures 89 and 90.

Using the pulse profiles specified above, piston velocities of the hydraulic system (Fig. 86) were established and mandrels of the pulses were machined. Measured pulse trains from in-place tests are also shown in Figures 89 and 90. Typical acceleration-time histories obtained are displayed in Figures 91 and 92. These figures are a three-way comparison of (1) criterion (predicted) response to nuclear threat, (2) pulse-simulated response, and (3) actual (measured) response of platforms to in-place pulse tests. The same three-way comparison for each platform is also shown in shock spectrum format in Figure 93.

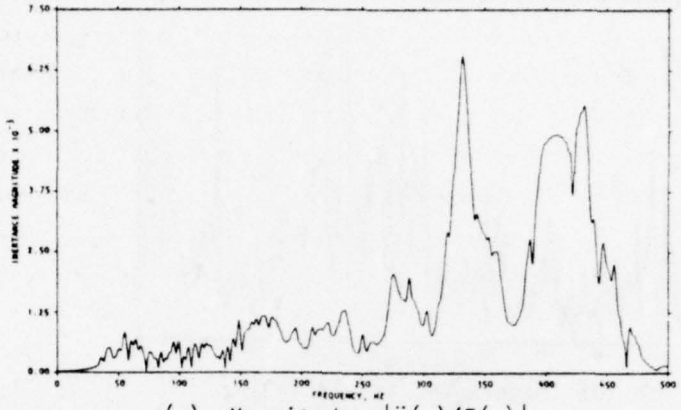

(a) Magnitude, $|\ddot{x}(\omega)/F(\omega)|$

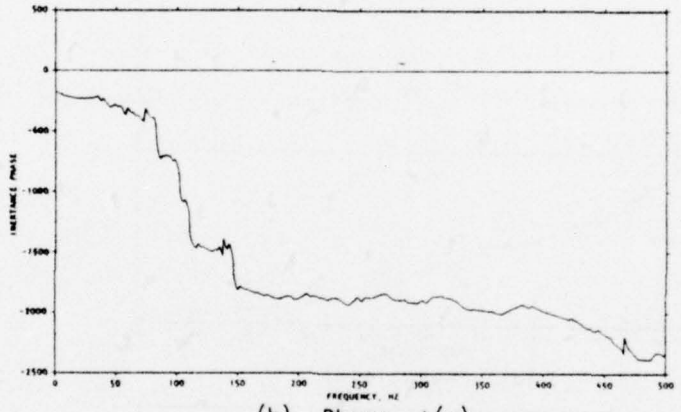

(b) Phase, $\phi(\omega)$

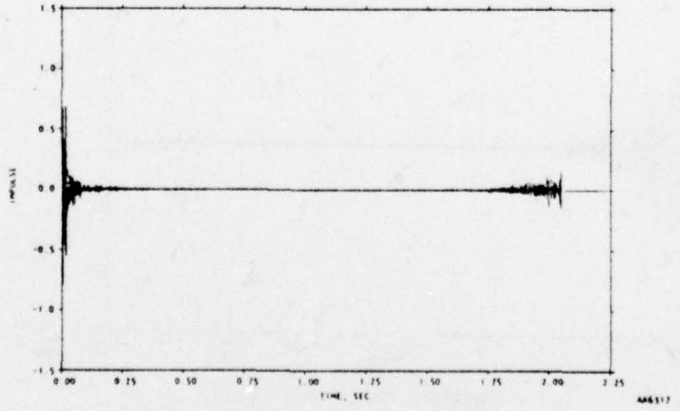

(c) Impulse, $h\ [\ddot{x}(t)/F(t)]$

FIGURE 87. PLATFORM D: TYPICAL TRANSFER INERTANCE FUNCTION, FROM PULSER ATTACHMENT POINT TO REFERENCE ACCELERATION POINT, N, ON PLATFORM

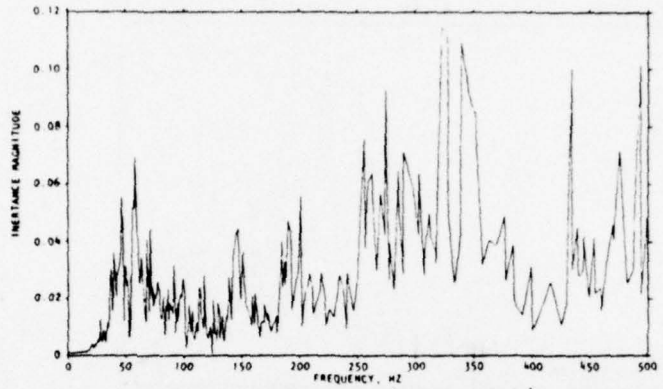

(a) Magnitude, $|\ddot{X}(\omega)/F(\omega)|$

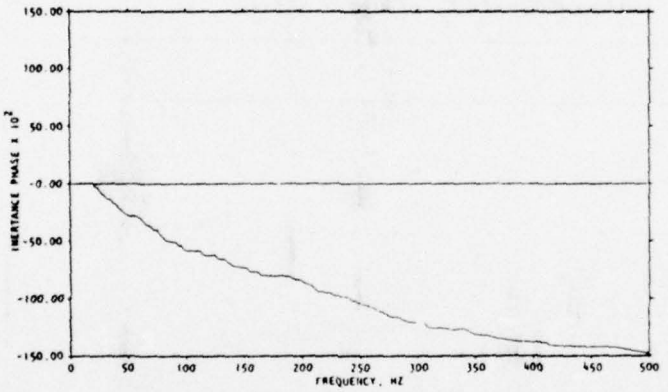

(b) Phase, $\phi(\omega)$

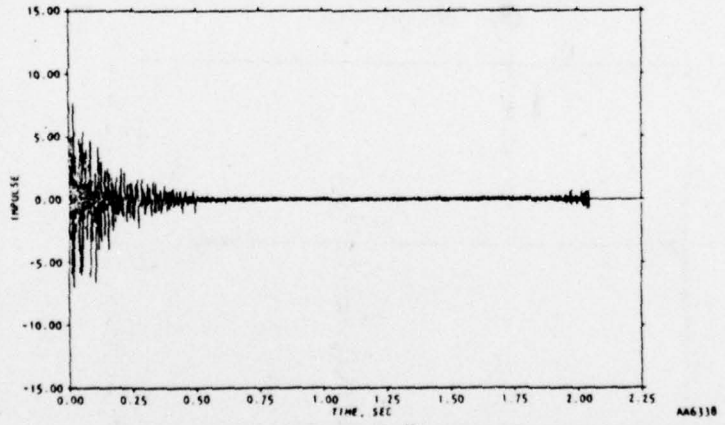

(c) Impulse, $h\ [\ddot{X}(t)/F(t)]$

FIGURE 88. CONTROL ROOM PLATFORM: TYPICAL TRANSFER INERTANCE FUNCTION, FROM PULSER ATTACHMENT POINT TO REFERENCE ACCELERATION POINT, NO. 1, ON PLATFORM

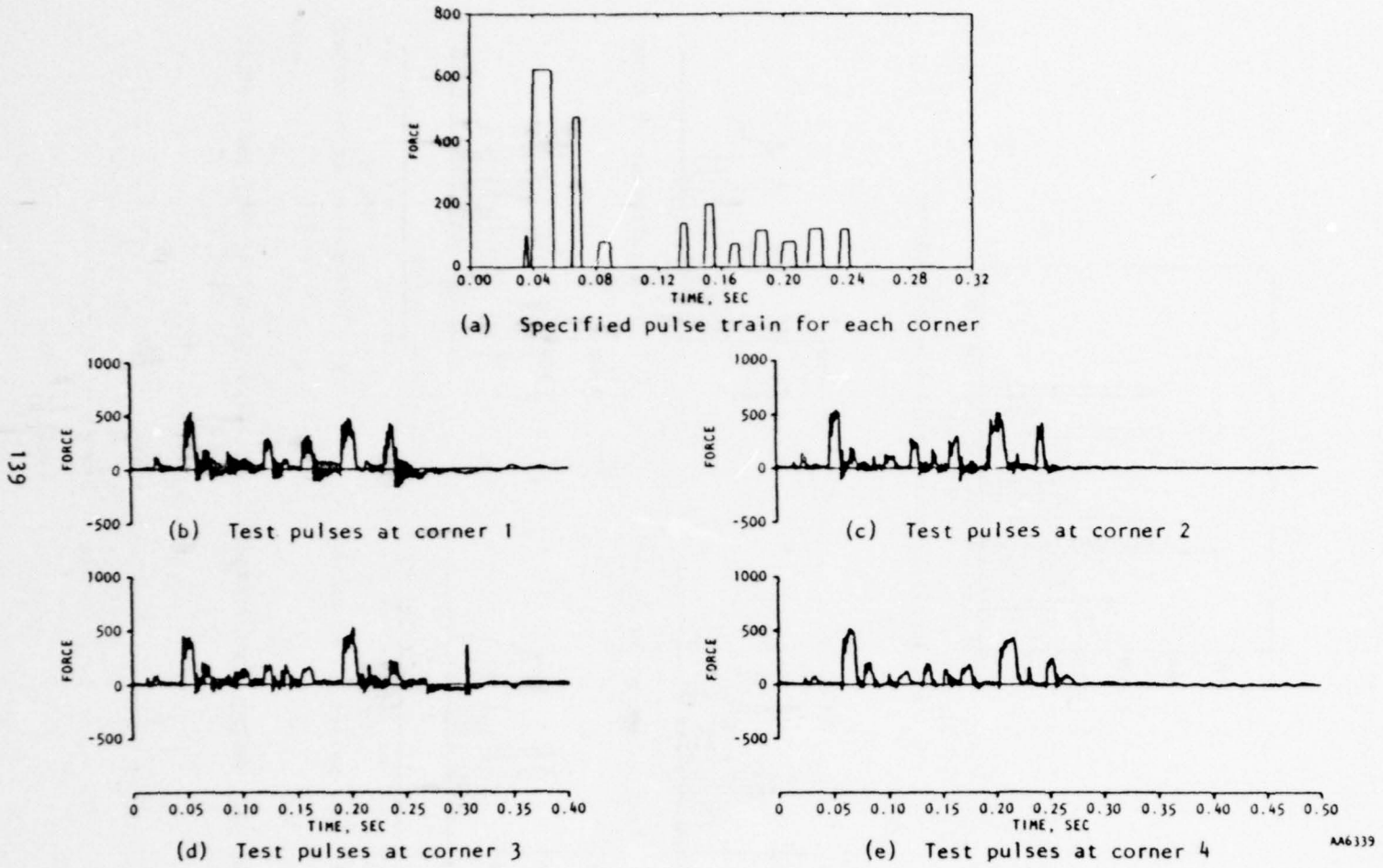

FIGURE 89. PLATFORM D: SPECIFIED AND ACTUAL TEST-INPUT PULSES

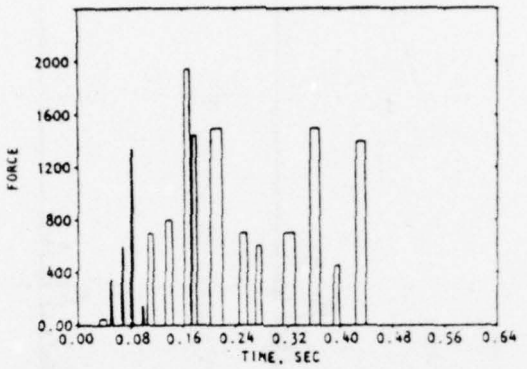

(a) Specified pulse train for each corner

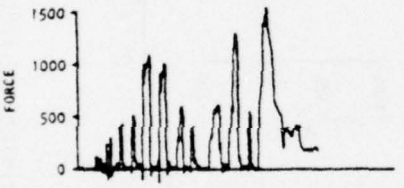

(b) Test pulses at SW corner

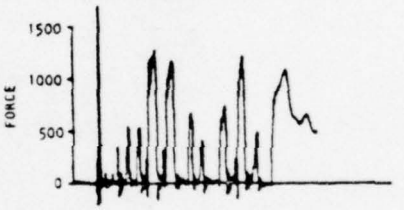

(c) Test pulses at SE corner

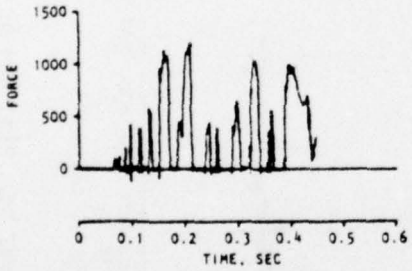

(d) Test pulses at NE corner

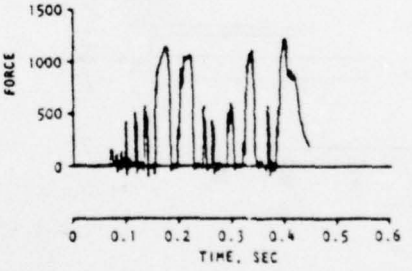

(e) Test pulses at NW corner

AA6345

FIGURE 90. CONTROL ROOM PLATFORM: SPECIFIED AND ACTUAL TEST-INPUT PULSES

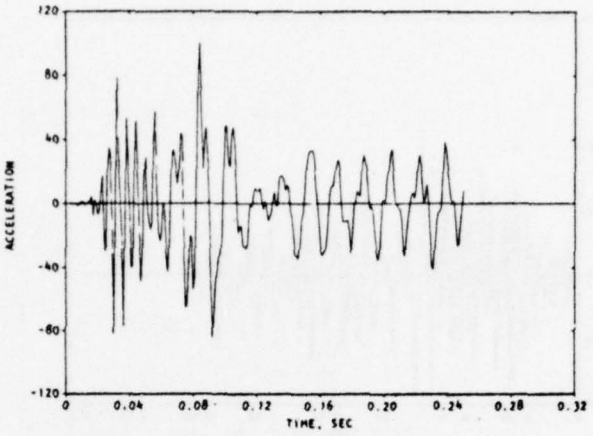

(a) Predicted

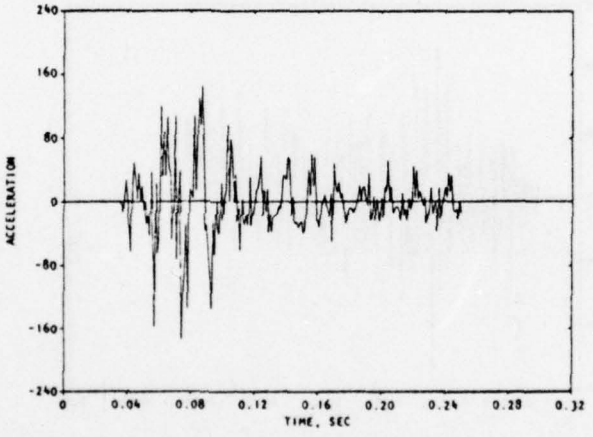

(b) Pulse simulated

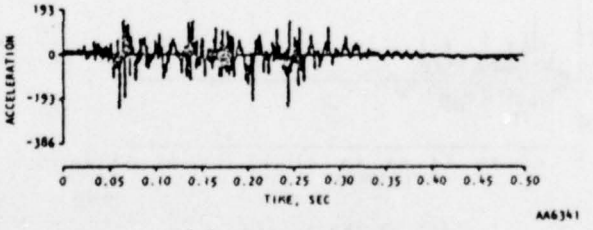

(c) Pulse tested

FIGURE 91. PLATFORM D: ACCELERATION-TIME HISTORIES OF PREDICTED, PULSE-SIMULATED, AND PULSE-TESTED MOTIONS

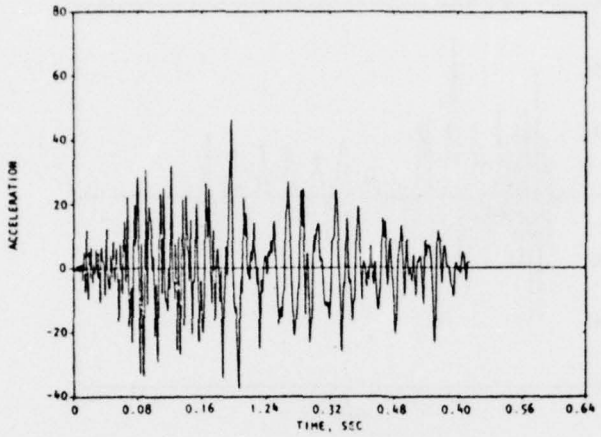

(a) Predicted

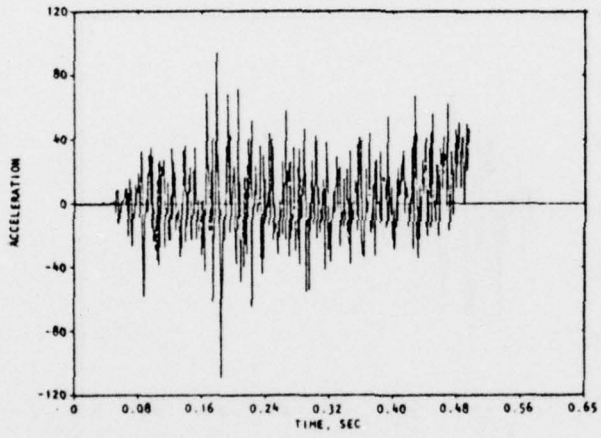

(b) Pulse simulated

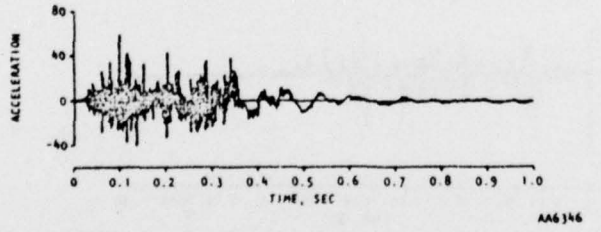

(c) Pulse tested

FIGURE 92. CONTROL ROOM PLATFORM: ACCELERATION-TIME HISTORIES OF PREDICTED, PULSE-SIMULATED, AND PULSE-TESTED MOTIONS

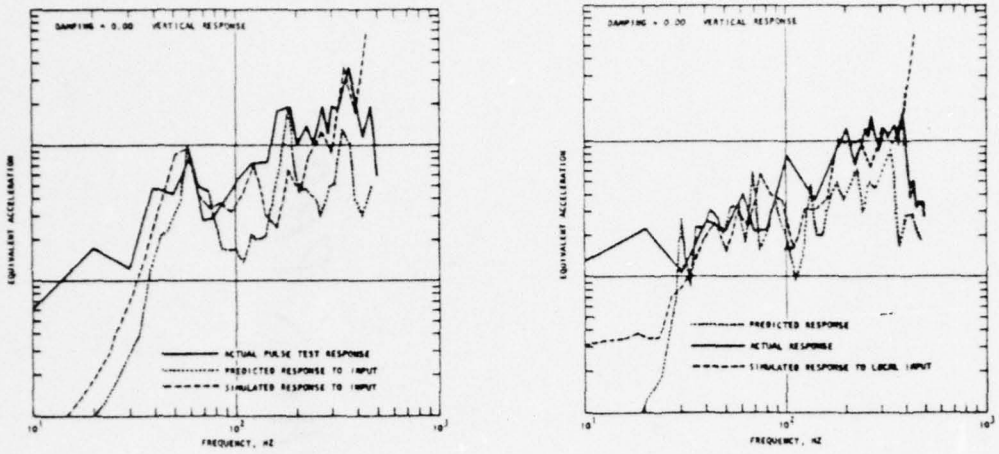

(a) Platform D

(b) Control room platform

FIGURE 93. COMPARISON OF SHOCK SPECTRA FOR THE PREDICTED, PULSE-SIMULATED AND PULSE-TESTED PLATFORMS

SECTION 3

IMPEDANCE USAGE AND APPLICATIONS

The previous section set forth practical engineering projects of impedance, and of motion predictions and environmental simulation based on impedance. A notable feature of some of these projects was their dismayingly large size and massiveness. Numerous data measurements were necessary for such projects, with subsequent complex chains of multiplications, divisions, and summations that required compatibility in both the time and the frequency domains.

However, the demonstrated practicality of impedance and mobility provides means by which certain types of problems may become tractable. For example, the results of previous tests could be processed by impedance/mobility for scaling the data from one type of ship for application to another type, or for equipment changes and replacements. Other applications would include quasi-linear systems, nonlinear systems, parameter identification, multivariate regression analysis, and pulsed environmental simulation. These areas are further discussed in this section.

Throughout this report, the term *impedance* has been used in a broad sense because it is widely accepted and understood. In practice, however, *mobility* and its derivative *inertance* are applied almost exclusively, not only for ease of computation and for visual interpretation but also because they are independent of the number and locations of other measurement points (Ref. 41).

3.1 LINEAR SYSTEMS

Section 2 covered the use of impedance and transfer functions for response-motion prediction based on linear or quasi-linear systems. Currently, five major projects on this subject have been completed or are in the process

of completion, with results that are considered quite good. As a practical matter, many systems exist where the main load-bearing structure (ship or submarine hulls) remains essentially linear over a wide range of attacks, yet internal equipment may exhibit nonlinear response with failure, malfunction, or degradation. The nonlinear interaction of equipment on the linearly responding main load-bearing structure needs to be assessed on a case-by-case basis. Previous projects indicate that these nonlinear effects are not severe enough to adversely affect impedance measurements. Response predictions made at equipment locations at criterion or postulated attack levels provide input functions for individual laboratory-environmental tests on the equipment.

Response motions (acceleration-time histories) determined from impedance measurements may be made quite accurately for a large class of linear and quasi-linear systems. The accuracy depends on the formulation of appropriate input loads. Scale-model tests for air-blast and underwater shock have been found to be very effective for formulating the input to represent the transient-load engulfment of the target facets. Improvement in the accuracy of impedance data using time-series digital data analysis, noise minimization procedures, and new measurement devices largely accounts for the practicality of applications in predicting response motions. Each succeeding project exhibits continuing improvements in reduction of costs, ease of testing, and accuracy. In the near future, many analytic models will be checked against impedance measurements for accuracy.

3.2 NONLINEAR SYSTEMS

New methods of approach can be employed that provide a means of improved predictions for nonlinear response of structures. By proper design of tests, data can be extracted in a specific manner to yield nonlinear

describing functions. These functions, which are discussed below, quantitatively specify inelastic and damage phenomena and permit nonlinear response predictions.

In the parametric identification approach, the mathematical structure of the model is postulated but its parameters are not. Most of the work done so far in structural-system identification has been considered from the parameter estimation approach. The identification task in this parametric model approach eventually reduces to a search in parameter space where system parameters are iterated repeatedly until values are obtained that meet a specified error criterion. Among the techniques used in this approach are gradient or random search methods.

In the describing function identification approach, no a priori assumptions are made regarding the structural configuration of the mathematical model of the system to be identified. The identification problem becomes a search in "functional space." The basic mathematical statement supporting this process is presented below.

Let $u(t)$ be a random noise input signal, and g_i be a function of n variables. The response $y(t)$ of a nonlinear system can be expressed as

$$y(t) = \sum_{i=1}^{n} G_i[g_i, u(t)]$$

where $G_i[g_i, u(t)]$ is a functional of the i^{th} degree, which is orthogonal to all functions G_j, $j < i$:

$$\overline{G_i[g_i, u(t)] \times G_j[g_j, u(t)]} = 0 \qquad \text{for } i < j$$

The first few terms of the functionals are:

$$G_1[g_1, u(t)] = \int_{-\infty}^{\infty} g_1(\tau_1)\, u(t - \tau_1)\, d\tau_1$$

$$G_2[g_2, u(t)] = \iint_{-\infty}^{\infty} g_2(\tau_1,\tau_2)\, u(t - \tau_1)\, u(t - \tau_2)\, d\tau_1 d\tau_2 - k\int_{-\infty}^{\infty} g_2(\tau_2,\tau_2)\, d\tau_2$$

$$G_3[g_2, u(t)] = \iiint_{-\infty}^{\infty} g_3(\tau_1,\tau_2,\tau_3)\, u(t - \tau_1)\, u(t - \tau_2)\, u(t - \tau_3)\, d\tau_1 d\tau_2 d\tau_3 - 3k\iint_{-\infty}^{\infty} g_3(\tau_1,\tau_2,\tau_2)\, u(t - \tau_1)\, d\tau_1 d\tau_2$$

where k = average power of random noise.

Since the parametric identification requires a priori assumptions regarding the characteristics of the system, large errors can be introduced in modeling complex structures if the order of the mathematical model does not agree with the order of the actual structure. This problem becomes particularly acute for the response in the nonlinear range. However, for the describing function identification approach, the order of the system need not be assumed, but is allowed to develop to optimally satisfy the measured characteristics.

For the general solutions of nonlinear systems, the Volterra Series may be used to represent an explicit input/output relation. One of the main problems in the application of the theory is the explicit determination of the kernels appearing in the Volterra Series. A solution improvement set forth by Wiener was to expand these kernels in terms of a set of orthogonal functions, such as Laguerre functions. Practical solution was achieved by cross correlation.

Studies of nonlinear effects (Ref. 1) disclosed nonlinearities that could be very sensitively detected by rapid sine sweeps (CHIRP tests) without requiring excessively large forces that could drive the test structure into the damage region. From this information, an alternative procedure has evolved in the form of state variables, by which Chebychev polynomials are used as functionals relating input to output.

3.3 PARAMETRIC IDENTIFICATION

By extending parameter identification to nonlinear systems, a series of impedance measurements at different force levels is obtained. This approach provides a group of nonparametric impedance curves from which parameters are identified. From the parameters obtained, functional relations are set forth in the model, as for nonlinear springs and damping, to provide an approximate model of the nonlinear transmission path. The parametric approach can also be used in conjunction with the functional approach to determine system parameters once the functionals (describing functions) are determined. This combined approach presages an improved means of extracting physical phenomena for application to nonlinear modeling of structures.

Random search algorithms for parameter optimization have been widely applied and documented. They have the advantage of (1) leading to global solutions of nonlinear systems, (2) guaranteeing convergence, and (3) easing computer implementation. On the negative side, random search algorithms may converge very slowly, particularly in criterion surfaces of high dimensionality. Several procedures have been tried in the past to circumvent slow convergence.

The algorithm used in several impedance and pulse simulation projects is another approach to the determination of the optimal step size (Ref. 40). Rather than a fixed-length step, steps used are random in both length and direction. Hence, the adaptation described below is based on the selection of the optimal variance of the step-size distribution as the search progresses. Large variances are desirable in the early, exploratory portions of a search. However, in the vicinity of a local optimum, a smaller value of the standard deviation, σ, will decrease the probability of overshoot.

The algorithm for the adaptive random search consists of alternating sequences of a global random search with a fixed value for the step size variance followed by searches for the locally optimal σ. This adaptive random search method was used, as shown in the following example, to optimize 17 parameters of a nonlinear soil model.

In specific applications, data are given in the form shown in Table 4, where ε and σ are the vertical soil strain and stress, respectively, obtained from a uniaxial test, and where

J_1 = First stress invariant $(\Sigma\sigma_i)$

J_2' = Second reduced stress (stress deviation) invariant $= \frac{1}{6} \Sigma (\sigma_i - \sigma_j)^2$

σ_i, σ_j = Principal stress components

The stress invariants depend on ε, σ, and the loading history, as well as numerous other soil parameters that are to be identified. Among the present soil models that are being widely used in ground-shock computations are elastic, perfectly plastic, variable moduli, and an elastic-plastic model with a movable cap.

Once a candidate mathematical model is selected, the problem is then to determine the "best" set of parameters that will result in a loading/unloading curve and stress path that will simultaneously match both sets of experimental data such as given in Table 4. Thus, the identification problem is reduced to a search in parameter space that will yield the extremum (minimum) value of a suitable penalty function.

The cap model used to represent soils employs a yield surface that combines both strain hardening and ideal plasticity. The ideally plastic modified Drucker-Prager criterion represents the ultimate shear strength of the material and is associated with fracture or sustained plastic flow in laboratory experiments. The form of the yield criterion is

$$f_1 = (J_1, J_2') = 0$$

TABLE 4. REFERENCE DATA

Point No.	Strain Increment	Strain	Stress	J_1	$\sqrt{J_2'}$
1	-1.000-03	-1.000-03	-1.669-03	-3.000-03	5.774-04
2	-6.900-02	-7.000-02	-2.097-02	-3.890-02	6.928-03
3	3.000-03	-6.700-02	-5.000-03	-9.000-03	1.732-03
4	-5.000-03	-7.200-02	-1.828-02	-3.290-02	6.371-03
5	-2.800-02	-1.000-01	-3.841-02	-7.490-02	1.155-02
6	-5.000-02	-1.500-01	-7.552-02	-1.500-01	2.194-02
7	-2.500-02	-1.750-01	-1.080-01	-2.249-01	2.887-02
8	-2.300-02	-1.980-01	-1.400-01	-3.000-01	3.464-02
9	-1.200-02	-2.100-01	-1.680-01	-3.749-01	3.811-02
10	-1.500-02	-2.250-01	-1.960-01	-4.500-01	4.041-02
11	-5.000-03	-2.300-01	-2.220-01	-5.249-01	4.157-02
12	-5.000-03	-2.350-01	-2.490-01	-6.000-01	4.328-02
13	-5.000-03	-2.400-01	-2.760-01	-6.749-01	4.444-02
14	-5.000-03	-2.450-01	-3.010-01	-7.500-01	4.503-02
15	-1.000-03	-2.460-01	-3.270-01	-8.249-01	4.563-02
16	-1.000-03	-2.470-01	-3.596-01	-9.180-01	4.619-02
17	2.000-04	-2.468-01	-3.240-01	-8.249-01	4.272-02
18	2.000-04	-2.466-01	-2.950-01	-7.500-01	3.982-02
19	3.000-04	-2.463-01	-2.670-01	-6.749-01	3.635-02
20	3.000-04	-2.460-01	-2.389-01	-6.000-01	3.404-02
21	1.000-03	-2.450-01	-2.110-01	-5.249-01	3.118.02
22	1.000-03	-2.440-01	-1.830-01	-4.500-01	2.887-02
23	1.000-03	-2.430-01	-1.540-01	-3.749-01	2.540-02
24	1.000-03	-2.420-01	-1.260-01	-3.000-01	2.250-02
25	1.000-03	-2.410-01	-9.683-02	-2.249-01	1.903-02
26	5.000-04	-2.405-01	-6.910-02	-1.500-01	1.672-02
27	5.000-04	-2.400-01	-4.083-02	-7.490-02	1.386-02

As the plastic volumetric strain increases or decreases, the strain-hardening cap expands or contracts, respectively. The cap is denoted by

$$f_2 = (J_1, J_2', \varepsilon^P) = 0$$

where ε^P is plastic strain.

It is assumed that elastic behavior is governed by

$$d\sigma_{ij} = Kd\varepsilon_{kk}\delta_{ij} + 2G\left(d\varepsilon_{ij} - \frac{1}{3}\, d\varepsilon_{kk}\delta_{ij}\right)$$

where

$d\sigma_{ij}$ = Stress increment tensor

$d\varepsilon_{ij}$ = Strain increment tensor

$d\varepsilon_{kk}$ = Linear dilatation $(= d\varepsilon_{11} + d\varepsilon_{22} + d\varepsilon_{33})$

δ_{ij} = Kronecker delta $(= 1$ if $i = j, = 0,$ if $i \neq j)$

K = Bulk modulus, which is a function of pressure

G = Constant shear modulus

The basic cap model used in this study consists of the following parts: (1) a variable bulk modulus, (2) a constant shear modulus, (3) a fracture surface, and (4) a cap. The cap model is defined by the following equations and an associated flow rule:

Bulk and Shear Modulus

$$K = B_1\left\{1 - B_2 e^{B_3 J_1} - B_4 e^{B_5 J_1}\right\}$$

where

G = Constant

B_1 through B_5 = Empirical coefficients

Fracture Surface (f_1)

$$f_1 = 0 = \sqrt{J_2'} - \left[Y_1 - Y_2 e^{Y_3 J_1} \right]$$

Cap (f_2)

$$f_2 = 0 = (L - J_1)^2 + Y_4^2 J_2' - (L - x)^2$$

$$X = \frac{1}{Y_5} \ln \left(\frac{I_1^P + Y_7}{Y_6} + 1 \right)$$

$$L + Y_4 \left(Y_2 e^{Y_3 L} - Y_1 \right) - x = 0$$

$$I_1^P = \varepsilon_1^P + \varepsilon_2^P + \varepsilon_3^P$$

where

I_1^P = First invariant of plastic strain
$= \sum_{i=1}^{3} \varepsilon_1^P .$

L = Distance to the center of the elliptical cap

X = Intersection of elliptical cap with J_1 axis

Y_1 through Y_7 = Empirical coefficients

In the application of this model to soils, the cap movement is controlled by the change of plastic volumetric strain; hence, strain hardening can be reversed.

The computer implementation of this model results in a code that, when supplied with a strain time history, will generate the corresponding state of stress, and subsequently the stress invariants, at every point in the stress path.

In view of the complexity of the aforementioned model, its computer implementation has required a substantial effort and resulted in a large computer code that performs a significant number of computations for every incremental change in the strain level in order to determine the corresponding state of stress.

Given n discrete data points with coordinates

$$[\varepsilon_i, \sigma_i(\varepsilon_i, \vec{P})] \quad \text{and} \quad \left[J_{1_i}(\varepsilon_i, \vec{P}), \sqrt{J'_{2_i}(\varepsilon_i, \vec{P})}\right]$$

of the type shown in Table 4 where

ε_i = Value of independent variable (strain), i=1, 2,..., n

$\vec{P}$ = Parameter vector whose k components correspond to the parameters to be identified

$\sigma_i(\varepsilon_i, \vec{P})$ = Digitized values of stress, i=1, 2,..., n

$J_{1_i}(\varepsilon_i, \vec{P})$ = Digitized values of stress invariant

$J'_{2_i}(\varepsilon_i, \vec{P})$ = Digitized values of stress invariant

The penalty function J used in the present example is:

$$J = \sqrt{W_1 S_1 + W_2 S_2 + W_3 S_3}$$

where

$$S_1 = \sum_{i=1}^{n} [\sigma(\varepsilon_i) - \hat{\sigma}(\varepsilon_i)]^2$$

$$S_2 = \sum_{i=1}^{n} [J_1(\varepsilon_i) - \hat{J}_1(\varepsilon_i)]^2$$

$$S_3 = \sum_{i=1}^{n} \left[\sqrt{J_2'(\varepsilon_i)} - \sqrt{\hat{J}_2'(\varepsilon_i)}\right]^2$$

W_1, W_2, W_3 = Weighting functions

n = Number of data points

and where ε, σ, J_1, J_2' represent measurement data and $\hat{\sigma}$, $\hat{J}_1$, $\hat{J}_2'$ are the corresponding quantities obtained by specifying the sequence of strain increments $\Delta\varepsilon_i = \varepsilon_{i+1} - \varepsilon_i$, $i = 1,2,\ldots, n-1$, and then determining the state of stress in accordance with the predictions of a suitable mathematical model.

The random search algorithm was used to fit soil data by performing the following steps:

a. The discretized values of the stress/strain and the stress path of Table 4 were used as data.

b. A judicious choice was made for the soil cap model fitting parameter values, which were subsequently used as initial parameter values to start the random search algorithm. These initial values are listed in Table 5.

TABLE 5. PARAMETER VALUES

Cap Model Parameters	Initial Values	Optimized Values	% Change
A	0.0468	0.047	
B	4.5	4.5	
C	0.0456	0.0456	
R_0	2.0	2.24	12
R_1	2.5	2.25	-10
R_2	5.0	4.54	- 9
R_3	0	0	
R_4	0	0	
R_5	0	0	
W	0.237	0.237	
D	4.96	4.54	- 8.5
α	1.0	1.0	
D_1	100.0	100.0	
D_2	1000.0	1000.0	
W_1	50.0	45.46	- 9.1
D_F	31.0	31.0	
W_2	-0.009	-0.009	
D_3	0.5	0.5	
K_{EI}	123.2	139.2	13
K_S	3.144	7.050	
δ	-0.900	-0.958	6.4

Cap Model Parameters	Initial Values	Optimized Values	% Change
β	1.25	1.36	8.8
K_1	1.0	0.92	- 8.0
K_2	1000.0	1078.0	7.8
K_3	450.0	418.0	- 7.1
K_4	0.0015	0.0015	
K_5	0	0	
G_{EI}	24.0	21.8	- 9.2
G_S	0.968	1.057	9.2
γ	-0.9	-0.996	11.0
η	4.0	3.58	-10.5
G_1	0	0	
G_2	16.0	13.95	-12.8
G_3	5000.0	5510.0	10.2
G_4	0	0	
G_5	0	0	

AA8797

c. Using the initial values given in Table 5 in conjunction with an appropriate cap model computer code, Figure 94 shows a comparison of this "initial solution" and the experimental data. Note that this "initial solution" was obtained by merely substituting the parameter values given in Table 5 into the material package subprograms. The optimization section of the parameter identification code was not exercised in this step.

d. Using equal error weighting functions $w_1 = w_2 = w_3 = 1$ in the criterion function, the deviation error between the "initial solution" and the given data was 0.272.

e. Again using the "initial values" listed in Table 5 as a starting estimate to initiate the parameter identification code and then operating the code for a few hundred iterations, an optimum set of parameters was found. These parameters are listed in Column 3 of Table 5. The optimized solution is shown in Figure 95 and its corresponding deviation error is 0.070 (~ 1/4 of the starting error).

Note that the reduction of the deviation error was achieved by optimizing the values of 17 parameters listed in Table 5. The percentage change in these parameters ranged from -12.8% to +13%.

3.4 SCALING AND CORRELATION

3.4.1 MULTIVARIATE REGRESSION ANALYSIS

Multivariate regression analysis may be viewed as the problem of determining a linear relationship between two or more variables. It may also be viewed as a linear curve fitting procedure in which--

$$Y = \beta_0 + \beta_1 X_1 + \beta_2 X_2 + \ldots + \beta_n X_n$$

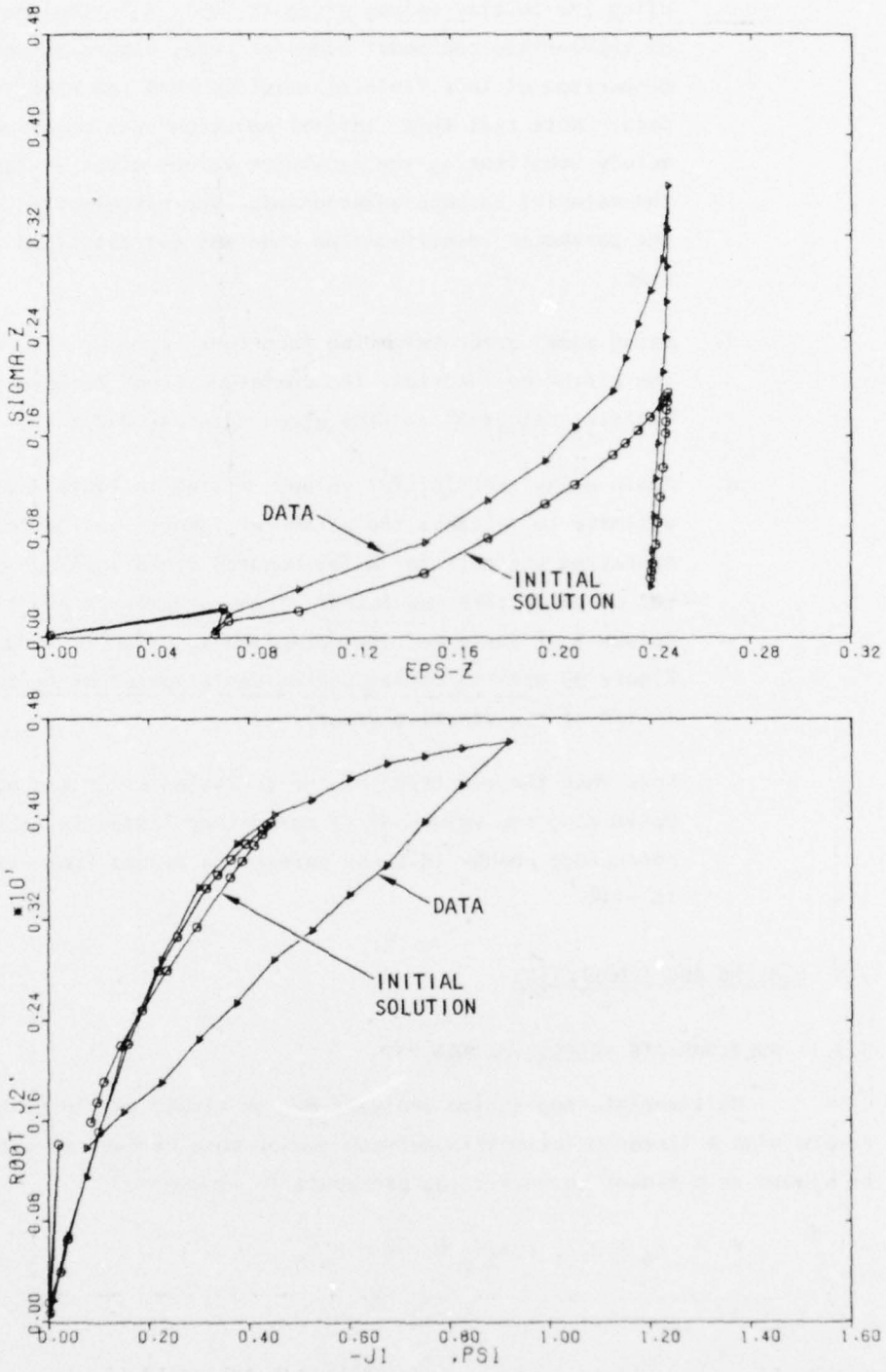

FIGURE 94. COMPARISON OF EXPERIMENTAL DATA AND INITIAL SOLUTION

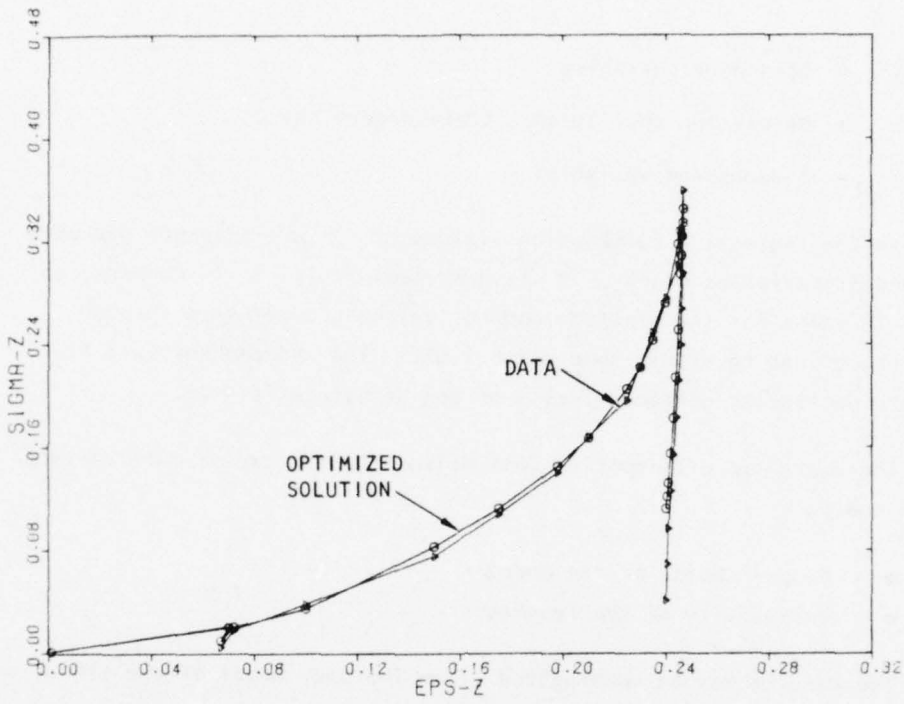

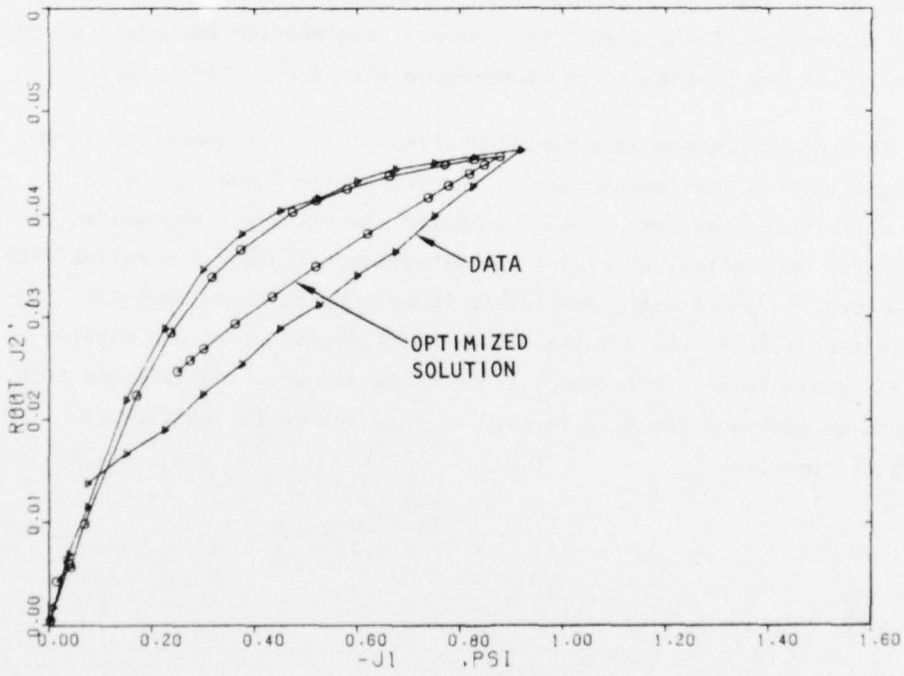

FIGURE 95. COMPARISON OF EXPERIMENTAL DATA AND OPTIMIZED SOLUTION

where

Y = Dependent variables

β_n = Regression coefficients to be determined

X_n = Independent variables

In the regression computation, values of β are assumed; and with the independent variables of X_n, Y is computed. This Y is compared to the known Y value for the platform and β values are adjusted through iterative procedures to within some error limit. The independent variables, X_n, are the particular characteristics of any structural system.

There are two difficulties that arise from the use of multivariate regression analysis:

- Proper choice of the model
- Variability of the results

The results may be meaningless if an improper model of the situation is employed, or at least be less meaningful than some other model. Stepwise regression procedures can be used, and a general engineering awareness of the dimensionality of the problem tends to overcome this first difficulty.

The second problem is a function primarily of the number of structural systems used in the computations: the larger the number or more uniformly distributed the data base, the better the results. Procedures for the analysis of variability of errors can be applied to judge the reliability of the results. In particular, confidence bounds may be calculated and placed on either side of the results. These confidence bounds are usually given at a certain level. For example, one frequent way of calculating them is such that chances are the true results will be inside the confidence bounds 95% of the time.

Comparison of systems is made both by similarities and by differences. In formulating trial models, the independent parameters reflect the similarities, and the specific values assigned thereto provide the differences. In shock or Fourier response-spectra-estimation procedures for a ship, multivariate regression analysis is applied once for each frequency being examined. For example, the X and Y variables could be defined as follows:

Y = Fourier pressure spectra for frequency f_i on ship's hull

X_1 = Depth-charge size

X_2 = Depth-charge depth below surface

X_3 = Depth-charge distance from ship

X_4 = Length of ship (water line)

X_5 = Beam of ship

X_6 = Length/beam ratio

X_7 = Hull thickness

X_8 = Displacement vol/weight

. .
. .
. .

The units of these parameters are immaterial; the multivariate regression analysis procedure automatically accounts for the units. It should be noted that the X variables may be composite. That is, they might be equal to functions such as $\ell^2 + w^3$, $w^2 f^4$, $\exp(-af)$, etc., where ℓ is length, w is weight, f is frequency, and a is a constant.

Grouping of parameters as in the foregoing permits formulation of reasonable representative system models or functional relationships, rather than brute force polynomial fits to data.

For example, shock-isolated platforms protecting equipment comprise 62 different configurations totaling 107 platforms distributed throughout a hardened facility (Ref. 9, 30). Prediction of response-motion for each

platform and for each environmental location within the system was required for hardness/survivability assessments of equipment. The a priori selection of platforms as a representative sample for transfer-function measurements permitted interpolation methods to be used to estimate with acceptable confidence the response motions of all platforms. A simple environmental scaling rule then allowed these estimates of platform motions to be adjusted to the threat environments for a particular building and floor location.

A multivariate regression method was used to predict responses for all types of platforms, measured and unmeasured. The platforms can be classified in terms of their physical characteristics (i.e., length, width, density, etc.) and local input environments. Transfer-function measurements and subsequent response analysis of the 10 selected platforms resulted in 10 shock-response spectra for prediction analysis.

The polynomial approach was generated by representing the shock-isolated platforms in the form of plates. Since the dynamic response of a plate (hence its shock spectrum) is directly related to its frequency spectrum, it is reasonable to choose the following characteristic parameters as independent parameters for the regression analysis: ℓ, w, ρ, wt/iso. On the basis of several trial cases, the following nonlinear multivariate regression was evolved:

$$\ddot{x}(ss) = \beta_0 + \beta_1\ell + \beta_2\ell^2 + \beta_3\ell^3 + \beta_4\rho + \beta_5\rho^2 + \beta_6\rho^3 + \beta_7(\ell/w) + \beta_8(wt/iso)$$

where

$\ddot{x}(ss)$ = Acceleration shock spectra

β_n = Coefficients of regression for each frequency point

ℓ = Length

ρ = Weight/area (calculated density)

w = Width

wt/iso = Total weight per isolator

The particular data bases used for this analysis were the dependent variable values of the shock-spectrum responses of the 10 measured platforms over the frequency range of 35 to 500 Hz, and the independent variable platform characteristics: length, width, density, length/width, and weight per isolator. Characteristics of the measured platforms are provided in Table 6. To ensure optimum predictive results, the error limit for the response data was set at $\pm 1\sigma$ about the mean for the 10 measured platforms. Also, because of the optimum distributive sampling of the platforms for testing, the upper and lower bounds of the 62 sets of platforms did not exceed the upper and lower bounds of the 10 platforms investigated (see Fig. 96).

Figures 97 and 98 show two platform responses to the referent overall environment input as computed from impedance and transfer function data. Overlaid on each plot is the predicted shock spectrum for that same platform, derived by multivariate regression analysis.

The predicted shock spectra show a good correlation with the actual shock spectra if all 10 platforms are viewed in a statistical relationship. Individually, 7 of the 10 platforms are almost perfectly predicted to within $\pm 1/4$ standard deviations.

The shock-spectrum responses of the remaining unmeasured 52 types of platforms were predicted by using their specific characteristics (length, width, length/width, density, wt/iso) with the coefficients generated by multivariate regression analysis. These values are the platform responses to the overall input. Typical examples of responses predicted for unmeasured platforms by the regression method are shown in Figures 99 and 100.

To develop the platform shock spectrum for its particular location (local shock spectrum), a scaling technique was developed. This scaling method was used to develop the response of the 62 types of platforms to the local input environments. The procedure calls for dividing the shock spectrum

TABLE 6. REGRESSION PARAMETERS FROM 10 IMPEDANCE-MEASURED PLATFORMS (DATA BASE)

Platform	Length, ℓ (ft)	Width, w (ft)	Total Weight (lb)	Number of Isolators	ℓ/w	Density ρ (lb/ft^2)	Weight per Isolator (lb/unit)
PARPP-H	14	5	7,500	4	2.8	107	1,875
RLOB-124B	10	8	11,000	4	1.25	137	2,750
PARPP-D	12	4	13,100	4	3.0	273	3,275
PARPP-G	13	5.5	13,700	4	2.36	192	3,425
RLOB-124C	23	7	23,500	6	3.29	146	3,917
MSCB-125B	31	9	32,600	4	3.44	117	8,150
MSRPP-9-10	26	24	66,600	20	1.08	107	3,330
PARPP-A	52	14	109,300	17	3.71	150	6,429
PARPP-CR	64	49	198,000	18	1.31	63	11,000
MSRPP-2W	77	16	244,000	20	4.81	198	12,200

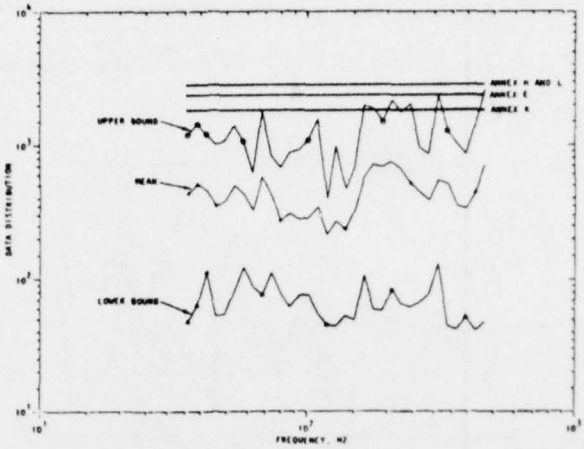

FIGURE 96. DISTRIBUTION OF SHOCK SPECTRA FOR 10 PLATFORMS MEASURED IN PLACE. Response computations determined from overall Annex M input. Environmental levels for equipment tested on vibration shakers are also shown (Annexes E, H, L, and K).

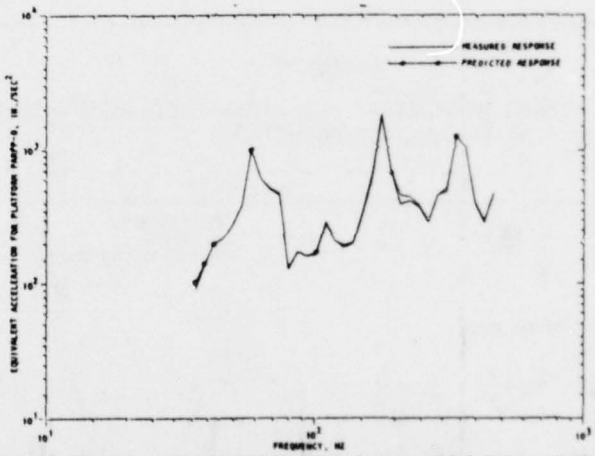

FIGURE 97. PLATFORM PARPP-D: COMPARISON OF SHOCK SPECTRA DETERMINED FROM IMPEDANCE MEASUREMENTS AND FROM REGRESSION-PREDICTION METHOD

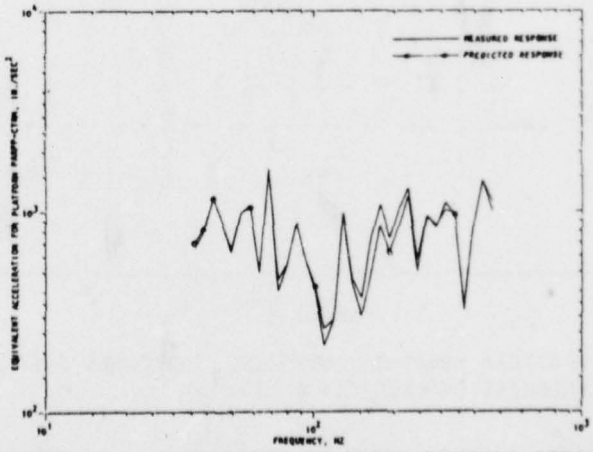

FIGURE 98. PLATFORM PARPP-CR: COMPARISON OF SHOCK SPECTRA DETERMINED FROM IMPEDANCE MEASUREMENTS AND FROM REGRESSION PREDICTION METHOD

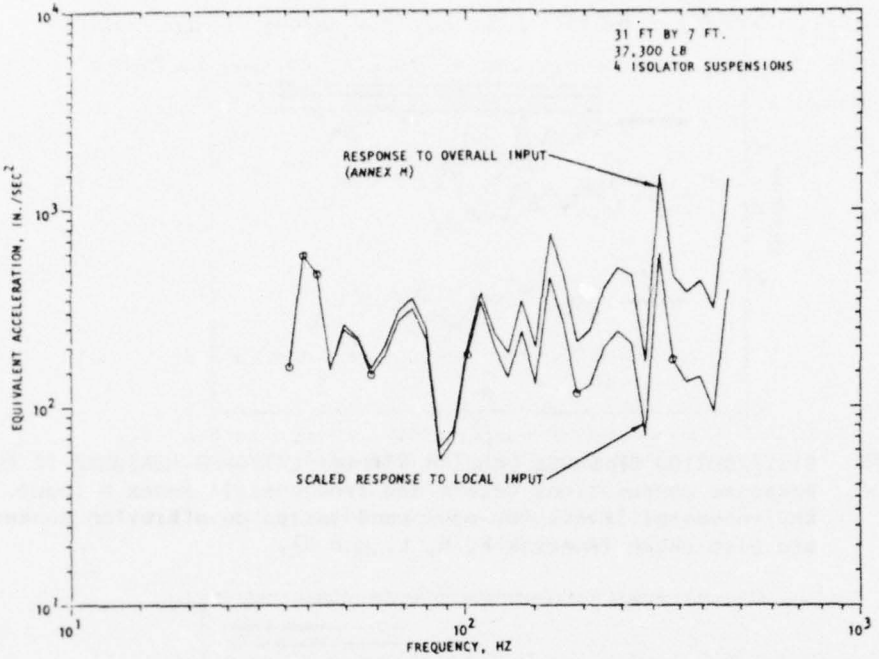

FIGURE 99. PLATFORM MSCB-250A: VERTICAL SHOCK-RESPONSE SPECTRA (REGRESSION PREDICTION METHOD)

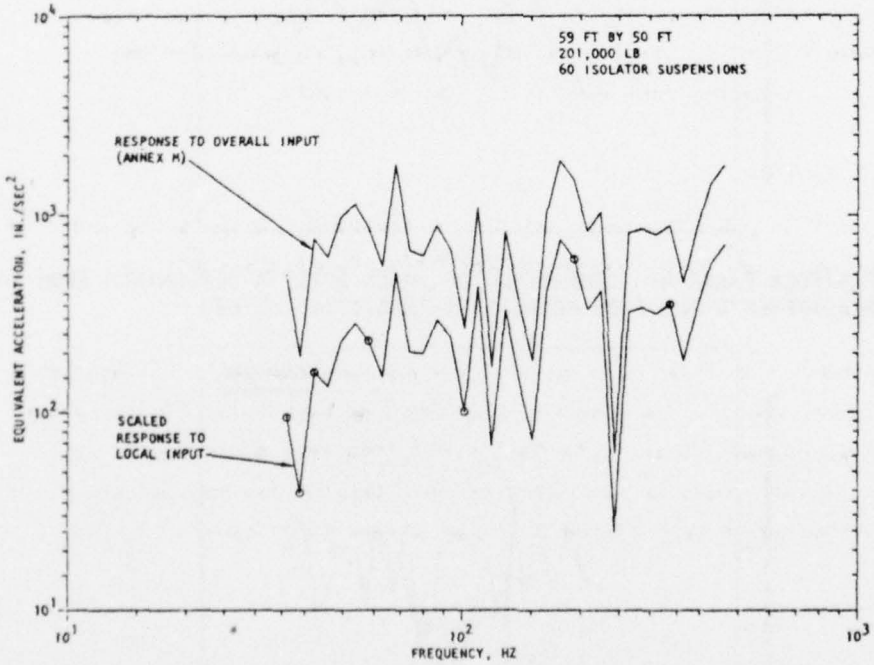

FIGURE 100. PLATFORM MSRPP-1: VERTICAL SHOCK-RESPONSE SPECTRA (REGRESSION PREDICTION METHOD)

values of the local environments by the shock spectrum values of the overall (reference) environment. A relationship can be drawn as follows to form a pseudotransfer function:

$$\ddot{y}_{local}^{(ss)} = \ddot{y}_{ref.}^{(ss)} \frac{\text{local input ss}}{\text{ref. input ss}}$$

where

$\ddot{y}_{local}^{(ss)}$ = Platform response shock spectrum to local input environment

$\ddot{y}_{ref.}^{(ss)}$ = Platform response shock spectrum to overall (reference) input environment

local input ss = Input shock spectra specified for a particular building and floor

ref. input ss = Overall (reference) shock spectrum

Figures 99 and 100 also show platform response to local shock spectrum input environments determined from the scaling techniques. Scaling of shock spectra as above must be performed with some caution. Where large changes in waveform and time durations exist, errors in response estimates can result. However, for estimating the high-frequency response for any isolated platform, this is a very useful and low-cost tool.

3.4.2 IMPEDANCE SCALING

Systems with similar dimensions may be scaled for response by matching impedance functions, even though extensive not-to-scale elements may be present (Ref. 32, 42).

One method of optimal scaling overlays each matched pair of impedance functions from naval vessels and compares them for the best curve fit (minimum error). The resulting magnitude-scale factor and frequency-scale factor are then used to scale, for example, such data as the response due to a depth charge on one submarine to predict the response of another type or class of submarine.

Another method conforms more to conventional network theory in accordance with the following representation:

$$\ddot{x}_1(t) (=) \ddot{X}_1(j\omega) = \mathcal{A}_1(j\omega)\ F_1(j\omega)$$

where

$\ddot{x}_1(t)$ = Acceleration time history at an internal location in vessel

$\ddot{X}_1(j\omega)$ = Complex acceleration-frequency response of $\ddot{x}(t)$

$\mathcal{A}_1(j\omega)$ = Generalized inertance functions $\left|\frac{\ddot{X}}{F}(j\omega)\right|$ (impedance) measured on Vessel No. 1

$F_1(j\omega)$ = Generalized input force on Vessel No. 1

For the second vessel, generalized inertance functions (impedance) $\mathcal{A}_2(j\omega)$ are measured and formulated such that response prediction on the second vessel may be scaled from the first vessel as:

$$x_2(t)\ (=)\ \ddot{X}_2(j\omega) = \left[\frac{\mathcal{A}_2(j\omega)}{\mathcal{A}_1(j\omega)}\right] \ddot{X}_1(j\omega)$$

The predicted response for Vessel No. 2 is based on equivalent input loading for Vessel No. 1. Depending on the geometric differences of the vessel, scaling may also be required for input loads. Scaling of input loads may also be used to determine equivalent response motion (shock or Fourier spectra) of the second vessel. The inverse problem, i.e., defining the external loads from the above formulation, is quite difficult and will not be looked into here.

The generalized inertance function may be viewed as a network equivalent system, a matrix array, or a sample. The form of representation can be developed for the application required. In References 32 and 42, single representative samples for each of the four locations scaled were used with quite good results even though their factors differed significantly (see Sec. 2.1.6.1, Table 2).

3.5 PULSE APPLICATION

Pulse train excitation of structures was covered in Section 1.1 and in more detail in Section 2.3.2. In addition to mechanical pulse generators that require fixed reaction points or inertial reaction masses, fluid and chemical pulse generators are under application development and should be available in the next 12 to 15 months. These new pulse generators depend on the mass-flow reaction, and as a consequence permit considerable flexibility in applications, including underwater use. Applications will determine the pulse generator type best suited for use, such as:

a. Peak force required
b. Pulse durations (max and min)
c. Number of pulses required
d. Turn-on/turn-off timing
e. Test bandwidth frequency
f. Number of pulse units required
g. Number of test axes for simultaneous testing

Force generation may be configured for environmental response simulation, systems (impedance) measurements, modal surveys, and diagnostic testing. Diagnostic testing is performed in terms of structure response, of equivalent sine, chirp, and random. The latter two types of excitation are particularly suited for studies of nonlinear phenomena.

In-place testing of large equipment, subsystems, and systems can be accomplished by pulse-simulation methods. Transmission of shock loads from the hull of a vessel through the structure to the multiple-mounting points of a ship's equipment alters the input to complicated acceleration time-history vectors. Section 4.1 covers projects for predicting these time-history motions for each mounting point and for each orthogonal direction as well as for selected points on the equipment itself. Pulse generators would be used to match these motion predictions in a vector sense on the equipment. Physical duplication of expected or actual motions of equipment

provides the most reliable means for determining failure, malfunction, degradation, and damage as a function of attack threat. Experience has also shown that once fragility data on equipment is obtained, hardness upgrade may be significantly improved. Typical nitty-gritty details of a fragility test and upgrade hardening on electronic communication equipment is given in Tables 7 and 8 from Reference 3. This transient shock-fragility program objectively demonstrated that the equipment would meet, and exceed with high probability, the weapon-system mission requirements for nuclear-weapon effects of shock and vibration.

Fragility of systems/components (Ref. 2) is categorized in terms of failure, malfunction, and damage/degradation. These terms demonstrate that fragility is more comprehensive than expected after a cursory throught: its operational connotation extends the meaning well beyond structural breakage. However, even the fragility categories are subject to different interpretation in the range of technical fields involved. Therefore, the categories are defined as follows:

- Failure is defined as an irreversible, environment-induced, inoperative condition or operation outside of tolerances. *Irreversible* refers to the system/component remaining inoperative or out of tolerance after the environment is removed.

- Malfunction also represents an environment-induced inoperative condition or out-of-tolerance operation. However, the process is reversible, i.e., the system/component returns to satisfactory operation upon removal of the environment.

- Damage/degradation has multiple meanings. It may be considered as a mild form of failure (i.e., irreversible but borderline operation). It also represents permanent degradation in performance, reduction in hardness, or limitation of survivability. Damage also applies to system/component attributes that are unrelated to performance.

TABLE 7. QUALIFICATION (100%) LEVEL TEST SUMMARY (Ref. 3)

Equipment	Failure/Malfunction/Degradation				Test Level Intensity, Percent	Corrective Action	Results
	Operational Effect	Mode	Mechanism	Cause			
IIIA Power Equipment	Degradation (reduced capacity)	Fuse holder fell off	Low spring tension on connectors	Design	100	Fuse panel restrained	Hardened to 100%+
	None	Voltmeter panel fell off	Low friction restraint	Design	100	Panel restraints or latches	Hardened to 100%+
		Doors swing open		Design	50	Door latches	Hardened to 100%+
Inverter	None	None	--	--	100	--	Passed qualification level 100%
Battery Rack	None	None	--	--	100	--	Passed qualification level 100%
Crypto	None	None	--	--	100	--	Passed qualification level 100%
203/303 Data Equipment	None	None	--	--	100	--	Passed qualification level 100%
46A Multiplex Unit No. 1	Degradation (reduced capacity)	4 kHz Generator module disengaged	Low spring tension on connector	Design	50	Module restraint brackets	Hardened to 100%+
46A Multiplex Unit No. 2	Degradation (high error counts in data stream)	Intermittent shorts	Loose wire	Quality control	100	Discovered and corrected at 200% test	See fragility test
46C Terminal Equipment	Malfunction (error counts and interruptions, 1 kHz tone)	Line input unit, loose jumper assy	Low spring tension and friction, connector jumper assy	Quality control or design	50	Split end connectors spring force increased	Hardened to 100%+
46C Dependent Terminal	Degradation (minor effect on isolator)	One friction damper failed to operate	Isolator damper guide pin fell out	Quality control	100	Reassembled damper	Passed qualification level 100%

AA5763

TABLE 8. FRAGILITY (200%) LEVEL TEST SUMMARY

Equipment	Failure/Malfunction/Degradation				Test Level Intensity, Percent	Corrective Action	Results
	Operational Effect	Mode	Mechanism	Cause			
111A Power Equipment	Degradation (reduced capacity)	Fuse holder disengaged	Low spring tension and friction of connector	Design	200	Fuse panel restrained	Hardened to 200% +
Inverter	None	1/4" bolt sheared	Cumulative fatigue	Test dependent	150	Bolt replaced	Passed fragility level 200%
	Failure	Short circuit	Loose bolt on capacitor	Quality control	200	Capacitor remounted	Passed fragility level 200%
Battery Rack	None	None	--	--	• 200 Vertical • 150 X- and Y-axis	--	• Passed fragility level 200% vertical • Passed level 150% horizontal axes
Crypto	None	None	--	--	--	--	200% level
203/303 Data Equipment	Failure (data signals lost)	Power supply fell out of rack	Weak mounting bracket	Design	X-axis 200 and Y-axis 200	Support bracket installed	Hardened to 200% +
46A Multiplex Unit No. 1	Failure (data signals lost)	Plug-in modules disconnected	Low spring tension on connector	Design	150	Restraint bars added	Hardened to 200% +
	Degradation (slight signal interruption)	Relay contact chatter	Armature dynamics	Design	150	None	Passed fragility level 200%
46A Multiplex Unit No. 2	Failure (data signals lost and 1 kHz tone interruptions)	Fuse operated, lost power to capacitor bank	Extraneous loose wire, electrical short	Quality control	200	Removed loose wire	Passed fragility level 200%
46C Terminal Equipment	None	--	--	--	200	See qualification test	Passed fragility level 200%
46C Dependent Repeater	None	--	--	--			• 150% X and Y axis • 200% vertical axis

AA8807

In matching the response of a structure to a specific input-dynamic environment, it is recognized that this approach is not as fruitful for nonlinear systems as it is for linear systems. It is planned to use the pulse technique to compare calculated (from nonlinear-mathematical models) and measured responses due to applied diagnostic-pulse trains. The results would be approximate with the resulting error as an index to the degree of nonlinearity encountered. Thus, a base is provided (if the approximation is poor) for improving the analysis and validating or identifying the nonlinear system characteristics.

SECTION 4

APPLICATIONS TO ONGOING NAVAL NEEDS

Intensive and extensive applications of impedance/mobility can be made to ongoing naval needs. The benefits that justify such efforts are outlined briefly in the nine projects suggested in this section.

Although impedance has a solid analytic foundation (see p. 6), the examples shown in Section 2 and the projects described in this section are all based upon physical measurements. Impedance data provide useful knowledge of systems in as-built configurations. In contrast, analytical models must use engineering material-properties data, estimates of joints and workmanship, and modeling simplification. The need to use abstract or simplified data rather than actual measurements has given rise in recent years to probabilistic solutions with associated confidence levels. The large uncertainties that result may lead to pessimism for hardness and survivability. An interesting check on the validity of probabilistic solutions could be the collection and statistical analysis of matched impedance measurements from ships of the same class and type.

Finite element models and impedance methods can be complementary. For the same bandwidth, impedance measurements may be used to verify and improve the finite element models. For high frequencies, impedance measurements are more effective; whereas for highly nonlinear systems, finite element methods are preferable. The two methods are not mutually exclusive but can be melded together in the frequency bands where each is most effective.

We feel that important information can be gleaned from the following projects. They are suggested for review, extension, and elaboration by the naval community.

4.1 IMPEDANCE APPLICATIONS

4.1.1 PROJECT 1: PREDICTION OF BASE (ATTACHMENT-POINT) MOTIONS OF THE SHIP'S STRUCTURE WHEN LOADED WITH EQUIPMENT OR FOR CHANGE OF EQUIPMENT

a. Purpose: To determine input motion to equipment for devising shock and vibration tests on this equipment for vulnerability and hardness requirements.

b. Theory: The shock environment at equipment locations in a naval vessel is specified from tests and procedures. Dynamic interaction at the mounting locations is modified by interaction of the ship's structure and equipment. If new equipment is to be substituted and dynamically differs from the original equipment, then the originally specified motion is altered.

c. Procedure: Inertance measurements are made on the ship's structure and on the equipment. Ratios of these functions are multiplied by the free (unloaded) velocity (or acceleration) motion of the ship at the mounting locations to predict the motion with equipment attached.

$$v'(t) (=)\ V'(\omega) = V(\omega) \left[\frac{\mathscr{A}_{33}(\omega)}{\mathscr{A}_{33}(\omega) + \mathscr{A}_{22}(\omega)} \right] \qquad (4\text{-}1)$$

where

$v'(t)$ = Velocity time history at ship's structure/equipment mounting

$V'(\omega)$ = Velocity-frequency spectrum of $v'(t)$

$V(\omega)$ = Velocity-frequency spectrum of ship structure only

$\mathcal{A}_{22}(\omega)$ = Driving-point inertance of ship's structure

$\mathcal{A}_{33}(\omega)$ = Driving-point inertance of equipment

d. Demonstration and Verification: Demonstration and verification of this project may be performed on the U.S. Navy Medium-Weight Shock Machine and on the U.S. Navy Floating Shock Platform (FSP) or the Large Floating Shock Platform (LFSP). Tests would be made with and without equipment mounted on both the shock machine and the FSP/LFSP, and velocity records would be taken. Subsequent inertance measurements would be used in Equation 4-1 to predict motions. These predictions, when compared to actual test records, would determine the accuracy and suitability of the method.

e. Applications to the Fleet:

- Standardized inertance measurement procedures and equipment could be established to determine threat motions to equipment.
- The ensemble of threat motions on equipment could be used to establish survivability, vulnerability, and fragility by tests in naval laboratories or by naval contractors.
- Hardening and upgrading of marginal equipment may be implemented.
- Shock and vibration transmitted from ship's structure to equipment can be attenuated by the use of isolation and damping devices.
- Shock-sensitive equipment may be relocated to locations more environmentally benign in a ship.

4.1.2 PROJECT 2: SCALING HULL PRESSURE AND RESPONSE OF NAVAL VESSELS TO EXPLOSIVE LOADINGS

a. Purpose. To scale the response motions and hull pressure loadings generated by explosive loads on one type of naval vessel to similar or different types of vessels, when not-to-scale effects exist.

b. Theory. In addition to presently available scaling procedures, inertance scaling and multivariate regression analysis may be used on an empirical basis.

c. Procedure: Procedures for multivariate regression analysis and inertance scaling are given in Section 3.

d. Demonstration and Verification: An array of inertance measurements taken on two different ships are matched for approximately equivalent paths (e.g., control room to similar hull position). Ratios of these paired measurements are used to scale the response of one vessel to the other. The predicted responses are compared for accuracy to actual test records.

e. Applications to Fleet: Empirical procedures will be developed and verified by impedance methods and/or multivariate regression analysis to scale explosive tests on naval vessels to various classes and types.

Multivariate regression analysis requires a reasonable data base and has the characteristics of correlation. Inertance scaling is functionally related and requires only measurements of the two systems that are to be related.

Multivariate regression analysis requires a data base sufficient to make reasonably accurate predictions. It may be more appropriate to examine hull response or pressure loading as the dependent variable, since inertance measurements and scaling can be used to determine responses elsewhere within the ship. Parameters required would include charge weight, depth of charge (below surface), target distance, depth of water, target orientation (including surface or below surface), hull parameters, and vessel velocity. Iterative models of the parameters would be generated, and would be expected to be a combination of linear and nonlinear terms.

Of particular importance is the scalability of the shock motions of equipment tested on the FSP or LFSP to their locations on naval vessels. In another sense, for the same or dynamically similar equipment motion, what is the explosive threat required to induce this motion on another ship?

4.1.3 PROJECT 3: PREDICTION BY IMPEDANCE TECHNIQUES OF NAVAL-VESSEL RESPONSE TO EXPLOSIVE CHARGES

a. Purpose: To determine acceleration time histories and associated acceleration Fourier frequency spectra and shock spectra at critical equipment locations in U.S. naval ships and submarines. These responses can be determined for a range of threats and for various orientations of the vessel with respect to the threat source. Both single attack and multiple attacks from several directions can be predicted. Response predictions would be based upon quasi-linear hull response.

b. Theory: Response motions at selected interior points of a naval vessel may be predicted by complex multiplication of transfer impedance functions and transient hydraulic-pressure loadings over the surface of the hull. Transient-pressure loadings on the hull may be formulated analytically from scale model tests and from low-level depth charges on full-size naval vessels.

c. Procedure: Transfer impedance measurements are taken from critical equipment location to the ship's hull, as illustrated in Figure 101. Spacing of the measurements is determined by the gradient observed between contiguous measurements on the hull and the engulfing velocity of the shock wave from the weapon (see Fig. 58). The impedance functions are arranged with respect to shock-wave engulfment of the vessel. It is to be noted that the surface area of the hull of a Polaris submarine has about the same area as the roof of the PARB building, which was measured for impedance/motion prediction (see Sec. 2.2.1.2). Hull pressure-time histories for a range of attack levels and directions would be established at input threat criteria and obtained from scale model tests, calculations, and full-scale tests.

d. Demonstration and Verification: Demonstration and verification of the procedures may be applied to any naval vessel that was used for explosive tests and for which test records exist or for which new tests can be made. As a practical convenience, the Floating Shock Platform (FSP), the Large Floating Shock Platform (LFSP), and the Submersible Submarine Test Vehicle (SSTV) can be used. The resulting acceleration time-history records from a test would be compared to predicted motions based on pressure loadings and impedance functions to assess the degree of accuracy obtained.

e. Application to Fleet:

- Impedance measurements on naval vessels can be made with minimal disruptions of operations and no damage/risk even for measurements at high-input-force levels.
- Response predictions can be made prior to explosive tests on surface vessels and submarines to assess the safety of the test.

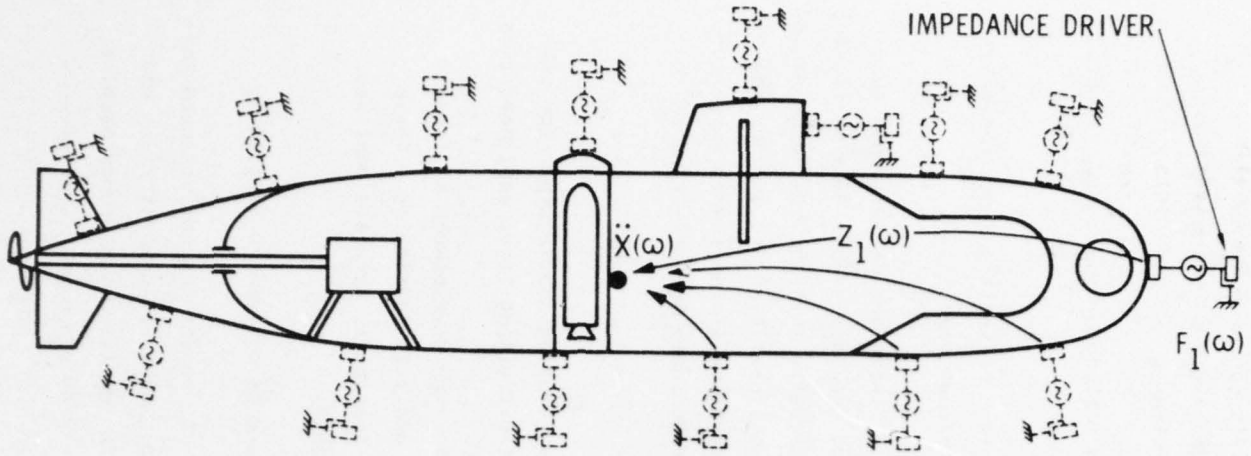

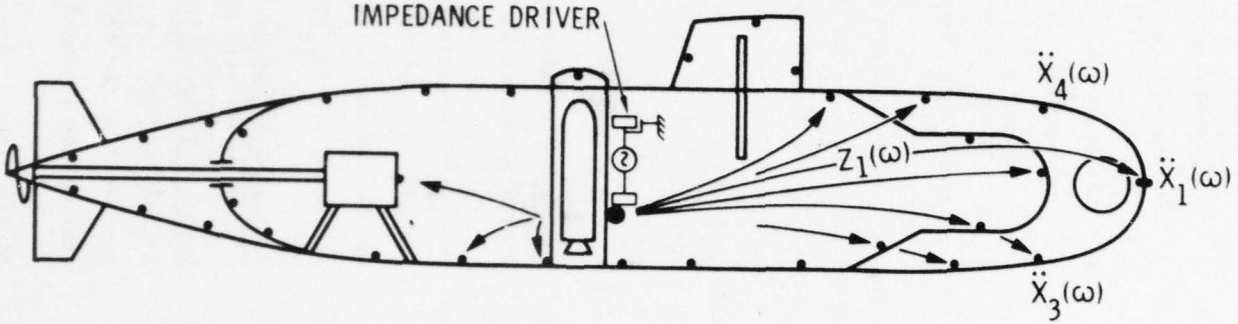

RECIPROCITY MEASUREMENTS FROM INTERNAL POINT
TO LOADING SURFACES (INTERNAL FACE)

FIGURE 101. SYSTEM FUNCTION MEASUREMENTS TO DETERMINE RESPONSE OF SUBMARINE TO DEPTH CHARGES

- Worse-case single- and multiple-attack scenarios can be developed, and response levels can be compared to laboratory-determined damage levels of equipment for hardness/survivability assessments.

- Response predictions may be scaled to other naval vessels as discussed in Project 2.

- Improvements can result in test criteria and environmental specifications for shipboard equipment.

Projects 1 through 3 are predicated on linear and quasi-linear systems. "Quasi-linear" is taken in the sense that the ship's hull remains linear, and other elements in the system may respond partially into the nonlinear range, as in damping and stiffness. For cases where nonlinearities are greater than known, response motions predicted will be conservative (larger) with some frequency shifts expected. This situation will predominate in early times.

4.1.4 PROJECT 4: NONLINEAR SYSTEMS

a. Purpose: To extract functionals relating input/output for subsystem's components or equipment exhibiting large nonlinearities.

b. Theory: Several methods exist for the development of functionals, such as Wiener kernels and state variables. These can be combined with multilevel testing to generate nonlinear parameter models from measured data.

c. Procedure: General procedures are as covered in Section 3.

d. Demonstration and Verification: A project has not yet been completely defined for this subject. However, demonstration and verification can be applied to the medium-weight shock machine when driven to its stops and to shipboard piping systems.

e. Applications to Fleet:

- Nonlinear shock-isolation systems for shipboard equipment
- Shipboard piping systems

4.2 SHOCK-SIMULATION PROJECTS

4.2.1 PROJECT 5: PULSE-SIMULATION TESTS ON U.S. NAVY MEDIUM-WEIGHT SHOCK MACHINE

a. Purpose: To demonstrate pulse-simulation methods and to increase the testing flexibility of the medium-weight shock machine.

b. Procedure: Response of the test structure and anvil is calculated for a pressure time history as shown in Figure 102. A pulse train is computed to generate an equivalent response from which pulse tests are conducted.

c. Verification: Accuracy of the test is determined by comparing the predicted motions to test records.

4.2.2 PROJECT 6: PULSE-SIMULATION TESTS ON MAJOR SUBSYSTEMS

a. Purpose: To qualify a major subsystem to criteria shock loads, to determine hardness/fragility levels, to identify failure modes, and to upgrade hardness levels where required.

b. Procedure: On selection of the major subsystem for testing--for example, the missile-launch tube shown in Figure 103--response motions determined from the previous impedance studies of Project 4 are used to generate pulse-equivalent motions. Shock tests are performed simultaneously in the three orthogonal axes. Testing may be accomplished as installed aboard ship if space permits, or at a Navy yard, naval laboratory, or contractor facility.

c. Verification: The tests are validated by comparison of test motion to prediction and to environmental tests on the vessel.

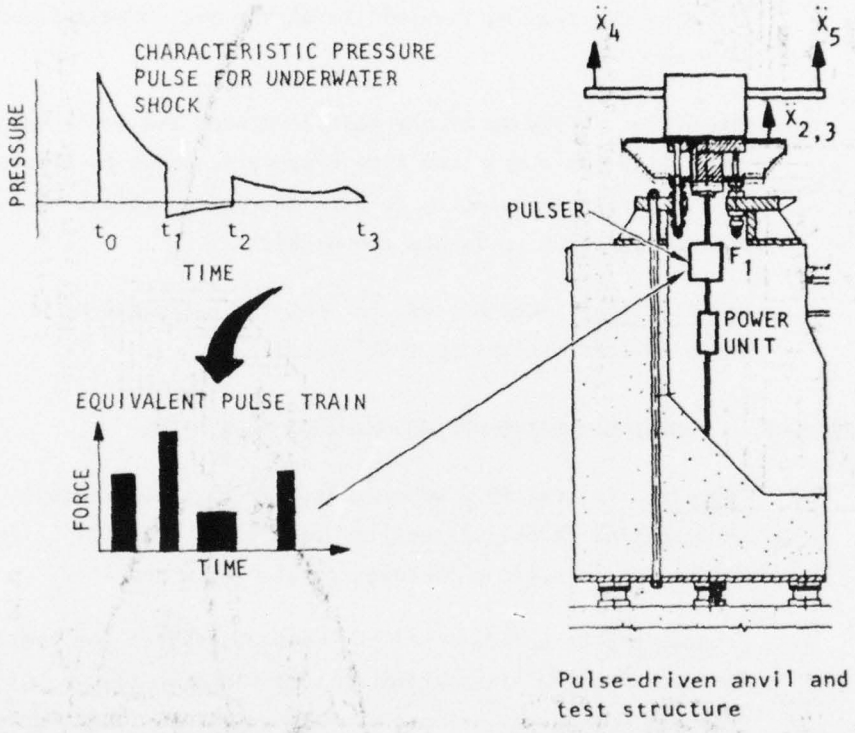

FIGURE 102. PULSE DRIVEN MEDIUM-WEIGHT SHOCK MACHINE SIMULATING UNDERWATER SHOCK MOTION ON TEST STRUCTURE

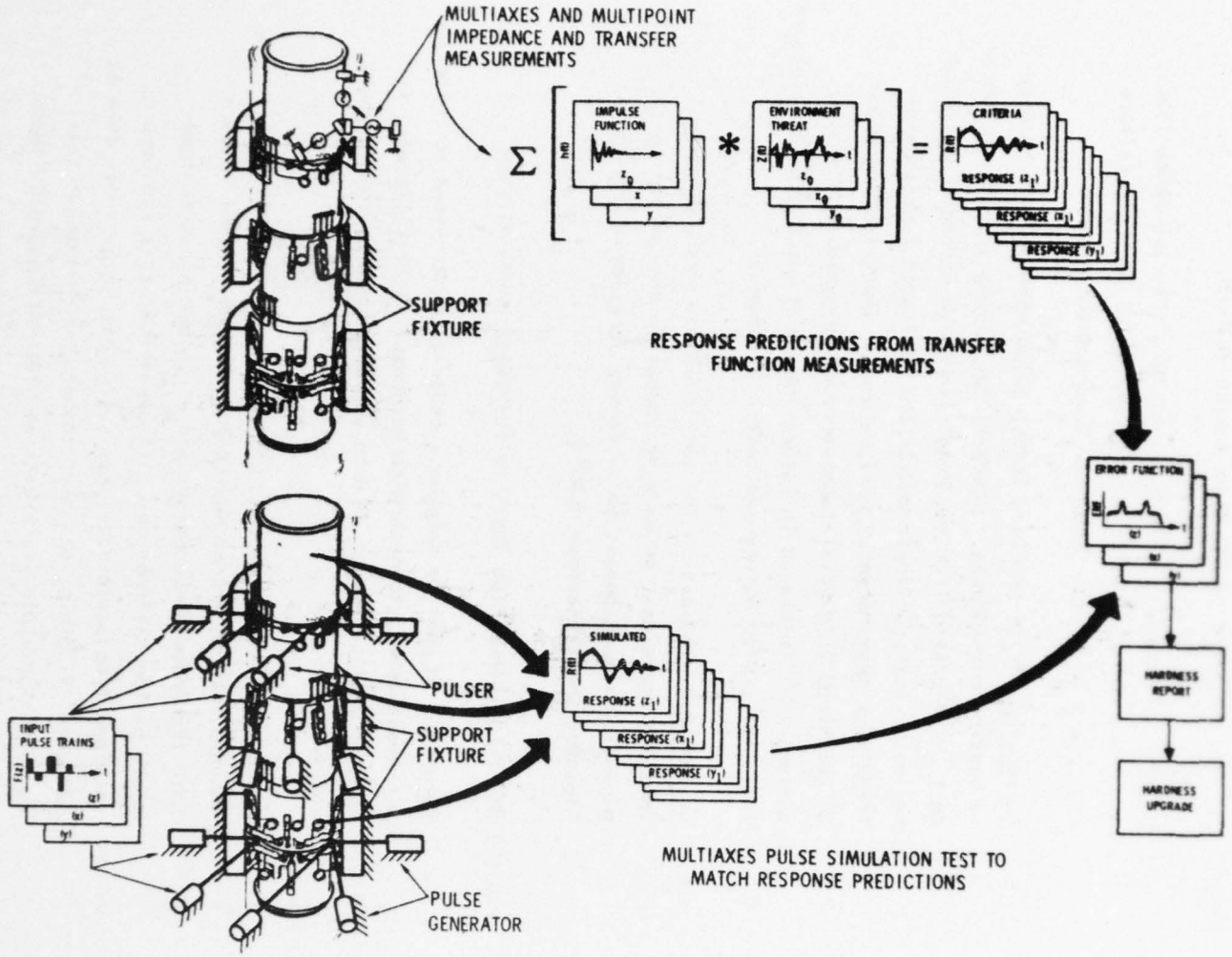

FIGURE 103. LABORATORY TESTING OF MAJOR SUBSYSTEMS

4.2.3 PROJECT 7: PULSE-SIMULATION TESTS ON PIPING SYSTEMS

a. Purpose: To qualify piping systems to criterion shock loads, to determine hardness/fragility levels, to identify failure modes, and to upgrade hardness levels where required.

b. Procedure: As in previous tests, pulse methods will be used to duplicate responses. However, for piping systems, responses must be generated from the quasi-linear to strongly nonlinear regions. Both nonlinear models and nonlinear functionals (from test measurements) will be used. Shock testing would be performed in a naval laboratory or shipyard on a piping system, as illustrated in Figure 104, that duplicates a shipboard installation for safety and test efficiency.

c. Validation: Validation for the levels of shock severity involved could best be made by comparing the pulsed-test piping-system responses to responses obtained on the Large Floating Shock Platform (LFSP).

4.2.4 PROJECT 8: PULSE-SIMULATION TESTS ON SHIPBOARD RADAR ANTENNA

a. Purpose: To qualify shipboard radar-antenna system to criterion air-blast loads, to determine hardness/fragility levels, to identify failure modes, and to upgrade hardness levels where required.

b. Procedure: Response prediction and pulse simulation of antenna systems are as depicted in Figure 105 and require both impedance measurements and air-blast pressure load-distribution information. Air-blast load data are best obtained from scale-model tests from the large shock tube at Dahlgren, Virginia, and supplemented by full-scale tests in such high-explosive events as DIAL PACK and DICE THROW. Experimental air-blast data on truss-type structures will provide necessary information on transient-drag coefficients and shading effects.

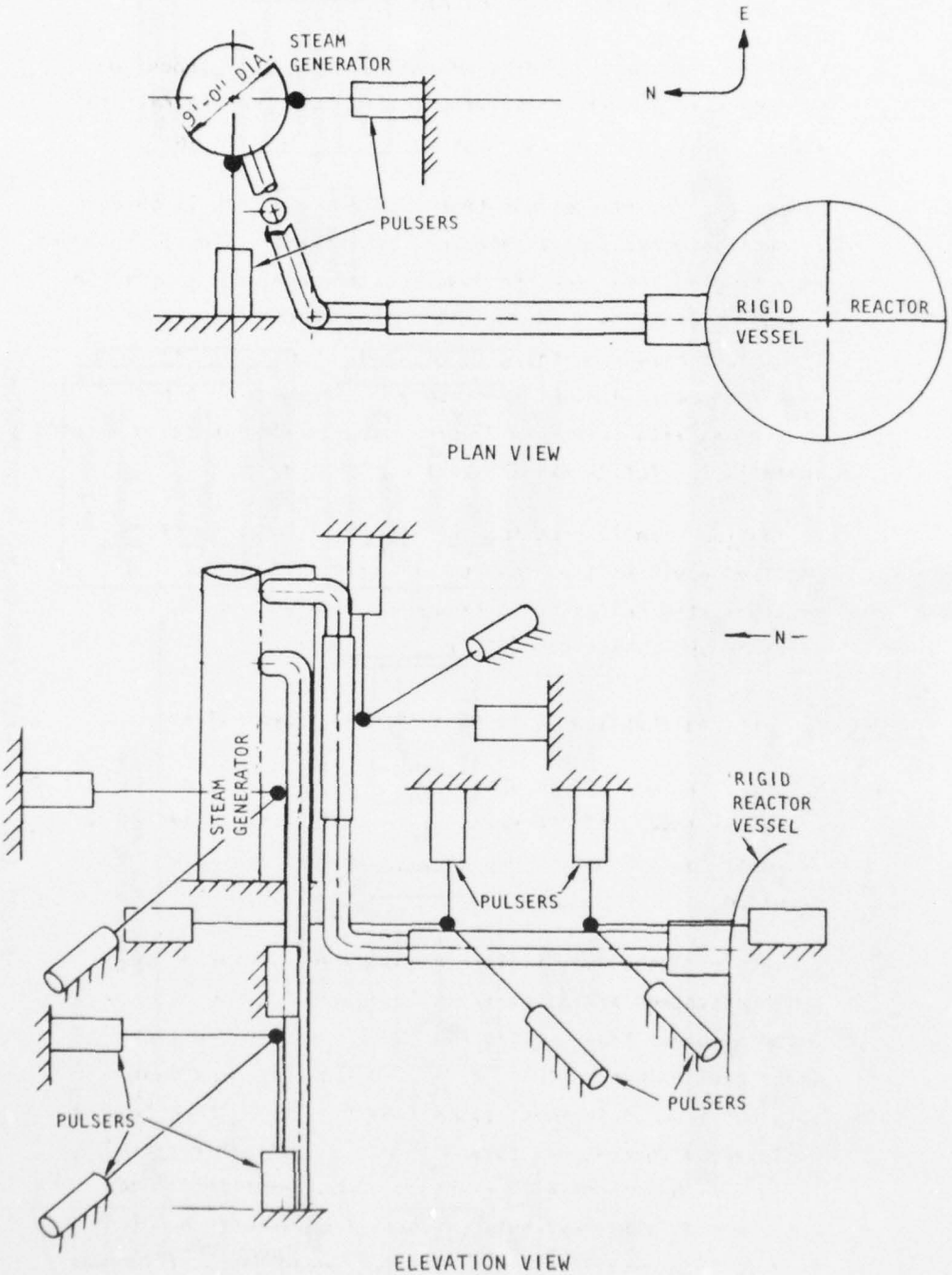

FIGURE 104. TESTS ON SHIPBOARD PIPING SYSTEM

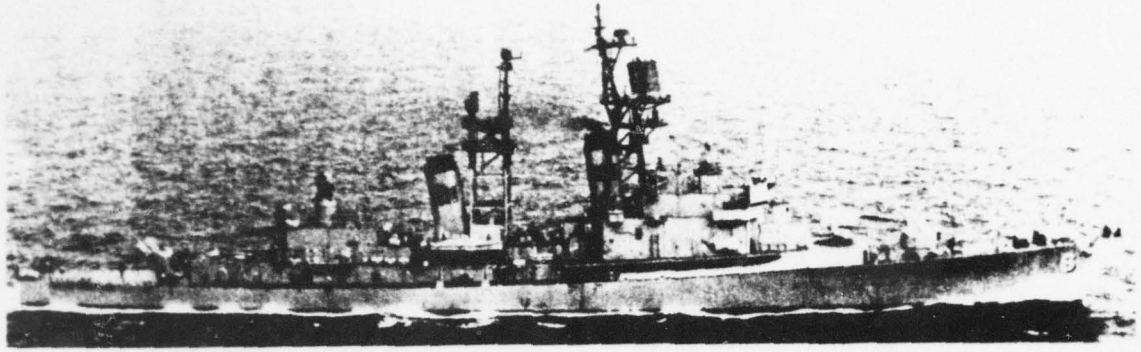

FARRAGUT (DLG 6)

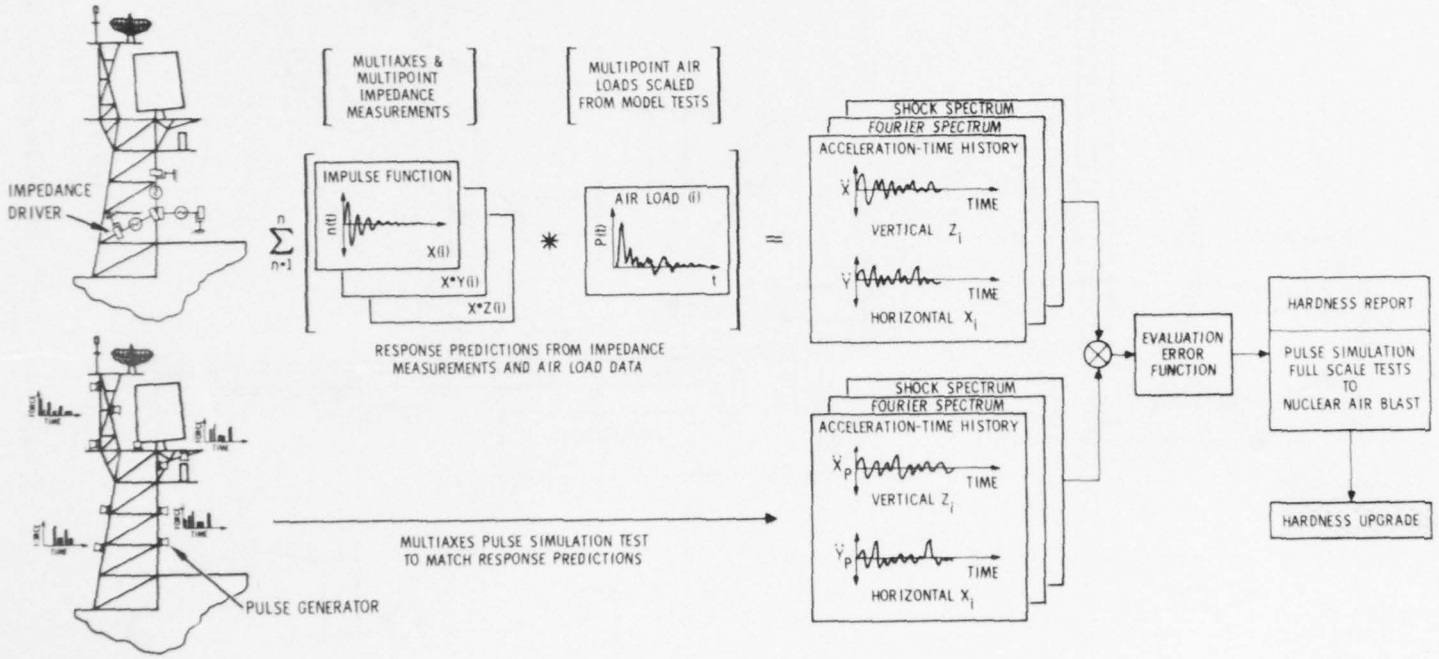

FIGURE 105. IN-PLACE TESTS OF MAJOR SUBSYSTEMS

c. Validation: Validation of pulse-simulated responses would be limited to scale-model tests in shock tubes and to full-scale tests in high-explosive events.

4.2.5 PROJECT 9: PULSE-SIMULATION TESTS ON A WEAPON'S SYSTEM

a. Purpose: To simulate underwater shock response of a naval vessel.

b. Procedure: Response-motion predictions as performed in Project 3 are used to specify the pulse generators and their spatial distribution over the ship's hull (Fig. 106a). For manned or tethered-operational vessels, pulse testing would be at a level to preclude damage consistent with safety. High-level tests would be accomplished on the Submersible Submarine Test Vehicle (SSTV), Floating Shock Platform (FSP), and Large Floating Shock Platform (LFSP). Pressure-load distribution over the hull, as shown in Figure 106b, must be determined from analysis, scale-model tests, and full-scale depth charges.

c. Validation: Validation of pulse-simulated responses is made by comparison to equivalent depth-charge tests on the weapon's system or test vehicle.

AD-A050 116 AGBABIAN ASSOCIATES EL SEGUNDO CALIF F/G 20/11
IMPEDANCE-BASED MOTION PREDICTION, SCALING, AND ENVIRONMENTAL S--ETC(U)
DEC 77 F B SAFFORD N00173-76-C-0249
UNCLASSIFIED AA-R-7710-4500 NRL-MR-3676 NL

3 OF 3
AD
A050116

END
DATE
FILMED
3-78
DDC

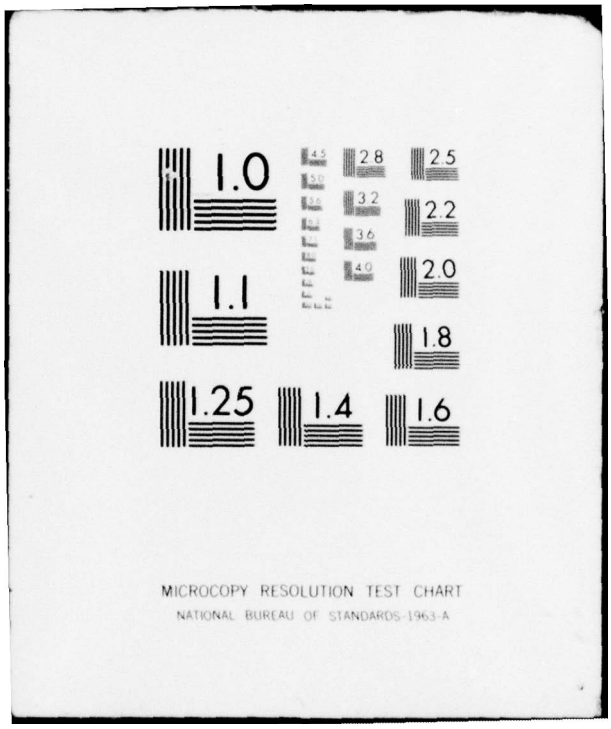
1.0
1.1
1.25
1.4
1.6
1.8
2.0
2.2
2.5
2.8
3.2
3.6
4.0
4.5
5.0
MICROCOPY RESOLUTION TEST CHART
NATIONAL BUREAU OF STANDARDS-1963-A

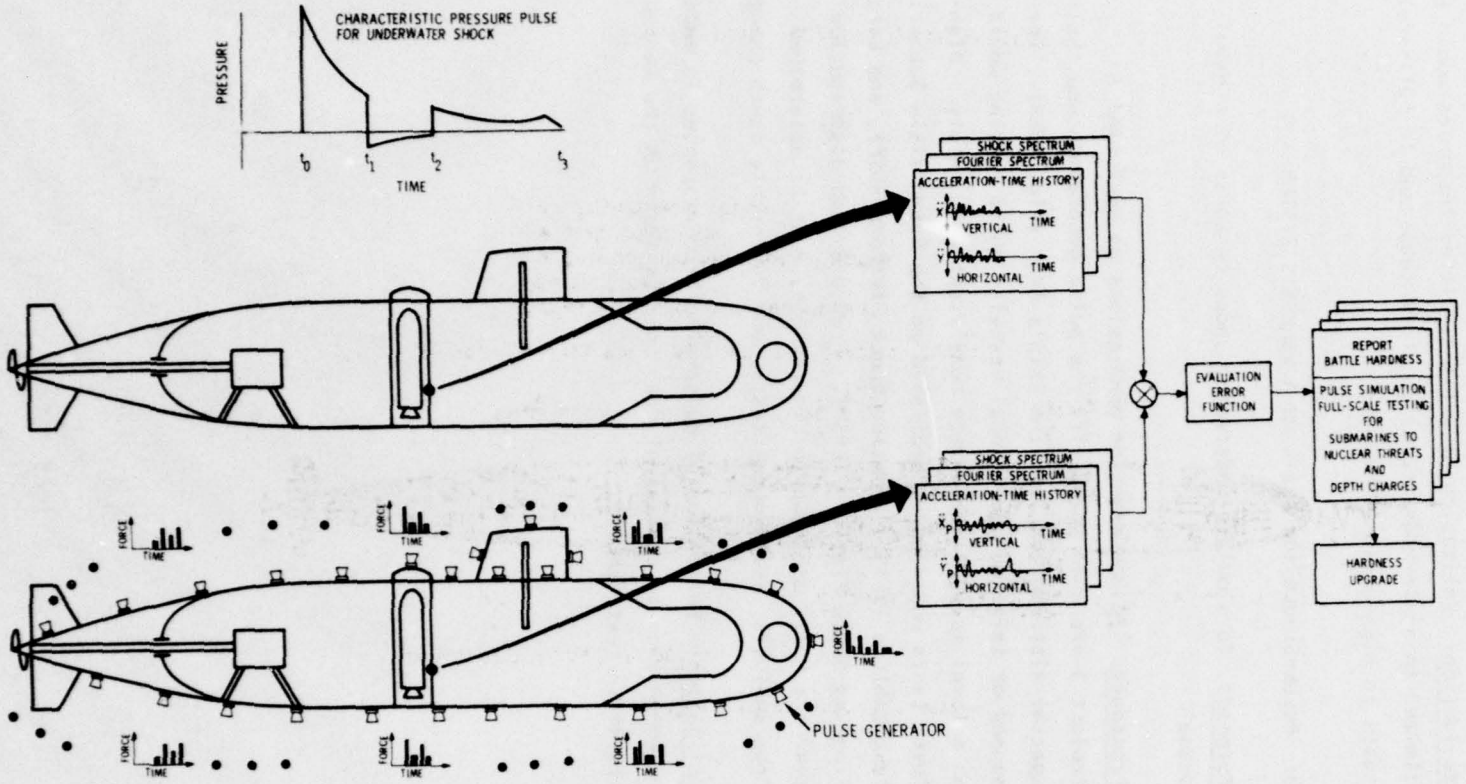

PULSE SIMULATION TO GENERATE STRUCTURAL RESPONSE MOTIONS EQUIVALENT TO MOTIONS INDUCED BY NUCLEAR OR DEPTH CHARGE UNDERWATER SHOCK

(a)

FIGURE 106. WEAPONS SYSTEMS TEST

DETERMINE AND SPECIFY INTERFACE PRESSURE LOADS

FREE FIELD

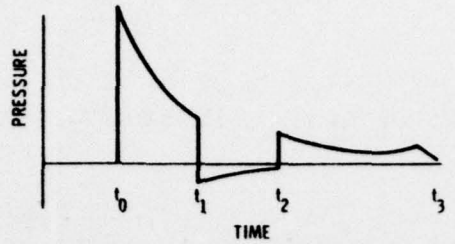

Free-field pressure pulse for underwater shock

INTERFACE PRESSURE LOADS

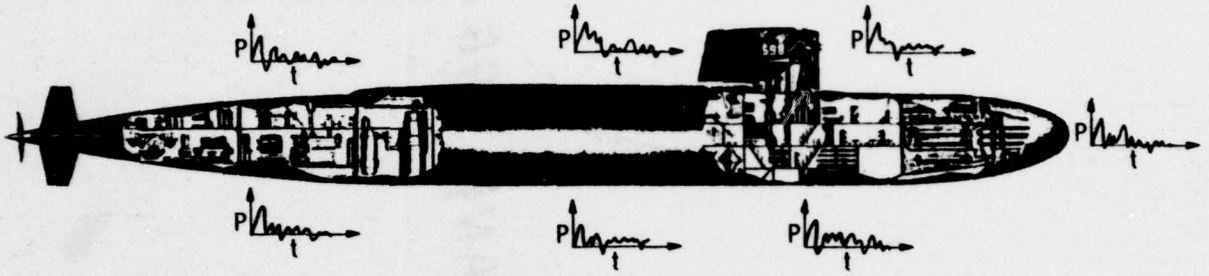

SPECIFY INTERFACE PRESSURE LOADS FOR RANGE OF THREATS

Spatial distribution over hull surface
Determine from:

- Analytic/finite difference calculation
- Scale model tests
- Low-yield depth charges

(b)

FIGURE 106. WEAPONS SYSTEMS TEST

SECTION 5

RECOMMENDATIONS

This report has summarized current activities in the measurement of structural dynamic functions, practical methods of response prediction to environmental threats, and a new means of environmental testing. The scaling of systems, particularly by impedance/mobility techniques, also offers opportunities for refining information from ongoing and past projects for hardness assessment and upgrade.

It is shown in this report that mechanical impedance/mobility techniques have come of age. Impedance and mobility, long a tool of the experimenter, have evolved to practical methods under engineering conditions. The ability to accurately predict and simulate acceleration-time histories at the mounting locations of weapons system equipments and components provides additional knowledge for protecting and hardening these elements to meet mission requirements of naval ships and submarines.

It is therefore recommended that the responsible authorities in the Navy Codes consider projects for applying the methods presented and for elaboration of them for specific naval projects.

The projects outlined in the previous section started with demonstration/proof examples and proceeded to hardness/survivability levels for naval subsystems and systems. The following recommended projects are listed by priority, starting with the less complex tests to ensure proper application of the methods, procedures, and techniques involved. The next group provides for measurements and tests where a potentially high yield of information may be obtained for a minimal expenditure of funds. The final, more complex projects then benefit from evolving refinements in test and measurements and the learning curve of personnel and of management.

(1) U.S. NAVY MEDIUM-WEIGHT SHOCK MACHINE (PROJECTS 1 AND 5)

- Determine motion of shock machine as altered by addition of equipment mounted thereon.
- Pulse-test the shock machine with mounted equipment, to simulate response motions induced by an underwater depth charge.

(2) FLOATING SHOCK PLATFORM/LARGE FLOATING SHOCK PLATFORM (PROJECT 1)

- Determine motions at equipment mounting points on FSP/LFSP with and without mounted equipment.

(3) SCALING RESPONSE MOTIONS (PROJECT 2)

- Scale response motions from one naval vessel to another and verify, by explosive tests on second vessel, that the predicted motions are accurate within acceptable error bounds.
- Scale transient-shock tests made of equipment on the Floating Shock Platform or Large Floating Shock Platform to shipboard installations and verify with test records.
- Scale explosive tests for Floating Shock Platform or Large Floating Shock Platform to yield the equivalent motion (energy spectra, Fourier spectra, shock spectra) of equipment aboard a ship.

(4) RESPONSE PREDICTIONS TO UNDERWATER DEPTH CHARGE(S) (PROJECT 3)

- Convolve pressure loads from depth charge(s) with systems (impedance) functions of naval vessels to predict motions. Candidate vessels are submarine, Submersible Submarine Test Vehicle (SSTV), Floating Shock Platform, Large Floating Shock Platform, or other vessels to be designated. Predicted motions are to be verified by tests.

(5) NONLINEAR RESPONSE (PROJECTS 4 AND 7)

- Predict motions of shipboard piping system by extraction from data of nonlinear functionals. Pulse simulation of nonlinear motion of shipboard piping system would duplicate a shipboard installation and be tested in a laboratory.

(6) PULSE SIMULATION TESTS OF MAJOR SUBSYSTEMS (PROJECT 6)

- Make simultaneous tests in three orthogonal axes by pulse-simulated response-motion equivalents on major subsystems in the weight range of 20,000 lb to 400,000 lb. These tests may be accomplished in place as installed aboard ship, in naval laboratories, naval shipyards, or at contractors' plants. Verification of simulation will be by comparison to motion-response records from shock-barge tests.

(7) RADAR ANTENNA (PROJECT 8)

- Perform pulse-simulation tests on deck-mounted equipment of surface ships by simultaneous tests in three orthogonal axes. These tests induce responses caused by air-blast loading and may be performed in place and as installed.

(8) PULSE SIMULATION OF COMPLETE WEAPONS SYSTEMS (PROJECT 9)

- Test a surface ship or submarine to equivalent underwater depth charge(s) by attachment of pulse generators to the hull. Repeat tests for different levels of attack, for different directions, and for multiple attacks. For environmental protection, this test method would kill fewer fish than present methods.

SECTION 6

REFERENCES

1. Safford, F.B. "Experiments for Resistance-Analysis Technology Development for Dynamic Response of Flush Buried Structures," R-7734-1-4404, El Segundo, CA: Agbabian Assoc., Apr 1977.

2. Rountree, R.C. and Safford, F.B. "Methodology and Standardization for Fragility Evaluation," *Shock & Vibration Bull.* No. 41, Pt. 5. Washington, DC: Naval Research Lab., Dec 1970.

3. Safford, F.B. and Tuttle, R.J. "Transient Shock Fragility and Hardness Assessment of Commercial Communications Equipment," Paper No. 740801. *Nat'l Aerospace Eng. and Manufacturing Meeting, Soc. of Automotive Engineers, San Diego, CA, Sep 30, 1974.*

4. Calkins, J.C. and Piersol, A.G. "Simulation of the Sparrow Flight Vibration Environment," Paper No. 730939. *Nat'l Aerospace Eng. and Manufacturing Meeting, Soc. of Automotive Engineers, Los Angeles, CA, Oct. 16, 1973.*

5. Meeker, D.B. and Piersol, A.G. "Accelerated Reliability Testing under Vibroacoustic Environments," Paper to be presented at the Annual Meeting, Amer. Soc. of Mech. Engineers, New York City, NY, Dec 1974.

6. Safford, F.B. and Masri, S.F. "Analytical and Experimental Studies of a Mechanical Pulse Generator," *Jnl of Eng. for Industry,* 96:2, May 1974, pp 459-470.

7. Safford, F.B. "Mechanical Force Pulse Generator for Use in Structural Analysis," U.S. Patent No. 4,020,672.

8. Safford, F.B. "Pulse Application and Parameter Identification for U.S. Navy Medium Weight Shock Machine," R-7710-4502. El Segundo, CA: Agbabian Assoc., Sep 1977.

9. Safford, F.B.; Carlson, L.E.; Walker, R.E.; and Huang, C.C. "Air-Blast and Ground-Shock Simulation Testing of Massive Equipment by Pulse Techniques," *5th Int. Symp. on Military Application of Blast Simulation, Stockholm, Sweden, May 23-26, 1977.*

10. Nuclear Power Eng. Test Center (NPETC). *On Aseismic Proving Test Project Using a Large-Scale Vibration Table: Large Capacity Earthquake Shaking Table Project-Japan.* Tokyo, Japan: NPETC, Jun 1977.

11. White, R.G. "The Resolution of Close Natural Frequencies in the Impulse Response and Several Truncation Effects," ISVR-R-17. Southampton, UK: Inst. of Sound & Vibration, Univ. of Southampton, Jun 1969.

22. Klosterman, A.L. "Modal Surveys of Weakly Coupled Systems," Paper No. 760876. *Soc. of Auto Engrs., Aerospace Eng. Meeting, San Diego, CA, Dec 1976.*

23. Richardson, M. and Kniskern, J. "Identifying Modes of Large Structures from Multiple Input and Response Measurements," Paper No. 760875. *Soc. of Auto Engrs., Aerospace Eng. Meeting, San Diego, CA, Dec 1976.*

24. Ibanez, P. "Force Appropriation by Extended Asher's Method," Paper No. 760873. *Soc. of Auto Engrs., Aerospace Eng. Meeting, San Diego, CA, Dec. 1976.*

25. Hamma, G.A. and Smith, S. "An Evaluation of Excitation and Analysis Methods for Modal Testing," Paper No. 760872. *Soc. of Auto Engrs., Aerospace Eng. Meeting, San Diego, CA, Dec 1976.*

26. Leppert, E.L. et al. "Comparison of Modal Test Results: Multipoint Sine Versus Single Point Random," Paper No. 760879. *Soc. of Auto Engrs., Aerospace Eng. Meeting, San Diego, CA, Dec 1976.*

27. Otnes, R.K. and Enochson, L.D.:

    Digital Time Series Analysis. New York: Wiley, 1972.

    MAC/RAN III Reference Manual. Los Angeles, CA: University Software Systems, 1973.

28. Bendat, J.S. and Piersol, A.G. *Random Data, Analysis and Measurement Procedures.* New York: Wiley-Interscience, 1971.

29. Malthan, J.A. *Task 4--Data and Correlation Analysis for Structural Response Measurements--Event DIAL PACK,* R-7124-4-2484, El Segundo, CA: Agbabian Assoc. Jan 1973.

30. Safford, F.B. and Walker, R.E. *In-Place Testing of SAFEGUARD Shock-Isolation Systems,* HNDSP-75-346-ED-R. Vicksburg, MS: Army Eng. Waterways Exp. Station, and El Segundo, CA: Agbabian Assoc., Mar 1975.

31. Bendat, J.S. "Solutions for the Multiple Input/Output Problem," *Jnl of Sound and Vibration,* 44:3, 1976, pp 311-325.

32. Safford, F.B.; Walker, R.E.; and Kennedy, T.E. *Prediction of Model and Prototype PARB Structure Responses Using Impedance Analysis Techniques,* R-7240-4036. Vicksburg, MS: Army Eng. Waterways Exp. Station; and El Segundo, CA: Agbabian Assoc., 1975.

33. White, R.G. "Evaluation of the Dynamic Characteristics of Structures by Transient Testing," *Jnl of Sound and Vibration*, 15:2 Mar 1971.

34. Crum, J.D. and Grant, R.L. "Transient Pulse Development," *Shock & Vibration Bull.*, No. 41, Pt. 5. Washington, D.C.: Naval Res. Lab., Dec. 1970.

35. Blake, R.E. and Belsheim, R.O. "Significance of Impedance in Shock and Vibration" in *Colloquium on Mechanical Impedance Methods*, edited by R. Plunkett. New York: Amer. Soc. of Mech. Eng., 1958.

36. Masri, S.F.; Bekey, G.A.; and Safford, F.B. "Optimum Response Simulation of Multidegree Systems by Pulse Excitation," *Jnl of Dyn. Systems, Measurement & Control*, 97:1, Mar 1975, p 46.

37. Crowson, R.D. and Kiger, S.A. "The Effect of Earth Cover on the Dynamic Response of Hardened Reinforced Concrete Structures," *Shock & Vibration Bull.* No. 47, Pt. 4. Washington, DC: Naval Res. Lab., Sep 1977.

38. Yang, R.C. *Development of a Waveform Synthesis Technique*, SAF-64. Los Angeles: Ralph M. Parsons Co., Aug. 1970.

39. Masri, S.F. and Safford, F.B. "Dynamic Environment Simulation by Pulse Techniques," *Proc. ASCE Eng. Mech. Div.* 101:EM1, Feb 1976, pp 151-169.

40. Masri, S.F.; Bekey, G.A.; and Safford, F.B. "Adaptive Random Search Method for Identification of Large-Scale Nonlinear Systems," *4th Symp. for Identification and System Parameter Estimation, Int. Federation of Automatic Control, Tbilisi, USSR, Sep 1976.* (to be published in Automatica)

41. O'Hara, G.J. *Mechanical Impedance and Mobility Concepts*, NKL Report 6406. Washington, DC: Naval Research Laboratory, July 29, 1966.

42. Safford, F.B.; Walker, R.E.; and Kennedy, T.E. "Scaling and Response Predictions of Both Model and Prototype Protective Structures to Air-Blast Loads by Impedance Techniques." *Shock & Vibration Bull. No. 48.* Washington, DC: Naval Res. Lab., Oct 1978.

DISTRIBUTION LIST

ASSISTANT TO THE SECRETARY DEFENSE
ATOMIC ENERGY
WASHINGTON , DC 20301
ATTN DONALD COTTER

DIRECTOR
DEFENSE ADVANCED RSCH PROJ AGENCY
ARCHITECT BUILDING
1400 WILSON BLVD
ARLINGTON VA. 22209
ATTN A TACHMINDJI
ATTN STO KENT KRESA
ATTN TECHNICAL LIBRARY
ATTN R CHAPMAN

DIRECTOR
DEFENSE INTELLIGENCE AGENCY
WASHINGTON D.C. 20301
ATTN DI-7D E. OFARRELL
ATTN DI-7E
ATTN DT-1C J. VERONA
ATTN DT-2 WPNS + SYS DIV
ATTN TECHNICAL LIBRARY

DIRECTOR
DEFENSE NUCLEAR AGENCY
WASHINGTON D.C. 20305
ATTN STTL TECH LIBRARY (2 COPIES)
ATTN STST ARCHIVES
ATTN DDST
ATTN SPSS (2 COPIES)

CHAIRMAN
DEPT OF DEFENSE EXPLO SAFETY BOARD
RM-GB270, FORRESTAL BUILDING
WASHINGTON D.C. 20301
ATTN DD/S+SS

DIR OF DEFENSE RSCH + ENGINEERING
WASHINGTON D.C. 20301
ATTN AD/SW
ATTN DD/TWP
ATTN DD/S+SS
ATTN AD/NP

COMMANDER
FIELD COMMAND
DEFENSE NUCLEAR AGENCY
KIRTLAND AFB, NM 87115
ATTN FCTA
ATTN FCTA-D

INTERSERVICE NUCLEAR WEAPONS SCHOOL
KIRTLAND AFB, NM 87115
ATTN TECH LIB

DIRECTOR
JOINT STRAT TGT PLANNING STAFF JCS
OFFUTT AFB
OMAHA, NB 68113
ATTN STINFO LIBRARY

WEAPONS SYSTEMS EVALUATION GROUP
400 ARMY NAVY DRIVE
ARLINGTON VA 22202
ATTN DOC CON

CHEIF OF RES, DEV * ACQUISITION
DEPARTMENT OF THE ARMY
WASHINGTON D.C. 20310
ATTN TECHNICAL LIBRARY
ATTN DAMA-CSM-N LTC E. DEBOESER JR

COMMANDER
HARRY DIAMOND LABORATORIES
WASHINGTON D.C. 20438
ATTN AMXDO-NP
ATTN AMXDO-TI TECH LIB

DIRECTOR
U S ARMY BALLISTIC RESEARCH LABS
ABERDEEN PROVING GROUND, MD 21005
ATTN TECH LIB E. BAICY

COMMANDER
U S ARMY COMM COMMMAND
FORT HUACHUCA, AZ 85613
ATTN TECHNICAL LIBRARY

COMMANDER
U S ARMY MAT + MECHANICS RSCH CTR
WATERTOWN, MA 02172
ATTN R SHEA

COMMANDER
U S ARMY NUCLEAR AGENCY
FORT BLISS, TX 79916
ATTN TECH LIB

COMMANDER
U S ARMY WEAPONS COMMAND
ROCK ISLAND ARSENAL
ROCK ISLAND, IL 61201
ATTN TECHNICAL LIBRARY

CHIEF OF NAVAL MATERIAL
NAVY DEPT
WASHINGTON D.C. 20360
ATTN MAT 0323

CHIEF OF
NAVY DEPA
WASHINGTO
ATTN
ATTN

CHIEF OF
DEPARTMEN
ARLINGTON
ATTN
ATTN

OFFICER I
CIVIL ENG
NAVAL CON
PORT HUEN
ATTN
ATTN

COMMANDER
NAVAL ELE
NAVAL ELE
WASHINGTO
ATTN

COMMANDER
NAVAL FAC
HEADQUART
WASHINGTO
ATTN

SUPERINTE
NAVAL POS
MONTEREY
ATTN

CHIEF OF NAVAL OPERATIONS
NAVY DEPARTMENT
WASHINGTON D.C. 20350
ATTN OP 03FG
ATTN OP 985F

CHIEF OF NAVAL RESEARCH
DEPARTMENT OF THE NAVY
ARLINGTON VA 22217
ATTN N PERRONE CD 474
ATTN TECHNICAL LIBRARY

OFFICER IN CHARGE
CIVIL ENGR LAB
NAVAL CONST. BATTALION CTR
PORT HUENEME CA 93041
ATTN R ODELLO
ATTN TECH LIB

COMMANDER
NAVAL ELECTRONIC SYSTEMS COMMAND
NAVAL ELECTRONIC SYSTEMS COMMAND HQS
WASHINGTON D.C. 20360
ATTN PME 117-21A

COMMANDER
NAVAL FACILITIES ENGINEERING COMMAND
HEADQUARTERS
WASHINGTON D.C. 20390
ATTN TECHNICAL LIBRARY

SUPERINTENDENT
NAVAL POSTGRADUATE SCHOOL
MONTEREY CA 93940
ATTN CODE 2124 TECH RPTS LIBRARIAN

COMMANDER
NAVAL SHIP RESEARCH AND DEV CENTER
BETHESDA MD 20034
ATTN CODE 17 WW MURRAY
ATTN CODE 142-3 LIBRARY
ATTN CODE 174
ATTN CODE 11
ATTN CODE 2740 Y WANG
ATTN CODE 1962
ATTN CODE 1903
ATTN CODE 1731C
ATTN CODE 1171
ATTN CODE 19

COMMANDER
NAVAL SURFACE WEAPONS CENTER
WHITE OAK
SILVER SPRING MD 20910
ATTN CODE 241 J PETES
ATTN CODE 1224 NAVY NUC PRGMS OFF
ATTN CODE 730 TECH LIB
ATTN CODE 240 H SNAY
ATTN CODE 243 G YOUNG

COMMANDER
NAVAL SURFACE WEAPONS CENTER
DAHLGREN LABORATORY
DAHLGREN VA 22448
ATTN TECHNICAL LIBRARY

COMMANDER
NAVAL UNDERSEA CENTER
SAN DIEGO, CA 92152
ATTN TECHNICAL LIBRARY

COMMANDER
NAVAL WEAPONS CENTER
CHINA LAKE CA 93555
ATTN CODE 533 TECH LIB

SANDIA LABS
LIVERMORE LAB
P O BOX 969
LIVERMORE CA 94550
ATTN DOC CON FOR TECH LIB

SANDIA LABORATORIES
P.O. BOX 5800
ALBUQUERQUE NM 87115
ATTN DOC CON FOR 3141 SANDIA RPT COLL

U S ENERGY RSCH & DEV ADMIN
DIVISION OF HEADQUARTERS SERVICES
LIBRARY BRANCH G-043
WASHINGTON D C 20545
ATTN DOC CONTROL FOR CLASS TECH LIB

UNIV OF CALIFORNIA
LAWRENCE LIVERMORE LAB
P.O. BOX 808
LIVERMORE CA 94550
ATTN TECHNICAL LIBRARY

AGBABIAN ASSOCIATES
250 NORTH NASH STREET
EL SUGONDO CA 90245
ATTN M AGBABIAN

BATTELLE MEMORIAL INSTITUTE
505 KING AVENUE
COLUMBUS OH 43201
ATTN TECHNICAL LIBRARY

INST FOR DEFENSE ANALYSIS
400 ARMY NAVY DRIVE
ARLINGTON VA 22202
ATTN IDA LIBRARIAN R SMITH

J.L. MERRITT
CONSULTING + SPECIAL ENGR SVS INC
P.O. BOX 1206
REDLANDS CA 92373
ATTN TECHNICAL LIBRARY

KAMAN AVIDYNE
DIV OF KAMAN SCEINCES CORP
83 SECOND AVE
NW INDUSTRIAL PARK
BURLINGTON MA 01803
ATTN E CRISCIONE
ATTN TECHNICAL LIBRARY
ATTN G ZARTARIAN

KAMAN SCIENCES CORP.
P.O. BOX 7463
COLORADO SPRINGS CO 80933
ATTN TECHNICAL LIBRARY

LOCKHEED MISSILES AND SPACE CO.
3251 HANOVER ST
PALO ALTO CA 94304
ATTN TECH INFO CTR D/COLL
ATTN T GEERS D/52-33 BLDG 205

NATHAN M. NEWMARK
CONSULTING ENGINEERING SERVICES
1114 CIVIL ENGINEERING BLDG
URBANA IL 61801
ATTN N NEWMARK

URS RESEARCH CO.
155 BOVET RD.
SAN MATEO CA 94402
ATTN TECH LIB

WEIDLINGER ASSOCIATES
3000 SAND HILL ROAD
BUILDING 4 SUITE 245
MENLO PARK CA 94025
ATTN J. ISENBERG

WEIDLINGER ASSOCIATES
110 EAST 59TH STREET
NEW YORK, NY 10022
ATTN DR. M. BARON

ASSISTANT CHIEF FOR TECHNOLOGY
OFFICE OF NAVAL RESEARCH
ARLINGTON, VIRGINIA 22217
ATTN CODE 200

TELEDYNE BROWN ENG.
MAIL STOP 44
300 SPARKMAN DRIVE
RESEARCH PARK
HUNTSVILLE, ALABAMA 35807
ATTN DR. MANU PATEL

DIRECTOR
U S ARMY WATERWAYS EXPERIMENT STN
P.O. BOX 631
VICKSBURG MS 39180
ATTN J STRANGE
ATTN W FLATHAU
ATTN TECH LIB (UNCL ONLY)